

Medical University of South Carolina

MEDICA

MUSC Theses and Dissertations

2017

The 8p11-P12 Amplicon Oncogenes ASH2L and NSD3 Regulate Cell Cycle Progression via Epigenetic Alterations and Result in Overexpression and Estrogen-Independent Activation of ER α in Breast Cancer

Jamie Nicole Mills

Medical University of South Carolina

Follow this and additional works at: <https://medica-musc.researchcommons.org/theses>

Recommended Citation

Mills, Jamie Nicole, "The 8p11-P12 Amplicon Oncogenes ASH2L and NSD3 Regulate Cell Cycle Progression via Epigenetic Alterations and Result in Overexpression and Estrogen-Independent Activation of ER α in Breast Cancer" (2017). *MUSC Theses and Dissertations*. 335.

<https://medica-musc.researchcommons.org/theses/335>

This Dissertation is brought to you for free and open access by MEDICA. It has been accepted for inclusion in MUSC Theses and Dissertations by an authorized administrator of MEDICA. For more information, please contact medica@muscd.edu.

JAMIE NICOLE MILLS. The 8p11-p12 Amplicon Oncogenes ASH2L and NSD3 Regulate Cell Cycle Progression via Epigenetic Alterations and Result in Overexpression and Estrogen-Independent Activation of ER α in breast cancer. (Under the direction of STEPHEN P. ETHIER)

The 8p11-p12 Amplicon Oncogenes ASH2L and NSD3 Regulate Cell Cycle Progression via Epigenetic Alterations and Result in Overexpression and Estrogen-Independent Activation of ER α in breast cancer

by

Jamie Nicole Mills

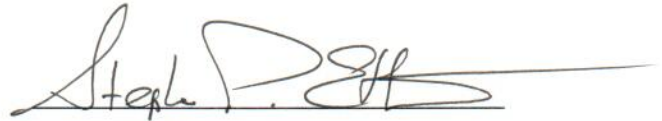
A dissertation submitted to the faculty of the Medical University of South Carolina in partial fulfillment of the requirements for the degree of Doctor of Philosophy in the College of Graduate Studies.

Department of Pathology and Laboratory Medicine

2017

Approved by:

Chairman, Advisory Committee



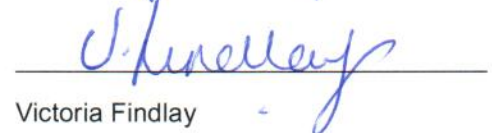
Stephen P. Ethier



Melissa Cunriningham



John Wrangle



Victoria Findlay



Amanda LaRue

TABLE OF CONTENTS

| | |
|--|------|
| Acknowledgements..... | ii |
| List of Figures..... | iii |
| List of Tables..... | iv |
| List of Appendices..... | v |
| List of Abbreviations..... | vi |
| ABSTRACT | viii |
| CHAPTER 1: Introduction and Review of Literature | 2 |
| CHAPTER 2: NSD3 amplification and overexpression results in overexpression and estrogen-independent activation of the estrogen receptor in human breast cancer | 55 |
| CHAPTER 3: ASH2L regulates gene expression via H3K4me3 in promoters and knockdown of ASH2L reduces expression of NSD3, ERα, and other genes important in cell proliferation processes | 70 |
| CHAPTER 4: Discussion and Future Directions | 94 |
| CHAPTER 5: Materials and Methods | 124 |
| REFERENCES CITED..... | 136 |
| Appendix Materials..... | 162 |

ACKNOWLEDGEMENTS

First and foremost, I would like to thank Steve Ethier for his mentorship. I appreciate all he taught me, the time and energy he invested in me, and the guidance he gave while also allowing me the freedom to explore scientific thought. Steve always challenged me and I will always be grateful to have had him as my mentor. I would also like to thank the members of the Ethier lab for support and advice through this process. It has been a pleasure working with Brittany Turner-Ivey, Christy Kappler, and Ericka Smith. Brittany has been a wonderful mentor and friend and I am thankful for all she taught me. Thank you to Jon Irish, Steve Guest, Ginny Davis, members of adjacent labs, and the Department of Pathology and Laboratory Medicine as a whole for your friendship and for acting as invaluable resources in my training process. I would like to thank my committee members, Melissa Cunningham, John Wrangle, Victoria Findlay, and Amanda LaRue for taking time from their busy schedules to invest in my scientific development. Perry Halushka, Amy Connolly, and my colleagues from the MSTP at MUSC have been an amazing source of support, as have the MUSC core facilities and personnel. Thank you to my clinical mentors and the faculty at MUSC as a whole for participating in my training. Finally, I would like to thank my friends and family. My husband, Ian Mills, always supported me and I could not have accomplished this without him. Thank you to my extended family, especially my mom, Diane Lingenfelter, and grandma, Vel Helton. I am grateful for support from my friends that have become family, especially Gerry Barnard, Renee Vick, Dawn Simmons, and the members of Redeemer Presbyterian Church. Last but not least, I have to thank my daughters, Gwendolyn and Eleanor. More than anyone, they have challenged me and shaped me in ways I never thought possible and I hope they continue to do so at every stage of life and career.

LIST OF FIGURES

Figure 1.1. Schematic representation of ER α structure.

Figure 1.2. Breast cancer intrinsic subtype proportions and characteristics of luminal tumors.

Figure 1.3. Schematic representation of the 8p11-p12 amplicon.

Figure 1.4. Frequencies of ASH2L and NSD3 alterations in primary tumors (TCGA).

Figure 1.5. Illustration of major histone modifications and effects on chromatin.

Figure 1.6. Hierarchical representation of histone lysine methyltransferase enzyme relationships.

Figure 1.7. Representation of the three isoforms of NSD3.

Figure 2.1. NSD3 is overexpressed in 8p11-p12 amplicon-bearing cell lines and is a verified oncogene.

Figure 2.2. NSD3 knockdown results in knockdown of estrogen receptor alpha (ER α).

Figure 2.3. NSD3 overexpression results in overexpression of estrogen receptor alpha (ER α).

Figure 2.4. SUM-44 cells are estrogen-independent despite high-level ER α expression.

Figure 2.5. SUM-44 cells are ER α -dependent.

Figure 3.1. ASH2L is overexpressed in ER+, 8p11-p12 amplicon-bearing breast cancer.

Figure 3.2. Overall H3K4 tri-methylation patterns in SUM-44 cells are similar between control and ASH2L knockdown on a global scale.

Figure 3.3. ASH2L is responsible for H3K4me₃ in the promoters of genes involved in breast cancer tumorigenesis.

Figure 3.4. ASH2L knockdown reduces expression of genes with decreased promoter H3K4me₃ levels.

Figure 3.5. ASH2L, NSD3, and ER α influence the expression of similar suites of genes related to cell cycle progression.

Figure 3.6. Knockdown of ASH2L results in decreased proliferation and clonogenicity in luminal B breast cancer.

Figure 3.7. Knockdown of ASH2L alters response to palbociclib.

Figure 4.1. Summary model of NSD3 functions.

Figure 4.2. Summary model of ASH2L functions.

Figure 4.3. Summary model.

LIST OF TABLES

Table 2.1. Genes with reduced transcript expression following knockdown of NSD3-S in SUM-44 cells.

Table 2.2. Biological processes to which genes with altered expression following knockdown of NSD3-S and ESR1 were annotated.

Table 3.1. Genes with promoter H3K4me3 ChIP-seq peaks called in control but not ASH2L knockdown datasets.

Table 3.2. Genes with reduced transcript expression following knockdown of ASH2L in SUM-44 cells.

Table 3.3. Summary of genes identified by ASH2L knockdown H3K4me3 ChIP-seq, ASH2L knockdown RNA-seq, NSD3-S knockdown array, or ESR1 knockdown array.

Table 3.4. Genes annotated to palbociclib response in ToppFun.

LIST OF APPENDICES

Appendix A. NSD3-S and ESR1 knockdown microarray results.

Appendix B. H3K4me3 ChIP-seq quality control and enrichment reports.

Appendix C. H3K4me3 ChIP-seq peak datasets: LacZ control and ASH2L knockdown.

Appendix D. Gene lists: overall H3K4me3 ChIP-seq peaks.

Appendix E. Gene lists and ToppFun analysis: promoter only H3K4me3 ChIP-seq peaks.

Appendix F. ASH2L knockdown RNA-seq results.

Appendix G. Gene lists and ToppFun analysis: ASH2L knockdown RNA-seq downregulated genes.

Appendix H. Gene lists and ToppFun analysis: ASH2L knockdown H3K4me3 ChIP-seq and RNA-seq.

Appendix I. Gene lists and ToppFun analysis: ASH2L, NSD3-S, and ESR1 knockdown expression analysis and ASH2L knockdown H3K4me3 ChIP-seq overlap.

LIST OF ABBREVIATIONS

| | |
|---|---|
| 4OH-tamoxifen – hydroxytamoxifen | HDAC(i) – histone deacetylase (inhibitor) |
| AF – activating function (ER α domain) | HER2 – human epidermal growth factor receptor 2 |
| AI – aromatase inhibitor | HOX – homeobox gene family |
| AML – acute myeloid leukemia | HMT – histone methyltransferase |
| ASH2L – Absent, Small, or Homeotic disc 2-Like | HMTi – histone methyltransferase inhibitors/inhibition |
| BET – bromodomain and extraterminal domain | hPTM – histone post-translational modification |
| CCND1 – cyclin D1 gene | IGV – integrated genome viewer |
| CDK – cyclin-dependent kinase | IHC - immunohistochemistry |
| CHD – chromodomain | IP - immunoprecipitation |
| ChIP – chromatin immunoprecipitation | IPTG – isopropyl β -D-1-thiogalactopyranoside |
| CNA – copy number alteration | K – lysine |
| CTD – comparative toxicogenomics database | LBD – ligand binding domain |
| DBD – DNA binding domain | LSCC – lung squamous cell carcinoma |
| DNMT – DNA methyltransferase | MLL – mixed lineage leukemia |
| EGFR – epidermal growth factor receptor | NLS – nuclear localization signal |
| ER/ERα – estrogen receptor (alpha) | NS – non-significant |
| ERE – estrogen response element | NSD – Nuclear-receptor binding SET Domain-containing |
| ESR1 – estrogen receptor alpha gene | NSD3-L – long isoform of NSD3 |
| FDR – false discovery rate | NSD3-S – short isoform of NSD3 |
| GISTIC – genomic identification of significant targets in cancer | NSD3-T – total NSD3 (both isoforms) |
| GO – gene ontology | PBS – phosphate buffered saline |
| GRH – gonadotrophin releasing hormone | PCA – principal component analysis |
| H – histone | PcG – polycomb group |
| HAT – histone acetyltransferase | PHD – plant homeodomain |
| HBSS – Hank's buffered saline solution | |

PR – progesterone receptor

PRC – polycomb repressive complex

PWWP – proline-tryptophan-tryptophan-proline

R – arginine

RT – room temperature

RT-PCR – reverse transcription polymerase chain reaction

SAC – SET-associated cysteine-rich

SERD – selective estrogen receptor degrader

SERM – selective estrogen receptor modulator

SET – Suppressor of variegation 3-9, Enhancer of zeste and Trithorax

-seq – high throughput sequencing

shRNA – short hairpin RNA

TAD – transcription activating domain

TBST – tris-buffered saline + Tween 20

TCGA – the cancer genome atlas

TNBC – triple negative breast cancer

trxG – trithorax group

WAR – WDR5-ASH2L-RbBP5 sub-complex

WRAD – WDR5-RbBP5-ASH2L-DPY-30 sub-complex

WHSC1L1 – Wolf-Hirschhorn Syndrome Candidate 1-Like 1

ABSTRACT

Breast cancer is a highly heterogeneous disease classified clinically by expression of estrogen receptor alpha ER α , progesterone receptor, and human epidermal growth factor receptor. Molecular expression profiling identified a luminal breast cancer sub-type that can be sub-divided into luminal A and B. Compared to luminal A, luminal B tumors have increased proliferation, poor prognosis, endocrine therapy resistance, and complex genomes, including amplification of the 8p11-p12 genomic region. This amplicon occurs in 15% of primary breast tumors, correlates with poor prognosis and tamoxifen resistance, and harbors several oncogenes. Two of these oncogenes, ASH2L and NSD3 (WHSC1L1), promote transcription via epigenetic modification of histone proteins. NSD3 has a long isoform that is associated with di-methylation of lysine 36 on histone 3 (H3K36me2) and a short isoform that lacks a catalytic SET domain but retains the ability to interact with chromatin. ASH2L also lacks a catalytic SET domain yet is tightly and specifically linked to tri-methylation of lysine 4 on histone 3 (H3K4me3) in gene promoters. In this study, we tested the hypothesis that ASH2L and NSD3 cooperate to regulate expression of a suite of genes important in breast cancer, including ESR1, which encodes ER α . We discovered that NSD3-short is the major oncogenic isoform of NSD3 and its amplification and overexpression leads to overexpression and estrogen-independent activation of ER α . We also demonstrated that knockdown of ASH2L reduces H3K4me3 specifically in promoters of genes important to cell cycle progression. ASH2L also regulates promoter H3K4me3 at NSD3 and expression of both NSD3 and ER α . Knockdown of ASH2L reduced sensitivity to the cell cycle inhibitor palbociclib in the 8p11-p12 amplicon-bearing SUM-44 cell line. Together, the data presented here identify a role for ASH2L and NSD3 in cooperative regulation of genes important to cell

cycle regulation, including ESR1, and demonstrate that ER α is active in an estrogen-independent manner in the context of overexpression of these oncogenes. We have discovered a novel mechanism of endocrine resistance in luminal B breast cancers and provided evidence for the 8p11-p12 amplicon as a biomarker of patients who will respond to cell cycle inhibitors and epigenetic therapies against histone methyltransferase enzymes.

CHAPTER 1: Introduction and Review of Literature

1.1. Breast Cancer Classification and Treatment

a. Breast cancer history, classification, and estrogen receptor alpha (ER α)

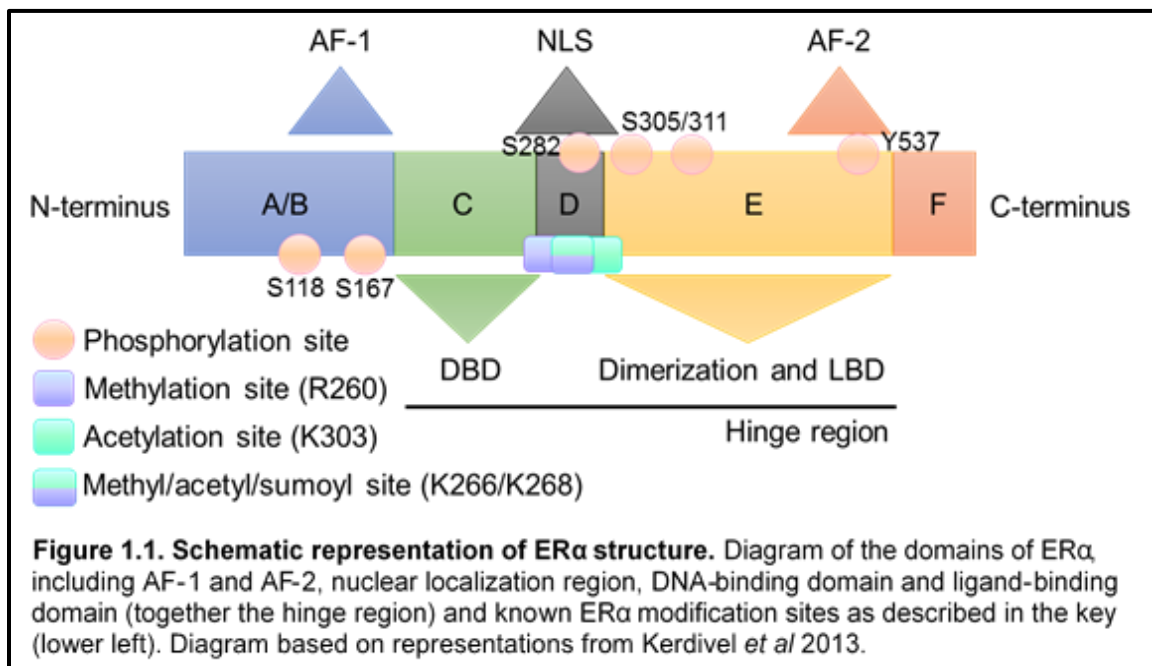
Breast cancer is the most common cancer in women worldwide and accounts for more than 40,000 deaths in the United States annually (Morris and Carey 2007, Chang 2012). As early as 1896, oophorectomy was described by Beatson as providing benefit to patients with advanced breast cancer (Cadoo *et al.* 2013, Mancuso and Massarweh 2016, Tabarestani *et al.* 2016), although the mechanism, now known to be estrogen deprivation, would not be understood until the discovery of estrogen receptor alpha (ER α) by Elwood Jensen *et al.* in 1958 (Hartman *et al.* 2009, Pritchard 2013). With this discovery, the importance of estrogen signaling in mammary gland ductal development and breast cancer genesis and progression was identified and became the focus of targeted therapies in breast cancer treatment.

Currently, breast cancer is diagnosed and treated based on clinicopathologic analysis (Geyer *et al.* 2012, Cadoo *et al.* 2013, Netanelly *et al.* 2016). Tumors are assessed by immunohistochemistry (IHC) for estrogen receptor (ER), progesterone receptor (PR), and human epidermal growth factor receptor 2 (HER2) (Cui *et al.* 2005, Reis-Filho and Pusztai 2011, Eroles *et al.* 2012). Tumors negative for all three markers are known as triple negative breast cancers (TNBC), are treated primarily with chemotherapy, and have the worst prognosis (Sorlie *et al.* 2001, Eroles *et al.* 2012, Cobain and Hayes 2015). HER2-amplified tumors are treated with chemotherapy and targeted HER2 antibody therapies (Yang *et al.* 2009, Cobain and Hayes 2015). Tumors expressing ER usually also express PR as its expression is under ER regulation, with

loss of PR acting as a marker of poorer prognosis (Margueron *et al.* 2004, Cui *et al.* 2005, Cornen *et al.* 2014). Tumors expressing both ER and PR are termed “hormone receptor-positive” and make up the majority of breast cancer cases (Scott *et al.* 2011, Geyer *et al.* 2012). Approximately 70-80% of breast cancers express ER α (ER+ breast cancer) and have the best prognosis due to the less aggressive nature of the tumors and availability of therapies targeting ER α function (Schiff *et al.* 2003, Cui *et al.* 2005, Howell 2006, Robertson 2007, Thomas and Munster 2009, Pathiraja *et al.* 2010, 2012, Chang 2012, Geyer *et al.* 2012, Cadoo *et al.* 2013, Ignatiadis and Sotiriou 2013, Kerdivel *et al.* 2013, Dabydeen and Furth 2014, Lumachi *et al.* 2015, Nagaraj and Ma 2015, Wang and Yin 2015, De Marchi *et al.* 2016, Selli *et al.* 2016).

ER α is encoded by the ESR1 gene and is a transcription factor that responds to estrogens, most predominantly 17 β -estradiol (Hartman *et al.* 2009, Pathiraja *et al.* 2010, Chang 2012). ER α is comprised of two transcriptional activating domains, AF-1 and AF-2, which flank a central hinge region that includes the ligand-binding and DNA-binding domains (Figure 1.1) (Cui *et al.* 2005, Nicholson and Johnston 2005, Hartman *et al.* 2009, Kerdivel *et al.* 2013, Wang and Yin 2015, Angus *et al.* 2016). AF-1 is ligand-independent and is activated by phosphorylation and other post-translational modification events while AF-2 is ligand-dependent (Cui *et al.* 2005, Dowsett *et al.* 2005, Nicholson and Johnston 2005, Hartman *et al.* 2009, Thomas and Munster 2009, Chang 2012, Kerdivel *et al.* 2013, Zhang *et al.* 2013, Nagaraj and Ma 2015, Wang and Yin 2015, De Marchi *et al.* 2016, Steelman *et al.* 2016, Tabarestani *et al.* 2016). Binding of estradiol at the ligand-binding domain stimulates dimerization and binding to chromatin, recruitment of co-regulatory molecules, and gene transcription (Cui *et al.* 2005, Nicholson and Johnston 2005, Howell 2006, Thomas and Munster 2009, Fedele *et al.*

2012, Kerdivel *et al.* 2013, Zhang *et al.* 2013, Nagaraj and Ma 2015, Wang and Yin 2015, De Marchi *et al.* 2016, Steelman *et al.* 2016, Tabarestani *et al.* 2016). The resulting effect on gene expression is highly cell- and tissue-type specific and is regulated by ligand type, post-translational modifications to ER α , other transcription factors, the balance of ER α co-activator versus co-repressor components available, the epigenetic state of the chromatin, growth factor signaling pathways, and many other factors (Schiff *et al.* 2003, Margueron *et al.* 2004, Cui *et al.* 2005, Kristensen *et al.* 2005, Nicholson and Johnston 2005, Thomas and Munster 2009, Pathiraja *et al.* 2010, Chang 2012, Fedele *et al.* 2012, Hervouet *et al.* 2013, Kerdivel *et al.* 2013, Zhang *et al.* 2013, Nagaraj and Ma 2015, Wang and Yin 2015, De Marchi *et al.* 2016). Transcript variants of ER α with non-genomic functions, such as cross-talk with growth factor receptor signaling pathways, have also been well-described in the literature but are beyond the scope of this review (Howell 2006, Chang 2012, Fedele *et al.* 2012, Kerdivel *et al.* 2013, Zhang *et al.* 2013, Wang and Yin 2015, Steelman *et al.* 2016). Generally, estrogens exert



mitogenic effects via ER α -mediated transcriptional activation of genes involved in cell cycle and other cellular growth processes (Sorlie *et al.* 2001, Allred *et al.* 2004, Kerdivel *et al.* 2013, Wang and Yin 2015).

b. Treatment of ER+ breast cancer

The selective estrogen receptor modulator (SERM) tamoxifen was introduced in the 1970s and has since been the most widely used endocrine therapy in advanced breast cancer (Morris and Wakeling 2002, Margueron *et al.* 2004, McKeage *et al.* 2004, Hartman *et al.* 2009, Huang *et al.* 2011, Chang 2012, Lumachi *et al.* 2015, Nagaraj and Ma 2015, De Marchi *et al.* 2016, Selli *et al.* 2016). The introduction of tamoxifen saw a reduction in breast cancer recurrence by 39% and mortality by 30% (Nagaraj and Ma 2015). Tamoxifen binds to ER α at the ligand-binding domain and prevents signaling through the ligand-dependent AF-2 domain but is unable to block the AF-1 domain, which is activated through phosphorylation in a ligand-independent manner (McKeage *et al.* 2004, Dowsett *et al.* 2005, Howell 2006, Hartman *et al.* 2009, Chang 2012). As a result, tamoxifen exerts both antagonist and agonist effects on ER α (Morris and Wakeling 2002, Schiff *et al.* 2003, Allred *et al.* 2004, Margueron *et al.* 2004, Dowsett *et al.* 2005, Nicholson and Johnston 2005, Hartman *et al.* 2009, Chang 2012, Dabydeen and Furth 2014, Lumachi *et al.* 2015, De Marchi *et al.* 2016, Selli *et al.* 2016).

The benefit of tamoxifen use in breast cancer is centered upon its role as an ER α antagonist in breast tissue. The active metabolite of tamoxifen, 4-hydroxytamoxifen (4OH-tamoxifen), binds ER α with 25% of the affinity of 17 β -estradiol and induces a conformational change to prevent recruitment of co-activators and instead favoring co-repressor recruitment, thereby blocking ER α -mediated transcription of proliferative

genes (Morris and Wakeling 2002, Margueron *et al.* 2004, Cui *et al.* 2005, Dowsett *et al.* 2005, Howell 2006, Chang 2012, De Marchi *et al.* 2016). Tamoxifen functions as an ER α agonist in bone to maintain bone density and blood to reduce serum cholesterol, positive effects for patients, but also in liver and uterus, increasing the risk of developing endometrial cancer with prolonged use (Morris and Wakeling 2002, Nicholson and Johnston 2005, Howell 2006, Hartman *et al.* 2009, De Marchi *et al.* 2016). Many adverse effects of tamoxifen are due to its agonist activity, including gastrointestinal disturbances (e.g. nausea, vomiting), hot flushes, joint pain, and headaches (McKeage *et al.* 2004, Howell 2006). The recommended duration of tamoxifen use is at least 5 years after diagnosis and initial treatment and these adverse effects are the primary cause of non-compliance during adjuvant therapy (Chanrion *et al.* 2008, Scott *et al.* 2011, Chang 2012, Ignatiadis and Sotiriou 2013, Lumachi *et al.* 2015, Nagaraj and Ma 2015).

Due in part to the agonist properties of tamoxifen, recurrence while on therapy occurs (Nicholson and Johnston 2005, Robertson 2007, Huang *et al.* 2011, Bilal *et al.* 2012, Chang 2012, Cadoo *et al.* 2013, Ignatiadis and Sotiriou 2013, Kerdivel *et al.* 2013, Nagaraj and Ma 2015, Kumler *et al.* 2016, Lim *et al.* 2016, Mancuso and Massarweh 2016, Selli *et al.* 2016, Tabarestani *et al.* 2016). As such, additional non-steroidal agents similar to tamoxifen have been developed, such as toremifene, idoxifene, and droloxifene, but none have treatment advantages over tamoxifen (Morris and Wakeling 2002). To circumvent tamoxifen resistance, another class of anti-estrogen therapies was developed to abrogate estrogen-mediated activation of transcription via ER α through a reduction in circulating estrogen levels (Morris and Wakeling 2002, Nicholson and Johnston 2005, Kerdivel *et al.* 2013, Robertson *et al.* 2014, Lumachi *et al.* 2015).

Estrogens are derived from androgens by the enzyme aromatase in peripheral tissues,

especially adipose tissue in postmenopausal women, as well as within the tumor in the context of breast cancer (Morris and Wakeling 2002, Nicholson and Johnston 2005, Pritchard 2013, Dabydeen and Furth 2014, Lumachi *et al.* 2015, Nagaraj and Ma 2015, Selli *et al.* 2016). First-generation aromatase inhibitors (AIs) did not demonstrate therapeutic benefit over tamoxifen, but the third-generation non-steroidal AIs anastrozole and letrozole and steroidal exemestane surpassed tamoxifen as first-line therapy for ER+ breast cancer in postmenopausal women (Morris and Wakeling 2002, Cui *et al.* 2005, Nicholson and Johnston 2005, Ariazi *et al.* 2006, Howell 2006, Robertson 2007, Hartman *et al.* 2009, Robertson *et al.* 2014). AIs increase gonadotropin releasing hormone (GRH) in premenopausal patients, which results in increased estrogen levels, therefore these compounds are under investigation in conjunction with GRH-inhibitors to extend their use to this patient population (Tabarestani *et al.* 2016). The introduction of AIs as treatment alternatives, both as first-line therapies and for patients who failed to respond to tamoxifen, was a major step forward in breast cancer management.

Aromatase inhibitors have shown improvement in patient survival and lack the increased risk of endometrial cancer of tamoxifen (Chang 2012). AIs have similar adverse effects otherwise, including disease recurrence despite initial response (Fedele *et al.* 2012, Ignatiadis and Sotiriou 2013, Nagaraj and Ma 2015, Mancuso and Massarweh 2016). More recently, pure ER α antagonists were developed, known as selective estrogen receptor degraders (SERDs), such as fulvestrant (ICI-182,780) (Dowsett *et al.* 2005, Howell 2006, Johnston and Cheung 2010). Fulvestrant binds to ER α at the ligand-binding domain with 89% the affinity of 17 β -estradiol, inducing a different conformational change than tamoxifen that results in inhibition of dimerization, blocking both the AF-1 and AF-2 domains from participating in transcription (Morris and

Wakeling 2002, McKeage *et al.* 2004, Dowsett *et al.* 2005, Nicholson and Johnston 2005, Howell 2006, Scott *et al.* 2011, Lumachi *et al.* 2015). This results in complete abrogation of transcription of ER α -target genes and destabilization of ER α , prompting degradation by the ubiquitin-proteasome complex (Morris and Wakeling 2002, Margueron *et al.* 2004, McKeage *et al.* 2004, Dowsett *et al.* 2005, Johnston and Cheung 2010, Scott *et al.* 2011). Clinical trials revealed that fulvestrant is at least as effective as anastrozole and was thus approved in 2002 for the treatment of hormone receptor-positive metastatic breast cancer that had failed other endocrine therapies (Dowsett *et al.* 2005). In 2010, fulvestrant was approved as a second-line therapy for postmenopausal patients with hormone receptor-positive breast cancer (Scott *et al.* 2011, Ignatiadis and Sotiriou 2013).

Due to the different mechanism of action of SERDs, cross-resistance to tamoxifen and anastrozole is rare (McKeage *et al.* 2004, Dowsett *et al.* 2005, Johnston *et al.* 2005, Howell 2006, Johnston and Cheung 2010, De Marchi *et al.* 2016). Adverse effects of fulvestrant are similar to the other endocrine therapies and slightly less common, with gastrointestinal disturbances and joint pain being most cited (McKeage *et al.* 2004, Howell 2006, Scott *et al.* 2011, Lumachi *et al.* 2015). Clinical trials focused on optimal dosing of fulvestrant, however, revealed the dose-dependent nature of this drug for reducing ER α levels (Robertson 2007, Scott *et al.* 2011, Robertson *et al.* 2014, Nagaraj and Ma 2015). The ability to achieve steady-state levels adequate for complete inhibition of ER α in patients, especially those with highly ER-positive tumors, without reaching the limits of adverse effects is difficult (Robertson 2007). This therapy is also given via intramuscular injection as opposed to orally, affecting patient compliance (McKeage *et al.* 2004). A second generation of SERD therapies are under development

and testing to attempt to combat these issues (Angus *et al.* 2016, Mancuso and Massarweh 2016).

Unfortunately, resistance to endocrine therapy of all types is common (Allred *et al.* 2004, Kerdivel *et al.* 2013, Pritchard 2013, Nagaraj and Ma 2015). Absence of ER α is a very good negative predictor of response to endocrine therapy and its expression is an accurate positive predictor of response in approximately 50% of ER+ breast cancers (Lonning *et al.* 2005, Thomas and Munster 2009, Shiu *et al.* 2010, Cobain and Hayes 2015, Wang and Yin 2015, Azim *et al.* 2016). Since half of ER+ breast cancer patients do not demonstrate durable response to endocrine therapy, there is a pressing need to discover novel biomarkers that will complement ER α in predicting endocrine therapy response (Chanrion *et al.* 2008, Thomas and Munster 2009, Reis-Filho and Pusztai 2011, Geyer *et al.* 2012, Habashy *et al.* 2012, Cobain and Hayes 2015, Mancuso and Massarweh 2016, Selli *et al.* 2016, Rakha and Green 2017). Similarly, many groups are investigating parallel processes, such as activation of the PI3K/AKT/mTOR pathway and the cyclin D1/CDK4/6-mediated cell cycle pathway, to determine if coupling endocrine therapy with inhibitors of these pathways will improve patient outcomes (Caldon *et al.* 2012, Ignatiadis and Sotiriou 2013, Dabydeen and Furth 2014, Lumachi *et al.* 2015, Nagaraj and Ma 2015, Azim *et al.* 2016, Knudsen and Witkiewicz 2016, Kumler *et al.* 2016, Lim *et al.* 2016, Mancuso and Massarweh 2016, Steelman *et al.* 2016). Indeed, these inhibitors have shown promising results in subsets of breast cancer patients in combination with endocrine therapy (Cornen *et al.* 2014, Nagaraj and Ma 2015, Azim *et al.* 2016, Knudsen and Witkiewicz 2016, Mancuso and Massarweh 2016, Steelman *et al.* 2016). Some of the mechanisms of endocrine therapy resistance are known, such as loss of ER α expression, ESR1 amplifications, point mutations in the ligand binding

domain of ER α , and aberrant activation of growth factor signaling pathways, but these alterations do not account for all patients with poor response to endocrine therapies (Cui *et al.* 2005, Loi *et al.* 2009, Pathiraja *et al.* 2010, Chang 2012, Fedele *et al.* 2012, Kerdivel *et al.* 2013, De Marchi *et al.* 2016, Selli *et al.* 2016, Tabarestani *et al.* 2016). More research is necessary to determine additional mechanisms behind endocrine therapy resistance in order to identify biomarkers for which patients will require combinatorial treatment strategies and to identify potential targets for novel therapies.

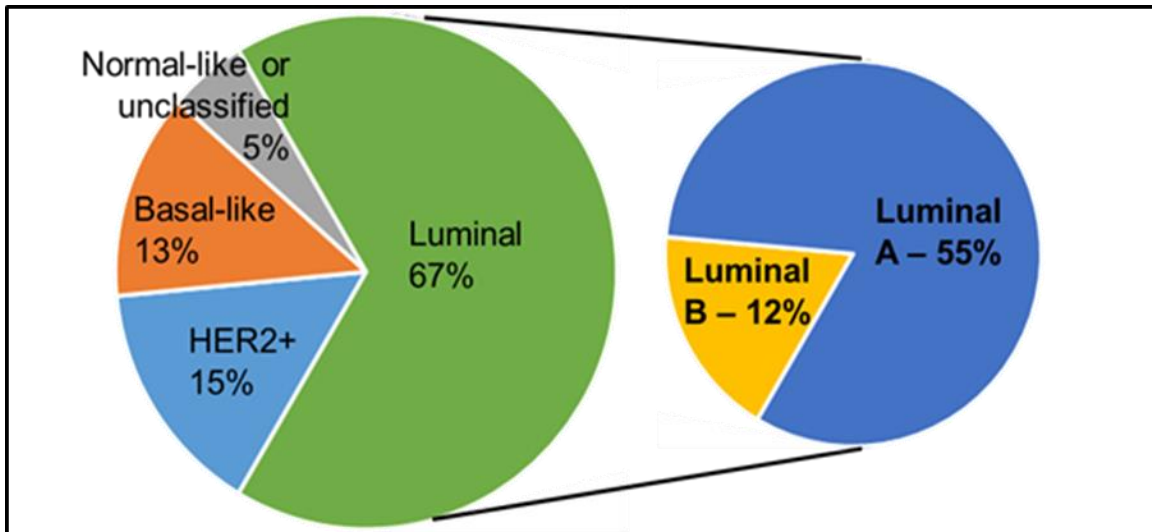
Breast cancer has long been described as a highly heterogenous disease (Carey *et al.* 2006, Morris and Carey 2007, Elsheikh *et al.* 2009, Kao *et al.* 2009, Ellis *et al.* 2012, Cadoo *et al.* 2013, Dabydeen and Furth 2014, Cobain and Hayes 2015, Selli *et al.* 2016). The current clinical and histopathologic parameters used to classify breast cancers are insufficient to capture this diversity and predict treatment response (Sorlie *et al.* 2001, Sorlie *et al.* 2003, Kao *et al.* 2009, Habashy *et al.* 2012, Tang and Tse 2016). With expansion of global-scale profiling techniques such as microarrays, next generation sequencing, and many others, there has been a paradigm shift toward breast cancer classification based on molecular expression profiling.

c. Molecular profiling of breast cancers

In 2000, Perou *et al.* identified two main types of breast cancer that correlate to ER α status of the tumors: those that express genes known to be associated with basal cells and those with a more luminal cell-like expression profile (Perou *et al.* 2000). Many groups since have advocated that the delineation of these two cancer types is so robust that they should be treated as different diseases and given their own cancer classes in large databases such as the cancer genome atlas (TCGA) (Sorlie *et al.* 2001, Reis-Filho

and Pusztai 2011, Geyer *et al.* 2012, Habashy *et al.* 2012). The basal tumors then subdivide into basal-like, normal-like, and HER2+ subtypes while the luminal group divides into luminal A and luminal B (Figure 1.2) (Sorlie *et al.* 2001). Even within the basal and luminal groups, a high degree of heterogeneity remains (Sorlie *et al.* 2001, Morris and Carey 2007, Shiu *et al.* 2010, Geyer *et al.* 2012, Ignatiadis and Sotiriou 2013, Cornen *et al.* 2014). Indeed, the luminal group, which are primarily ER+ and express ER-associated genes such as ESR1, XBP1, CCND1, and GATA3 (Perou *et al.* 2000, Sorlie *et al.* 2001, Sotiriou *et al.* 2003, 2012, Habashy *et al.* 2012, Shan *et al.* 2014, Tang and Tse 2016), has been a topic of controversy in the field. Some advocate for the existence of three subtypes, luminal A, B, and C, while others have focused on identifying clinically-useful markers to separate luminal A tumors from luminal B, and others still have argued that this tumor type actually comprises a continuum rather than individual and separable subtypes of breast cancer (Shiu *et al.* 2010, Geyer *et al.* 2012, Netanelly *et al.* 2016, Tang and Tse 2016). The St Gallen International Consensus on the Primary Therapy of Early Breast Cancer 2013 separated this group of tumors into luminal A, luminal B HER2-, and luminal B HER2+ (Judes *et al.* 2016).

Regardless of the specific breakdown, it is generally accepted that luminal A tumors differ from luminal B tumors in many characteristics (Figure 1.2). Luminal A tumors are the most common type of all breast cancers (approximately 55%) and have the highest ER α and ER α -target gene expression, including PR, low expression of genes associated with proliferation, no HER2 amplifications, low rates of GATA3 mutations, simple karyotypes, and higher rates of PIK3CA mutations than luminal B tumors (Raica *et al.* 2009, Shiu *et al.* 2010, Geyer *et al.* 2012, Ignatiadis and Sotiriou 2013, Tang and Tse 2016). These tumors tend to be well-differentiated and include all cases of lobular



| Characteristic | Luminal B | Luminal A |
|--|--|---------------------------------|
| Incidence | 12% | 55% |
| ER α expression | lower | high |
| ER α negativity | up to 6% | up to 15% |
| ER α target genes | lower | high |
| PR | +/- | + |
| Proposed PR IHC % cutoff | <20 | >20 |
| HER2 amplification | 30% | <10% |
| Proliferation-associated gene expression | higher | low |
| Proposed Ki-67 % cutoff | >14 | <14 |
| Histology | lobular/ductal and less differentiated | lobular and well-differentiated |
| Aggressiveness | higher | low |
| GATA3 mutation rate | higher | low |
| PIK3CA mutation rate | 32% | 45% |
| TP53 mutation rate | 32% | 13% |
| karyotypes | complex | simple |
| endocrine therapy response rate | lower | high |
| chemotherapy response rate | intermediate | poor |
| prognosis | intermediate | good |

Figure 1.2. Breast cancer intrinsic subtype proportions and characteristics of luminal tumors. Pie chart depicting the approximate percentage of all breast cancers accounted for by each molecular subtype. Together, the luminal subtype makes up approximately 67% with luminal A and B accounting for approximately 55% and 12% of total breast cancers, respectively. Corresponding table describes selected characteristics of luminal A and luminal B tumors.

carcinoma *in situ* as well as most cases of invasive lobular carcinoma and multiple other histologic subtypes (Shiu *et al.* 2010, Eroles *et al.* 2012, Dabydeen and Furth 2014). Luminal A tumors tend to be highly responsive to endocrine therapies and have significantly better prognosis and relapse rates than luminal B tumors, which comprise approximately 12% of all breast cancers and have overall lower expression of ER α and associated genes (Raica *et al.* 2009, Turner *et al.* 2010, Tang and Tse 2016). Up to 6% of luminal B tumors are classified as ER-negative (Eroles *et al.* 2012). These tumors have higher expression of proliferation-associated genes, including MKI67, CCNB1, and MYBL2, and indeed these genes are often cited as the major distinction between luminal A and B tumors (Cheang *et al.* 2009, Sircoulomb *et al.* 2011, Eroles *et al.* 2012, Ades *et al.* 2014). The luminal B subtype also tends to be more aggressive, higher grade, less differentiated, primarily invasive ductal carcinoma of multiple histologic types, usually HER2-negative (although half of HER2+ tumors fall under this category), and less commonly PR+ than luminal A (Raica *et al.* 2009, Eroles *et al.* 2012, Ignatiadis and Sotiriou 2013, Tang and Tse 2016). Complex karyotypes with multiple copy number aberrations are common with a lower PIK3CA (32% vs 45%) but higher TP53 (32% vs 13%) mutation rate and more frequent gain of MDM2 and cyclin D1 (Geyer *et al.* 2012, Ades *et al.* 2014, Tang and Tse 2016). Luminal B tumors also tend to have poorer response to endocrine therapy than their luminal A counterpart (Turner *et al.* 2010, Tang and Tse 2016). Although luminal B tumors do respond better to chemotherapy than luminal A, response is still much poorer than the other breast cancer subtypes, leaving few good therapeutic options for these patients (Sircoulomb *et al.* 2011, Eroles *et al.* 2012, Cadoo *et al.* 2013, Ignatiadis and Sotiriou 2013, Kerdivel *et al.* 2013).

Defining molecular subtypes has major implications for identifying and developing novel therapeutic strategies for breast cancer management, therefore a means by which luminal A and luminal B tumors can be clinically differentiated, both from the other intrinsic subtypes as well as from each other, is essential for improving therapeutic interventions (Miller *et al.* 2009, Cornen *et al.* 2014, Tang and Tse 2016, Rakha and Green 2017). Several attempts have been made to identify a genetic signature based on the initial intrinsic gene sets that would function as a prognostic and predictive clinical assay (van 't Veer *et al.* 2002, Morris and Carey 2007, Chanrion *et al.* 2008, Cheang *et al.* 2009, Geyer *et al.* 2012, Ignatiadis and Sotiriou 2013, Luo *et al.* 2017). Though there is moderate clinical utility, these attempts have largely been unable to capture the biologic complexity and accurately predict tumor classification (Sorlie *et al.* 2006, Reis-Filho and Pusztai 2011, Geyer *et al.* 2012, Ignatiadis and Sotiriou 2013, Selli *et al.* 2016, Tang and Tse 2016). The exception has been Oncotype DX, an RT-PCR-based test that predicts benefit of chemotherapy and risk of distant recurrence and has demonstrated usefulness in predicting patients who will derive minimal benefit from chemotherapy (Morris and Carey 2007, Reis-Filho and Pusztai 2011, Bilal *et al.* 2012, Geyer *et al.* 2012, Cobain and Hayes 2015).

Clinicopathologic markers in addition to ER, PR, and HER2 have also been proposed to distinguish the intrinsic subtypes. The addition of IHC assessment of basal cytokeratin expression, such as CK5, has improved the identification of luminal- versus basal-type tumors (Raica *et al.* 2009, Eroles *et al.* 2012, Tang and Tse 2016). The two major proteins proposed to differentiate luminal A and B by IHC are PR and Ki-67, which is a marker of proliferation. Cutoffs of 20% for PR and 14% for Ki-67 have been endorsed by the 2011 St. Gallen International Breast Cancer Conference, with luminal A

tumors having higher PR expression and luminal B having higher Ki-67 (Eroles *et al.* 2012, Geyer *et al.* 2012, Ignatiadis and Sotiriou 2013, Ades *et al.* 2014, Tang and Tse 2016). Due to the lack of true bimodal distribution of these subtypes, these cutoffs are subjective, arbitrary, and vary widely based on tumor heterogeneity, even within one tumor biopsy (Geyer *et al.* 2012, Tang and Tse 2016). Additionally, lack of standardization of these tests poses another complicating factor in using IHC to define tumor subtypes (Eroles *et al.* 2012, Geyer *et al.* 2012). Indeed, even IHC assessment of ER α expression is highly variable and subjective. ER+ tumors are defined by at least 1% of the cells staining positive for nuclear ER α and are treated with endocrine therapy, despite studies demonstrating that tumors with 1-10% ER α staining behave much more like basal tumors (Allred *et al.* 2004, Dabydeen and Furth 2014, Lumachi *et al.* 2015, Tang and Tse 2016). Identification of reliable biomarkers that can encompass the vast heterogeneity of breast cancers is essential to moving this field forward and improving patient outcomes.

1.2. Breast Cancer Genomics

a. Genomic alterations in luminal B breast cancer

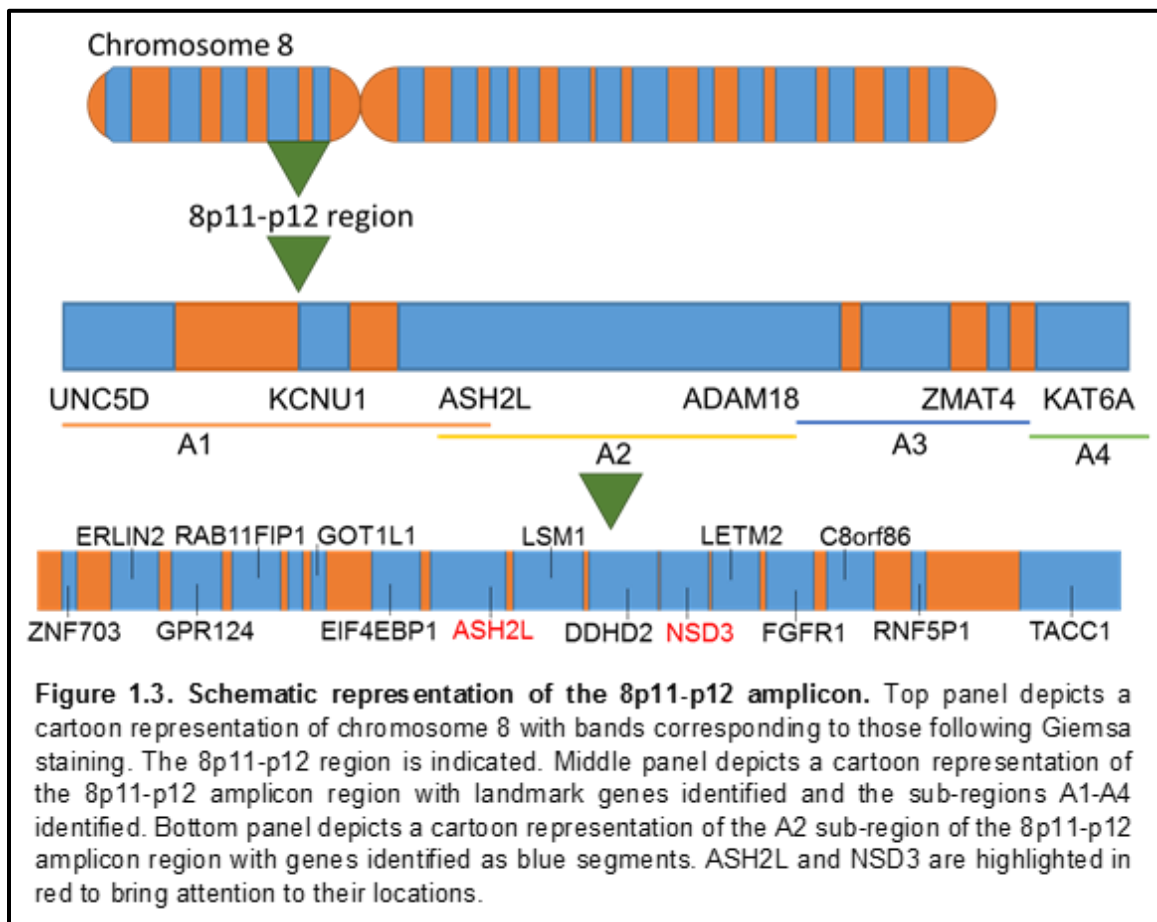
Although breast cancer classification by molecular profiling is complicated, evolving, and not yet ready for full clinical use, some of the information obtained from these studies can be immediately utilized to inform clinical trial design and spark novel scientific studies that will improve understanding of breast cancer pathogenesis and lead to identification of potential therapeutic targets. One of the major differences between luminal A and B breast cancer subtypes, other than the difference in expression of genes associated with proliferation, is the genomic instability associated with luminal B

tumors (Kristensen *et al.* 2005, Geyer *et al.* 2012, Cornen *et al.* 2014). As previously mentioned, luminal A tumors tend to have relatively simple karyotypes (Kao *et al.* 2009, Geyer *et al.* 2012). They are often diploid with infrequent translocations and copy number alterations (CNAs), although low-level gains of 1q and 16p and deletions of 16q are not uncommon, especially as the tumors become higher grade and ER α and proliferation gene expression patterns move more toward the luminal B profile (Bergamaschi *et al.* 2006, Shiu *et al.* 2010, Geyer *et al.* 2012, Reynisdottir *et al.* 2013, Ades *et al.* 2014, Cornen *et al.* 2014). This tendency again highlights the continuum pattern rather than bimodal distribution of these two luminal breast cancer subtypes.

Three major genomic phenotypes have been described in breast cancer (Shiu *et al.* 2010). In contrast to the “simplex” phenotype of luminal A, luminal B tumors have much greater genomic instability and frequency of high-level CNAs and aneuploidy (Shiu *et al.* 2010, Cornen *et al.* 2014). These tumors fall into a “firestorm” or “amplifier” pattern characterized by multiple recurrent amplifications (Shiu *et al.* 2010, Sircoulomb *et al.* 2011). The third breast cancer genomic phenotype is termed “sawtooth” or “complex” pattern, which demonstrates alternating low-level gains and deletions that affect multiple chromosomes in the same tumor type (Shiu *et al.* 2010). These three phenotypes are highly correlated with tumor grade (Shiu *et al.* 2010, Geyer *et al.* 2012, Habashy *et al.* 2012, Cornen *et al.* 2014). Luminal B tumors often have losses of Xp, 22q, 18p, 16q, 17q, 14q, 13q, 11q, 10q, 9p, 8p, 6q, 4p, and 1p and gains of 20q, 17q, 16p, 11q, 10p, 8q, and 1q (Garcia *et al.* 2005, Reis-Filho *et al.* 2006, Bernard-Pierrot *et al.* 2008, Haverty *et al.* 2008, Shiu *et al.* 2010, Sircoulomb *et al.* 2011, Geyer *et al.* 2012, Habashy *et al.* 2012).

In addition to large areas of chromosomal gains and losses, luminal B tumors often have more focal CNAs (Yang *et al.* 2006, Sircoulomb *et al.* 2011, Geyer *et al.* 2012, Ades *et al.* 2014, Cornen *et al.* 2014). High level amplification of specific genomic regions known as amplicons is a common mechanism of overexpression of the oncogenes found in that location (Ray *et al.* 2004, Bergamaschi *et al.* 2006, Ellis *et al.* 2007, Shiu *et al.* 2010, Yang *et al.* 2010, Bilal *et al.* 2012). Since amplicons frequently harbor multiple candidate oncogenes, identifying the “drivers” from the “passengers” is key to elucidating drug targets (Garcia *et al.* 2005, Haverty *et al.* 2008, Shiu *et al.* 2010, Mahmood *et al.* 2013, Chen *et al.* 2014, Irish *et al.* 2016). For example, amplification of 17q12 is well-known to induce overexpression of the HER2 oncogene and is associated with poor endocrine response and outcome (Still *et al.* 1999, Sorlie *et al.* 2001, Yang *et al.* 2004, Bilal *et al.* 2012). As HER2 is a driving oncogene, targeted therapies such as trastuzumab, a monoclonal antibody directed toward HER2, has been a highly successful intervention (Yang *et al.* 2010). Similarly, other amplicons are known to harbor driver oncogenes. C-MYC is found on the 8q24 amplicon (Still *et al.* 1999, Ray *et al.* 2004, Yang *et al.* 2004, Yang *et al.* 2006, Bernard-Pierrot *et al.* 2008, Yang *et al.* 2010). The 11q12-q14 amplicon, which harbors CCND1, an ER α -target gene associated with cell cycle progression, is found in up to 30% of breast cancers and is commonly associated with endocrine resistance and poorer outcome in ER+ tumors (Still *et al.* 1999, Ray *et al.* 2004, Yang *et al.* 2004, Yang *et al.* 2006, Bernard-Pierrot *et al.* 2008, Kwek *et al.* 2009, Shiu *et al.* 2010, Yang *et al.* 2010, Sircoulomb *et al.* 2011, Bilal *et al.* 2012, Ignatiadis and Sotiriou 2013, Lim *et al.* 2016). Despite frequent losses of 8p in luminal B breast cancers, a small region near the centromere is commonly amplified, known as the 8p11-p12 amplicon (Figure 1.3) (Ray *et al.* 2004, Garcia *et al.* 2005, Gelsi-

Boyer *et al.* 2005, Cooke *et al.* 2008, Shiu *et al.* 2010, Turner *et al.* 2010, Sircoulomb *et al.* 2011, Geyer *et al.* 2012, Ades *et al.* 2014, Cornen *et al.* 2014). This amplicon is fairly prevalent, found in 15% of all breast cancers but up to 32% of luminal B breast cancers, and is associated with worse outcome in these cancers (Ray *et al.* 2004, Yang *et al.* 2004, Gelsi-Boyer *et al.* 2005, Shiu *et al.* 2010, Sircoulomb *et al.* 2011, Reynisdottir *et al.* 2013, Zhang *et al.* 2013).

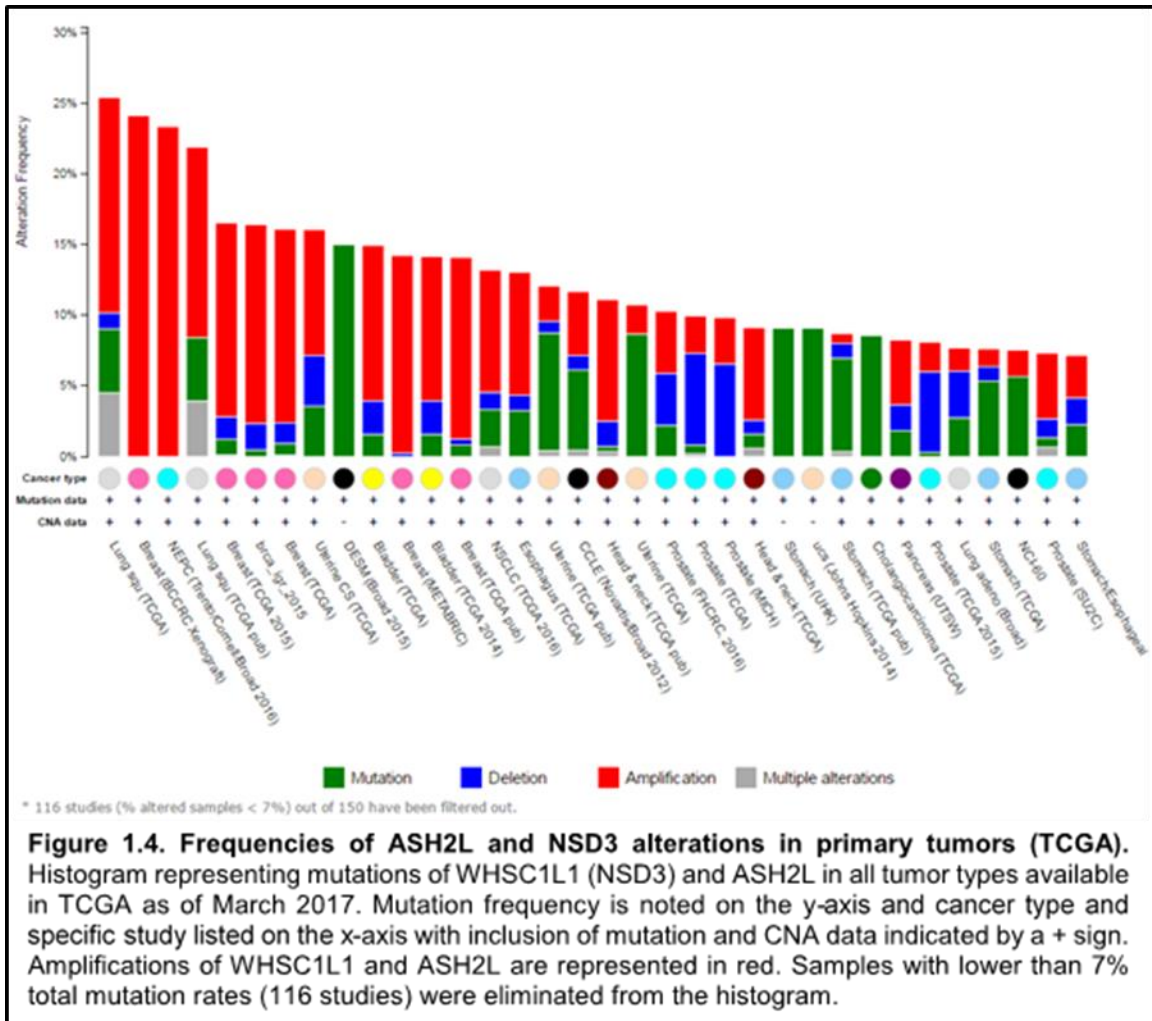


b. The 8p11-p12 amplicon and candidate oncogenes

Several groups have identified and validated oncogenes from the 8p11-p12 region and linked this amplicon to luminal B, ER+ tumors with poor metastasis-free survival, high histologic grade and Ki-67 proliferation indices, and resistance to

endocrine therapy (Ray *et al.* 2004, Garcia *et al.* 2005, Streicher *et al.* 2007, Bernard-Pierrot *et al.* 2008, Elsheikh *et al.* 2009, Shiu *et al.* 2010, Yang *et al.* 2010, Sircoulomb *et al.* 2011, Bilal *et al.* 2012, Geyer *et al.* 2012, Wu *et al.* 2012, Mahmood *et al.* 2013, Cornen *et al.* 2014). The 8p11-p12 amplicon ranges in size from 1 to 11 Mb but is most commonly approximately 5 Mb in length (Garcia *et al.* 2005, Yang *et al.* 2006, Melchor *et al.* 2007). Although there is variation in the specific start and end sites among tumors and cell lines that have been mapped, the NRG1 gene is the most common telomeric breakpoint site and usually includes loss of the remaining p arm of chromosome 8 (Ray *et al.* 2004, Garcia *et al.* 2005, Gelsi-Boyer *et al.* 2005, Melchor *et al.* 2007, Cooke *et al.* 2008), which harbors important tumor suppressor genes such as DLC1, SGCZ, and TUSC3 (Reis-Filho *et al.* 2006, Cooke *et al.* 2008). The amplicon has four sub-regions of amplification, named A1-A4 from telomere to centromere (Gelsi-Boyer *et al.* 2005, Melchor *et al.* 2007, Sircoulomb *et al.* 2011, Reynisdottir *et al.* 2013, Turner-Ivey *et al.* 2014), with up to 21 genes demonstrating coordinated amplification and overexpression in breast cancer, depending on the technique used, thereby identified as candidate oncogenes (Ray *et al.* 2004, Yang *et al.* 2004, Garcia *et al.* 2005, Yang *et al.* 2006, Bernard-Pierrot *et al.* 2008, Cooke *et al.* 2008, Kwek *et al.* 2009, Yang *et al.* 2010, Holland *et al.* 2011, Bilal *et al.* 2012, Cornen *et al.* 2014, Turner-Ivey *et al.* 2014, Irish *et al.* 2016). Additionally, this amplicon is not unique to breast cancer, but has also been implicated in lung, bladder, pancreatic, and ovarian cancers (Figure 1.4) (Bernard-Pierrot *et al.* 2008, Yang *et al.* 2010, Dutt *et al.* 2011, Mahmood *et al.* 2013, Luo *et al.* 2017).

Many amplicons are well-known to play major roles in breast tumorigenesis and amplification is a common mechanism of overexpression on oncogenes. For example, the 17q12 amplicon contains HER2 (ERBB2) and identification and characterization of



this oncogene has led to the development of targeted therapies, such as trastuzumab (Still *et al.* 1999, Sorlie *et al.* 2001, Yang *et al.* 2004, Yang *et al.* 2010, Bilal *et al.* 2012). This oncogene has been considered the only driving oncogene from the 17q12 locus, but more recent studies have identified other genes, once thought of as passengers, to have driving roles in a subset of breast cancers with this amplicon, including GRB7 and STARD3 (Sorlie *et al.* 2001, Ray *et al.* 2004, Bernard-Pierrot *et al.* 2008, Haverty *et al.* 2008, Mahmood *et al.* 2013). Similarly, the 8q24 amplicon is common in breast tumors and harbors C-MYC, a well-known breast cancer oncogene (Still *et al.* 1999, Ray *et al.* 2004, Yang *et al.* 2004, Yang *et al.* 2006, Bernard-Pierrot *et al.* 2008). The 11q12-q14

Chapter 1: Introduction Page | 20

amplicon, which contains CCND1, the gene encoding the cell cycle protein cyclin D1, has been shown in numerous studies to enhance breast cancer progression (Still *et al.* 1999, Ray *et al.* 2004, Yang *et al.* 2004, Yang *et al.* 2006, Bernard-Pierrot *et al.* 2008, Kwek *et al.* 2009, Shiu *et al.* 2010, Yang *et al.* 2010, Sircoulomb *et al.* 2011, Bilal *et al.* 2012, Ignatiadis and Sotiriou 2013, Lim *et al.* 2016). This amplicon also harbors CTTN (EMS1), GAB2, and other suspected oncogenes. Interestingly, the 11q12-q14 amplicon is commonly associated with the 8p11-p12 amplicon and cross-talk between these two genomic regions has been suggested, discussed in more detail below (Reis-Filho *et al.* 2006, Kwek *et al.* 2009, Sircoulomb *et al.* 2011, Bilal *et al.* 2012, Cornen *et al.* 2014).

Following discovery of the 8p11-p12 amplicon in breast cancer, several groups set out to map the region and identify the driver and passenger oncogenes (Still *et al.* 1999, Ray *et al.* 2004, Yang *et al.* 2004, Garcia *et al.* 2005, Gelsi-Boyer *et al.* 2005, Yang *et al.* 2006). Profiling of 8p11-p12 amplicon-bearing tumors and cell lines revealed incredible complexity and heterogeneity in this region, with multiple amplicon peaks observed (Yang *et al.* 2004, Reis-Filho *et al.* 2006, Melchor *et al.* 2007, Kwek *et al.* 2009, Wu *et al.* 2012, Luo *et al.* 2017). Several strong candidate oncogenes were identified based on commonality of amplification and coordinated overexpression, including: FGFR1, ZNF703, BRF2, RAB11FIP1, LSM1, PPAPDC1B, ASH2L, DDHD2, EIF4EBP1, KAT6A, TC-1, WHSC1L1, TACC1, ERLIN2, and PROSC (Ray *et al.* 2004, Garcia *et al.* 2005, Gelsi-Boyer *et al.* 2005, Yang *et al.* 2006, Bernard-Pierrot *et al.* 2008, Haverty *et al.* 2008, Elsheikh *et al.* 2009, Kwek *et al.* 2009, Yang *et al.* 2009, Reynisdottir *et al.* 2013, Zhang *et al.* 2013, Cornen *et al.* 2014). Indeed, many of these genes have been investigated further and their transforming properties validated. For example, TACC1 was implicated by Still *et al.* (1999) in cell transformation, anchorage-

independent growth, and proliferation. Similarly, LSM1 has been implicated by Streicher *et al.* (2007) as involved in grow-factor independent growth and soft agar colony-forming ability, both properties of transformed cells, when overexpressed in the non-transformed MCF10A breast cancer cell line. DDHD2 has also been implicated in regulating insulin-independent growth and disorganized acini formation in MCF10A cells grown in Matrigel when its overexpression is induced (Yang *et al.* 2010). PPAPDC1B was described by Bernard-Pierrot and colleagues as displaying transforming properties when overexpressed in a fibroblast cell line and having a negative regulatory effect on ER α while also promoting survival, proliferation, anchorage-independent growth in breast, lung, and pancreatic cancers (Bernard-Pierrot *et al.* 2008, Mahmood *et al.* 2013). This group also identified WHSC1L1, a histone methyltransferase, as a significant oncogene from the 8p11-p12 genomic region, but suggested it not to be the best avenue of investigation due to other oncogenes having greater potential as druggable targets (Bernard-Pierrot *et al.* 2008). They later pursued this gene further and cited its potential and importance as a drug target for epigenetic therapies, also mentioning ASH2L, another factor involved in histone methylation from the 8p11-p12 amplicon, as potentially interesting as well (Mahmood *et al.* 2013). These two oncogenes will be discussed in more detail in subsequent sections. Similarly, our group has also established KAT6A (MYST3), a histone acetyltransferase (HAT) discovered as an important gene via RNA-interference screening, to be essential for proliferation, colony formation, and anchorage-independent growth in the amplicon-bearing SUM-52 breast cancer cell line (Turner-Ivey *et al.* 2014). This study also identified several important cancer-related genes and biological pathways under control of this chromatin-modifying oncogene.

One hypothesis regarding amplicons is that the smallest area commonly amplified will contain the driving oncogene(s). To investigate this concept, a 1 Mb region in sub-region A1 was identified as the most conserved area of amplification (Garcia *et al.* 2005). Several groups identified five candidate oncogenes from this 1 Mb region based on coordinate amplification and overexpression: PROSC, ZNF703 (FLJ14299), ERLIN2 (C8orf2, SPFH2), BRF2, and RAB11FIP1 (ROC) (Garcia *et al.* 2005, Melchor *et al.* 2007, Haverty *et al.* 2008, Holland *et al.* 2011, Reynisdottir *et al.* 2013). Subsequent studies confirmed the transforming potential of several of these genes. ERLIN2 overexpression in the non-transformed MCF10A cell line resulted in cell proliferation in the absence of insulin and insulin-like growth factors, anchorage-independent growth, and highly proliferative colony formation (Yang *et al.* 2010). This gene has been shown to act as a “non-classical” oncogene, indirectly promoting cell survival via modulation of the stress response by the endoplasmic reticulum, an important adaptation in transformed cells (Wang *et al.* 2012). Little work has been done on BRF2 in 8p11-p12 amplicon-bearing cells. Our group demonstrated its overexpression can induce insulin-independent growth in MCF10A cells (Yang *et al.* 2010) but another group cited its elimination from consideration as a potential oncogene due to high expression in MCF10A cells at baseline (Kwek *et al.* 2009). Similarly, PROSC is often identified as a strong candidate oncogene (Reis-Filho *et al.* 2006, Haverty *et al.* 2008, Kwek *et al.* 2009, Yang *et al.* 2010, Holland *et al.* 2011, Reis-Filho and Pusztai 2011, Reynisdottir *et al.* 2013, Luo *et al.* 2017), but is understudied in the context of the 8p11-p12 amplicon. RAB11FIP1 is also understudied in this context, but has been implicated in PI3K/AKT/mTOR pathway activation in luminal B breast cancer and may play a role in protein trafficking (Yang *et al.* 2010, Cornen *et al.* 2014). Sircoulomb *et al.* (2011) and

Holland *et al.* (2011) simultaneously described ZNF703 (FLJ14299) as the only candidate oncogene of these five that is commonly and coordinately amplified and overexpressed across breast tumors harboring this site of focal amplification. These groups identified ZNF703 as a co-factor for a nuclear repressor complex that may contribute to transcriptional regulation and control of cell proliferation and clonogenicity via regulation of ER α and TGF- β , respectively, and both studies linked the 8p11-p12 amplicon to endocrine resistance.

Although not contained in this 1 Mb region, one of the more well-known oncogenes from this amplicon is fibroblast growth factor receptor-1 (FGFR1), which is located more proximally in sub-region A2 and amplified in 16-27% of breast cancers (Shiu *et al.* 2010, Turner *et al.* 2010, Ades *et al.* 2014). One study linked amplification and overexpression of FGFR1 to anchorage-independent proliferation, endocrine therapy resistance, and poor prognosis (Ignatiadis and Sotiriou 2013). Interestingly, FGFR1 is not always amplified, amplification does not always correlate with overexpression, its knockdown does not always result in decreased proliferation, and treatment with ligands FGF1 and FGF2 have been shown to actually inhibit proliferation of some 8p11-p12 amplicon-bearing breast cancer cells (Still *et al.* 1999, Ray *et al.* 2004, Yang *et al.* 2004, Haverty *et al.* 2008, Elsheikh *et al.* 2009, Turner *et al.* 2010, Mahmood *et al.* 2013). Therefore, FGFR1 is not universally accepted as a driver of all cancers with 8p11-p12 amplification and these tumors are more likely driven by oncogenes in close proximity to this gene (Melchor *et al.* 2007, Elsheikh *et al.* 2009, Turner *et al.* 2010, Bilal *et al.* 2012). More recent studies investigating the role of FGFR1 as a driving oncogene from this genomic region actually identified eight other amplicon genes as better predictors of FGFR1 amplification than FGFR1 itself, including ASH2L,

BAG4, BRF2, DDHD2, LSM1, PROSC, RAB11FIP1, and WHSC1L1 (NSD3) (Luo *et al.* 2017). Two of these genes, ASH2L and NSD3, also mentioned above, are the focus of the work presented here and are discussed in detail below.

As investigation of the oncogenes from the 8p11-p12 amplicon has progressed, new insight has been gained into the function of this genetic change in breast cancer. This has led to the development of new hypotheses regarding the potential cooperation of the multiple driving oncogenes that have been identified and described. As mentioned previously, the 11q12-q14 amplicon has been hypothesized to cooperate with the 8p11-p12 amplicon due to their coordinated amplification, where amplification of 8p11-12 occurs in 40% of 11q12-14 amplified cases (Reis-Filho *et al.* 2006, Kwek *et al.* 2009, Shiu *et al.* 2010, Yang *et al.* 2010, Sircoulomb *et al.* 2011, Bilal *et al.* 2012, Ignatiadis and Sotiriou 2013, Lim *et al.* 2016). CCND1 (11q13) induces expression of ZNF703 (8p12) via the RB/E2F pathway and expression of ZNF703, BAG4, RAB11FIP1, and WHSC1L1 (NSD3), all 8p11-p12 amplicon genes, is increased when 11q12-q14 is amplified, independent of concomitant 8p11-p12 amplification (Kwek *et al.* 2009). Overexpression of CCND1 in the SUM-44 cell line, which harbors both amplicons, resulted in upregulation of these 8p11-p12 amplicon genes. Although not fully explored, this study also indicated evidence that FGFR1 and DDHD2 from the 8p11-p12 amplicon may interact with C-MYC, a commonly amplified oncogene from the 8q24 region (Kwek *et al.* 2009). Together, this study provides evidence that the complex genomic structures of luminal B tumors may be due in part to interactions between driving oncogenes from multiple amplicons.

It was suggested that oncogenes from the 8p11-p12 amplicon cooperate to promote tumorigenesis, a concept that is supported by groups studying this amplicon

(Gelsi-Boyer *et al.* 2005, Yang *et al.* 2006, Sircoulomb *et al.* 2011, Wu *et al.* 2012, Luo *et al.* 2017). This hypothesis of cooperation partially explains the complexity of this amplicon and the plethora of oncogenes in this “hot spot” of genomic activity (Ray *et al.* 2004). The candidate oncogenes from this region can often be grouped by similar function, such as regulation of RNA metabolism, vesicle trafficking, tyrosine kinase activity, chromatin maintenance, and regulation of ER α (Gelsi-Boyer *et al.* 2005, Yang *et al.* 2010, Turner-Ivey *et al.* 2014, Irish *et al.* 2016). The latter two functions are of particular interest to our group since all three of the 8p11-p12 oncogenes implicated in epigenetic regulation of chromatin structure, KAT6A (MYST3), WHSC1L1 (NSD3), and ASH2L, are also implicated in regulation of ER α and/or ESR1, the gene which encodes ER α (Ades *et al.* 2014, Qi *et al.* 2014, Turner-Ivey *et al.* 2014, Irish *et al.* 2016). Indeed, genetic abnormalities, such as amplifications, are increasingly linked to epigenetic dysregulation in cancers, leading to enhanced focus on understanding the role of chromatin modification in tumorigenesis and key players and processes that can become therapeutic targets in breast and other cancers.

1.3. Breast Cancer Epigenomics

a. Epigenetics overview

Epigenetics is emerging as an important mechanism of transcriptional dysregulation in cancer and understanding the effects of various chromatin-modifying enzymes on gene expression patterns related to cell proliferation, survival, DNA repair, and other carcinogenic processes is essential to prevention, diagnosis, and treatment of cancer. Epigenetics is defined as changes to the expression profile of a cell not accounted for by alterations to the DNA sequence (Miyamoto and Ushijima 2005,

Kristensen *et al.* 2009, Lustberg and Ramaswamy 2009, Jovanovic *et al.* 2010, Pathiraja *et al.* 2010, Grzenda *et al.* 2011, Lustberg and Ramaswamy 2011). It includes DNA methylation, histone post-translational modifications (hPTM), non-coding RNA, and nucleosome remodeling and is a multi-layer regulation system that is complex by its nature (Margueron *et al.* 2004, Jovanovic *et al.* 2010, Rijnkels *et al.* 2010, Lustberg and Ramaswamy 2011, Abdel-Hafiz and Horwitz 2015, Noberini and Bonaldi 2017).

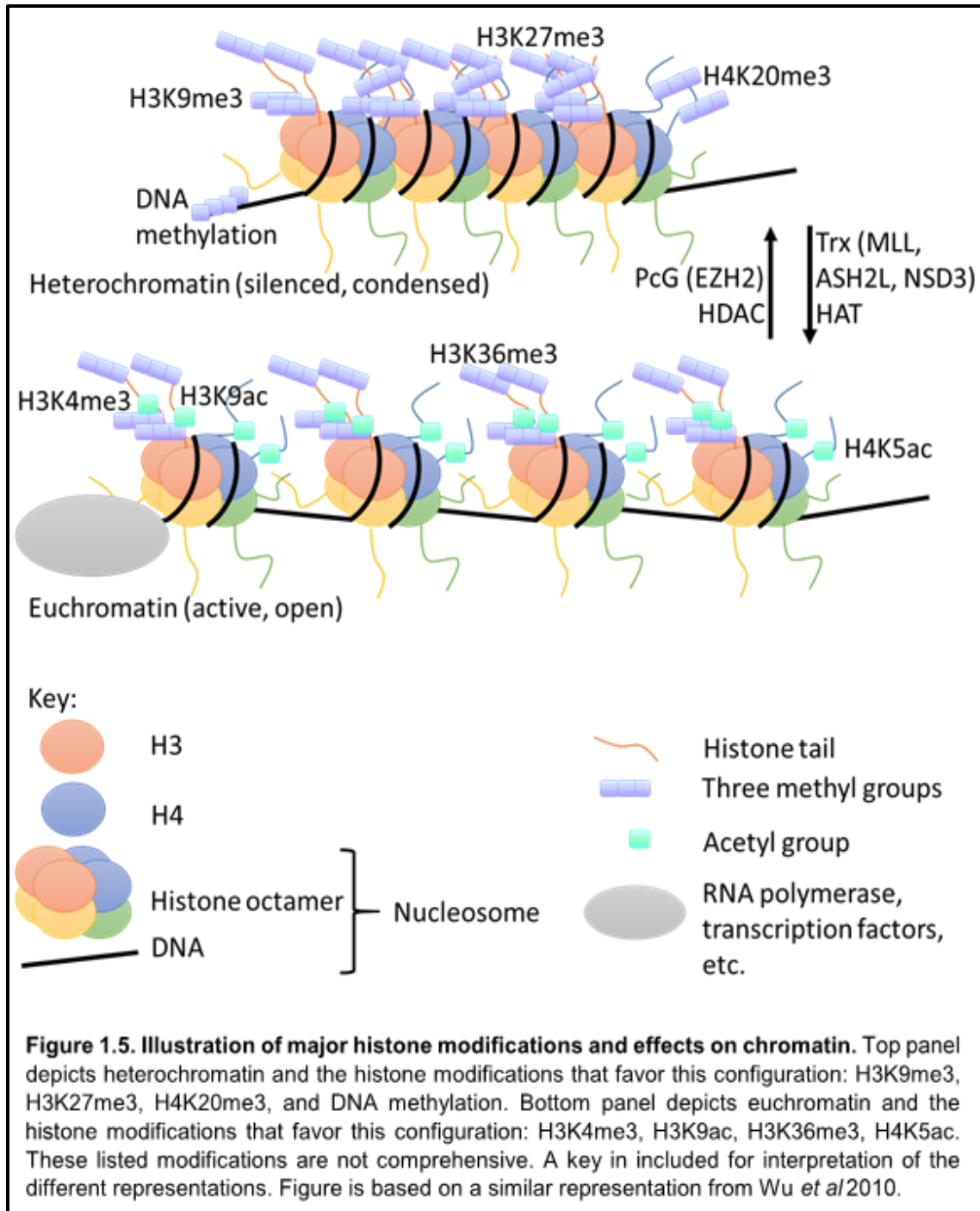
The first and best-characterized epigenetic modification investigated is DNA methylation at CpG islands in promoter regions by DNA methyltransferase (DNMT) enzymes (Lustberg and Ramaswamy 2009). In general, DNA methylation results in gene silencing and cancers tend to have global hypermethylation (suppression) with hypomethylation (expression) of specific genes, such as those involved in cell cycle progression (Lo and Sukumar 2008, Jovanovic *et al.* 2010, Pathiraja *et al.* 2010, Huang *et al.* 2011). For this reason, inhibitors of the methyltransferase enzymes responsible for these events have proven clinically successful at re-expression of heavily methylated genes and have a positive influence on patient survival (Cai *et al.* 2011, Falahi *et al.* 2014). One such example is the re-expression of ER α and subsequent re-sensitization of ER-negative breast cancers to endocrine therapy (Kristensen *et al.* 2009, Falahi *et al.* 2014, Abdel-Hafiz and Horwitz 2015).

In addition to methylation of the DNA, modifications to the chromatin structure and regulation of access to the genetic information contained therein is emerging as an essential component of tumor initiation and progression in breast and other types of cancer (Lo and Sukumar 2008, Grzenda *et al.* 2011, Kim *et al.* 2016). Chromatin is composed of nucleosomes, units of 147 base pair segments of DNA wrapped around octamers of histone proteins, made up of two each of histone proteins H2A, H2B, H3,

Chapter 1: Introduction Page | 27

and H4 (Lo and Sukumar 2008, Kristensen *et al.* 2009, Souza *et al.* 2009, Jovanovic *et al.* 2010, Grzenda *et al.* 2011, Kumar *et al.* 2016). These nucleosomes are linked via histone H1 and complexed with additional proteins into areas of highly condensed, transcriptionally inactive heterochromatin and open, transcriptionally active euchromatin (Lo and Sukumar 2008, Kristensen *et al.* 2009, Shan *et al.* 2014, Kumar *et al.* 2016). Within nucleosomes, the N-terminal tails of the histone proteins are left exposed, rendering them susceptible to post-translational modification by epigenetic enzymes (Liu *et al.* 2009, Jovanovic *et al.* 2010, Kim *et al.* 2016). Known hPTMs include acetylation, methylation, sumoylation, ubiquitination, phosphorylation, and ADP-ribosylation (Lo and Sukumar 2008, Souza *et al.* 2009, Jovanovic *et al.* 2010, Grzenda *et al.* 2011, Huang *et al.* 2011). Different modifications on different histone tail amino acid residues in different regions of the genome produce a variety of effects on the transcriptional program of the cell (Figure 1.5) (Liu *et al.* 2009, Kuo *et al.* 2011, Kim *et al.* 2014, Osmanbeyoglu *et al.* 2014, Kumar *et al.* 2016). These modifications have such a profound effect on gene expression that they account for much of the cellular programming during embryogenesis that produces a vast number of functionally differentiated cell and tissue types from a single set of genetic information, and conversely their dysregulation can aberrantly revert differentiated cells back to a pluripotent state, which has major implications in tumorigenesis (Lo and Sukumar 2008, Liu *et al.* 2009, Sircoulomb *et al.* 2011, Nagamatsu *et al.* 2012, Osmanbeyoglu *et al.* 2014).

Since epigenetic factors play a major role in altering the expression of large sets of genes simultaneously, it is no surprise that aberrant expression of these enzymes can lead to cancer (Lo and Sukumar 2008, Demircan *et al.* 2009, Liu *et al.* 2009, Yang *et al.* 2009, Kim *et al.* 2014, De Marchi *et al.* 2016, Kim *et al.* 2016). Global studies of hPTMs



demonstrate that early stage tumors have a different epigenomic profile than late stage tumors and the different molecular subtypes of breast cancer can be further clarified by analyzing their epigenomic states (Garapaty *et al.* 2009, Messier *et al.* 2016). An

important aspect of epigenetics is the ability of the modifications to chromatin structure to be both stable, with heritability of the epigenetic state of cells being an essential component of development and maintenance of phenotype, and dynamic, with different patterns of gene expression required throughout the life of a cell and the mitotic process (Miyamoto and Ushijima 2005, Lustberg and Ramaswamy 2009, Pathiraja *et al.* 2010, Allali-Hassani *et al.* 2014). As such, most epigenetic modifications, unlike genetic changes, are reversible (Lo and Sukumar 2008, Simon and Lange 2008, Kristensen *et al.* 2009, Lustberg and Ramaswamy 2009, Pathiraja *et al.* 2010, Cai *et al.* 2011, Morishita and di Luccio 2011, Liu *et al.* 2014, Michalak and Visvader 2016). These features make epigenetic enzymes and the chromatin alterations they generate key drug targets in cancer and other diseases.

b. Histone acetylation and methylation

The best-studied hPTM thus far is acetylation. Histone acetylation usually occurs on lysine (K) residues in the exposed histone tails, especially K4, K9, and K27 of H3 and K5, K8, K12, and K16 of H4 (Figure 1.5) (Lo and Sukumar 2008, Kristensen *et al.* 2009, Lustberg and Ramaswamy 2009, Huang *et al.* 2011, Judes *et al.* 2016, Messier *et al.* 2016). Histone acetylation weakens the charge interaction between DNA and histones, relaxing the chromatin, and therefore is generally associated with transcriptionally active genes (Lo and Sukumar 2008, Lustberg and Ramaswamy 2009, Pathiraja *et al.* 2010, Zhang *et al.* 2013). In normal cells, histone acetylation is regulated by opposing activity of histone acetyltransferase (HAT) and histone deacetylase (HDAC) enzymes (Margueron *et al.* 2004, Lo and Sukumar 2008, Huang *et al.* 2011). Acetylated histones also interact with other epigenetic changes, such as DNA methylation, to contribute to overall transcriptional balance (Lustberg and Ramaswamy 2009, Pathiraja *et al.* 2010).

Some cancer types have high levels of global histone acetylation associated with aberrant transcription of cell cycle progression programs while others have low levels, correlating to overactivity of HDACs that shut down transcription of tumor suppressors (Lo and Sukumar 2008, Elsheikh *et al.* 2009, Judes *et al.* 2016, Messier *et al.* 2016). HDAC inhibitors have been studied for their potential to promote hyperacetylation and transcription of pro-apoptotic genes and show promising results in clinical trials, especially in combination with DNMT inhibitors and endocrine therapies (Margueron *et al.* 2004, Lo and Sukumar 2008, Kristensen *et al.* 2009, Lustberg and Ramaswamy 2009, Cai *et al.* 2011, Connolly and Stearns 2012, Abdel-Hafiz and Horwitz 2015, Borbely *et al.* 2015, Connolly *et al.* 2016, Walsh *et al.* 2016). HDAC inhibitors can also promote acetylation of proteins such as HSP90, a chaperone protein for clients such as ER α , AKT, HER2, cRAF, and others, which are then destabilized and degraded (Lo and Sukumar 2008, Lustberg and Ramaswamy 2009). Depending on the tumor type and subtype, this can be beneficial in cancer treatment. HDAC inhibitors have shown success in several hematologic malignancies but have yet to demonstrate much benefit in breast cancer (Kerdivel *et al.* 2013, Falahi *et al.* 2014).

Histone methylation is less understood and more complex than histone acetylation (Lo and Sukumar 2008, Huang *et al.* 2011). Histone methylation occurs at lysine (K) and arginine (R) residues, though is almost exclusively found on K, and can be both activating and repressive depending on the specific residue, location within a gene and how many methyl groups are added (Lo and Sukumar 2008, Elsheikh *et al.* 2009, Morishita and di Luccio 2011). K residues can accept up to three methyl groups in a stepwise fashion, and different enzymes are involved in catalyzing mono-, di-, and trimethylation as well as de-methylation events (Li *et al.* 2009, Liu *et al.* 2009, Huang *et al.*

2011, Kim *et al.* 2014, Kim *et al.* 2016). In general, the most common activating methylation marks include H3K4me3, H3K36me3, and H3K79me3 and repressive marks include H3K9me3, H3K27me3, and H4K20me3 (Lo and Sukumar 2008, Elsheikh *et al.* 2009, Souza *et al.* 2009, Fang *et al.* 2010, Jovanovic *et al.* 2010, Huang *et al.* 2011, Morishita *et al.* 2014). Similarly, arginine residues can be methylated by protein-arginine methyltransferase family proteins, and H4R3me3 is associated with activated transcription (Elsheikh *et al.* 2009, Butler *et al.* 2011). Although the exact specificity of different histone methyltransferase (HMT) enzymes responsible for placing these marks is still controversial, some general patterns have emerged.

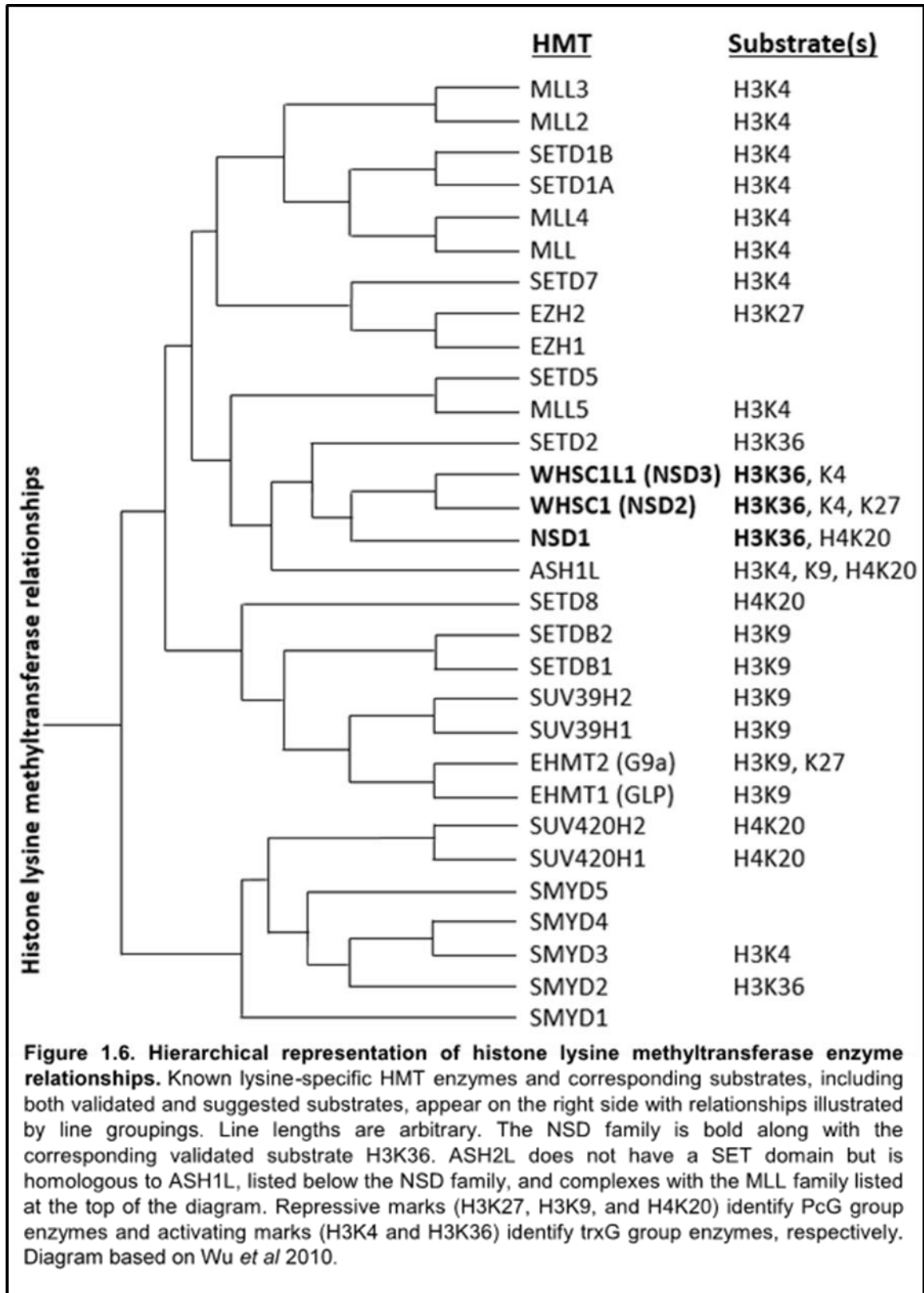
The first HMTs, though not yet known to function as such, were identified in the 1940s in *Drosophila melanogaster* when it was observed that loss of homeobox (HOX) gene expression in male flies produced extra sex combs, and the phenomenon was termed “polycomb” (Grzenda *et al.* 2011). These polycomb group (PcG) enzymes that negatively regulate HOX gene expression have since been identified as the SET (Suppressor of variegation 3-9, Enhancer of zeste and Trithorax) domain-containing HMTs EZH1 and EZH2 and their complex partners (Angrand *et al.* 2001, Lo and Sukumar 2008, Simon and Lange 2008, Grzenda *et al.* 2011). The SET domain provides the catalytic activity for the 4 subgroups, PRC1 (polycomb repressive complex), which is associated with transcriptional maintenance, and PRC2, PRC3, and PRC4 that are associated with transcriptional initiation (Grzenda *et al.* 2011, Huang *et al.* 2011, Yuan *et al.* 2011, Garapaty-Rao *et al.* 2013). PcG factors exert their repressive function primarily via tri-methylation of H3K27 and H3K9 and are critical for embryonic development, stem cell maintenance, differentiation, proliferation, and invasion (Rampalli *et al.* 2007, Simon and Lange 2008, Pathiraja *et al.* 2010, Grzenda *et al.* 2011, Yuan *et al.* 2011, Judes *et al.* 2011).

et al. 2016). EZH2 is one of the most studied HMTs to date and EZH2 inhibitors are now in clinical trials (Garapaty-Rao *et al.* 2013, Sato *et al.* 2017). Activity of PcG enzymes is found at both active and inactive genes and transcriptional repression and chromatin compaction is thought to be the “default” setting of cells, with activation of transcription occurring through “de-repression” in a tightly controlled fashion (Rampalli *et al.* 2007, Yuan *et al.* 2011).

Until the 1980s, it was unclear how PcG enzyme activity was counterbalanced (Grzenda *et al.* 2011). Also in *Drosophila melanogaster*, the trithorax group (trxG) of chromatin modifiers was discovered (Ikegawa *et al.* 1999, Luscher-Firzlaff *et al.* 2008, Grzenda *et al.* 2011, Yuan *et al.* 2011). This family of proteins is made up of HMT enzymes that also contain SET domains, which possesses the catalytic HMT function (Ikegawa *et al.* 1999, Angrand *et al.* 2001, Cao *et al.* 2010, Judes *et al.* 2016). TrxG enzymes counteract PcG repression primarily by H3K4 tri-methylation, mediated by MLL (mixed lineage leukemia) and other ASH2L-containing complexes, leading to active transcription (Guertin *et al.* 2006, Rampalli *et al.* 2007, Grzenda *et al.* 2011). Many promoters possess both H3K27me3 and H3K4me3 at high levels and are termed “poised” chromatin regions, though the “switch” that determines which direction gene transcription ultimately favors is unclear and may depend on cross-talk with other layers of epigenetic regulation, such as DNA methylation and histone acetylation (Grzenda *et al.* 2011, Wan *et al.* 2013, Ullius *et al.* 2014, Katoh 2016). MYC may be involved in recruitment of other enzymes, such as p300, that de-methylate and acetylate H3K27 for transcriptional activation in an ASH2L-dependent manner (Hervouet *et al.* 2013, Ullius *et al.* 2014, Erfani *et al.* 2015). SET domain-containing proteins also di-methylate H3K36, another marker of active gene transcription (Li *et al.* 2009, Liu *et al.* 2009, Kuo *et al.*

2011, Yuan *et al.* 2011, French *et al.* 2014, Liu *et al.* 2014, Zhu *et al.* 2016). These enzymes include ASH1L and the NSD family of HMTs, discussed in more detail along with ASH2L and the MLL complexes in subsequent sections (Figure 1.6).

Although chromatin-modifying enzymes are often studied individually, the reality is that many of these enzymes are found in complexes together, and activation of one tends to facilitate recruitment of others (Wang *et al.* 2007, Nguyen *et al.* 2008, Simon and Lange 2008, Li *et al.* 2009, Yates *et al.* 2010, Huang *et al.* 2011, Kumar *et al.* 2016). This is exemplified in the SWI/SNF and similar complexes that have been well-characterized and are known to have a vast selection of subunits that contribute to chromatin architecture in a plethora of biological contexts (Yates *et al.* 2010, Kumar *et al.* 2016). Similarly, transcription factors such as ER α rely on several epigenetic proteins for local remodeling of nucleosomes to facilitate transcription, create positive feedback loops to maintain transcription, and auto-regulate shutting down of these pathways to prevent aberrant gene expression (Margueron *et al.* 2004, Lo and Sukumar 2008, Li *et al.* 2009, Fang *et al.* 2010, Jacques-Fricke and Gammill 2014, Locke *et al.* 2015). Some of the better-characterized binding partners of ER α include the HATs p300/CBP, PCAF, and SRC1 (NCoA1, nuclear co-activator 1), which function as co-activators to destabilize the nucleosomes and open the chromatin for transcription (Margueron *et al.* 2004, Garapaty *et al.* 2009, Hervouet *et al.* 2013, Zhang *et al.* 2013). Various HMT, demethylase, and DNMT enzymes, including HMTs MLL1 and MLL2, also complex with ER α to close the chromatin once the transcriptional pattern is complete (Cui *et al.* 2005, Huang *et al.* 2011, Hervouet *et al.* 2013, Zhang *et al.* 2013, Ades *et al.* 2014). In addition to histones, epigenetic factors can modify non-histone proteins. For example, SMYD2, a HMT, methylates K266 in the hinge region of the ER α protein itself in the absence of



17 β -estradiol and LSD1, a demethylase, must first remove this inhibitory K26me prior to acetylation at the same residue by p300/CBP, which contributes to ER α activation upon stimulation with 17 β -estradiol (Zhang *et al.* 2013). Many other enzymes are also implicated in direct modification of ER α , particularly related to the hinge-region ligand-binding and ligand-independent AF-1 domains (Margueron *et al.* 2004, Kerdivel *et al.* 2013). When any of the mechanisms contributing to transcriptional access are disrupted, tumorigenesis can result.

An essential feature of epigenetics is the ability for precise interpretation of the combinatorial nature of histone modifications and translation to transcriptional signals (Grzenda *et al.* 2011, Hervouet *et al.* 2013). This is accomplished by the various “reader” domains possessed by epigenetic enzymes. Bromodomains recognize acetylated histones and recruit additional factors to the chromatin (Lo and Sukumar 2008, Grzenda *et al.* 2011, Rahman *et al.* 2011, Wagner and Carpenter 2012). The bromodomain and extraterminal domain (BET) family of proteins, BRDT, BRD2, BRD3, and BRD4, have been implicated as “linker” or “bridge” proteins in various cancer types between acetylated histones and other epigenetic factors and have been the focus of drug development leading to clinical trials in recent years (Morishita and di Luccio 2011, Rahman *et al.* 2011, Feng *et al.* 2014, Zou *et al.* 2014, Nagarajan *et al.* 2015, Shen *et al.* 2015, Crowe *et al.* 2016, Kumar *et al.* 2016, Zhang *et al.* 2016). Other common domains include WD40, ADD, and chromodomains (CHD), which recognize methylated lysine residues (Guccione *et al.* 2007, Lo and Sukumar 2008, Grzenda *et al.* 2011, Kim *et al.* 2016). Plant homeodomains (PHD) are zinc finger motifs that recognize methylated lysines and arginine residues, preferentially H3K4me3 and H3K9me3 (Huang *et al.*

et al. 2014, Morishita *et al.* 2014, Kim *et al.* 2016). PWWP (Pro-Trp-Trp-Pro) domains are highly conserved and preferentially recognize H3K36me1 and H3K36me2 (Yang *et al.* 2010, Grzenda *et al.* 2011, Wagner and Carpenter 2012, Allali-Hassani *et al.* 2014, Morishita *et al.* 2014, Wen *et al.* 2014, Shen *et al.* 2015, Kim *et al.* 2016). The PHD5-C5HCH domain unique to the NSD family of HMTs also plays an important role in directing these enzymes to chromatin, preferentially binding H3K4me0 and H3K9me3 (He *et al.* 2013). These reader domains generally bind multiple histone and non-histone PTMs with substrate affinities dependent upon the three-dimensional structures of the domains, presence of coregulatory factors that cause conformational changes to those binding pockets, nearby histone and DNA modifications that can have allosteric effects on HMTs, and other factors, increasing the complexity of the rich language of the histone code.

As the field of epigenetics has expanded exponentially over the past two decades (Huang *et al.* 2011), it has become clear that the complexity and interaction between all the chromatin regulatory marks, together termed the “histone code” (Grzenda *et al.* 2011, Hervouet *et al.* 2013), needs further evaluation. There is a clear link between aberrant expression of epigenetic modifiers of chromatin and pathology, especially tumorigenesis (Miyamoto and Ushijima 2005, Lo and Sukumar 2008, Demircan *et al.* 2009, Li *et al.* 2009, Kim *et al.* 2014, Paska and Hudler 2015, Kim *et al.* 2016, Zhu *et al.* 2016). Globally-targeted inhibition of some of these enzymes, such as the DNMT, HDAC, and bromodomain inhibitors, have proven that this pathway of investigation is worthwhile and has highlighted the need to fine-tune pharmacologic control of epigenetic editing in a cancer subtype-specific manner (Lo and Sukumar 2008, Falahi *et al.* 2014, French *et al.* 2014). For a more detailed discussion of the topics

briefly addressed in this section, interested readers are referred to several comprehensive review articles (Lo and Sukumar 2008, Lustberg and Ramaswamy 2009, Jovanovic *et al.* 2010, Rijnkels *et al.* 2010, Veeck and Esteller 2010, Cai *et al.* 2011, Connolly and Stearns 2012, Falahi *et al.* 2014, Lin *et al.* 2015, Paska and Hudler 2015, Michalak and Visvader 2016, Walsh *et al.* 2016, Damaskos *et al.* 2017). Only the implications of histone methylation on lysine residues 4 and 36 of histone 3 will be discussed further as these groups are regulated by the two 8p11-p12 amplicon factors involved in histone methylation, ASH2L and NSD3, respectively.

1.4. Histone Methyltransferases from the 8p11-p12 Amplicon

a. NSD3 (WHSC1L1) and H3K36me2

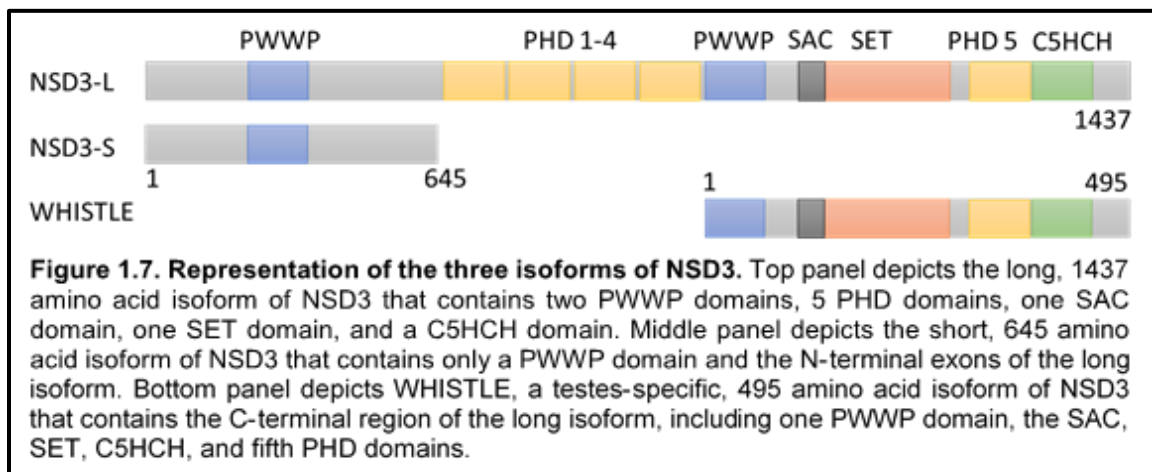
The Nuclear-receptor binding SET Domain-containing (NSD) family of proteins is part of the trithorax (trx) group of chromatin-modifying enzymes and has three main members: NSD1, NSD2 (WHSC1/MMSET), and NSD3 (WHSC1L1 for Wolf-Hirschhorn Syndrome Candidate 1-Like 1) (Huang *et al.* 1998, Yang *et al.* 2010). These enzymes are HMTs and share a large degree of homology with one another as well as with other SET domain-containing proteins conserved throughout evolution (Angrand *et al.* 2001, Li *et al.* 2009, Wu *et al.* 2010, Yang *et al.* 2010, Zhou *et al.* 2010, Morishita and di Luccio 2011, Kato 2016). All three family members are dysregulated in a number of benign and malignant disease states and they have all been established as oncogenes (Douglas *et al.* 2005, Yang *et al.* 2010, Morishita and di Luccio 2011, He *et al.* 2013). Much of the work on these enzymes has been done in hematological malignancies, primarily acute myeloid leukemia (AML) for NSD1 and NSD3 and multiple myeloma for NSD2, but they have also been implicated in lung, pancreatic, colorectal, liver, bladder,

glioblastoma, neuroblastoma, head and neck carcinoma, and breast cancers (Stec *et al.* 2001, Li *et al.* 2009, Taketani *et al.* 2009, Zhou *et al.* 2010, Morishita and di Luccio 2011, Morishita and di Luccio 2011, He *et al.* 2013, Morishita *et al.* 2014, Suzuki *et al.* 2015, Saloura *et al.* 2016). Though there has been much debate over the specificity of these HMTs and some controversy remains, it has been established that they all possess H3K36 methylation ability and NSD3 is unambiguously implicated in di-methylation of this lysine residue, which is generally associated with active transcription (Li *et al.* 2009, Kuo *et al.* 2011, Morishita and di Luccio 2011, Rahman *et al.* 2011, Wagner and Carpenter 2012, He *et al.* 2013, Allali-Hassani *et al.* 2014, Feng *et al.* 2014, French *et al.* 2014, Jacques-Fricke and Gammill 2014, Morishita *et al.* 2014, Saloura *et al.* 2016, Bennett *et al.* 2017). NSD2 is implicated in the greatest number of histone methylation events (Li *et al.* 2009, Morishita and di Luccio 2011, Morishita *et al.* 2014). In addition to histone methylation, NSD1 has demonstrated methylation of NF- κ B and NSD3 has been shown to methylate the epidermal growth factor receptor (EGFR), activating downstream events in the absence of EGF that lead to DNA replication in squamous cell carcinomas of the head and neck (Morishita and di Luccio 2011, Saloura *et al.* 2017). NSD2 and NSD3 share the highest degree of homology compared to NSD1, and all three have highly conserved sequences (Angrand *et al.* 2001, Yang *et al.* 2010, Zhou *et al.* 2010, Morishita and di Luccio 2011). Knockout mouse models confirm that the functions of these three enzymes are non-redundant and they likely perform unique roles in development and, then, in tumorigenesis as well (He *et al.* 2013, Allali-Hassani *et al.* 2014, Bennett *et al.* 2017).

NSD3 has three isoforms (Figure 1.7). The longest isoform, dictated NSD3-L, is 1437 amino acids from 24 exons located at 8p11.23 and contains an N-terminal PWWP

domain followed by 4 sequential PHD fingers, a second PWWP domain, a SAC (SET-associated cysteine-rich) domain, SET domain (catalytic HMT domain), and a final PHD finger linked to a C5HCH (cys-his-rich) domain that is unique to the NSD family (Angrand *et al.* 2001, Stec *et al.* 2001, Yang *et al.* 2010, Zhou *et al.* 2010, Morishita and di Luccio 2011, Morishita and di Luccio 2011, He *et al.* 2013, Saloura *et al.* 2016).

WHISTLE is a shorter, C-terminal version of this protein generated by a downstream promoter that is specific to testes and bone marrow (Kim *et al.* 2007, Zhou *et al.* 2010, Bennett *et al.* 2017). It recruits HDAC1 with its PWWP domain and methylates H3K4 and H3K27 to repress transcription and may also induce apoptotic cell death through activation of caspase-3 (Kim *et al.* 2007, Zhou *et al.* 2010). This isoform has not been shown to have a role in tumorigenesis (Bennett *et al.* 2017). Alternative splicing of the NSD3 gene at exon 9 produces a truncated 645 amino-acid protein, NSD3-S, that contains only the first PWWP chromatin-binding domain and lacks the catalytic SET and other binding domains (Angrand *et al.* 2001, Stec *et al.* 2001, Yang *et al.* 2010, Zhou *et al.* 2010, Saloura *et al.* 2017). While both the long and short isoforms of NSD3 demonstrate overexpression at the transcript and protein levels in tumor versus normal tissues in multiple cancer types, NSD3-S is consistently identified as expressed to a



higher degree than NSD3-L (Stec *et al.* 2001, Yang *et al.* 2010, Shen *et al.* 2015, Irish *et al.* 2016).

There is mounting evidence to indicate that NSD3-S is more transforming than NSD3-L despite lacking the catalytic SET domain. The 8p11-p12 amplicon often contains breakpoints and deletions in the 3' end of the NSD3 sequence, originally leading to the conclusion that it was not a driving oncogene from this amplicon (Yang *et al.* 2010, Dutt *et al.* 2011). Several studies have alternatively suggested that the short isoform actually is the dominant oncogenic form of this protein and is under selective pressure during the amplification process to preserve the 5' end of the transcript (Nagamatsu *et al.* 2012). Shen *et al.* (2015) demonstrated NSD3-S as the essential oncogenic isoform in AML by serving as an adaptor protein to link BRD4 to other chromatin-modifying enzymes such as CHD8, and the PWWP domain was necessary for this function. This group also identified a new domain on NSD3-S, a transcription activating domain (TAD) comprised of the highly acidic first 100 amino acids, suggesting that NSD3 can exert oncogenic function and transcriptional activation independent of HMT activity. This is consistent with other studies that have demonstrated the necessity of NSD3 in regulating gene transcription but with obvious disconnect between transcriptional outcome and H3K36me2 alterations (Jacques-Fricke and Gammill 2014). Others have postulated that NSD3-S acts by binding to chromatin through its PWWP domain and preventing the methyltransferase function of NSD3-L by occupying the binding sites (Stec *et al.* 2001, Irish *et al.* 2016). It is important to note that, although NSD3-S somewhat unexpectedly has been shown to play a more transforming role than NSD3-L in some studies, there is also evidence to indicate that the enzymatic activity of NSD3-L that generates H3K36me2 is also important in some tumors (Chen *et al.* 2014,

Liu *et al.* 2014, Suzuki *et al.* 2015). While the distinction between the two main isoforms of NSD3 remains to be fully understood, it has become clear that NSD3 is an important oncogene in many cancer types.

Although one study demonstrated that knockdown of NSD3-L in non-NSD3-amplified cell lines resulted in increased cell cycle progression and proliferation, suggesting that NSD3-L may be a tumor suppressor gene (Zhou *et al.* 2010), all others have confirmed it is a bona fide oncogene (Morishita and di Luccio 2011, He *et al.* 2013, Chen *et al.* 2014). This study also demonstrated increased NSD3-L transcript levels compared to NSD3-S (Zhou *et al.* 2010), a finding that is challenged by the body of literature on this gene as well as findings from our laboratory in the same MCF7 breast cancer cell line (Stec *et al.* 2001, Yang *et al.* 2010, Shen *et al.* 2015, Irish *et al.* 2016). NSD3, like NSD1, has been shown to create an oncogenic fusion protein with NUP98 in AML and is associated with poor prognosis and increased aggressiveness, possibly by competing with EZH2-mediated repression of HOX-A gene expression (Rosati *et al.* 2002, Wang *et al.* 2007, Li *et al.* 2009, Taketani *et al.* 2009). Similarly, a fusion protein of the first 7 exons of NSD3 with the NUT gene in NUT midline carcinomas of the lung and mediastinum produced a phenotype of high proliferation and lack of differentiation (French *et al.* 2014). This cancer is highly aggressive with few treatment options and poor patient survival and would benefit from inhibition of NSD3, which induced differentiation and reduced proliferation in a NUT midline carcinoma model cell line (French *et al.* 2014, Suzuki *et al.* 2015). Increased NSD3 expression is associated with reversion of cell phenotype toward pluripotency in other models as well (Yang *et al.* 2010, Nagamatsu *et al.* 2012), consistent with a role in tumorigenesis. NSD3 has been implicated in pancreatic cancer and non-small cell lung cancer progression through its

chromatin modifying behavior (Zhou *et al.* 2010, Morishita and di Luccio 2011, Mann *et al.* 2012, Kang *et al.* 2013, Mahmood *et al.* 2013, Jacques-Fricke and Gammill 2014, Suzuki *et al.* 2015).

NSD3 has been shown to bind several other proteins. BRD4, whose bromodomain recognizes acetylated histones, also possesses an extraterminal (ET) domain that binds NSD3 and other chromatin-modifying enzymes (Rahman *et al.* 2011, Wagner and Carpenter 2012, Feng *et al.* 2014, Shen *et al.* 2015, Crowe *et al.* 2016, Zhang *et al.* 2016). The BRD4-NSD3 unit participates in activating transcription at several important target genes, including CCND1 (Rahman *et al.* 2011, Wagner and Carpenter 2012). This complex is found primarily in the gene body and is associated with H3K36me₂, the histone mark for which NSD3 is responsible (Rahman *et al.* 2011). Rahman *et al.* (2011) also identified BRD2 as an NSD3-binding partner. The unique PHD5-C5HCH domain of the NSD family members has been extensively studied by He *et al.* (2013) and, though each member has different binding affinity, this motif in NSD3 was demonstrated to prefer H3K4me₀ and H3K9me₃, both markers of repressed chromatin. This is consistent with previous studies demonstrating that NSD3 complexes with LSD2, a H3K4 demethylase, and G9a, another SET enzyme responsible for the repressive H3K9me₃ mark (Morishita and di Luccio 2011, Wagner and Carpenter 2012, He *et al.* 2013, Feng *et al.* 2014). It has been proposed that these proteins coordinate the precise dynamic balance of H3 modifications that facilitate optimal transcriptional elongation while simultaneously preventing unwanted initiation of intragenic transcription at target genes (Feng *et al.* 2014).

Methylation of H3K36 is generally associated with transcriptional activity.

H3K36me₂, the major histone-methyl mark of NSD3, is an important hPTM for the

recruitment of other enzymes involved in transcriptional activation (Li *et al.* 2009, Wagner and Carpenter 2012). Methylated H3K36 tends to shift from me2 at the promoter to me3 at the 3' end (Li *et al.* 2009, Rahman *et al.* 2011, Wagner and Carpenter 2012, Zhu *et al.* 2016). There is only one human enzyme known to trimethylate H3K36: SETD2 (Wagner and Carpenter 2012, Michalak and Visvader 2016, Zhu *et al.* 2016). Knockdown of NSD3 or its binding partner BRD4 often indirectly decreases H3K36me3 levels by preventing the di-methylation step upon which SETD2 builds and these two factors have been shown to form a complex together with RNA polymerase II to keep tight regulation on chromatin structure and prevent transcriptional initiation outside the transcriptional start site (Li *et al.* 2009, Fang *et al.* 2010, Rahman *et al.* 2011, Wagner and Carpenter 2012, Jacques-Fricke and Gammill 2014, Katoh 2016). Increased levels of H3K36 methylation are associated with cancers such as AML (Morishita *et al.* 2014, Shen *et al.* 2015). H3K36me3 recruits corepressors, such as HDAC complexes and LSD2, to aid in this regulation (Fang *et al.* 2010, Zhu *et al.* 2016). H3K36 methylation is important early step in activation of transcription by antagonizing repressive marks, such as H3K27me3, and these hPTMs rarely coexist (Yuan *et al.* 2011). Additionally, H3K36 methylation is implicated in alternative splicing events, X-inactivation, and DNA repair and recombination (Wagner and Carpenter 2012). Due to the dynamic nature of chromatin regulation and complexity of the histone code, H3K36me2 has also been implicated in transcriptional repression (Morishita and di Luccio 2011, Wagner and Carpenter 2012). The PWWP domains of the NSD family members are able to read H3K36me0 and H3K36me1 to recruit these enzymes for further methylation by the catalytic SET domain, which all HMT proteins possess, including non-NSD family members such as ASH1L, which shares similarities with NSD1

(Wagner and Carpenter 2012, Liu *et al.* 2014, Katoh 2016). With the tightly coordinated balance associated with H3K36me2 in regulating transcription, it is no surprise that aberrant expression of the enzymes that alter this control have vast implications in disease state such as cancer.

In breast cancer, NSD3 has been identified as one of the top most important HMTs in tumorigenesis. One study analyzed a dataset of 958 breast tumors using TCGA copy number and expression data and GISTIC analysis and determined that, of the 51 known human HMTs, NSD3 has the highest correlation between copy number amplification and coordinate overexpression, thus emphasizing the importance of understanding this oncogene in breast cancer (Liu *et al.* 2014). NSD3 was found amplified in 19% of luminal B breast cancers and was expressed to a higher degree in luminal versus other breast cancer subtypes (Liu *et al.* 2014). Overexpression of NSD3 in the non-transformed MCF10A resulted in a transformed phenotype while knockdown in NSD3-overexpressing breast cancer cell lines reduced proliferation (Yang *et al.* 2010, Liu *et al.* 2014, Irish *et al.* 2016). Knockdown of NSD3 in the amplicon-bearing luminal B breast cancer cell line SUM-44 by our group resulted in decreased expression of ESR1 by microarray, and chromatin immunoprecipitation followed by high throughput sequencing (ChIP-seq) with an ER α antibody cocktail demonstrated ER α actively bound to chromatin without estrogen in a FOXA1-dependent manner, which was then abrogated by knockdown of NSD3 (Irish *et al.* 2016). Together, these data provided the foundation for further exploration of the role of NSD3 in luminal B breast cancer as described in this work.

Although there has been much progress in elucidating the function of NSD3 and its role in tumorigenesis over the past decade, there remains much to be determined

about this driving oncogene. Due to the highly conserved SET domain and mounting evidence that inhibition of this enzyme would be beneficial in multiple cancer types, several groups have suggested NSD3 and its family members as an excellent model for drug development that would revolutionize the field of epigenetic therapies in cancer (Chen *et al.* 2014, Katoh 2016, Michalak and Visvader 2016, Saloura *et al.* 2016). In addition to the catalytic SET domain, drug targets that would inhibit the PWWP domain common to both NSD3-S and NSD3-L would be highly beneficial for blocking non-enzymatic effects as well (Shen *et al.* 2015). This study seeks to identify the role of NSD3 amplification and overexpression in 8p11-p12 amplicon-bearing breast cancer cell lines and to extend the work previously done in our laboratory linking knockdown of NSD3 to a reduction in ER α expression in this context.

b. ASH2L and MLL complexes

The human ASH2L (Absent, Small, or Homeotic disc 2-Like) gene was first discovered by Ikegawa *et al.* in 1999 by large scale genome sequencing and computer-based gene prediction methods as being homologous to the *Drosophila melanogaster* trithorax group (trxG) gene *ash2*. This group of proteins antagonizes transcriptional silencing by the polycomb group (PcG) of epigenetic factors as discussed in previous sections. ASH2L has two isoforms: a 628-amino acid ASH2L1 and a 501-amino acid ASH2L2 protein (Wang *et al.* 2001). ASH2L has a PHD finger motif and thus has been implicated in transcriptional regulation since its discovery (Ikegawa *et al.* 1999). It also has a WH (winged helix) motif for DNA binding, a SPRY domain, and a DPY-30 binding motif, but it lacks the SET domain characteristic of the trxG family and related ASH1L protein (Ikegawa *et al.* 1999, Chen *et al.* 2012). ASH2L is implicated in tight regulation of H3K4 methylation, which is associated with activated transcription (Dou *et al.* 2006,

Chapter 1: Introduction Page | 46

Guccione *et al.* 2007, Luscher-Firzlaff *et al.* 2008, Wan *et al.* 2013, Judes *et al.* 2016). Specifically, ASH2L knockdown primarily affects H3K4me3 levels as opposed to mono- or di-methylation (Steward *et al.* 2006, Demers *et al.* 2007, Fossati *et al.* 2011).

H3K4 tri-methylation was originally thought to be irreversible, barring histone protein turnover, and its regulation in cells of utmost importance to transcriptional regulation in differentiation and development (Steward *et al.* 2006). While the latter is still true, H3K4me3 is now known to be de-methylated by LSD1 (Blobel *et al.* 2009, Fang *et al.* 2010, Huang *et al.* 2011, Hervouet *et al.* 2013, Kim *et al.* 2014, Abdel-Hafiz and Horwitz 2015). The primary H3K4 HMT family in mammalian cells is the SET1 family, which includes MLL proteins 1-4, SET1A, and SET1B, and is named for their highly conserved SET domain that is also found in other HMT groups, such as the NSD family as previously described (Dou *et al.* 2006, Steward *et al.* 2006, Tan *et al.* 2009, Cao *et al.* 2010, Wu *et al.* 2010, Xiao *et al.* 2011, Chen *et al.* 2012, Kim *et al.* 2014, Qi *et al.* 2014, Katoh 2016). MLL proteins actually have very weak enzymatic activity and require binding partners, one of which is ASH2L (Southall *et al.* 2009, Chen *et al.* 2012). In contrast to H3K4me1 and H3K4me2, H3K4me3 is strictly associated with active gene transcription and its distribution closely overlaps that of elongating RNA polymerase II (Demers *et al.* 2007, Guccione *et al.* 2007, Luscher-Firzlaff *et al.* 2008). H3K4me3 is often localized to the 5' (proximal promoter) end of target genes and ASH2L is also confined to this region, though MLL may spread further along the gene (Demers *et al.* 2007, Luscher-Firzlaff *et al.* 2008). In contrast, H3K4me2 has a greater distribution, suggesting a major role for ASH2L as the primary activator of H3K4 tri-methylation in promoter regions (Guccione *et al.* 2007).

Since ASH2L does not possess a SET domain like other trxG proteins, it is known to form complexes with the MLL family of SET domain proteins and is a component of all H3K4 HMTs characterized to date (Ikegawa *et al.* 1999, Butler *et al.* 2011, Ernst and Vakoc 2012, Wan *et al.* 2013, Qi *et al.* 2014, Butler *et al.* 2017). MLL proteins are preferentially H3K4 mono-methylases with weak enzymatic activity and ASH2L is critical for enhancement of HMT function and regulation of MLL-mediated catalysis of H3K4me3 (Patel *et al.* 2009, Chen *et al.* 2012). RbBP5, another MLL complex member, is implicated in activating MLL-mediated catalysis of the intermediate H3K4me2 state (Dou *et al.* 2006, Ernst and Vakoc 2012). The third critical MLL complex participant is WDR5, which is important for the stability of the protein-protein interactions and recruitment to chromatin (Dou *et al.* 2006, Steward *et al.* 2006). Menin, encoded by the MEN1 gene, is also often found together with the WDR5-ASH2L-RbBP5 (WAR) subunit and has demonstrated properties of tumor suppression as well as the ability to directly bind RNA polymerase II (Guertin *et al.* 2006, Guccione *et al.* 2007, Luscher-Firzlaff *et al.* 2008). DPY-30 is also commonly associated with WAR and ASH2L has a DPY-30 binding domain on its C-terminal end (Patel *et al.* 2011, Chen *et al.* 2012, Ali and Tyagi 2017). The sub-complex containing all 4 subunits, known as WRAD, can exist independent of MLL, with and without additional binding partners, implying that these genes may coordinate to recruit other chromatin-modifying enzymes or may have actions outside of hPTM (Patel *et al.* 2011, Ernst and Vakoc 2012, Ali *et al.* 2014, Ali and Tyagi 2017). Interestingly, although knockdown of ASH2L usually reduces global levels of H3K4me3, MLL-dependent H3K4 mono- and di-methylation at some genes is maintained, suggesting it may still interact with the chromatin and act as an HMT, but cannot perform tri-methylation without ASH2L (Guertin *et al.* 2006, Tan *et al.* 2009,

Butler *et al.* 2011, Fossati *et al.* 2011, Chen *et al.* 2012). Knockdown of MLL, however, does not alter methylated H3K4 levels, implying that ASH2L may be responsible for H3K4me3 catalysis by other HMT enzymes as well, perhaps by interaction with other SET domain-containing enzymes, and emphasizing the essential role that ASH2L plays in this histone methyl mark (Steward *et al.* 2006, Demers *et al.* 2007, Blobel *et al.* 2009, Butler *et al.* 2011, Wan *et al.* 2013).

The requirement of the non-SET binding partners ASH2L, RbBP5, and WDR5 for HMT activity at H3K4me3 is unique (Patel *et al.* 2011). As such, several studies have attempted to understand the biological role of the WRAD sub-complex without a SET domain-containing component (Steward *et al.* 2006, Patel *et al.* 2009, Ernst and Vakoc 2012, Ali and Tyagi 2017). One study demonstrated that the sub-complex interacts with nuclear hormone transcription factor coregulatory proteins NRC and NIF-1 and maintained affinity for H3 in this context (Garapaty *et al.* 2009), but the role of ASH2L in promoting HMT activity outside SET domain-containing proteins remained undefined. Patel *et al.* (2009) suggested that the sub-complex itself may possess H3K4-specific methylation ability when MLL is not present, although this activity is not through a SET domain and the mechanism is unknown. This finding was confirmed by their 2011 description of this phenomenon as well (Patel *et al.* 2011). Later, Cao *et al.* (2010) demonstrated that HMT activity is intrinsic to the ASH2L-RbBP5 heterodimer and requires the highly conserved SPRY domain of ASH2L. This group also suggested that ASH2L and the SET domain of MLL1 form a joint catalytic subunit for promoting H3K4 methylation and that overall activity of the MLL complex is dependent upon binding of the methyl-donor SAM to ASH2L (Cao *et al.* 2010). The WRAD sub-complex HMT activity has also been suggested as a second active site in the MLL complex, one

contributing factor to enhanced H3K4 methylation when the entire complex is assembled (Ernst and Vakoc 2012, Patel *et al.* 2014). These findings provided the foundation for the “two-step” hypothesis of MLL complex activation whereby a minimal association between ASH2L and RbBP5 is required to provide a second catalytic pocket in the three-dimensional structure of the complex, thus enhancing the overall methylation ability of the MLL family of proteins (Ernst and Vakoc 2012, Patel *et al.* 2014, Li *et al.* 2016, Ali and Tyagi 2017). This hypothesis explains the ability of ASH2L to act as an HMT even in the absence of a SET domain.

MLL complexes are known to interact with a plethora of proteins, including other epigenetic factors, transcription factors, and basal transcription machinery (Dou *et al.* 2006, Demers *et al.* 2007). ASH2L has similarly been shown to directly bind transcription factors such as AP2 δ , as well as the basal transcriptional machinery (Tan *et al.* 2008). This study suggested that the critical role of ASH2L is as a mediator between chromatin-modifying enzymes and factors involved in transcription. Yates *et al.* (2010) demonstrated binding of the WAR sub-complex, and specifically ASH2L, to CHD8, an APT-dependent chromatin remodeler that alters H3 methylation patterns of HOX genes. Additionally, MLL complexes have been shown by several groups to interact directly with ER α , modifying the histone code near ER α -target genes to promote transcription via promotion of catalysis of H3K4me3 by ASH2L (Hervouet *et al.* 2013, Zhang *et al.* 2013, Bhan *et al.* 2014, Qi *et al.* 2014). ASH2L and the complexes in which it participates have major effects on gene expression during embryogenesis and beyond (Dou *et al.* 2006, Butler *et al.* 2011). Tight regulation of ASH2L is therefore required but poorly understood. One study identified arginine residues on ASH2L that can be di-methylated by PRMT1, but the biological effect of this modification is unknown (Butler *et al.* 2011).

Similarly, MLL1 can auto-methylate ASH2L in the MLL-WRAD complex and, although the function of this methylation is unknown, one possibility is that it acts as a mechanism of autoregulation (Patel *et al.* 2014). WDR5 binds acetylated H3 tails with high affinity, preventing the HMT activity of ASH2L-containing MLL complexes (Guccione *et al.* 2007, Avdic *et al.* 2011). Of course, the actions of PcG proteins are well-known to antagonize H3K4 methylation by these trxG enzymes as well (Grzenda *et al.* 2011). The balance of other epigenetic marks, transcription factors, and protein-protein interactions could also play a role in keeping ASH2L and associated complexes in check, but these events currently remain unclear and are understudied to date (Dou *et al.* 2006, Butler *et al.* 2011, Vedadi *et al.* 2017).

Clearly, ASH2L plays a major role in regulation of gene expression. It is especially implicated in transcription of genes associated with development, stem cell divisions, and mitotic regulation (Ikegawa *et al.* 1999, Demers *et al.* 2007, Butler *et al.* 2011, Kawabe *et al.* 2012, Ali *et al.* 2014). Knockdown of ASH2L results in decreased expression of genes associated with cell cycle, proliferation, and survival in a range of tissue types, including hematologic cells, breast tumors, skeletal muscle, osteosarcomas, and gliomas (Wang *et al.* 2001, Rampalli *et al.* 2007, Luscher-Firzlauff *et al.* 2008, Pullirsch *et al.* 2010, Schram *et al.* 2013, Ali *et al.* 2014, Erfani *et al.* 2015, Zhu *et al.* 2016). Knockdown of ASH2L in embryonic stem cells results in reduced pluripotency due to globally decreased H3K4me3 and increased H3K9me3 levels, a mark of silenced chromatin (Wan *et al.* 2013). Similarly, MLL and the WRAD sub-complex is linked to cell cycle progression through S and M phases (Ali *et al.* 2014). Given the link to stem cell potential and cell cycle regulation, dysregulation of ASH2L can be linked to tumorigenesis.

Similar to NSD3, much of the work on ASH2L in cancer has been done in hematologic models. It was first identified as an oncogene by Lüscher-Firzlaff *et al.* (2008) where they demonstrated that ASH2L cooperates with MYC and RAS, is overexpressed in human tumor samples, and results in decreased tumor growth upon knockdown. The interaction of ASH2L with MYC was later confirmed and implicated in regulation of bivalent chromatin with high levels of both activating marks H3K4me3 and H3K27ac (Ullius *et al.* 2014). ASH2L is important for differentiation of erythroid cell lineages and its aberrant expression is implicated in hematologic malignancies (Wang *et al.* 2001, Cao *et al.* 2010). MLL is often involved in translocations or is mutated or deleted in these cancers (Luscher-Firzlaff *et al.* 2008, Southall *et al.* 2009, Ali *et al.* 2014), thus raising questions about ASH2L function outside of MLL complexes in this context. Additionally, ASH2L has been described as transforming in some osteosarcomas and recently was implicated in regulation of EGFR expression via H3K4me3 in gliomas (Schram *et al.* 2013, Erfani *et al.* 2015). Interestingly, ASH2L demonstrated tumor suppressor characteristics in cell lines from several cancer types with enriched H3K4me3 at p53 pro-apoptotic gene promoters (Mungamuri *et al.* 2015). The authors implicated ASH2L in promoting stability of the initiation complex, though the specific role of ASH2L in this setting was not clearly defined. A dataset of 511 AML patient samples analyzed by reverse phase protein array (RPPA) revealed that ASH2L expression is inversely correlated with patient survival and expression of cell adhesion and cell cycle inhibition genes (Butler *et al.* 2017).

ASH2L is not well-characterized in breast cancer. Along with other 8p11-p12 amplicon genes, ASH2L was identified as one of the core luminal B genes associated with cell cycle and proliferation (Cornen *et al.* 2014). Multiple analyses attempting to

identify the driver oncogene(s) from the 8p11-p12 amplicon called out the potential of ASH2L as such (Garcia *et al.* 2005, Yang *et al.* 2006, Kwek *et al.* 2009, Yang *et al.* 2010, Cornen *et al.* 2014, Turner-Ivey *et al.* 2014), but investigation into its biological function has not yet been fully explored in a luminal B breast cancer model. One group demonstrated recruitment of ASH2L to the promoter of ESR1 by GATA3, where ASH2L potentiated the effects of the GATA3 transcription factor to induce ER α overexpression in breast cancer cell lines and primary tumors (Qi *et al.* 2014). Since ASH2L is one of the most coordinately overexpressed 8p11-p12 amplicon genes when it is amplified (Sircoulomb *et al.* 2011), and given the link between this amplicon and ER α as reported by our work on NSD3 (see Chapter 2) and its prevalence in the ER+ luminal subtype of breast cancer, understanding the link between ASH2L, ER α , and other amplicon genes such as NSD3 could provide exciting new insight into an understudied oncogene and lead to new therapeutic opportunities in this patient subset. This study seeks to explore the role of ASH2L in epigenetic regulation of gene expression in luminal B breast cancer cells with the goal of understanding another step in the mechanism of breast tumorigenesis.

1.5. Significance

ER+ breast cancer, once thought to be a relatively straightforward disease dependent upon estrogen, has since proven to be an incredibly heterogeneous set of diseases with varying degrees of ER α expression and activity that makes reliable prediction of response to endocrine therapy nearly impossible. The call to discover oncogenic signatures that will inform individualized therapy for breast cancer patients is urgent. At the cross-roads of cancer genomics and epigenomics is amplification-induced

overexpression of chromatin-remodeling enzymes. The 8p11-p12 amplicon harbors two histone methyltransferases, NSD3 and ASH2L, which are capable of exerting a vast array of aberrations in the expression profiles of the tumors in which they are overexpressed, and therefore are the focus of the remainder of this work. HMTs have been cited as promising candidates for suppression in the treatment of various cancers (Chen *et al.* 2014, Liu *et al.* 2014, Michalak and Visvader 2016), and understanding how these enzymes function in the amplified and overexpressed state often observed in breast cancer will facilitate drug development in this field. Indeed, recent studies utilizing large-scale databases have identified several HMTs as compelling targets for drug development in cancer therapeutics and suggested that the NSD family of HMTs will provide the optimal starting place for structure-based design (Chen *et al.* 2014, Bennett *et al.* 2017). These studies have called for an improved understanding of chromatin-modifying enzymes as a whole and NSD3 and ASH2L and the complexes in which they function specifically. These oncogenic enzymes have the potential to serve both as biomarkers for therapy response and as novel therapeutic targets themselves and represent an exciting new arm of investigation in breast cancer research and treatment.

CHAPTER 2: NSD3 amplification and overexpression results in overexpression and estrogen-independent activation of the estrogen receptor in human breast cancer.

2.1. NSD3 is overexpressed in 8p11-p12 amplicon-bearing cell lines and is a verified oncogene.

Nuclear Receptor Binding SET Domain protein 3 (NSD3; formerly known as WHSC1L1) was verified as an oncogene by our laboratory (Yang *et al.* 2006, Yang *et al.* 2010, Irish *et al.* 2016). We surveyed a panel of normal breast, breast cancer, and lung squamous cell carcinoma cell lines for expression of NSD3 and discovered that NSD3 is overexpressed at both the message and protein levels in amplicon-bearing cell lines compared to control and that expression is highest in the luminal B breast cancer cell line SUM-44 (Figure 2.1-A). Additionally, we noted that the short isoform of NSD3 (NSD3-S) is expressed to a higher degree than the long isoform (NSD3-L), a finding consistent with data from our lab and others that have demonstrated a role for NSD3-S as the primary transforming isoform of this oncogene (Yang *et al.* 2010, Shen *et al.* 2015). These data correlate with the Cancer Genome Atlas (TCGA), which also showed that, for a group of 964 breast cancer tumors, NSD3-S was overexpressed compared to NSD3-L in the context of NSD3 amplification (Figure 2.1-B) (Gao *et al.* 2013).

Since the effects of the two isoforms of NSD3 on cell proliferation had not been previously differentiated, we performed growth assays following knockdown of NSD3-S or total (NSD3-T) using shRNA that targeted either a unique sequence in the 3'UTR of the NSD3-S transcript or a sequence common to the coding region of both isoforms, respectively. Knockdown with either construct did not affect cell proliferation compared to LacZ control in the amplicon-null MCF7 breast cancer cell line or amplicon-bearing DMS-114 lung squamous cell cancer (LSCC) cell line (Figure 2.1-C and Figure 2.1-D).

Knockdown of NSD3 with both constructs in the amplicon-bearing SUM-44 breast

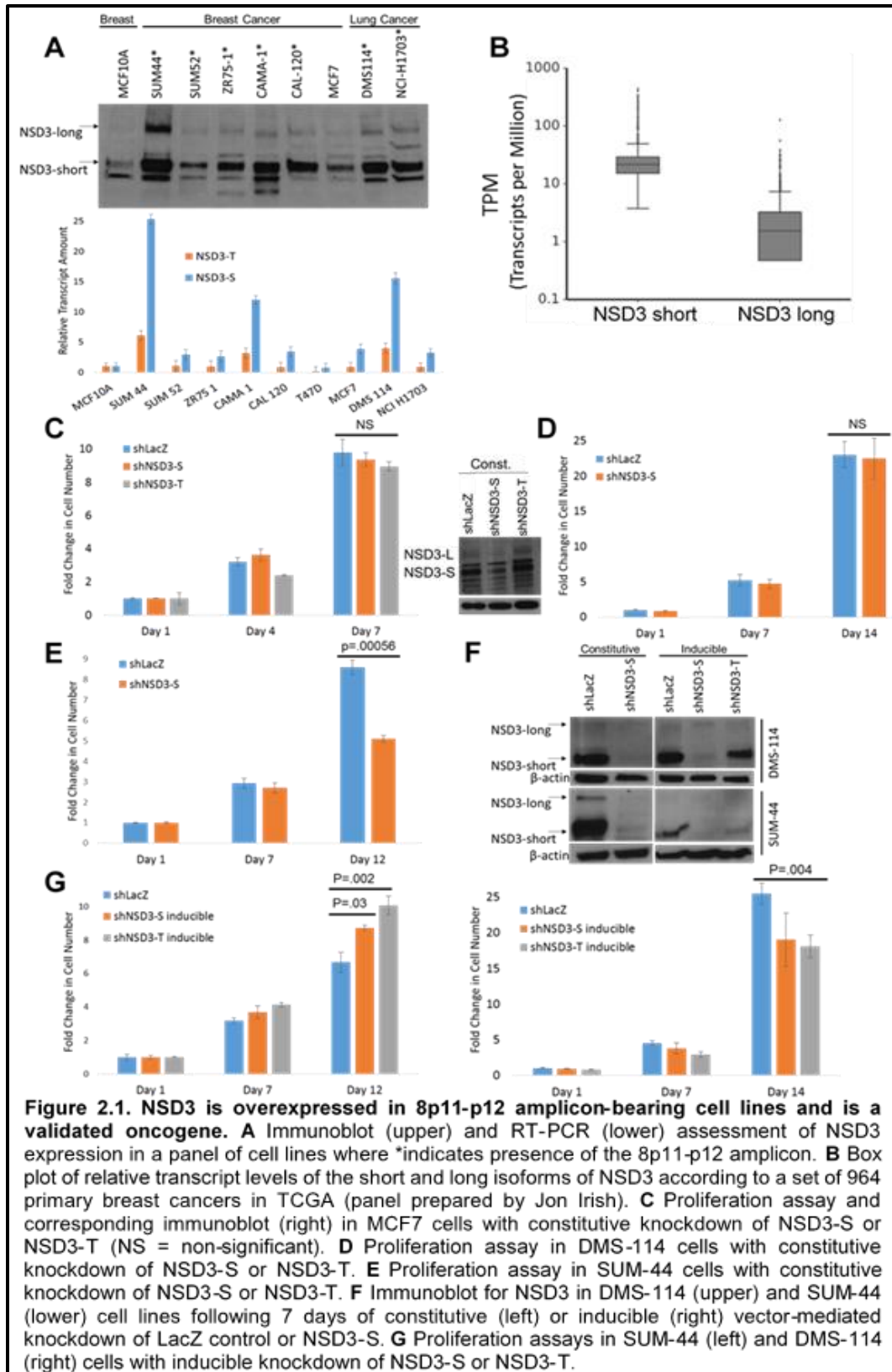


Figure 2.1. NSD3 is overexpressed in 8p11-p12 amplicon-bearing cell lines and is a validated oncogene. **A** Immunoblot (upper) and RT-PCR (lower) assessment of NSD3 expression in a panel of cell lines where *indicates presence of the 8p11-p12 amplicon. **B** Box plot of relative transcript levels of the short and long isoforms of NSD3 according to a set of 964 primary breast cancers in TCGA (panel prepared by Jon Irish). **C** Proliferation assay and corresponding immunoblot (right) in MCF7 cells with constitutive knockdown of NSD3-S or NSD3-T (NS = non-significant). **D** Proliferation assay in DMS-114 cells with constitutive knockdown of NSD3-S or NSD3-T. **E** Proliferation assay in SUM-44 cells with constitutive knockdown of NSD3-S or NSD3-T. **F** Immunoblot for NSD3 in DMS-114 (upper) and SUM-44 (lower) cell lines following 7 days of constitutive (left) or inducible (right) vector-mediated knockdown of LacZ control or NSD3-S. **G** Proliferation assays in SUM-44 (left) and DMS-114 (right) cells with inducible knockdown of NSD3-S or NSD3-T.

cancer cell line, however, did reduce cell proliferation (Figure 2.1-E). Interestingly, the inhibitory effect on growth was greater with knockdown of NSD3-S compared to NSD3-T (Irish *et al.* 2016), again underscoring the oncogenic role of the short isoform in particular. These proliferation assays were repeated using IPTG-inducible shRNA constructs and, although these constructs were able to achieve similar levels of NSD3 knockdown as the constitutive vectors in SUM-44 and DMS-114 cells (Figure 2.1-F), the effects on cell growth were not recapitulated in either cell line (Figure 2.1-G). This and other data (Figure 2.2-A and Figure 2.2-B) prompted our lab to discontinue the use of the IPTG-inducible shRNA system.

To investigate the role of this oncogene further, our lab generated a transgenic FVB mouse model with targeted overexpression of NSD3 to the mammary epithelium (Turner-Ivey *et al.* 2017). NSD3 transgenic females exhibited morphological abnormalities during mammary gland development that resulted in a lactation defect due to the inability of alveoli to undergo full functional differentiation. By 40 weeks of age, these NSD3 transgenic females also developed mammary gland dysplasias, hyperplasias, carcinomas in situ, and invasive carcinomas. Together, these data validate previous work demonstrating the transforming ability of NSD3 and confirm its role as an important driving oncogene in human breast cancer.

2.2. NSD3 knockdown results in reduced expression of estrogen receptor alpha (ER α).

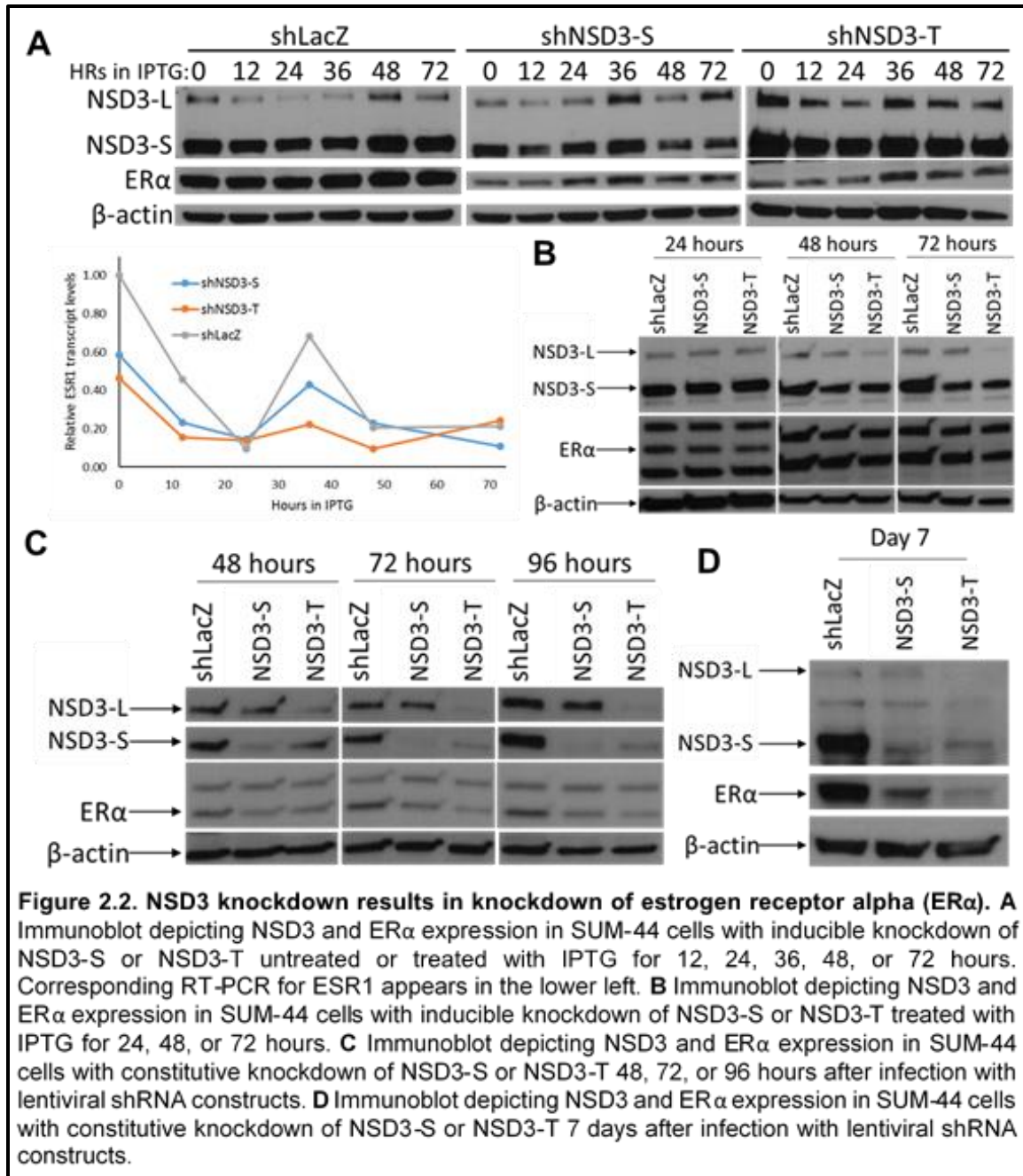
To investigate further the role of NSD3 in breast cancer, we performed microarray analysis following NSD3-S knockdown in SUM-44 cells and noted decreased expression of multiple important genes, including ESR1, which encodes ER α (Table 2.1). To confirm and explore this relationship, SUM-44 cells were infected with LacZ

Table 2.1. Genes with reduced transcript expression following knockdown of NSD3-S in SUM-44 cells. Changes in gene expression by microarray analysis of select genes following knockdown of NSD3-S in SUM-44 cells. Data collected by Jon Irish.

| Gene Symbol | Fold Change | P-value (corrected) |
|-------------|-------------|---------------------|
| MYCN | -7.43 | .03 |
| ESR1 | -7.33 | .004 |
| CXCR4 | -4.88 | .007 |
| ID2 | -4.30 | .004 |
| RET | -3.70 | .008 |
| MYB | -2.92 | .016 |
| CD24 | -2.62 | .010 |
| ALDH2 | -2.55 | .002 |
| ERBB3 | -2.50 | .009 |
| ERBB4 | -2.12 | .002 |

control or IPTG-inducible NSD3-S or NSD3-T shRNA constructs and harvested at 12 hour intervals following initiation of IPTG-treatment to assess NSD3 and ER α levels by western blotting and ESR1 levels by RT-PCR. This system demonstrated very poor knockdown of either NSD3 isoform and relatively little

change in ER α or ESR1 levels (Figure 2.2-A). A second attempt at this experiment demonstrated similar results (Figure 2.2-B). Coupled with the inconsistent results observed on growth patterns using this inducible shRNA system (Figure 2.1-F and 2.1-G), we concluded this system was unreliable and switched to the constitutive shRNA system exclusively. Knockdown of NSD3-S and NSD3-T reduced ER α levels compared to control beginning at 72 hours post-infection (Figure 2.2-C). ER α expression consistently reached peak knockdown at 7 days post-infection with shNSD3-S or NSD3-T virus (Figure 2.2-D). This elucidation of the timing of NSD3-induced reduction in ER α levels was essential to begin to understand the mechanism and implications of this relationship.



2.3. NSD3 overexpression results in overexpression of estrogen receptor alpha (ERα).

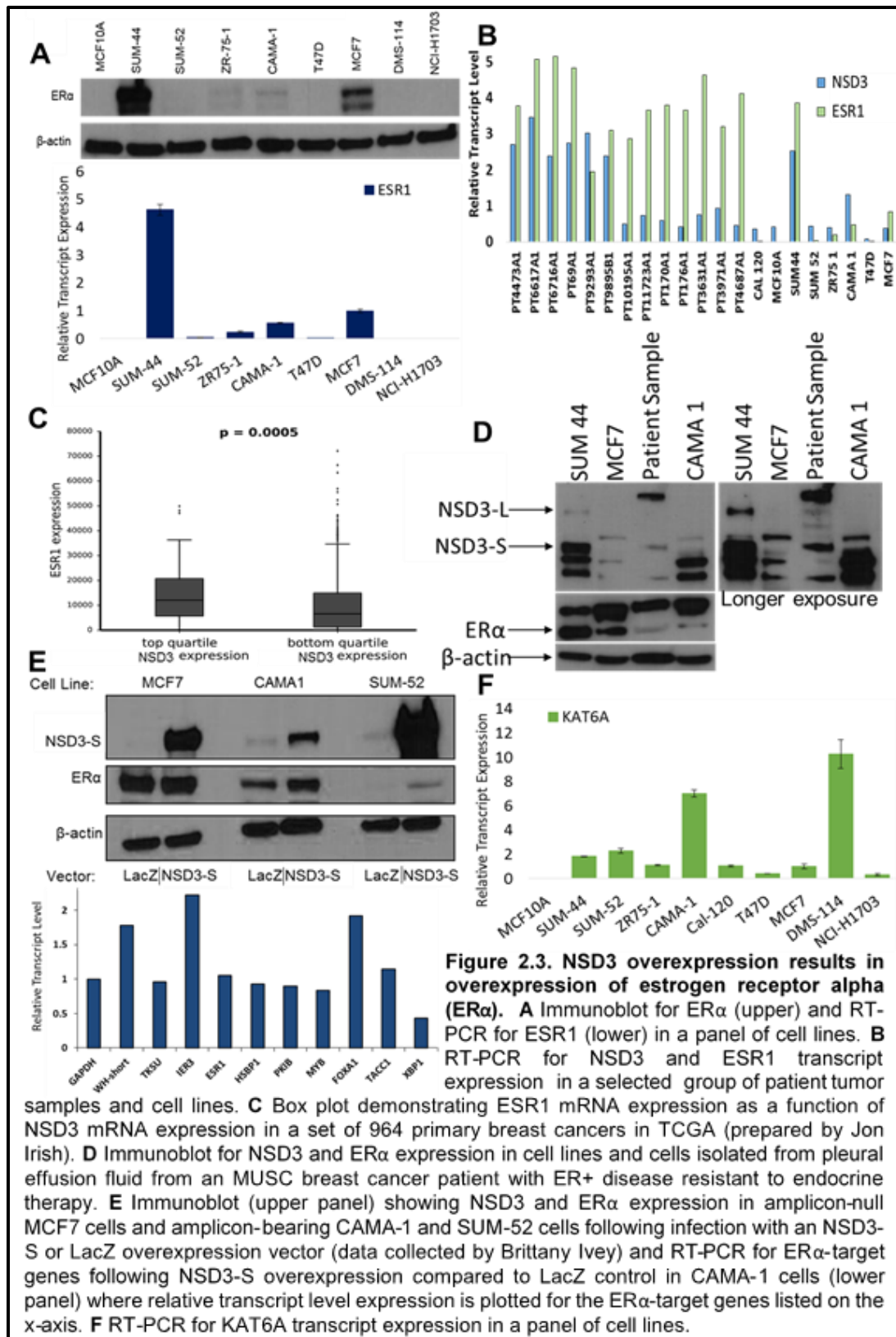
To explore further the effect of NSD3 amplification and overexpression on ERα expression, we assessed ERα levels by immunoblot in a panel of breast and LSCC cell

lines and determined that that SUM-44 cells express extremely high levels of ER α protein (Figure 2.3-A, upper). This finding was especially interesting considering that MCF7 cells are held as the benchmark ER+ cell line for ER α expression *in vitro* and ZR-75-1, CAMA-1, and T47D are also described as ER+ and widely used to study ER α biology in breast cancer cell lines. SUM-44 cells have markedly increased ER α expression compared to all of these lines. RT-PCR for ESR1 expression in this panel of cell lines revealed that message level expression followed the same pattern as protein expression (Figure 2.3-A, lower).

To assess the biological relevance of the dramatic overexpression of ER α in SUM-44 cells in relation to ER α levels observed in patients, we performed RT-PCR to determine message level expression of NSD3 and ESR1 in a group of patient tumor specimens compared to the panel of cell lines (Figure 2.3-B). While we noted 7 cases of high ESR1 expression without corresponding overexpression of NSD3, indicating that ESR1 can be overexpressed without NSD3, we discovered that every case of NSD3 overexpression also displayed high levels of ESR1. TCGA also demonstrates this link between NSD3 and ESR1 overexpression (Figure 2.3-C). We obtained a pleural effusion sample from a breast cancer patient at MUSC with metastatic ER+ breast cancer resistant to endocrine therapy and performed immunoblots for NSD3 and ER α (Figure 2.3-D). While we were unable to isolate a homogeneous population of cells from this specimen, even this heterogeneous sample demonstrated NSD3 expression greater than MCF7 and CAMA-1 cells and ER α expression comparable to the ER+ CAMA-1 line. From these data we concluded that ESR1 can be overexpressed without NSD3 overexpression, suggesting that there are multiple mechanisms for ER α upregulation in

human breast cancer, but not vice versa, demonstrating an important link between the NSD3 oncogene and the transcription factor ER α . Importantly, we found that only the SUM-44 cell line recapitulated the expression levels of these two genes in patient tumors (Figure 2.3-B). SUM-44 is the only *in vitro* model that represents this important subgroup of breast cancer patients and serves as a means by which to study the biology of tumors with NSD3-induced overexpression of ER α .

Since we previously demonstrated that knockdown of NSD3-S reduced ER α expression in SUM-44 cells (Figure 2.2), we next tested whether overexpression of NSD3-S in amplicon-null MCF7 (ER+) cells or amplicon-bearing CAMA-1 (ER+) and SUM-52 (ER-negative) cells would induce overexpression of ER α as detected by immunoblot. NSD3-S overexpression did not alter ER α levels in MCF7 cells but did increase ER α protein levels in both of the amplicon-bearing cell lines (Figure 2.3-E, upper). Message level expression of ER α downstream target genes in CAMA-1 cells also increased, suggesting that the upregulated ER α by NSD3-S overexpression is transcriptionally active (Figure 2.3-E, lower). This suggests that NSD3 is necessary but not sufficient to overexpress ER α and requires one or more additional factors present on the 8p11-p12 amplicon. Since NSD3 is an epigenetic modifier of chromatin, we assessed a panel of cell lines for expression of the two other chromatin modifiers present in the 8p11-p12 genomic region: KAT6A and ASH2L. RT-PCR revealed that, of the breast cancer cell lines, CAMA-1, SUM-52, and SUM-44 have the highest levels of KAT6A (Figure 2.3-F) and SUM-44 expresses the highest ASH2L protein levels, followed by SUM-52, CAMA-1, and MCF7 (Figure 3.1-A). Together, these data led to our hypothesis that these three 8p11-p12 amplicon oncogenes, ASH2L, KAT6A, and NSD3,



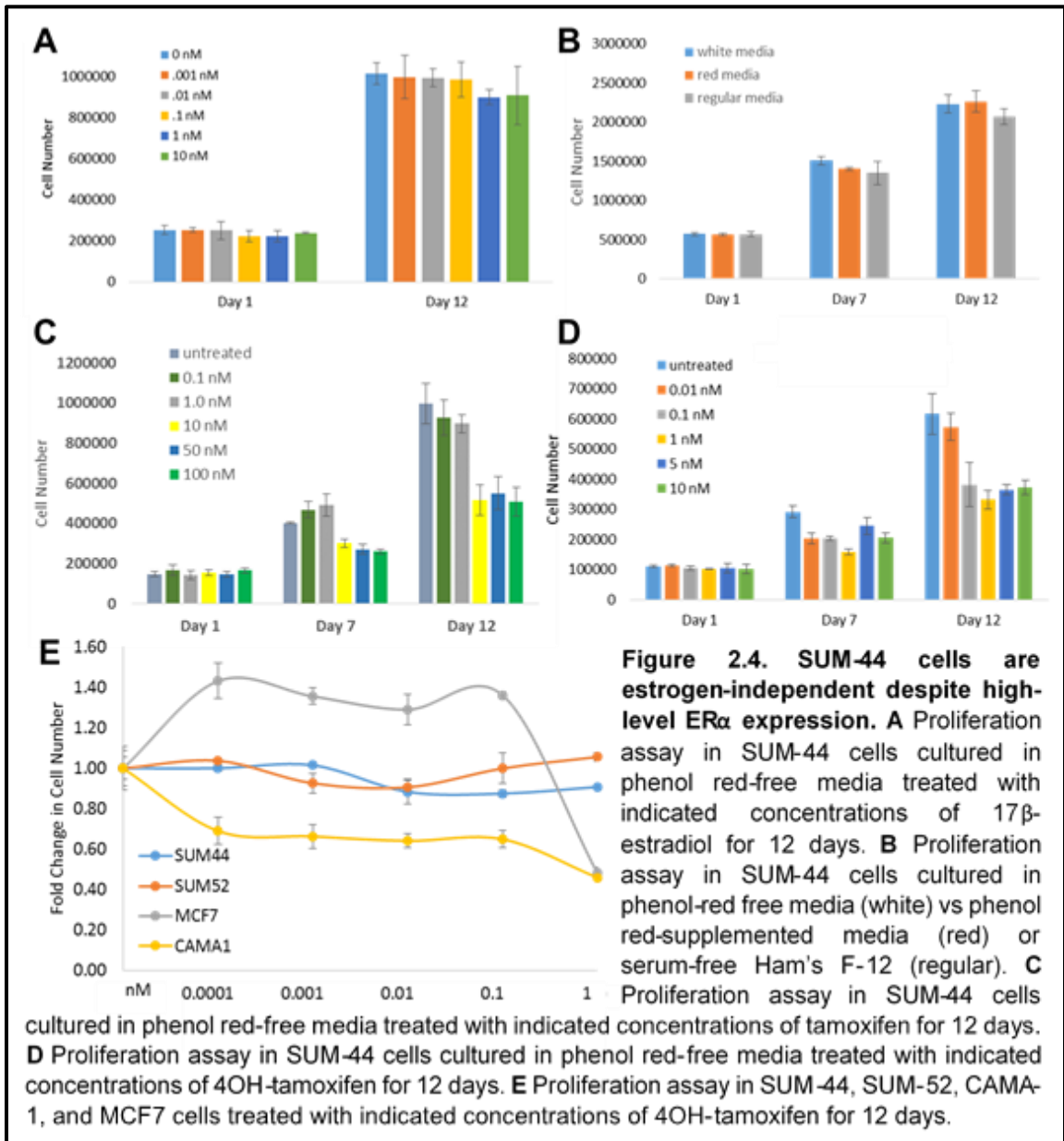
work cooperatively to promote tumorigenesis in luminal B breast cancer. This work discovered a clear link between NSD3 amplification and overexpression and overexpression of ER α in human breast cancer and identified SUM-44 as a unique model by which this patient group can be studied further.

2.4. SUM-44 cells are estrogen-independent despite high-level ER α expression.

Since SUM-44 cells have extremely high levels of ER α expression, we hypothesized that this line would be highly responsive to its mitogenic ligand, 17 β -estradiol, and highly sensitive to the SERM tamoxifen as this drug is used clinically to treat ER+ breast cancers. To test this hypothesis, we measured the proliferation of SUM-44 cells grown in phenol red-free media and treated with increasing doses of estrogen over 12 days and observed no difference in growth across these concentrations (Figure 2.4-A). Since SUM-44 cells are routinely grown in serum free, low phenol red media, we tested the effect of phenol red, often cited as having a stimulatory effect on ER α (Wesierska-Gadek *et al.* 2006), in this cell line using “white” phenol red-free, “red” phenol red-supplemented, and “regular” low phenol red Ham’s F-12 media. We observed no difference in cell growth due to the phenol red content of the media (Figure 2.4-B).

We next tested the effect of the SERM Tamoxifen on SUM-44 cells and, while higher concentrations of the drug did inhibit the growth of these cells, they were still able to proliferate and reached a plateau where increasing the amount of drug did not have a corresponding increase in response (Figure 2.4-C). We repeated this assay, performed in phenol red-free media, using 4OH-tamoxifen, the active metabolite of tamoxifen, and again observed a plateau in the proliferation response of this cell line (Figure 2.4-D). To

assess how this observation compared to other cell lines, we treated the 8p11-p12 amplicon-bearing lines SUM-52, SUM-44, and CAMA-1 as well as the amplicon-null MCF7 line with 4OH-tamoxifen and observed that SUM-44 cells had little response up to the 1 nM treatment dose, mirroring the ER-negative SUM-52 line rather than the tamoxifen-sensitive ER+ CAMA-1 line (Figure 2.4-E). Interestingly, 4OH-tamoxifen



elicited an agonistic effect on the ER+ MCF7 cell line before achieving antagonistic concentrations (Figure 2.4-E). These results are an important step toward understanding patients with highly ER+ tumors that do not respond to traditional endocrine therapies.

In addition to these findings, ER α chromatin immunoprecipitation and high-throughput sequencing (ChIP-seq) was performed in our laboratory (Irish *et al.* 2016). These data demonstrated that ER α maintained the ability to bind to chromatin without estrogen in SUM-44 cells. This work also showed that treatment with estrogen increased the number of peaks per gene and size of those peaks, indicating that these cells are capable of responding to estrogen, but no significant alterations of the interaction of ER α with the chromatin were observed in this context. Knockdown of NSD3-S abrogated the ability of ER α to bind to chromatin without estrogen, suggesting that the estrogen-independent activity of ER α is dependent upon NSD3. Based on these observations, we concluded that, despite high-level ER α expression, the SUM-44 cell line is independent of estrogen signaling for growth and survival.

2.5. SUM-44 cells are ER α -dependent.

One explanation for the estrogen-independent state of ER α in this model is that the receptor is no longer functional. Indeed, loss of ER α or its function is a known mechanism of endocrine resistance in ER+ human breast tumors (Kerdivel *et al.* 2013). Since we clearly demonstrate here that SUM-44 cells maintain ER α expression and previous characterization of this cell line detected wild-type ER α (Ethier 1996), we next sought to determine whether the receptor was functional in SUM-44 cells. Previously performed ChIP-seq experiments demonstrated that ER α is indeed capable of binding to chromatin without estrogen and ChIP-PCR validated enrichment of several important

ER α -target genes (Figure 2.5-A). Enrichment was enhanced by treatment with estrogen, again underscoring that this receptor maintains its normal structure and function. In MCF7 cells, there was no enrichment of target genes over negative control until estrogen was added. Interestingly, enrichment of the gene encoding the progesterone receptor (PR), an ER α pioneer factor associated with good prognosis genes that is lost in SUM-44 cells, was dramatically increased with estrogen treatment in MCF7 cells but not in SUM-44, further confirming that ER α is active in these cells but is behaving differently than in MCF7 cells (Mohammed *et al.* 2015). Indeed, ER α ChIP-seq in SUM-44 cells identified FOXA1 binding motifs in addition to estrogen response elements (ERE) (Irish *et al.* 2016), consistent with reports that alternative pioneer factors are involved in ER α -mediated gene transcription upon loss of PR (Ross-Innes *et al.* 2012).

To test the ability of ER α to alter the expression of target genes, we performed RT-PCR following siRNA-mediated knockdown of ESR1 or FOXA1. ER α target gene expression decreased with knockdown of both ESR1 and FOXA1 (Figure 2.5-C). When ESR1 was knocked down using three different shRNA constructs, MCF7 cells demonstrated reduced proliferation while SUM-44 cells were unable to survive or proliferate (Figure 2.5-D), suggesting that SUM-44 cells are highly dependent on ER α for growth and survival. Array analysis following knockdown of either NSD3-S or ESR1 revealed that the top-scoring biological processes of the genes affected by knockdown of both ESR1 and NSD3-S are related to cell cycle regulation and DNA replication (Table 2.2; Appendix A). Together, these data demonstrate that SUM-44 cells are highly dependent on ER α signaling for growth, survival, and gene transcription. We conclude

that ER α is active in an estrogen-independent manner in the 8p11-p12-amplified SUM-44 cell line.

Since the SUM-44 cell line represents the group of patients who respond poorly to AIs and SERMs yet maintain high-level ER α expression, we tested the sensitivity of this cell line to the SERD Fulvestrant. At increasing doses of drug, we observed corresponding decreasing levels of ER α expression and proliferation of the cells (Figure 2.5-E). When this response was compared to other cell lines, we noted that SUM-44 cells are not as sensitive as the other ER+ MCF7 and CAMA-1 cell lines (Figure 2.5-F). Since the mechanism of action of the SERD compounds is dose-dependent and directly proportional to the ability of the drug to degrade the receptor, it is expected that a cell

Table 2.2. Biological processes to which genes with altered expression following knockdown of NSD3-S and ESR1 were annotated. Top scoring biological processes and corresponding p-values in common between NSD3-S and ESR1 knockdown microarrays in SUM-44 cells.

| Biological Process | P-value |
|---|----------|
| Mitotic cell cycle | 1.00E-24 |
| Cell Cycle | 1.00E-24 |
| Mitotic cell cycle process | 1.00E-24 |
| DNA metabolic process | 1.00E-24 |
| Cell cycle process | 1.00E-24 |
| Mitotic nuclear division | 1.60E-22 |
| Organelle fission | 9.30E-22 |
| Nuclear Division | 1.00E-21 |
| Organelle organization | 1.20E-21 |
| DNA replication | 4.40E-21 |
| Cell division | 4.70E-21 |
| Mitotic cell cycle phase transition | 1.50E-20 |
| Cell cycle phase transition | 2.80E-20 |
| DNA strand elongation | 8.80E-19 |
| DNA strand elongation involved in DNA replication | 8.90E-19 |

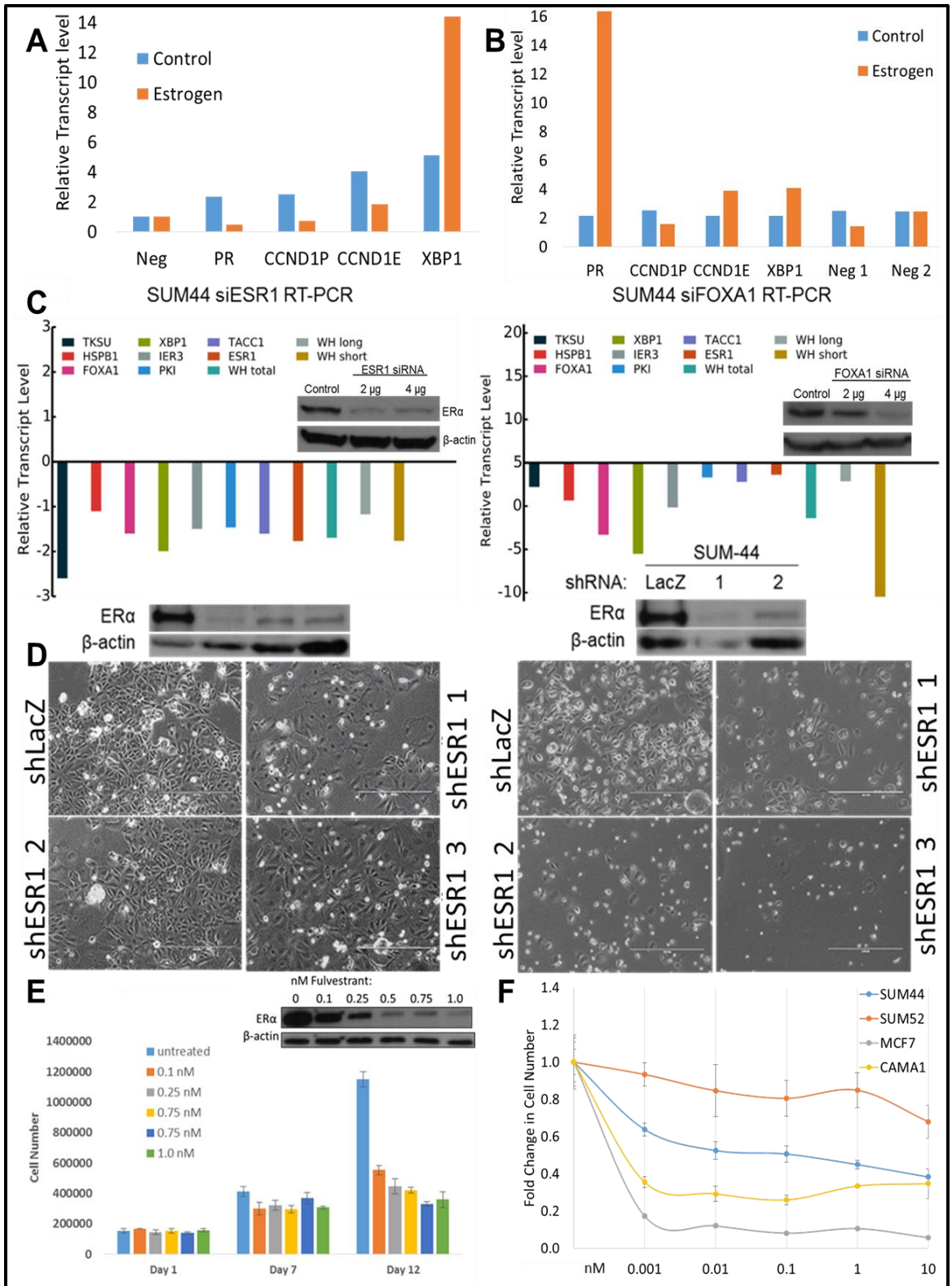
line such as SUM-44, which has the highest ER α expression of the cell lines tested (Figure 2.3-A), would appear to be resistant to fulvestrant due to the increased requirement to achieve effective dose.

This is an important finding for breast cancer patients who fall into this subtype of cancer and provides foundational evidence for the 8p11-p12 amplicon as a marker for those patients who would benefit from addition of a SERD therapy to their AI/SERM regimen. These findings also underscore the need for development of additional SERD compounds that can achieve adequate degradation of ER α without subjecting patients to intolerable adverse effects.

2.6. Summary

Together, these data demonstrate that amplification and subsequent overexpression of the NSD3 oncogene results in overexpression of the transcription factor ER α . Under these circumstances, the receptor is activated in an estrogen-independent manner, rendering traditionally-used endocrine therapies, such as Tamoxifen, ineffective. These cells do, however, respond to the SERD Fulvestrant, but require high-dose treatment for adequate degradation of ER α . These data provide rationale for continued SERD development and offer a foundation for implementation of these types of therapies in patients using the 8p11-p12 amplicon and NSD3 overexpression as a biomarker. Further investigation is required to elucidate the mechanism of NSD3-induced overexpression and activation of ER α , which could provide additional therapeutic strategies to combat endocrine-resistant breast cancer.

Figure 2.5. SUM-44 cells are ER α -dependent. **A** ER α ChIP-PCR in SUM-44 cells after treatment with 17 β -estradiol for 6 hours. **B** ER α ChIP-PCR in MCF7 cells after treatment with 17 β -estradiol for 6 hours. **C** Immunoblot (inset) for protein expression and RT-PCR for transcript expression of selected ER α -target genes following siRNA-mediated knockdown of ESR1 (left) or FOXA1 (right) in SUM-44 cells. **D** Immunoblot for ER α expression (upper) and corresponding cell photographs (lower) following shRNA-mediated knockdown of LacZ control or ESR1 by three different shRNA constructs in MCF7 (left) and SUM-44 (right) cells. **E** Proliferation assay in SUM-44 cells treated with indicated concentrations of fulvestrant for 12 days with corresponding immunoblot demonstrating dose-dependent degradation of ER α (inset). **F** Proliferation assay in SUM-44, SUM-52, CAMA-1, and MCF7 cells treated with indicated concentrations of fulvestrant for 12 days. (Figure on page 69).



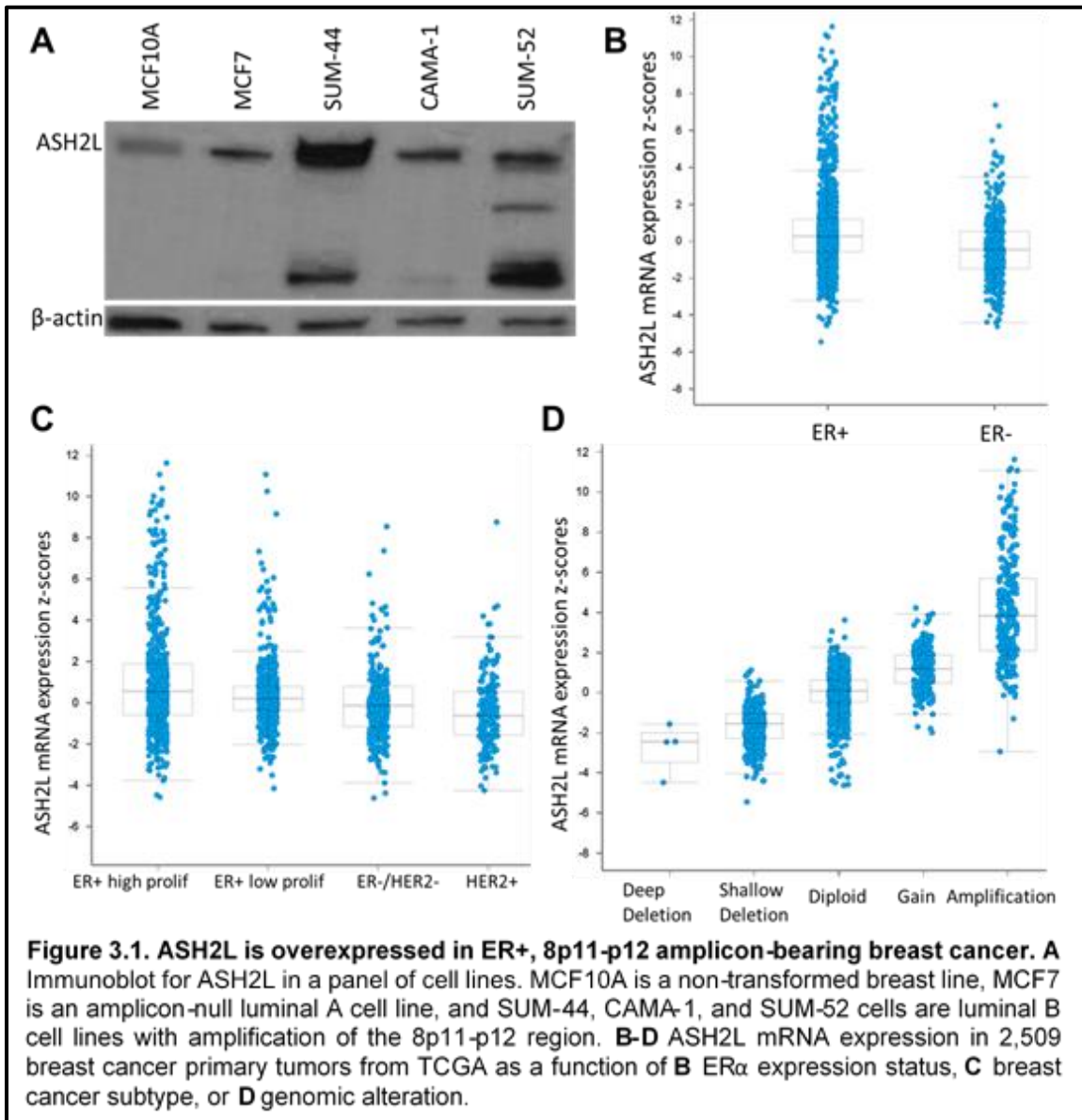
CHAPTER 3: ASH2L regulates gene expression via H3K4me3 in promoters and knockdown of ASH2L reduces expression of NSD3, ER α , and other genes important in cell proliferation processes.

3.1. ASH2L is overexpressed in ER+, 8p11-p12 amplicon-bearing breast cancer.

ASH2L (Absent, Small, or Homeotic disc 2-Like) is a chromatin-modifying factor located in the 8p11-p12 genomic region and is amplified in approximately 12% of breast cancers (TCGA). In a panel of breast cancer cell lines, ASH2L is overexpressed to varying degrees compared to the non-transformed MCF10A breast cell line (Figure 3.1-A). Of note, ASH2L is known to have two isoforms expressed in human tissues and multiple bands observed in ASH2L immunoblots suggest the presence of at least one other ASH2L isoform expressed in the amplicon-bearing SUM-44, CAMA-1, and SUM-52 cell lines (Figure 3.1-A). This possibility was not explored further and only the highest molecular weight ASH2L isoform was pursued in this study as this is the major isoform.

According to TCGA, ASH2L mRNA expression is higher in clinically-defined ER+ breast tumors compared to ER-negative tumors (Figure 3.1-B). Similarly, mRNA expression is greatest in the TCGA-defined highly proliferative subgroup of ER+ breast tumors as compared to low proliferation ER+, ER-negative, and HER2-amplified tumors (Figure 3.1-C). Amplification of ASH2L is highly correlated with overexpression at the message level (Figure 3.1-D), consistent with our observations at the protein level by immunoblot in cell lines with ASH2L amplification (Figure 3.1-A), as well as several large-scale studies of the 8p11-p12 amplicon which identified ASH2L as one of the candidate oncogenes where amplification is well-correlated with overexpression. These studies suggest ASH2L as a potential driving oncogene from this genomic region, but it remains understudied in breast cancer.

ASH2L is implicated in the tumorigenesis of osteosarcoma, glioma, and leukemia and is known to be primarily involved in tri-methylation of lysine (K) 4 on histone H3 (H3K4me3) by interacting with binding partners, such as WDR5, RbBP5, DPY-30, and MLL proteins, which are SET domain-containing histone methyltransferases (HMTs) (Dou *et al.* 2006). ASH2L has demonstrated HMT activity on H3K4 as a heterodimer with RbBP5 even without a SET domain-containing collaborator and is part of all known



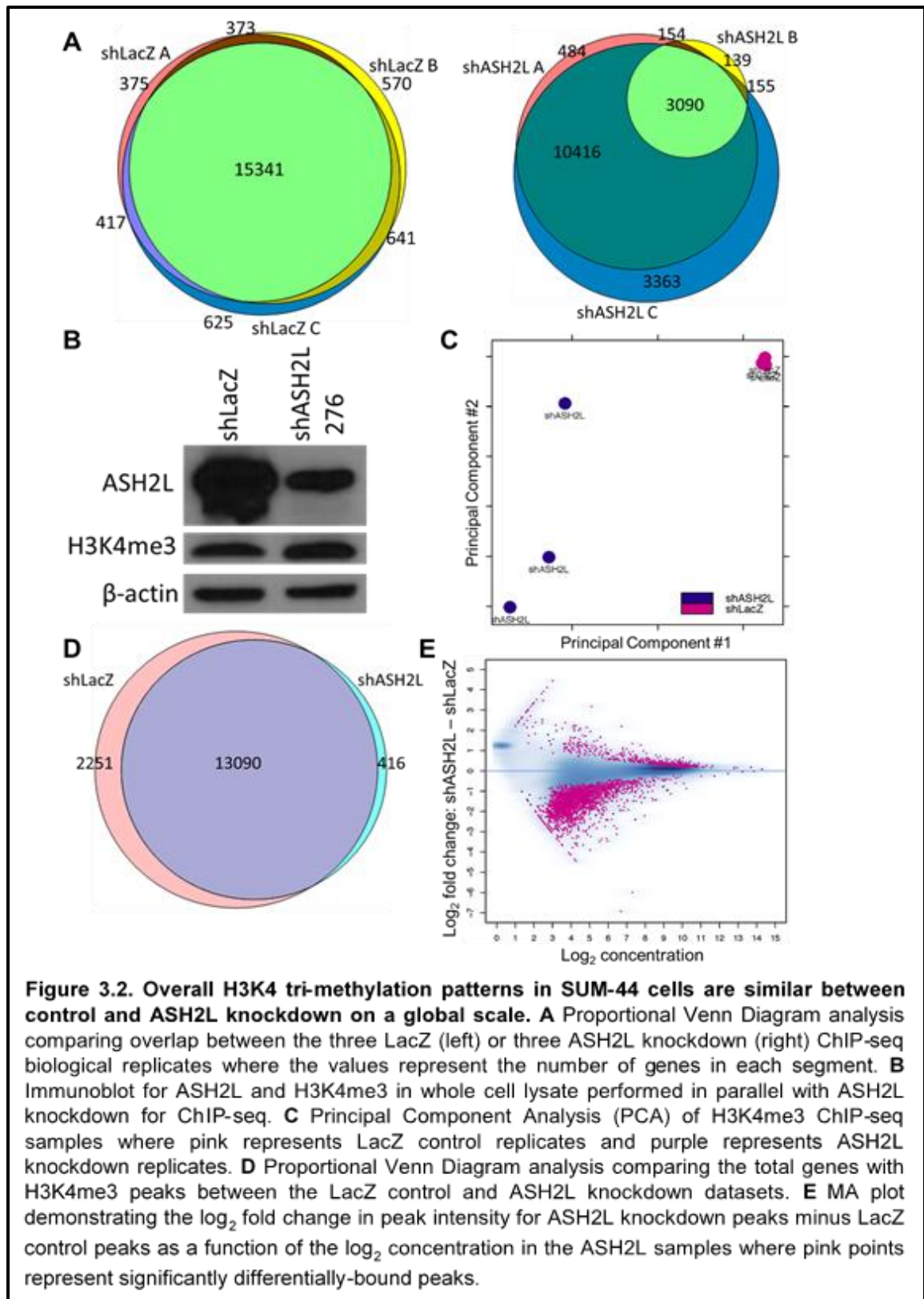
H3K4 HMT complexes characterized to date (Butler *et al.* 2017). As such, we sought to determine the influence of ASH2L on the H3K4me3 status in a luminal B breast cancer model. We selected the SUM-44 cell line, in which ASH2L is amplified and overexpressed to the highest degree of the cell lines tested (Figure 3.1-A).

3.2. Overall H3K4 tri-methylation patterns in SUM-44 cells are similar between control and ASH2L knockdown on a global scale.

To assess the influence of ASH2L overexpression on H3K4 tri-methylation, we performed chromatin immunoprecipitation and high throughput sequencing (ChIP-seq) utilizing an H3K4me3 antibody following shRNA-mediated knockdown of ASH2L or LacZ control in SUM-44 cells. Three biological replicates for each of shLacZ control and shASH2L were performed, designated A, B, and C. Quality control measures can be found in Appendix B and complete gene lists and peak data can be found in Appendix C. Sequences were aligned and annotated and the overlap between these annotated gene names corresponding to peaks called for the replicates was analyzed by Venn Diagram comparison (Figure 3.2-A). Similar numbers of peaks were called across the three LacZ control replicates with near complete overlap, corresponding to 15,341 genes with H3K4me3 enrichment in common. Overlap between ASH2L knockdown replicates A and C was also nearly identical with peaks called in a similar number of genes, both to each other as well as the shLacZ samples. Replicate B of the ASH2L knockdown group demonstrated overall poor enrichment for H3K4me3 in the paired ChIP versus input samples (Appendix B), and thus a much smaller number of genes were called in this sample. Nevertheless, the degree of overlap of this gene set with the other two ASH2L knockdown replicates was high. Due to the discrepancy in enrichment in this ChIP compared to the other two, accepting only the genes enriched in all three replicates would erroneously suggest that overall H3K4me3 levels were reduced by ASH2L

knockdown. However, western blot analysis of whole cell lysates isolated in parallel with these CHIP samples indeed showed that global levels of H3K4me3 were not reduced by knockdown of ASH2L (Figure 3.2-B). Principal component analysis also demonstrated the very close similarity between the LacZ control replicates and relative variability in the ASH2L knockdown replicates, confirming the observations by the Venn Diagram-style comparisons of annotated gene names (Figure 3.2-C). Based on these data, the genes were summed across the three replicates within each shRNA type for further analysis.

To determine the set of genes with reduced H3K4me3 enrichment due to knockdown of ASH2L, the LacZ control gene set was compared to that of the ASH2L knockdown group (Figure 3.2-D; Appendix D). We had hypothesized that there would be a significant proportion of genes with decreased enrichment of H3K4me3 upon knockdown of ASH2L, corresponding to the far left segment of the Venn Diagram in Figure 3.2-D, which represents the genes with peaks called in the LacZ control but not ASH2L knockdown group. While 2,251 genes do indeed fall into this category, the vast majority (13,090) of genes demonstrated enrichment in common between LacZ control and ASH2L knockdown. Since this Venn Diagram strategy of comparison employed a binary, presence or absence assessment of the two gene sets, differences in peak concentration between the two conditions were not taken into account. Analysis of the \log_2 fold change between the ASH2L knockdown and LacZ groups as a function of the \log_2 concentration of each sequence represented did indeed show that overall H3K4me3 enrichment was reduced following knockdown of ASH2L (Figure 3.2-E). These data demonstrate that knockdown of ASH2L does reduce the robustness of H3K4me3 peaks, but does not cause them to completely disappear. This is likely due to residual



expression of ASH2L in the knockdown samples (Figure 3.2-B). The implications of this scenario on gene transcription are unknown.

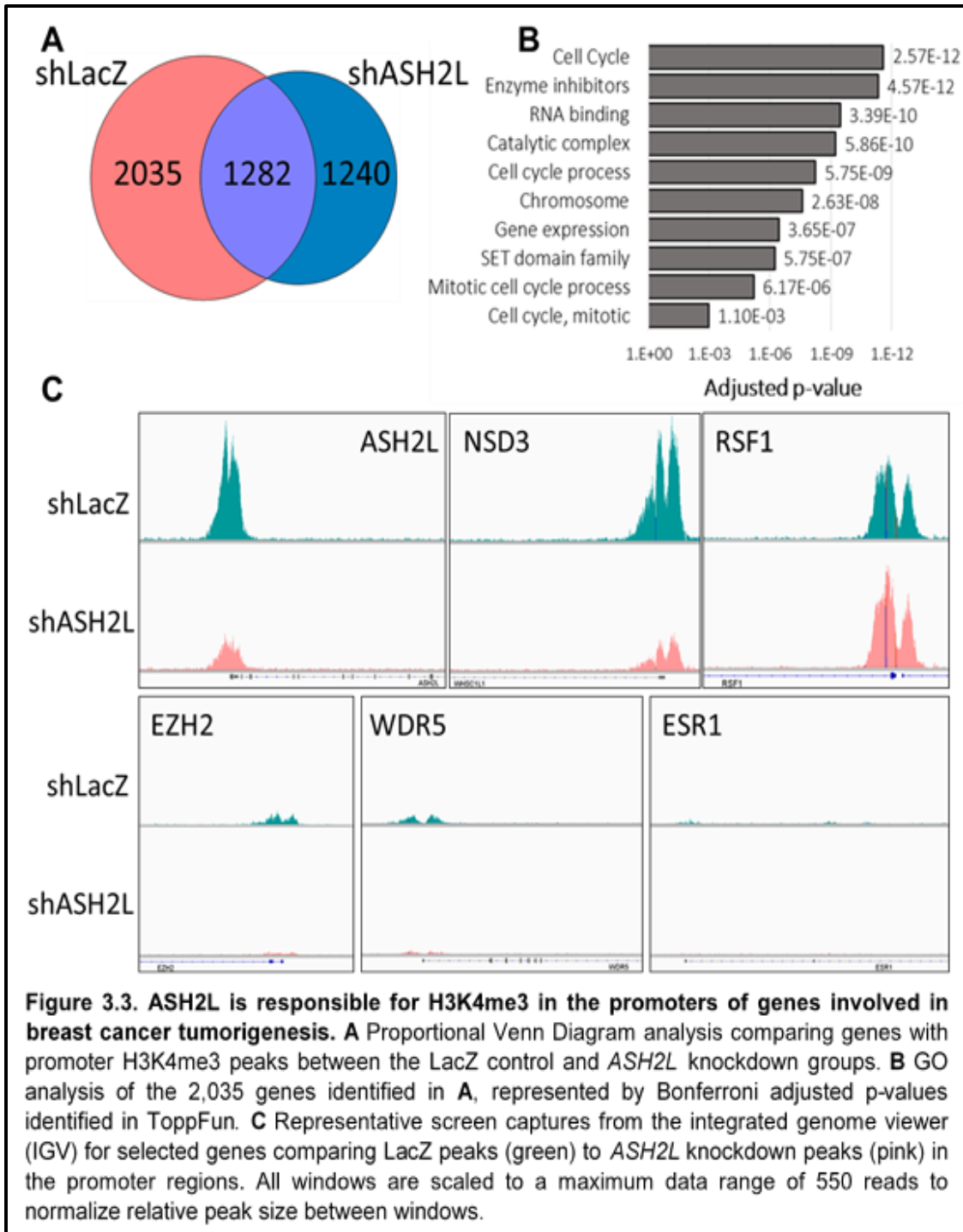
Together, the results of the ChIP analysis demonstrated that knockdown of ASH2L reduced the size of H3K4me3 peaks in SUM-44 cells, but the number of peaks and the overall distribution of H3K4 tri-methylation between control and ASH2L knockdown groups was largely unchanged. This observation was in contrast to our original hypothesis that knockdown of ASH2L would reduce global patterns of H3K4me3 in SUM-44 cells. Instead, we discovered that H3K4me3 peaks are similar between control and ASH2L knockdown, which then led us to the hypothesis that ASH2L may play a role in H3K4 tri-methylation in a more specific set of genes.

3.3. ASH2L is responsible for H3K4me3 in the promoters of genes involved in breast cancer tumorigenesis.

H3K4me3 is known to be most abundant in the 5' proximal promoter regions of actively transcribed genes (Demers *et al.* 2007, Luscher-Firzlaff *et al.* 2008). Similarly, ASH2L has been shown to be confined to these regions as well (Demers *et al.* 2007). In order to identify the specific gene set with ASH2L-regulated H3K4me3 peaks, we sorted the overall peak data sets by detailed annotation and isolated the peaks with promoter annotations only. Promoter H3K4me3 peaks were found in 3,317 genes from the LacZ group and 2,522 genes from the ASH2L knockdown group. Comparison between the two gene sets identified 2,035 genes that lose H3K4 tri-methylation following knockdown of ASH2L and are therefore found uniquely in the LacZ control gene set (Figure 3.3-A). These genes annotate primarily to cell cycle processes by ToppFun analysis (Figure 3.3-B and Appendix E). Somewhat unexpectedly, there were also a significant number of genes (1,240) with promoter H3K4 tri-methylation that demonstrated enrichment upon

ASH2L knockdown only. This is especially interesting since ASH2L is tightly and specifically linked to H3K4me3 and may indicate that another HMT gains H3K4 trimethylation ability in the context of 8p11-p12 amplification in breast cancer.

Several interesting patterns emerged upon closer inspection of the 2,035 genes that lost H3K4me3 enrichment following ASH2L knockdown. Twelve of the 21 candidate oncogenes from the 8p11-p12 amplicon region are contained in this 2,035 gene set, including ADAM9, ASH2L, DDHD2, DUSP4, FGFR1, IKBKB, LSM1, PLEKHA2, POMK, SMIM19, UBXN8, and WHSC1L1 (NSD3), and thus we predict have increased H3K4me3 in their promoter regions due to ASH2L overexpression when the amplicon is present. These genes have some of the strongest peak scores and most have multiple peaks called in their promoter region in the shLacZ control group but do not have any peaks called in the ASH2L knockdown group (Table 3.1). Examination of the peaks in the integrated genome viewer (IGV) demonstrated the robust nature of the promoter H3K4me3 peaks in these genes, including WHSC1L1 (NSD3) and ASH2L itself, as opposed to other significant genes identified in this dataset, such as EZH2 and WDR5 (Figure 3.3-C). RSF1 was included here to illustrate the dramatic decrease in peak size in the promoter peaks of NSD3 and ASH2L upon ASH2L knockdown since RSF1 was not identified as differentially regulated between control and ASH2L knockdown datasets. ESR1 was included here to demonstrate negative CHIP data as neither the control nor ASH2L knockdown samples identified H3K4me3 peaks at the ESR1 gene promoter. These data highlight the cooperative nature of this amplicon and suggest that ASH2L may be involved in generating a positive feedback loop of active transcription of amplicon genes.



In addition to the 8p11-p12 amplicon genes listed above, several important epigenetic regulators were identified in this 2,035 gene set (Table 3.1). As mentioned,

the other oncogenic 8p11-p12 amplicon HMT NSD3 was found in this set, as was EZH2, the major HMT of the polycomb group complexes that are antagonized by trithorax group proteins such as ASH2L. The ASH2L sub-complex member WDR5 appeared here, as did KMT2B (MLL4), one of the SET domain-containing enzyme family that is activated by ASH2L to generate H3K4me3. These data again suggest that knockdown of ASH2L breaks several positive feedback loops in which it participates to maintain active transcription via chromatin remodeling. While the loss of H3K4me3 peaks upon ASH2L knockdown provides some insight into the genes that may be under epigenetic control of this oncogene, this dataset does not provide information regarding the transcriptional effect that loss of this histone modification induces. Therefore, additional exploration of the effects of ASH2L knockdown on the transcriptome was carried out.

3.4 ASH2L knockdown reduces expression of genes with decreased promoter H3K4me3 levels.

To determine the influence of ASH2L knockdown on gene expression, total RNA was harvested and sequenced in triplicate following ASH2L knockdown using two different shRNA constructs in SUM-44 cells. The resulting datasets (Appendix F) were compared to RNA-seq from shLacZ control triplicate samples run in parallel. We identified 6,473 genes downregulated in common between control and ASH2L knockdown with the ASH2L 275. We similarly identified 5,766 genes downregulated in common between control and knockdown with the ASH2L 276 construct. We used a false discovery rate (FDR) cutoff of 0.4 for this analysis, a measure of the probability of type I error, in this case the assumption that these genes were significantly differently expressed from control when they actually were not. To increase statistical stringency, we next compared the differentially expressed genes from the two ASH2L shRNA constructs compared to control and identified 3,278 genes that were downregulated in

Table 3.3: Selected genes with promoter H3K4me3 peaks unique to shLacZ ChIP-seq samples. Known processes or associations of the gene are described and the average peak score of promoter region peaks, log₁₀ p-value, and log₁₀ q-value are reported for each gene.

| Gene Name | Description | Peak Score | log ₁₀ p-value | log ₁₀ q-value |
|----------------|---|------------|---------------------------|---------------------------|
| DDHD2 | 8p11-p12 amplicon gene | 1548 | 165.33 | 161.63 |
| LSM1 | 8p11-p12 amplicon gene | 1483 | 163.67 | 160.04 |
| ASH2L | 8p11-p12 amplicon gene | 1284 | 151.53 | 148.00 |
| FGFR1 | 8p11-p12 amplicon gene | 1420 | 145.81 | 142.05 |
| WHSC1L1 (NSD3) | 8p11-p12 amplicon gene | 1405 | 144.25 | 140.51 |
| ADAM9 | 8p11-p12 amplicon gene | 1024 | 109.46 | 106.39 |
| CCNE2 | cell cycle regulation | 889 | 99.71 | 96.84 |
| PLEKHA2 | 8p11-p12 amplicon gene | 748 | 86.65 | 83.86 |
| CDK6 | cell cycle regulation | 649 | 76.49 | 73.85 |
| NCOA7 | transcription-associated factor | 574 | 73.66 | 71.05 |
| BRD2 | chromatin-associated factor | 657 | 70.71 | 68.13 |
| IKBKB | 8p11-p12 amplicon gene | 579 | 68.71 | 66.14 |
| WDR5 | ASH2L binding partner | 476 | 43.78 | 41.35 |
| IRX2 | embryogenesis | 482 | 54.34 | 51.91 |
| FGFR4 | cell signaling pathway | 441 | 51.58 | 49.16 |
| UBE2C | associated with tamoxifen resistance | 485 | 51.04 | 48.52 |
| EZH2 | polycomb group HMT | 482 | 50.68 | 48.28 |
| POMK | 8p11-p12 amplicon gene | 465 | 49.00 | 46.50 |
| ASF1B | associated with tamoxifen resistance | 369 | 46.63 | 42.27 |
| RECQL4 | transcription-associated factor | 440 | 46.54 | 44.09 |
| SMIM19 | 8p11-p12 amplicon gene | 360 | 41.93 | 39.63 |
| AURKA | cell cycle regulation | 392 | 41.67 | 39.26 |
| PIK3CA | cell signaling pathway | 345 | 41.51 | 39.19 |
| SETD2 | HMT (SET family) | 388 | 41.35 | 39.03 |
| KMT2B (MLL4) | ASH2L binding partner, HMT (SET family) | 347 | 38.48 | 36.18 |
| UBXN8 | 8p11-p12 amplicon gene | 318 | 38.43 | 36.13 |
| DUSP4 | 8p11-p12 amplicon gene | 353 | 37.77 | 35.40 |

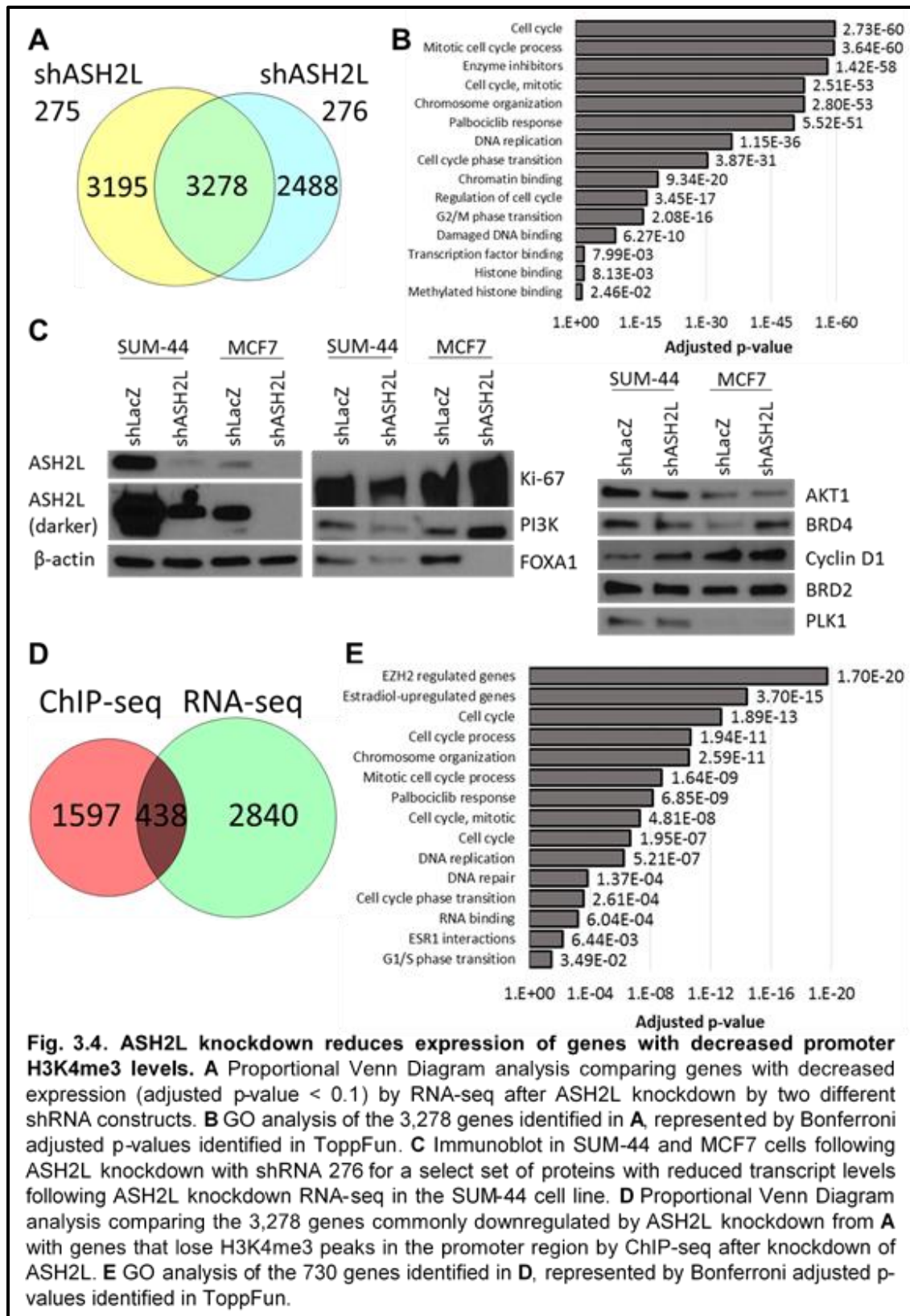
common between them (Figure 3.4-A; Table 3.2; Appendix G). In order to assess the biological processes affected by this suite of genes, we performed ToppFun analysis on the 3,278 genes and discovered that they are involved in cell cycle regulation, DNA replication, and chromatin organization (Figure 3.4-B). These results are consistent with previously implicated functions of ASH2L. We validated knockdown of several of these genes by immunoblot, including Ki-67, PI3K, and FOXA1 (Figure 3.4-C). Expression of

Table 3.4: Selected genes commonly downregulated between shASH2L 275 and shASH2L 276 in SUM-44 cells. Known processes or associations of the gene are described and log₂ fold change from shLacZ control and associated p-value and adjusted p-value are reported for each of the two shRNA constructs.

| Description | shASH2L 275 | | shASH2L 276 | |
|---|------------------------------|------------|------------------------------|-----------|
| | log ₂ fold change | p-value | log ₂ fold change | p-value |
| H3K4me3 (activating) | -4.33 | <1.05E-305 | -2.65 | <2.92E-74 |
| Luminal B marker | -1.74 | <1.05E-305 | -0.88 | 2.92E-74 |
| Transcription-associated, tamoxifen resistance | -1.92 | <1.05E-305 | -0.55 | 1.31E-45 |
| Transcription factor | -1.78 | 1.05E-305 | -0.49 | 4.62E-41 |
| Luminal B marker, transcription factor, ER α -associated | -1.50 | 6.65E-198 | -0.51 | 3.61E-09 |
| Cell cycle regulation | -1.46 | 3.50E-137 | -0.75 | 4.35E-36 |
| Cell cycle regulation, tamoxifen resistance | -1.09 | 2.83E-112 | -0.47 | 3.93E-27 |
| Cell cycle regulation | -0.57 | 4.71E-80 | -0.12 | 1.09E-04 |
| Luminal B marker, transcription factor, ER α -associated | -0.73 | 1.37E-73 | -0.27 | 8.91E-16 |
| H3K37me3 (repressive) | -0.87 | 9.83E-71 | -0.54 | 4.95E-24 |
| Transcription factor | -0.68 | 8.73E-54 | -0.73 | 4.65E-10 |
| Transcription factor | -0.74 | 1.45E-50 | -0.07 | 6.86E-02 |
| Cell cycle regulation, tamoxifen resistance | -0.62 | 1.50E-32 | -0.59 | 2.95E-07 |
| Transcription factor | -0.47 | 2.94E-26 | -0.32 | 6.74E-15 |
| Luminal B marker, proliferation | -1.01 | 8.32E-20 | -0.71 | 5.30E-06 |
| Cell cycle regulation, ER α -associated | -0.47 | 9.47E-19 | -0.37 | 1.24E-02 |
| 8p11-p12 amplicon gene | -0.25 | 1.39E-14 | -0.50 | 6.47E-58 |
| Cell cycle regulation | -0.28 | 1.80E-12 | -0.14 | 1.75E-05 |
| 8p11-p12 amplicon gene; Histone acetyltransferase | -0.25 | 1.94E-08 | -0.12 | 5.86E-03 |
| ASH2L binding partner | -0.31 | 3.97E-07 | -0.33 | 1.52E-09 |
| 8p11-p12 amplicon gene; H3K36me2 (activating) | -0.18 | 4.69E-06 | -0.22 | 6.97E-09 |
| H3K36me3 (activating) | -0.19 | 2.35E-04 | -0.17 | 8.09E-04 |
| Bromodomain protein | -0.10 | 4.15E-03 | -0.42 | 5.65E-42 |
| | | | | 1.57E-40 |

these genes did decrease upon knockdown of ASH2L in SUM-44 cells but had varied changes in expression in MCF7 cells, in which ASH2L is not amplified and its expression is much lower than in SUM-44 cells. These data validate the RNA-seq results and confirm that knockdown of ASH2L reduces gene expression. Interestingly, several of the genes with reduced transcript expression following ASH2L knockdown RNA-seq analysis did not demonstrate reduced protein levels (Figure 3.4-C), suggesting a disconnect between transcript- and protein-level expression for a subset of ASH2L-regulated genes.

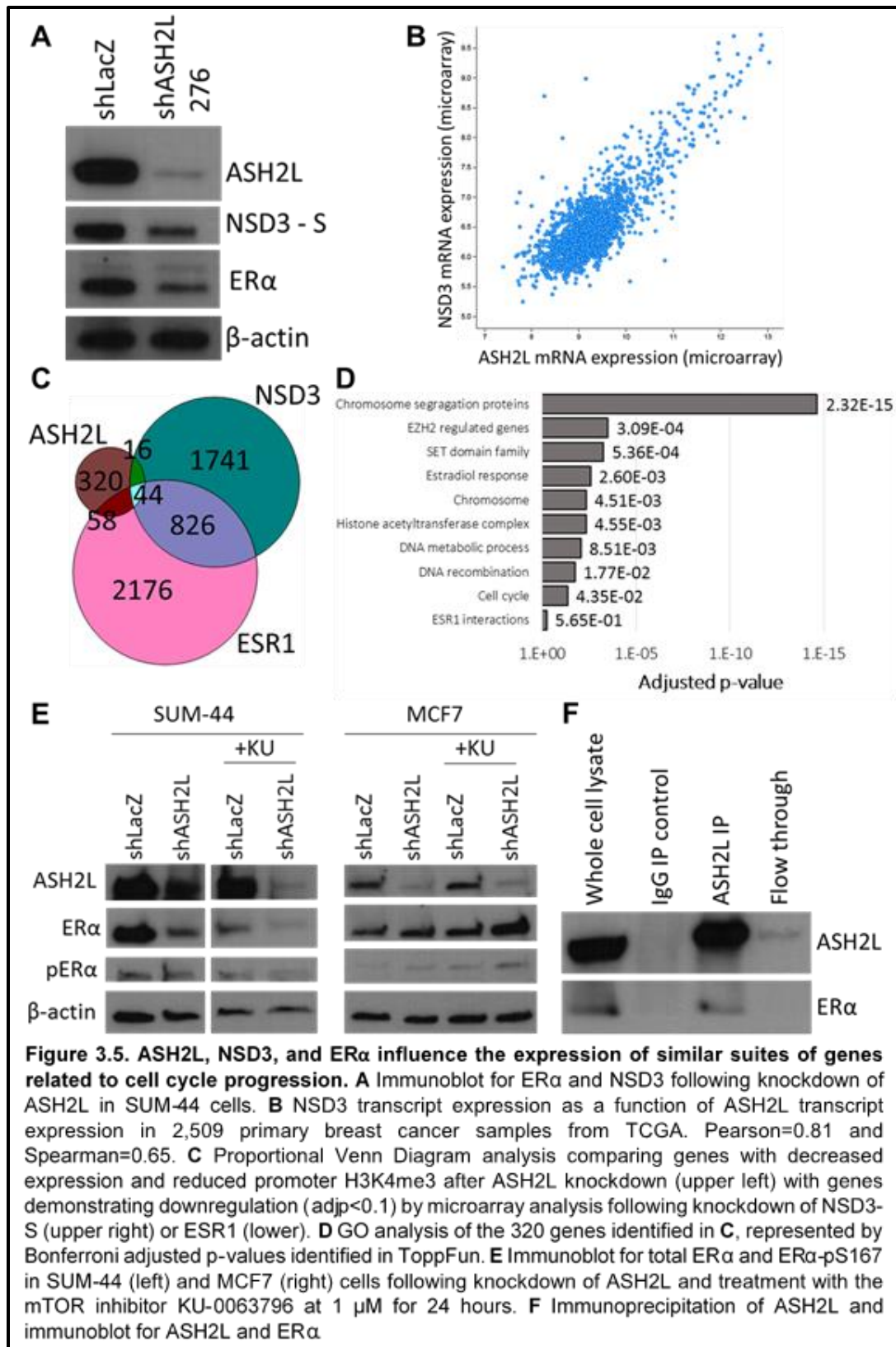
In order to determine which of the genes with decreased H3K4me3 promoter peaks in ASH2L knockdown cells also demonstrated decreased expression upon knockdown of ASH2L, the 3,278 genes downregulated in common between both ASH2L knockdown constructs compared to control were then cross-referenced with the 2,035 genes that lost H3K4me3 peaks after knockdown of ASH2L. This strategy identified 438 genes with coordinated decreased expression and H3K4me3 peak loss (Figure 3.4-D). ToppFun analysis of this set of genes assigned many of the same processes and pathways as the RNA-seq gene set alone, including palbociclib response, cell cycle processes, and chromosome organization (Figure 3.4-E and Appendix H). This gene set, however, was also assigned to several additional processes and pathways, such as genes that are upregulated in MCF7 cells upon treatment with estradiol, proteins that interact with ESR1/ER α , DNA and RNA binding, and histone methyltransferase activity. Together, these results demonstrate that ASH2L regulates H3K4me3 in the promoter regions of important genes related to breast cancer, primarily related to cell cycle and chromatin modification, and some of these genes are downregulated at the transcript and protein level as a result.



3.5 ASH2L, NSD3, and ER α influence the expression of similar suites of genes related to cell cycle progression.

The 438 genes identified in the previous section as downregulated upon loss of promoter H3K4me3 due to ASH2L knockdown were also implicated in ESR1 interactions and response to estradiol (Figures 3.4-D and 3.4-E; Appendix H). Given these results, the inclusion of NSD3 in this group of 438 ASH2L-regulated genes, and the link between NSD3 overexpression and estrogen-independent activation of ER α (see Chapter 2), we hypothesized that ASH2L is responsible for promoter H3K4me3-mediated NSD3 overexpression in the context of amplification of these two oncogenes, thus influencing ER α expression and activity and perpetuating the alterations to the transcriptome in the setting of 8p11-p12 amplified breast cancer. Knockdown of ASH2L resulted in reduced protein expression of NSD3 and ER α in SUM-44 cells (Figure 3.5-A), supporting the hypothesis that these three factors are cooperating to alter transcription in luminal B breast cancer models. Additionally, preliminary evidence in support of this hypothesis from TCGA demonstrates that ASH2L and NSD3 overexpression at the transcript level is highly correlated in a cohort of 2,509 primary breast tumors, with a Pearson correlation score of 0.81 and Spearman rank of 0.65 (Figure 3.5-B).

To test this hypothesis further, we compared the 438 genes with reduced H3K4me3 and expression upon ASH2L knockdown with genes that were downregulated upon ESR1 or NSD3-S knockdown using a p-value cutoff of 0.1 (Figure 3.5-C). In this analysis, 320 genes were unique to the ASH2L knockdown H3K4me4 ChIP-seq/RNA-seq downregulated group. We ran ToppFun analysis on this set of 320 genes and discovered they align with processes primarily involved in DNA repair and chromosome organization. (Figure 3.5-D and Appendix I). Interestingly, “ESR1 interactions” was



identified as a significant process ascribed to the 320 genes regulated by ASH2L, indicating that the group of genes under ASH2L transcriptional regulation are ER α - interacting proteins. As expected, these genes include chromatin remodeling enzymes and factors associated with transcription, such as TOPBP1, ZNF131, SMARCE1, TADA3, and several ribosomal proteins. PIK3CA also appears in this set of 320 genes, and the PI3K/AKT/mTOR pathway is known to play a role in activation of ER α via phosphorylation of S167 of the ER α protein. Treatment of LacZ control or ASH2L knockdown SUM-44 cells with 1 μ M of the mTOR inhibitor KU-0063794 for 24 hours did not reduce ER α -pS167 levels in SUM-44 or MCF7 cells, however (Figure 3.5-E). ASH2L and its sub-complex binding partner WDR5 are included in the list of genes that annotate in ToppFun to ESR1 interactions, suggesting that these proteins themselves may cooperate with ER α . ASH2L immunoprecipitation (IP) followed by ER α blotting identified a possible interaction between these two proteins (Figure 3.5-F). Although the MLL proteins are known to bind to ER α , this is the first study to provide evidence that ASH2L and ER α may directly interact and this possibility should be explored further.

From the overlapping gene sets in Figure 3.5-C, the 58 genes commonly downregulated by ASH2L and ESR1 knockdown were primarily involved in the cell cycle and estradiol-regulated processes. The 16 genes commonly downregulated by ASH2L and NSD3 knockdown were involved in processes having to do with transcription and chromatin/DNA interactions (data not shown). We have previously analyzed the overlap between ESR1 and NSD3 function (Chapter 2; (Irish *et al.* 2016)). Since the set of genes here is specifically those which were found to be downregulated by microarray analysis ($p < 0.1$), we analyzed these genes by ToppFun and found that they annotate to

processes similar to what we previously reported, including cell cycle and estradiol-mediated processes (data not shown).

3.6 Knockdown of ASH2L results in decreased proliferation and clonogenicity in luminal B breast cancer and reduces sensitivity to palbociclib.

Since ASH2L knockdown reduces expression of NSD3 and ER α , we hypothesized that ASH2L indirectly mediates the expression of the genes regulated by these two factors. The H3K4me3 ChIP-seq data indicated that ASH2L directly affects epigenetic regulation of NSD3 but not ESR1 (Figure 3.3-C) and we already validated the causal relationship between knockdown of NSD3 and decreased ER α expression (Chapter 2), so it is possible that the downregulation of these two factors occurs sequentially following knockdown of ASH2L. To test this hypothesis, whole cell lysate was harvested from SUM-44 cells at 5, 7, 11, and 14 days following infection with ASH2L-specific or LacZ control shRNA vectors and probed for ASH2L, NSD3, and ER α protein expression (Figure 3.6-A). Although previous immunoblots for these proteins performed as knockdown validation steps for other experiments indicated that the reduction in NSD3 expression may precede that of ER α , and that shRNA-mediated NSD3 knockdown-induced reduction in ER α expression takes approximately seven days, this more controlled test did not reproduce the temporal aspect of ASH2L knockdown-mediated reduction of NSD3 and ER α expression.

Some of the 44 genes shown in Figure 3.5-C derived by comparison of the ASH2L knockdown H3K4me3 ChIP-seq, ASH2L knockdown RNA-seq, and ESR1 and NSD3-S knockdown arrays gene sets appear in Table 3.3. This gene set is associated with several interesting processes by ToppFun analysis (Figure 3.6-B and Appendix I). Many of these processes are associated with the cell cycle. Since this is a common

theme associated with ASH2L-mediated transcriptomic alterations and high proliferation rates are associated with luminal B breast cancer and poor prognosis, we measured cell growth following shRNA-mediated knockdown of ASH2L in several cell lines (Figure 3.6-C). In both amplicon-bearing (SUM-44, CAMA-1, and SUM-52) and amplicon-null (MCF7) cell lines, knockdown of ASH2L by two different shRNA constructs reduced cell proliferation compared to shLacZ control. Knockdown levels were reported by immunoblot analysis for ASH2L expression in the four cell lines (Figure 3.6-C). Similarly,

Table 3.3. Summary of genes identified by ASH2L knockdown H3K4me3 ChIP-seq, ASH2L knockdown RNA-seq, NSD3-S knockdown array, or ESR1 knockdown array. Selected genes identified by RNA-seq as commonly downregulated between both shRNA constructs against ASH2L are reported in this table. Known processes and associations are described for each gene. Check marks indicate whether the gene was identified as having lost promoter H3K4me3 upon ASH2L knockdown (ChIP-seq), downregulated by both shRNA constructs against ASH2L (RNA-seq), downregulated by NSD3-S knockdown (NSD3 array), or downregulated by ESR1 knockdown (ESR1 array). Blank cells indicate the gene was not identified in that sample set.

| Gene Name | Description | ChIP-seq | RNA-seq | NSD3 array | ESR1 array |
|-----------|---|----------|---------|------------|------------|
| EZH2 | polycomb group HMT:H3K27 (repressive) | ✓ | ✓ | ✓ | ✓ |
| RECQL4 | associated with tamoxifen resistance | ✓ | ✓ | ✓ | ✓ |
| UBE2C | associated with tamoxifen resistance | ✓ | ✓ | ✓ | ✓ |
| CCNE2 | cyclin E2, cell cycle regulator | ✓ | ✓ | ✓ | ✓ |
| CKD2 | cyclin dependent kinase (cyclin E2), associated with tamoxifen resistance | ✓ | ✓ | ✓ | ✓ |
| BRD2 | bromodomain protein, chromatin-associated factor | ✓ | ✓ | ✓ | ✓ |
| ASF1B | associated with tamoxifen resistance | ✓ | ✓ | ✓ | ✓ |
| NSD3 | HMT: H3K36me2, 8p11 oncogene | ✓ | ✓ | ✓ | |
| AURKA | aurora A kinase, cell proliferation | ✓ | ✓ | | ✓ |
| ASH2L | H3K4me3, 8p11 oncogene | ✓ | ✓ | | |
| PIK3CA | PI3K, cell signaling oncogene/survival pathway | ✓ | ✓ | | |
| WDR5 | ASH2L binding partner | ✓ | ✓ | | |
| SETD2 | HMT: H3K36me3 | ✓ | ✓ | | |
| ESR1 | estrogen receptor alpha, transcription factor | | ✓ | ✓ | ✓ |
| CCNB1 | cyclin B1, cell cycle regulator | | ✓ | ✓ | ✓ |
| ATAD2 | bromodomain protein, ER co-activator | | ✓ | ✓ | ✓ |
| CCNB2 | associated with tamoxifen resistance | | ✓ | ✓ | ✓ |
| TK1 | associated with tamoxifen resistance | | ✓ | ✓ | |
| AURKB | aurora B kinase, cell proliferation | | ✓ | | ✓ |
| MYBL2 | proliferation marker of luminal B | | ✓ | | ✓ |
| CCNE1 | cyclin E1, cell cycle regulator | | ✓ | | ✓ |
| CCND1 | cyclin D1, cell cycle regulator, 11q14 amplicon | | ✓ | | ✓ |
| PLK1 | Kinase involved in cell proliferation | | ✓ | | |
| MLL5 | Mixed lineage leukemia family HMT | | ✓ | | |
| FOXA1 | ER pioneer factor | | ✓ | | |
| FLT3LG | ligand of FLT3 (cell proliferation and survival) | | ✓ | | |
| GATA3 | TF, ER partner, luminal BC marker | | ✓ | | |
| SMYD3 | HMT, transcription complex member | | ✓ | | |
| AKT1 | cell survival pathway signaling | | ✓ | | |

knockdown of ASH2L was performed in SUM-44 and MCF7 cells and clonogenicity measured by colony forming assay (Figure 3.6-D). Knockdown of ASH2L reduced clonogenicity in both cell lines to approximately the same degree, and the 276 ASH2L shRNA construct demonstrated a much greater effect than the 275 construct in both cell lines, although both achieved statistical significance (Figure 3.6-D, upper). Together, these data demonstrate that knockdown of ASH2L decreases cell proliferation and clonogenic potential in luminal breast cancer cell lines regardless of 8p11-p12 amplification status.

In addition to cell cycle processes, analysis of ASH2L-regulated genes consistently identified palbociclib response as a significant process to which they are annotated (Figure 3.4-B, Figure 3.4-E, Figure 3.6-B). Palbociclib selectively inhibits cyclin dependent kinases (CDK) 4 and CDK6, which bind cyclin D1 (CCND1) to advance cell cycle progression from G₁ to S phase (Nagaraj and Ma 2015). CCND1 is found on the 11q14 amplicon, which SUM-44 cells harbor in addition to the 8p11-p12 amplicon (Kwek *et al.* 2009). CDK6 is also amplified in this cell line and was identified by siRNA-based screening technique performed in our lab as essential for growth and survival of these cells. Palbociclib is approved for use in postmenopausal women with ER+/HER2-negative breast cancer and clinical trials are in progress for several similar compounds (Knudsen and Witkiewicz 2016). To determine the sensitivity of ASH2L-overexpressing cell lines to palbociclib, we treated a panel of cell lines with increasing doses of palbociclib and assessed cell number on day seven (Figure 3.7-A). We observed that the ASH2L-low MCF7 and CAMA-1 cell lines were more sensitive to palbociclib than the SUM-44 and SUM-52 cells. To validate the bioinformatic assignment of ASH2L-regulated genes to palbociclib response, we knocked down ASH2L in SUM-44 and

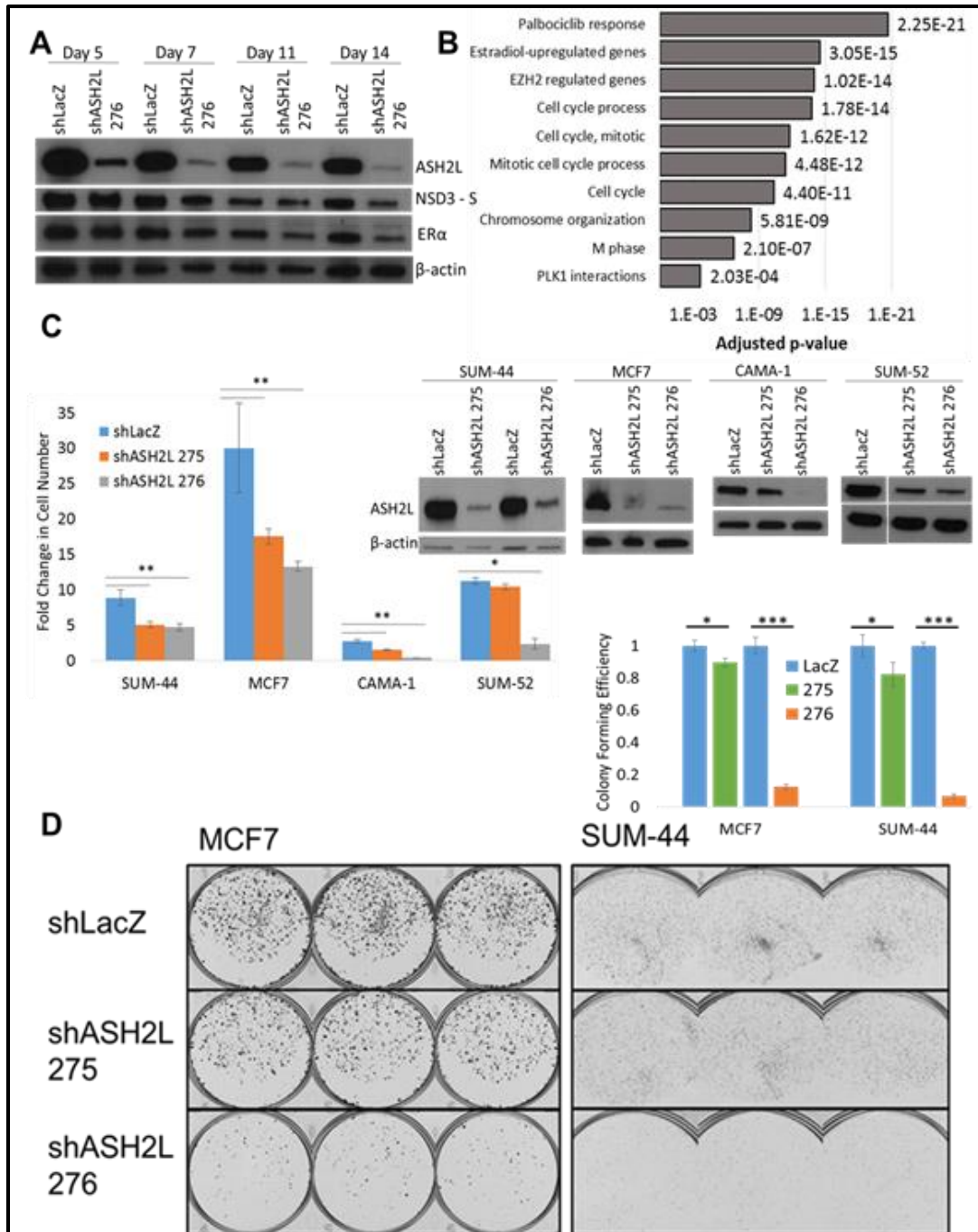
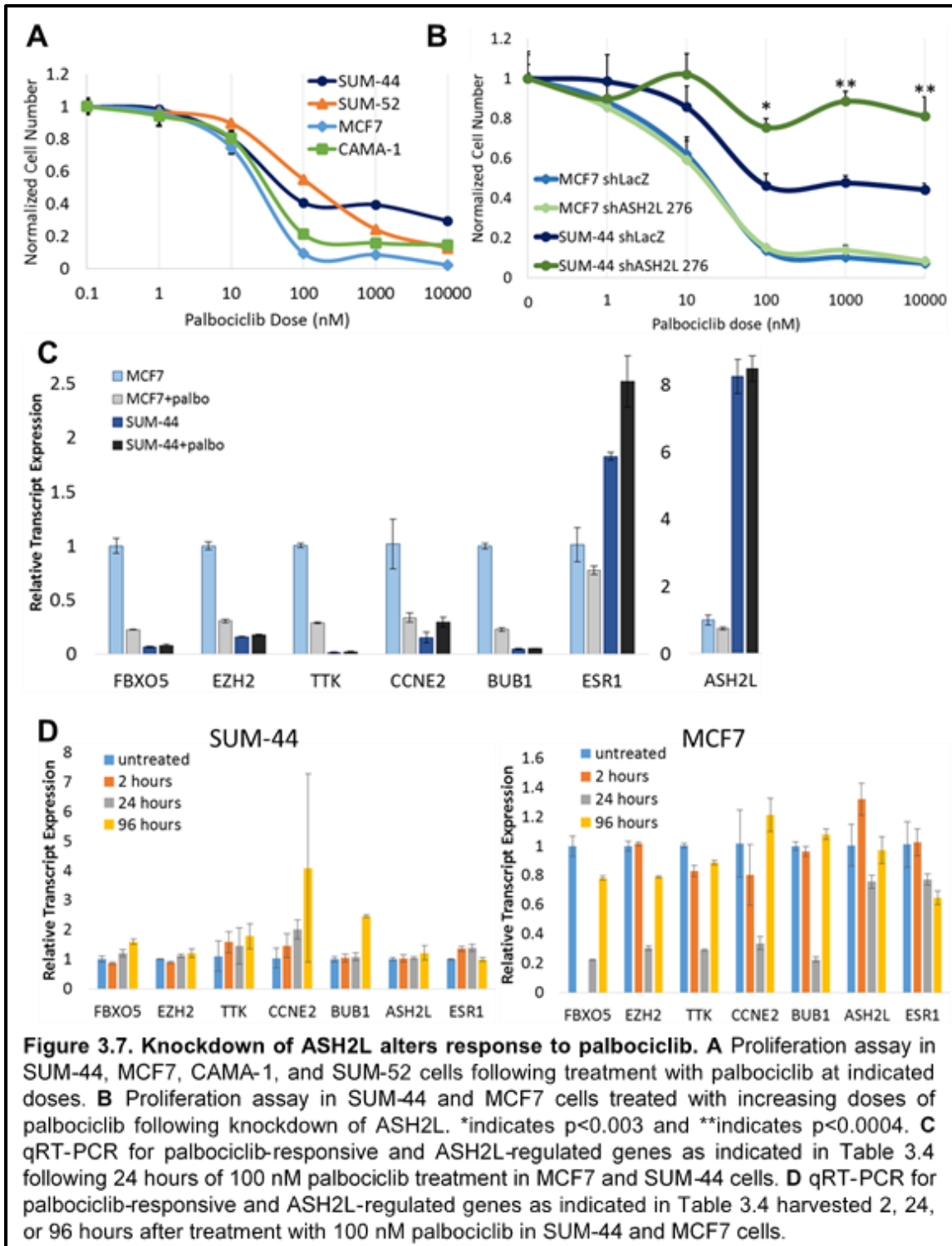


Figure 3.6. Knockdown of ASH2L results in decreased proliferation and clonogenicity in luminal B breast cancer. **A** Immunoblot for NSD3-S and ER α in SUM-44 cells 5, 7, 11, and 14 days after ASH2L knockdown. **B** ToppFun analysis on the 44 genes identified in **Figure 3.5-C**, represented by Bonferroni adjusted p-values identified in ToppFun. **C** Proliferation assay in SUM-44, MCF7, CAMA-1, and SUM-52 cells following ASH2L knockdown. Corresponding immunoblot for ASH2L appears in the upper right. **D** Colony forming assay plate photographs (stained with crystal violet) of MCF7 (left) or SUM-44 (right) cells following ASH2L knockdown and corresponding quantification (upper right). *indicates $p < 0.02$ and ***indicates $p < 6 \times 10^{-6}$.

MCF7 cells with increasing doses of palbociclib and measured their growth (Figure 3.7-B). Knockdown of ASH2L reduced sensitivity of SUM-44 cells to palbociclib but had no effect on MCF7 sensitivity to this compound. Of note, MCF7 had greater overall sensitivity to palbociclib than SUM-44 cells. MCF7 cells do not have amplification of 8p11-p12 or 11q14.

To further examine the relationship between genes regulated in expression by ASH2L, NSD3, and ESR1, and genes associated with response to palbociclib, a sub-set of genes was identified and expression level assessed by qRT-PCR. The set of 44 genes regulated by ASH2L, NSD3, and ESR1 included 10% (17 of 172) of the genes annotated as involved in response to palbociclib in ToppFun according to the comparative toxicogenomics database (CTD) (Table 3.4). From this set of 17 genes that lost promoter H3K4me3 upon ASH2L knockdown and were downregulated in response to knockdown of ASH2L, NSD3, and ESR1, we selected a sub-set of five genes that were downregulated in response to treatment with palbociclib according to CTD data, including *FBXO5*, *EZH2*, *TTK*, *CCNE2*, and *BUB1* (Table 3.4). To determine if treatment with palbociclib reduced expression of these genes in the context of ASH2L overexpression, we treated SUM-44 and MCF7 cells with palbociclib and harvested RNA 24 hours after treatment with 100 nM palbociclib for analysis of relative transcript expression by RT-PCR (Figure 3.7-C). Expression of *FBXO5*, *EZH2*, *TTK*, *CCNE2*, and *BUB1* was reduced in the palbociclib-sensitive MCF7 cell line, as predicted by the CTD data, however SUM-44 cells did not demonstrated a reduction in transcript level for these genes. ASH2L and ESR1 transcript levels were not significantly affected by palbociclib treatment (Figure 3.7-C). RNA was also harvested 2 and 96 hours following treatment with 100 nM palbociclib, demonstrating a recovery in gene expression at 96



hours post-palbociclib in the MCF7 cell line and an increase in transcript expression in

the SUM-44 line for the five genes assessed (Figure 3.7-D). These data indicate that

palbociclib resistance in the SUM-44 cells may be due to ASH2L-mediated transcriptional upregulation of genes that must be downregulated for response to palbociclib, thus preventing the cytostatic effects of this compound. This hypothesized mechanism should be investigated further.

The smallest set of genes analyzed in ToppFun, the 44 in common to ASH2L knockdown H3K4me3 ChIP-seq, ASH2L knockdown RNA-seq, NSD3-S and ESR1 knockdown microarrays (Figure 3.5-C), annotated to palbociclib response with the strongest p-value (Figure 3.6-B; Table 3.4), indicating that ASH2L, NSD3, and ER α all have a role in mediating expression of the suite of genes responsible for sensitivity to palbociclib and highlighting again the cooperative potential of these oncogenes in 8p11-p12-amplified breast cancer. This set of 44 overlapping genes (Appendix H) likely regulated by ASH2L, NSD3, and ESR1 requires further validation of their expression and investigation of the biological processes to which they connect that is beyond the scope of this study.

3.7 Summary

Little was known about ASH2L in breast cancer prior to these studies. Here, we demonstrated that ASH2L is involved in H3K4 tri-methylation specifically at the promoters of target genes without altering global H3K4me3 levels. Knockdown of ASH2L results in decreased expression of a subset of these genes with ASH2L-mediated promoter H3K4me3 marks, and these genes are implicated in cell cycle regulation and chromosome organization. ASH2L potentially exerts downstream effects by modulating several proteins important to cell signaling pathways, such as the PI3K/AKT1/mTOR pathway, and through expression of cell cycle proteins such as cyclin D1. Additionally,

ASH2L may be responsible for H3K4me3-mediated transcriptional regulation of itself as well as the co-amplified HMT NSD3, which has been shown to overexpress and activate ER α in an estrogen-independent manner (Chapter 2). Together, these data implicate ASH2L in the regulation of a large suite of genes, both directly and indirectly, when amplified and overexpressed in luminal B breast cancers. These studies identify ASH2L as an upstream regulator of many targetable pathways in breast cancer, and therefore this oncogene has the potential to inform drug discovery. Further investigation into the ASH2L complex composition in this setting and confirmation of the factors and pathways under control of this oncogene will be essential to extend these studies, ultimately leading to therapies that will benefit the breast cancer patient population with ASH2L amplification and overexpression.

Table 3.4. Genes annotated to palbociclib response in ToppFun. Genes from the input set that aligned to the ToppFun annotation set for Palbociclib Response are listed in this table. The input set consisted of 44 genes that were downregulated upon knockdown of ASH2L, NSD3-S, and ESR1 and lost promoter H3K4me3 peaks after ASH2L knockdown. Genes selected for validation by qRT-PCR are indicated.

| Gene Symbol | Gene Name | PCR |
|-------------|---|-----|
| KIF20A | Kinesin family member 20A | |
| HMGB2 | High mobility group box 2 | |
| MCM7 | Minichromosome maintenance complex component 7 | |
| HMMR | Hyaluronan mediated motility receptor | |
| FBXO5 | F-box protein 5 | ✓ |
| KIF15 | Kinesin family member 15 | |
| EZH2 | Enhancer of zeste 2 polycomb repressive complex 2 subunit | ✓ |
| CDC25C | Cell division cycle 25C | |
| CENPE | Centromere protein E | |
| TTK | TTK protein kinase | ✓ |
| CENPM | Centromere protein M | |
| ASF1B | Anti-silencing function 1B histone chaperone | |
| NCAPG2 | Non-SMC condensing II complex subunit G2 | |
| GMNN | Geminin, DNA replication inhibitor | |
| CCNE2 | Cydin E2 | ✓ |
| UBE2C | Ubiquitin conjugating enzyme E2 C | |
| BUB1 | BUB1 mitotic checkpoint serine/threonine kinase | ✓ |

CHAPTER 4: Discussion and Future Directions

4.1. 8p11-p12 Amplified Breast Cancer

a. Breast cancer *in vitro* models

Due to the incredible heterogeneity of breast cancer, a major challenge in research is acquiring laboratory models able to encompass the multiple patient subpopulations observed clinically (Benjamini and Hochberg 1995, Kao *et al.* 2009, Dabydeen and Furth 2014). The MCF7 cell line is considered the gold standard by which ER+ breast cancers are studied *in vitro* and *in vivo*, however this luminal A cell line does not sufficiently capture the complexity of the luminal type tumors as a whole (Comsa *et al.* 2015). This cell line has a simplex genomic pattern and is sensitive to endocrine therapies such as tamoxifen (Shiu *et al.* 2010, Comsa *et al.* 2015). While attempts have been made to induce tamoxifen resistance in MCF7 cells and these altered cell lines have been thoroughly investigated, this artificial representation of endocrine resistance does not translate to patient tumors and the genomic profiles of these modified MCF7 cell lines do not resemble patient-derived luminal B cell lines (Ross-Innes *et al.* 2012).

Model cell lines with intrinsic tamoxifen resistance have been reported but generally have lost ER α expression or dependence in culture, such as the SUM-52 cell line. While it is well-known that a significant number of patient tumors retain ER α expression even in the context of resistance to endocrine therapy, an *in vitro* model accurately representing this patient population has not previously been available (Cui *et al.* 2005). Similarly, although cell lines with amplification of the 8p11-p12 amplicon have been reported, these models have varying degrees of expression of the oncogenes contained in this region (Ray *et al.* 2004, Garcia *et al.* 2005, Gelsi-Boyer *et al.* 2005).

Approximately 15% of primary breast tumors have 8p11-p12 amplification and this number increases in metastatic samples, correlating with poor prognosis and ER α expression (Bernard-Pierrot *et al.* 2008, Tabarestani *et al.* 2016). Several groups have linked the 8p11-p12 amplicon with endocrine resistance (Shiu *et al.* 2010, Luo *et al.* 2017). Amplification is a major mechanism of oncogene overexpression and activation (Ray *et al.* 2004, Yang *et al.* 2006, Streicher *et al.* 2007, Bernard-Pierrot *et al.* 2008), and thus there is a need for more model cell lines by which to study the highly heterogenic 8p11-p12 amplicon.

The SUM-44 cell line, originating from metastatic cells in the pleural effusion fluid from a breast cancer patient with ER+ disease (Ethier *et al.* 1993), reflects the characteristics of a subset of breast cancer patients not previously represented *in vitro*, including intrinsic tamoxifen resistance and amplification of the 8p11-p12 genomic region (Ray *et al.* 2004, Irish *et al.* 2016). This cell line expresses ESR1/ER α to a higher degree than other ER+ cell lines, even MCF7 cells, a biologically relevant observation when compared to patient tumor sample ESR1 expression (Figure 2.3-B). SUM-44 cells have amplification of 8p11-p12 with abundant overexpression of the amplicon genes, even compared to other amplicon-bearing cell lines such as CAMA-1 and SUM-52 (Figure 2.3-A). Interestingly, the SUM-52 cell line, originally ER+, has lost ER α expression in culture and although the CAMA-1 cell line retains ER α expression, the level is very low compared to MCF7 and SUM-44. Together, the data presented in this work establish a model by which endocrine resistant, highly ER+ breast tumors can be investigated. Due to the heterogeneity of breast cancer patients, establishment of additional models is necessary, but here we offer an important advancement in the ability to understand the

8p11-p12 amplicon in luminal B breast cancer and the effects of the amplicon genes on constitutive activation of ER α as well as the transcriptome as it relates to tumorigenesis.

b. NSD3

NSD3 (WHSC1L1) was identified and validated as an 8p11-p12 amplicon oncogene in breast and other cancers (Yang *et al.* 2010, Bilal *et al.* 2012, He *et al.* 2013, Mahmood *et al.* 2013, Chen *et al.* 2014, French *et al.* 2014). We and others have demonstrated that the catalytic, SET domain-containing NSD3-L isoform is not the major oncogenic isoform (Shen *et al.* 2015, Irish *et al.* 2016). Instead, NSD3-S, produced by alternative splicing at exon 10 of the NSD3 (WHSC1L1) gene, is more highly expressed than NSD3-L (Figure 2.1-A) and has greater transforming ability when overexpressed in the MCF10A breast cell line (Yang *et al.* 2010). Knockdown of this isoform reduced cell proliferation and expression of ESR1, the gene that encodes ER α (Figure 2.2). Further investigation of this relationship identified that NSD3-mediated overexpression of ER α resulted in estrogen-independent activity of this receptor (Figure 2.5) and tamoxifen resistance (Figure 2.4). In the context of the 8p11-p12 amplicon, ER α is targeted to FOXA1 binding sites in addition to EREs (Irish *et al.* 2016), resulting in downstream transcription of a suite of genes correlating with poor prognosis in breast cancer (Figure 2.5-C). Knockdown of NSD3 and ESR1 identified altered expression of genes associated with cell cycle processes (Table 2.2), suggesting that one of the roles of NSD3-S is to mediate ER α activity and estrogen dependence.

The mechanism of NSD3-induced overexpression and estrogen-independent activation of ER α is poorly understood. Since the effect is mediated primarily by NSD3-S, investigation of the role of NSD3-S in general will elucidate possible effects on ER α .

Shen *et al.* (2015) identified NSD3-S as an adaptor protein between BRD4, a member of the bromodomain and extraterminal domain (BET) family of chromatin readers, and CHD8, a chromodomain helicase DNA binding protein involved in transcriptional regulation via nucleosome remodeling. BRD4 is tethered to chromatin by acetylated histones and is essential for maintenance of leukemia through interactions with other proteins. Identification of NSD3-S as an adaptor protein that aides BRD4 interactions with these other factors is a novel finding that has implications for breast cancer treatment. Preliminary studies in our laboratory indicate that SUM-44 cells may be sensitive to the BRD4 inhibitor JQ1 and that NSD3 binds BRD4 by co-IP (data not shown). BET inhibitors are currently under investigation in several cancer types (French *et al.* 2014), and inclusion of NSD-S as a potential biomarker for patient response would be an exciting arm of investigation.

In addition to its role as a linker protein, NSD3-S has been hypothesized to inhibit histone and non-histone protein methylation. NSD3-S retains the N-terminal PWWP domain and maintains the ability to read methylated H3K36 residues, thereby occupying potential binding sites of the NSD3-L isoform (Stec *et al.* 2001). In addition to the implications of such a role for NSD3-S on gene transcription, this hypothesis is applicable to ER α activation. In estradiol-mediated activation of ER α , the protein is demethylated and acetylated at the K266 residue (Zhang *et al.* 2013). In the context of NSD3-S amplification and overexpression, NSD3-S may bind ER α -K266 and prevent methylation, thereby leaving the protein susceptible to activation by acetylation, perhaps by another amplified and overexpressed 8p11-p12 amplicon oncogene, KAT6A, a HAT enzyme. The potential influence of NSD3-S on ER α PTM could be investigated by ER α proteomic analysis following knockdown of NSD3-S. Similarly, ER α is activated by

several phosphorylation events and any potential effects of NSD3-S on ER α phosphorylation could be identified by the same technique.

Since ER α is a receptor that is activated by ligand-stimulated dimerization, it is possible that NSD3-S does not affect the ER α protein itself and, instead, ER α is activated in an estrogen-independent manner by NSD3-induced overexpression leading to spontaneous dimerization. ER α is known to have a ligand-independent AF-1 domain (Cui *et al.* 2005), therefore abundant expression of the receptor as is observed with NSD3 amplification and overexpression may be sufficient to result in estrogen-independent ER α activity. AF-1 is known to be involved in transcription of a suite of genes different from those mediated by the ligand-dependent AF-2 domain (Wang and Yin 2015), consistent with ER α ChIP-seq and microarray results that demonstrated differential binding and expression profiles in 8p11-p12 amplicon-bearing SUM-44 cells compared to amplicon-null MCF7 cells (Irish *et al.* 2016). Testing the hypothesis that abundant overexpression of ER α is sufficient to induce estrogen-independent activation would require overexpression of the receptor in MCF7 cells and assessing ER α activity by reporter assay and RT-PCR for ER α target genes in the absence of estrogen. If these experiments indeed demonstrate estrogen-independent ER α activity, we would then predict that these MCF7 cells induced to recapitulate the ER α expression levels observed in SUM-44 cells would show tamoxifen resistance *in vitro* but would retain their sensitivity to fulvestrant.

If the estrogen-independent activation of ER α is due to its overexpression rather than PTM, then we would hypothesize that the effect of NSD3 overexpression to induce ER α overexpression reported here is due to epigenetic modifications by NSD3 that lead

to increased transcription of ESR1. Since NSD3-S is implicated in chromatin modification as an adaptor protein and NSD3-L is implicated in H3K36me3 in gene bodies of actively transcribed genes, analysis of the epigenetic landscape at the ESR1 gene with knockdown of NSD3-S and NSD3-T would identify the relationship between these two isoforms of NSD3 and their transcriptional effects on ESR1. Indeed we have shown that knockdown of NSD3 reduced ESR1 transcript and ER α protein levels (Figure 2.2), but the precise temporal relationship between these events has yet to be determined, therefore it remains unclear whether NSD3 knockdown first affects ESR1 transcription or ER α protein stability/activity/PTM that then results in a positive feedback loop whereby activated ER α is able to increase its own expression by its actions as a transcription factor. Other ER α co-factors and modifying proteins that may be involved in this process also remain yet unknown. Clearly, there is still a great deal of investigation necessary to elucidate the mechanism of ER α overexpression in the context of NSD3 amplification and overexpression.

The discovery of the relationship between overexpression of the 8p11-p12 amplicon oncogene NSD3 and overexpression and estrogen-independent activation of ER α has exciting implications for the treatment of amplicon-bearing luminal B breast cancers. We have demonstrated that these cells, though tamoxifen resistant (Figure 2.4-E), respond to the SERD fulvestrant (Figure 2.5-E and Figure 2.5-F) and treatment with fulvestrant recapitulates the cytotoxic effects of ESR1 knockdown in this cell line. The link between NSD3 and ER α described here is a novel mechanism of endocrine resistance in ER+ breast cancer.

In addition to breast cancer, the 8p11-p12 amplicon is present in several other cancer types (Gao *et al.* 2013, Mahmood *et al.* 2013). NSD3 is a validated oncogene in lung squamous cell carcinoma (LSCC), bladder carcinoma, and AML (Mahmood *et al.* 2013, Shen *et al.* 2015). These cancers are not ER α -dependent as is the case in breast cancer, and we demonstrated that two LSCC cell lines with high expression of NSD3 have undetectable levels of ER α expression (Figure 2.1-A and Figure 2.3-A). As such, we hypothesize that NSD3 has an important role in tumorigenesis outside of its effects on ER α . NSD3 is the least studied member of the NSD family of SET domain HMT proteins and the effects of NSD3 and its substrate, H3K36me₂, remain understudied in cancer. In order to investigate the genes under epigenetic regulation by NSD3, we attempted to perform ChIP-seq analysis in SUM-44 cells utilizing an NSD3 antibody developed by the Vakoc group at the Cold Spring Harbor Laboratory (Shen *et al.* 2015), but were unsuccessful. The H3K4me₃ ChIP-seq performed in this study in the context of ASH2L knockdown demonstrated the potential efficacy of employing a similar strategy to investigate the effects of NSD3 on H3K36me₂ in the SUM-44 cell line as a future direction of this project.

Figure 4.1 illustrates the three proposed mechanisms of NSD3 oncogenesis. Panel A depicts the epigenetic role of NSD3-L, which catalyzes H3K4me₂ in gene bodies to promote active transcription. We hypothesize that, in addition to a suite of genes involved in regulation of the cell cycle, NSD3 promotes transcription of ESR1, thereby inducing ER α overexpression. Since NSD3-S lacks the catalytic SET domain, its mechanism for promoting tumorigenesis remains largely unknown. Figure 4.1-B depicts a possible role for NSD3-S based on the model proposed by Shen *et al.* (2015). Here, NSD3-S acts as an adaptor protein for recruitment of additional chromatin-modifying

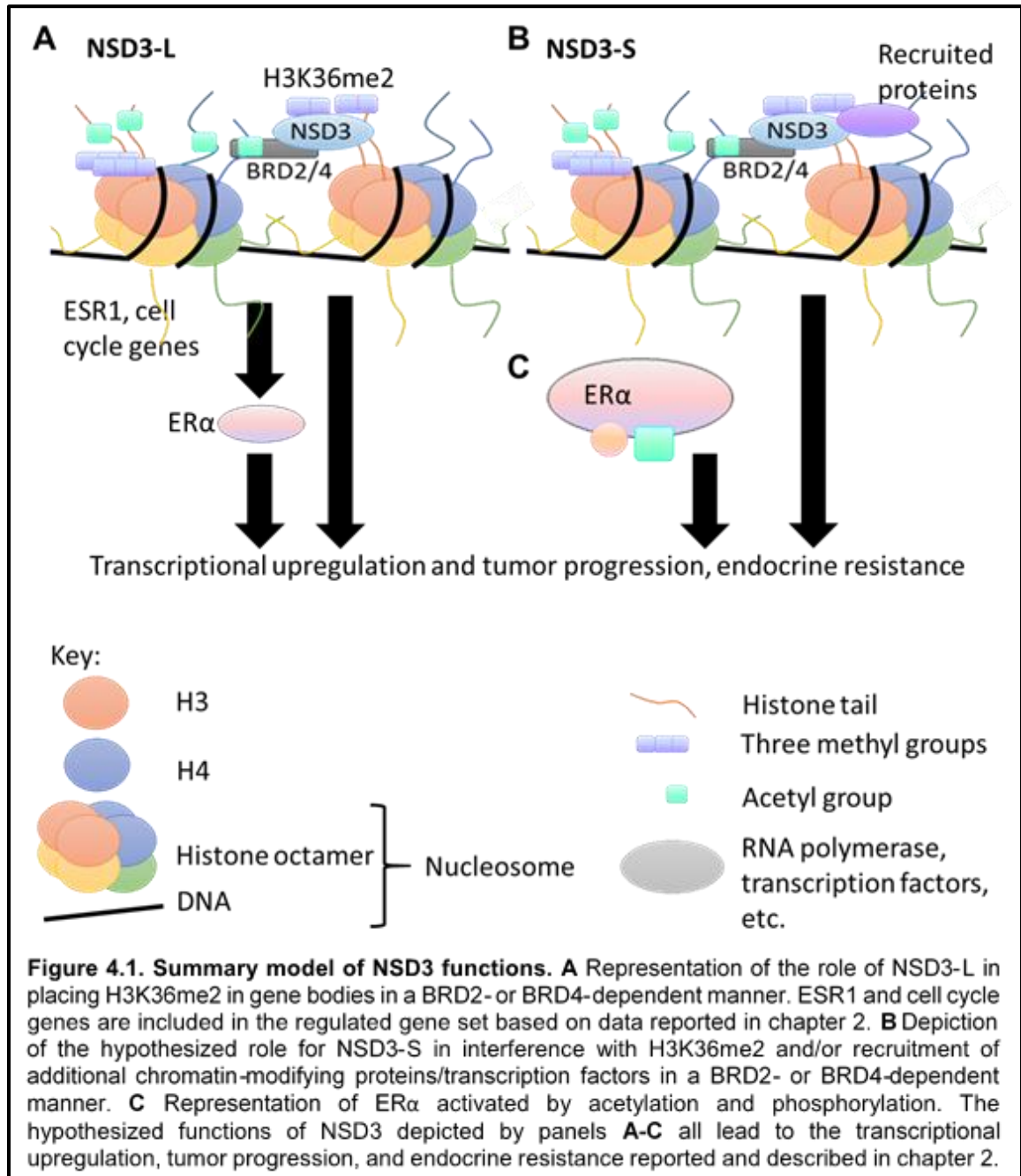
enzymes and transcription factors, thus affecting the transcriptome. This mechanism relies on chromatin binding by BRD protein family, which recognize acetylated histones (Lo and Sukumar 2008). We have previously hypothesized that the 8p11-p12 amplicon oncogene KAT6A is responsible for histone acetylation in this context. Alternatively, anchoring of NSD3-S to the chromatin by the BRD family proteins may act to prevent binding by NSD3-L, thus preventing H3K36me2 in those gene bodies. The exact mechanism and downstream implications of possible NSD3-S inhibition of NSD3-L remain to be elucidated. Finally, we have also hypothesized that NSD3-S binds K residues on the ER α protein itself, preventing its methylation and rendering it susceptible to activation by acetylation (Figure 4.1-C). These different mechanisms of action are not mutually exclusive and all potentially influence cell cycle progression, tumorigenesis, and endocrine resistance and therefore extension of the work reported here should explore each of these hypotheses.

c. ASH2L

ASH2L is understudied in breast cancer despite having been identified by several groups as a potential driving oncogene from the 8p11-p12 amplicon region (Garcia *et al.* 2005, Kwek *et al.* 2009, Cornen *et al.* 2014). Here, we identified a role for ASH2L in the regulation of H3K4me3 in promoter regions and expression of genes associated with cell cycle (Chapter 3). Knockdown of ASH2L resulted in decreased expression of an important set of genes, reduced proliferation and clonogenicity, and reduced sensitivity to the cell cycle inhibitor palbociclib. Together, the results of this study identify ASH2L as a driving oncogene in ER+ breast cancer and as a potential biomarker for palbociclib sensitivity in endocrine resistant tumors, a therapy currently in clinical trials for the treatment of ER+ breast cancer. Further investigation of ASH2L as a biomarker for drug

response and as a potential drug target itself could identify new therapeutic strategies to increase survival in patients with the 8p11-p12 amplicon.

ASH2L lacks the catalytic SET domain characteristic of HMT enzymes (Ikegawa *et al.* 1999). While this oncogene does possess methyltransferase activity when coupled



with its binding partner RbBP5 (Tan *et al.* 2009), ASH2L commonly relies on the formation of complexes with SET domain-containing proteins, such as the MLL family of HMTs, where the role of ASH2L lies primarily in promoting catalysis of H3K4me3 (Steward *et al.* 2006). ASH2L is present in all known complexes responsible for H3K4me3 and is tightly and specifically linked to this histone methyl mark (Butler *et al.* 2017). Here, we demonstrated that knockdown of ASH2L reduced the robustness of global H3K4me3 peaks across the genome in SUM-44 cells (Figure 3.2-E). Remaining H3K4me3 is likely a result of incomplete knockdown of ASH2L, which was not achieved due to the extreme level of ASH2L overexpression in the context of its amplification (Figure 3.2-B). Despite the reduction in robustness, ASH2L knockdown had little effect on the overall distribution of H3K4me3 peaks (Figure 3.2-D). We were, however, able to identify a major role for ASH2L in the elimination of H3K4me3 peaks specifically in the promotor regions of genes (Figure 3.3-A), a function in agreement with the previous studies on ASH2L-directed H3K4 tri-methylation (Demers *et al.* 2007).

The complex in which ASH2L functions in the context of the 8p11-p12 amplicon is yet unknown and investigation of the protein(s) assisting ASH2L would be an interesting future direction of this project. It is possible that ASH2L is forming a complex with the MLL family as is well-documented, but with the extremely high level of amplification-induced overexpression of ASH2L it is also possible that novel binding partners are favorable in this context. Since ASH2L lacks a catalytic SET domain, the direct versus indirect role of ASH2L on histone methylation is unclear. The effects of ASH2L on H3K4me3 elucidated in this study may be a reflection of indirect effects via the influence of ASH2L on binding partners. Indeed, we demonstrated here that the ASH2L binding partner WDR5 has reduced promoter H3K4me3 peaks and transcript

expression upon ASH2L knockdown (Tables 3.1 and 3.2). WDR5 is responsible for chromatin binding, recruitment of ASH2L and other MLL complex proteins, and stability of the ASH2L-MLL complex (Steward *et al.* 2006, Guccione *et al.* 2007, Ali and Tyagi 2017). Identification of regulation of WDR5 expression by ASH2L reveals a feedback loop by which ASH2L may increase its chromatin-binding ability. Lack of corresponding evidence of ASH2L-mediated regulation of MLL family members suggests that ASH2L is relying on alternative binding partners for its function in the context of amplification-induced overexpression in breast cancer. Suspected ASH2L binding partners, such as other SET domain-containing proteins, could be identified by ASH2L IP followed by immunoblotting for such factors, although novel ASH2L binding proteins would not be identified by this method and would require additional techniques such as proteomic analysis.

According to the ChIP-seq and RNA-seq analyses presented in Chapter 3, ASH2L mediates H3K4me3 at its own promoter as well as several other chromatin-modifying enzymes such as NSD3 and EZH2, suggesting that ASH2L amplification establishes a positive feedback loop whereby amplified ASH2L drives expression of itself, leading to increased transcription of cell cycle genes and chromatin-modifying enzymes that also alter downstream gene expression. Similarly, ASH2L knockdown abolished H3K4me3 in the promoter regions of over half of the candidate oncogenes from the 8p11-p12 amplicon region (Table 3.1), suggesting that ASH2L may have a role in modulating the expression of these amplified genes. Of these amplicon genes, however, RNA-seq analysis identified only POMK and NSD3 as transcriptionally downregulated upon knockdown of ASH2L but also identified the 8p11-p12 amplicon gene KAT6A, another epigenetic factor, as being under ASH2L transcriptional regulation

without corresponding modification of the H3K4me3 status of its promoter region (Table 3.2). Further investigation of the relationship between promoter H3K4me3 and transcription is required. Epigenetic regulation is complex and other chromatin-modifying or epigenetic reader enzymes may be altered in the context of ASH2L knockdown to modify the histone code, accounting for the discrepancy between H3K4me3 and transcription.

The ChIP-seq and RNA-seq datasets provide a plethora of avenues for further investigation of the role of this oncogene in cell and tumor biology. Importantly, the analysis presented in Chapter 3 focused solely on genes which lost H3K4me3 promoter tri-methylation with a corresponding reduction in gene expression upon ASH2L knockdown. Genes with increased expression following ASH2L knockdown may represent tumor suppressors that are reduced when ASH2L is amplified and overexpressed. Genes that gained H3K4me3 following knockdown of ASH2L may represent an interesting group of factors, especially considering other groups have reported ASH2L knockdown abolishes H3K4 tri-methylation as ASH2L is required to promote catalysis of this reaction. Of note, we did not recapitulate the global reduction in H3K4me3 upon ASH2L knockdown that other studies have demonstrated, indicating that either ASH2L is overexpressed to such a degree in SUM-44 cells that residual levels are sufficient to maintain H3K4me3 methyltransferase activity or that another factor is compensating for ASH2L reduction in the context of 8p11-p12 amplification. Identification of an HMT with H3K4 tri-methylation capabilities independent of ASH2L would be a novel finding in the field.

Finally, immunoblots designed to validate the ASH2L RNA-seq knockdown results identified several proteins with unchanged expression despite message-level

downregulation (Figure 3.4-C), suggesting a disconnect between transcriptional regulation and ultimate expression of several key factors. The complex nature of epigenetic alterations, transcriptional effects, and protein expression and stability leave several questions unanswered from these studies. The data indicate ASH2L influences H3K4me3 in the promoter of NSD3 and knockdown of ASH2L reduces NSD3 expression (Figure 3.3-C, Figure 3.5-A, and Table 3.2), therefore we hypothesize that amplification of ASH2L leads to overexpression of co-amplified NSD3, which then influences ESR1 and ER α expression and activity (Chapter 2), as well as cell cycle genes and ASH2L itself, establishing a positive feedback loop. This hypothesis is illustrated by Figure 4.2-A. More investigation into the complex biology of 8p11-p12 amplified breast tumors is required to fully understand the implications of ASH2L and its direct and indirect impact on breast cancer progression and therapy resistance.

d. Cooperating oncogenes and ER α

One hypothesis generated from this study is that ASH2L and NSD3 cooperate to alter epigenetic regulation of gene transcription and expression and activity of ER α in the context of 8p11-p12 amplified breast cancer. We demonstrated that knockdown of ASH2L abolished H3K4me3 in the promoter of NSD3 (Figure 3.3-C and Table 3.3), reduced NSD3 and ESR1 transcript levels (Table 3.2), and decreased NSD3 and ER α protein expression (Figure 3.5-A and Figure 3.6-A) in SUM-44 cells. Knockdown of NSD3 reduced ESR1 and ER α expression (Figure 2.2). From these data we conclude that ASH2L regulates NSD3 expression via promoter H3K4me3 and NSD3 then regulates expression and estrogen-independent activation of ER α . Further study is necessary to determine if ASH2L is directly involved in overexpression and/or activation

of ER α and whether these two oncogenes, ASH2L and NSD3, cooperate to modify the chromatin state in breast tumors in which they are amplified and overexpressed.

As discussed above, the complex in which ASH2L is found is essential to its function. Since ASH2L lacks the catalytic SET domain of other HMT enzymes, recruitment of SET proteins is essential to ASH2L function (Dou *et al.* 2006). NSD3-L possesses a SET domain that primarily catalyzes H3K36me₂ in gene bodies and is associated with active transcription (Li *et al.* 2009). NSD3-L has also been implicated in H3K4 methylation, but this histone mark has not been well-characterized for this enzyme (Jacques-Fricke and Gammill 2014). IP of ASH2L followed by immunoblot for NSD3 would determine whether ASH2L and NSD3 form a complex and, if so, which isoform of NSD3 is involved. These proteins do not necessarily need to bind one another, however, in order to coordinately regulate gene expression (Figure 4.2-C). ASH2L NSD3-S lacks a catalytic SET domain like ASH2L yet displays oncogenic characteristics when overexpressed in non-transformed breast cells (Yang *et al.* 2010). These two oncogenes may therefore provide similar functions in breast cancer cells outside of histone methylation. Since the stability and activity of several important proteins, ER α included, depends on PTM such as methylation (Zhang *et al.* 2013), global proteomic analysis of the methylome in breast cancer cell lines following knockdown of either ASH2L or NSD3-S would be an interesting future direction of this project.

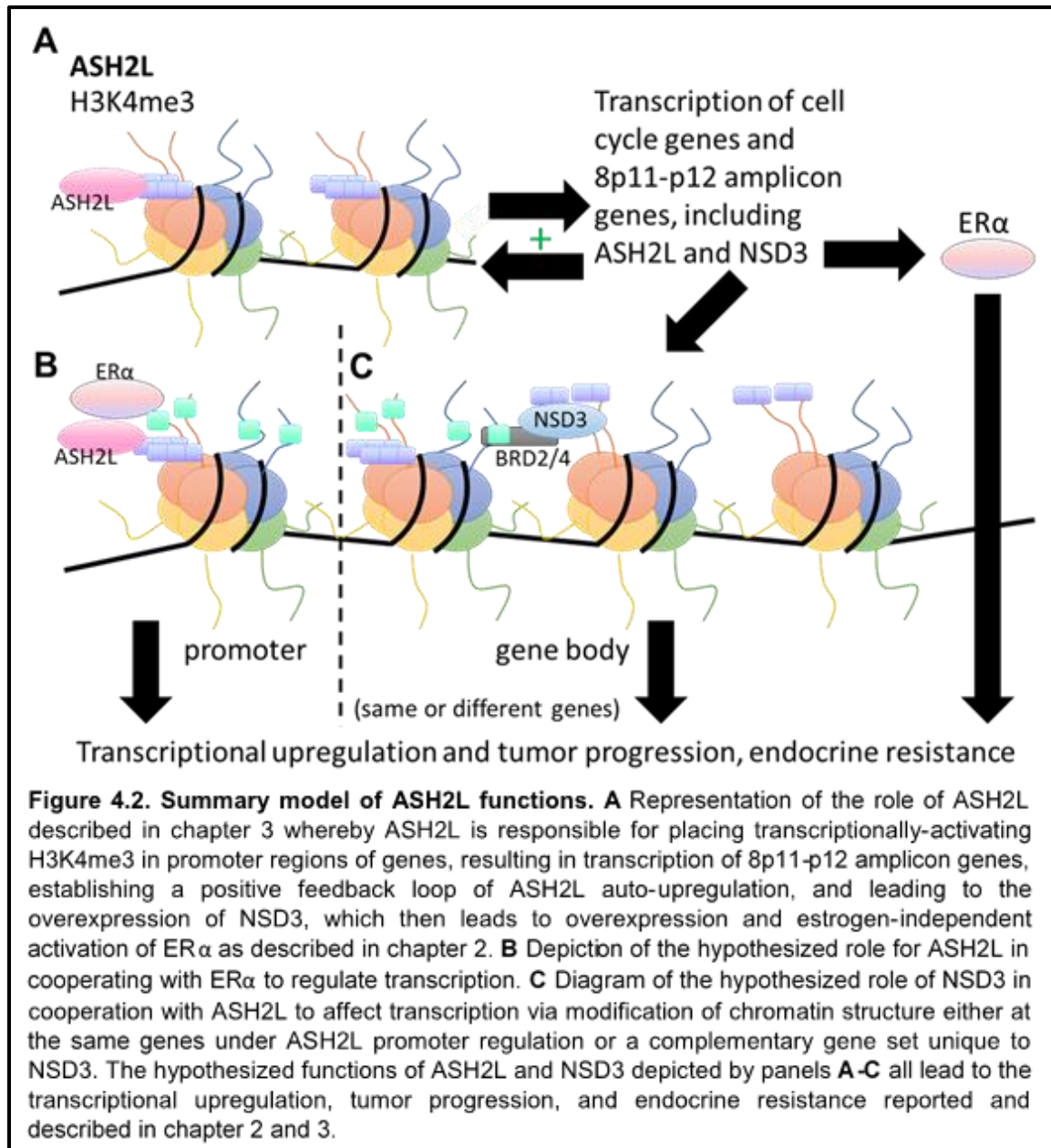
In order to interact with chromatin, NSD3 requires the assistance of chromatin reader proteins such as those of the BET family (Wagner and Carpenter 2012). Other studies have identified BRD4 as an NSD3 binding partner, but other BRD family proteins may also be involved (Shen *et al.* 2015). BRD2 was identified here by H3K4me₃ ChIP-seq and RNA-seq with ASH2L knockdown, NSD3-S knockdown array, and ESR1

knockdown array (Table 3.3). Immunoblot analysis following knockdown of ASH2L in SUM-44 and MCF7 cells did not reveal a change in BRD2 expression, however (Figure 3.4-C). Whole cell lysate was harvested for the blots shown in Figure 3.4-C seven days post infection with ASH2L shRNA constructs, therefore longer incubation may be required to detect changes in protein expression. Alternatively, a disconnect between promoter H3K4me3, transcription, and protein expression may be present in these cells and investigation of factors involved in translational regulation would be an interesting future direction of this project. One such factor, EIF4EBP1, is found on the 8p11-p12 amplicon, is amplified and overexpressed in SUM-44 cells, and is implicated in translational dysregulation in cancer (Karlsson *et al.* 2011). This factor may mediate the proteomic effects of transcriptional dysregulation by ASH2L, NSD3, and ER α .

While we discovered a direct link between knockdown of NSD3-S and reduced expression of ESR1 and ER α (Figure 2.2), we were not able to induce overexpression of ER α in the amplicon-null MCF7 cell line simply by overexpression of NSD3-S (Figure 2.3-E). Successful induction of ER α overexpression in the amplicon-positive cell lines CAMA-1 and SUM-52 suggests that other amplicon components are required for overexpression and activity of ER α in this setting. IP followed by immunoblot for ER α identified a potential interaction between these two proteins (Figure 3.5-F). The MLL complex, which includes ASH2L, is known to interact directly with ER α and ER α relies on histone- and chromatin-modifying enzymes to promote transcription at ER α -target genes (Cui *et al.* 2005, Turner-Ivey *et al.* 2014). Therefore, we hypothesize that ASH2L and ER α cooperate to alter gene transcription in the context of 8p11-p12 amplification, including increased transcription of ESR1 (Figure 4.2-B). Additional co-IP assays are

required to validate the interaction between ASH2L and ER α and close study of the transcriptional effects of these two factors would be necessary to explore this hypothesis.

The complex nature of amplification-induced overexpression and subsequent activation of oncogenes, epigenetic modifications, transcriptional regulation, and ER α -



signaling renders study of individual genomic alterations difficult. This study attempted to elucidate the roles of two important oncogenes, ASH2L and NSD3, and characterize the transcriptional effects of these two epigenetic factors. There are a multitude of pathways to investigate stemming from these studies, some of which are discussed here.

Ultimately, the goal of these *in vitro* studies is to identify novel mechanisms of drug treatments for patients with 8p11-p12 amplicon-bearing ER+ breast cancer. The implications of these studies on breast cancer management are discussed below.

4.2. ER+ Breast Cancer Treatment

a. Endocrine therapies

While tamoxifen and the aromatase inhibitors have made great strides in the treatment of ER+ breast cancer, not all patients with ER+ disease respond to these drugs. Mechanisms of endocrine resistance have long been the subject of investigation, and several have been identified. First, loss of ER α expression can occur (Cui *et al.* 2005). These cells are no longer dependent upon the receptor for growth and survival, therefore endocrine therapies are irrelevant to these processes, much like tumors that are ER-negative upon diagnosis. Second, point mutations in the ligand-binding domain of ER α can abrogate the ability of tamoxifen to bind and activate the ligand-independent AF-1 domain of ER α (Chang 2012, Angus *et al.* 2016). This mechanism renders Als ineffective as well since ER α is no longer dependent upon estrogen for activation and is capable of signaling through the ligand-independent AF-1 domain. Third, amplification of ESR1, though rare, does occur (Tabarestani *et al.* 2016). This mechanism is not yet well-characterized, but does correlate with endocrine resistance. Finally, we demonstrate here a novel mechanism of endocrine resistance: overexpression and

estrogen-independent activation of ER α by the 8p11-p12 amplicon oncogene NSD3, perhaps in cooperation with other amplicon-oncogenes (Chapter 2). This mechanism also requires further investigation, as discussed above, but highlights again the diversity of breast tumors and the genomic alterations that can have vast effects on drug sensitivities, underscoring the need to better characterize luminal B breast cancers to identify novel treatment strategies to overcome endocrine resistance.

Several drugs have undergone clinical trials for the treatment of endocrine-resistant, ER+ breast cancer. Fulvestrant was developed in an attempt to expand the SERM repertoire to pure ER α antagonists (Howell 2006). Fulvestrant (ICI 182,780; Faslodex) binds ER α and induces a conformational change different than that of tamoxifen, preventing dimerization and targeting the receptor for degradation by the proteasome system (Dowsett *et al.* 2005). Fulvestrant binding also inactivates both the AF-1 and AF-2 domains of ER α , unlike tamoxifen, completely abolishing ER α -mediated gene transcription (McKeage *et al.* 2004). Since the mechanism of action of Fulvestrant is primarily due to degradation of ER α , cross-resistance with tamoxifen and anastrozole is minimal (De Marchi *et al.* 2016). Several clinical trials assessing efficacy and dosing of Fulvestrant led to its approval in 2010 for the treatment of post-menopausal women with ER+ breast cancer nonresponsive to other endocrine therapy (Ignatiadis and Sotiriou 2013).

While Fulvestrant has been a major step forward in breast cancer treatment, the ability of this drug to degrade ER α is dose-dependent and achieving steady-state doses adequate for tumors with high-level ER α expression is a major clinical challenge (Robertson 2007). Several other SERDs are under development and testing, but interest

in this drug class has diminished due to apparent resistance in patients. This so-called resistance, however, may be due the dose-dependent nature of Fulvestrant, reflecting inadequate bioavailability. The work presented here is an important step toward shifting the paradigm regarding ER α expression and endocrine therapy resistance. Most luminal B tumors have relatively low ER α expression and it has long been thought that these tumors are not dependent upon the receptor for growth and survival, thereby accounting for the overall poor response to endocrine therapies (Ades *et al.* 2014). Here, we demonstrate that high-level ER α expression does occur in patient tumors with endocrine resistance, this receptor is a driving oncogene in this setting, and abolishing ER α expression is detrimental to these cancer cells (Chapter 2). The data presented in this work support continued development of the SERD drug class and underscore the need for such a drug that can effectively eliminate high ER α overexpression in patients.

b. Signaling pathway therapies

In addition to therapies targeting ER α signaling, several other pathways have been implicated in ER+ breast tumors. The “non-genomic” effects of ER α have been described in detail in several review articles, all concluding that cytoplasmic and/or membrane-bound ER α cross-talks with growth factor receptor pathways such as EGFR (McKeage *et al.* 2004, Dowsett *et al.* 2005, Johnston *et al.* 2005, Kristensen *et al.* 2005, Nicholson and Johnston 2005, Ariazi *et al.* 2006, Howell 2006, Chang 2012, Fedele *et al.* 2012, Ignatiadis and Sotiriou 2013, Kerdivel *et al.* 2013, Nagaraj and Ma 2015, Wang and Yin 2015, Tabarestani *et al.* 2016). In breast cancer, ER α expression (ER α -66) is essentially exclusively nuclear, as demonstrated by IHC staining of patient biopsies and ER α ChIP experiments identifying chromatin-bound ER α prior to treatment with 17 β -

estradiol (Cui *et al.* 2005, Howell 2006, Angus *et al.* 2016, Irish *et al.* 2016). Smaller ER α isoforms, most commonly ER α -36 and ER α -46, have been described as mediating these non-genomic ER α activities and the sensitivity of these isoforms to endocrine therapy is unknown, though both retain the DNA-binding and ligand-binding domains (Wang and Yin 2015). Additionally, the role of ER β in breast cancer is not fully characterized (Hartman *et al.* 2009). Despite the questions that still remain surrounding non-genomic ER α signaling, it is known that cross-talk with cell signaling pathways does occur in the form of post-translational modifications.

The PI3K/AKT/mTOR pathway is known to activate ER α by phosphorylation of several serine residues, including S118, S167, and S305 (Kerdivel *et al.* 2013, Zhang *et al.* 2013, Steelman *et al.* 2016). The EGFR pathway can phosphorylate ER α tyrosine residue Y537 and p38/MAPK is implicated in threonine phosphorylation on ER α -T311 (Cui *et al.* 2005, Kerdivel *et al.* 2013). Several drugs targeting these pathways have been tested in ER+ breast cancer, but success is limited and biomarkers of response are unknown (Morris and Wakeling 2002, Fedele *et al.* 2012). Since the PI3K/AKT/mTOR pathway was identified as possibly regulated by ASH2L (Chapter 3), we hypothesized that inhibition of mTOR would alter ER α phosphorylation, possibly identifying the mechanism behind estrogen-independent activation of ER α in the SUM-44 cell line. Reduced PI3K expression by ASH2L knockdown was confirmed by immunoblot but AKT1 was unchanged (Figure 3.4-C) and immunoblot for ER α -pS167 following treatment with the mTOR inhibitor KU-00063794 did not identify reduction of phosphorylation at this site (Figure 3.5-E), therefore the mechanism of estrogen-independent ER α activation remains unknown.

Another strategy for overcoming endocrine resistance is to target genes downstream of ER α (Mancuso and Massarweh 2016). ER α drives cell cycle progression from G₁ to S phase through activation of its transcriptional program (Wang and Yin 2015). CCND1 (cyclin D1) is an ER α -target gene that mediates G₁ to S phase transition by binding to CDK4 or CDK6 and stimulating transcription (Dabydeen and Furth 2014). Cyclin D1 is associated with several types of cancer, including breast, and is correlated with endocrine resistance (Dabydeen and Furth 2014, Nagaraj and Ma 2015). As discussed in section 1.2b, amplification of CCND1, located at 11q13, occurs in a subset of breast cancer patients and the 11q12-q14 amplicon often co-occurs with the 8p11-p12 amplicon (Still *et al.* 1999, Reis-Filho *et al.* 2006, Kwek *et al.* 2009, Karlsson *et al.* 2011, Sircoulomb *et al.* 2011, Bilal *et al.* 2012, Cornen *et al.* 2014). Cooperation of 11q14 oncogenes with oncogenes from the 8p11-p12 amplicon has been suggested (Kwek *et al.* 2009, Karlsson *et al.* 2011) and the data presented here supports this hypothesis. The CDK4/6 inhibitor palbociclib is in clinical trials in ER+ breast cancer and is demonstrating increased progression free survival in conjunction with endocrine therapy in luminal breast cancers (Nagaraj and Ma 2015, Turner *et al.* 2015, Angus *et al.* 2016, Knudsen and Witkiewicz 2016, Mancuso and Massarweh 2016). Genes with reduced H3K4me3 promoter peaks and transcript expression following ASH2L knockdown in SUM-44 cells annotated to the “palbociclib response” with a p-value of 5.7×10^{-7} , suggesting that knockdown of ASH2L reduces the expression of a suite of genes that sensitize cells to palbociclib (Figure 3.4-E). We tested response to palbociclib in the SUM-44 and MCF7 cell lines following knockdown of ASH2L and validated that ASH2L knockdown reduces palbociclib response in SUM-44 cells (Figure 3.6-E). MCF7 cells were more sensitive to palbociclib than SUM-44 cells and ASH2L knockdown did not

alter sensitivity. Interestingly, CCND1 was identified as downregulated by knockdown of ASH2L (Table 3.2), yet immunoblot for cyclin D1 expression demonstrated increased cyclin D1 protein levels in SUM-44 cells and no change in MCF7 following knockdown of ASH2L (Figure 3.4-C). MCF7 cells do not have either the 8p11-p12 or 11q12-q14 amplicons present in SUM-44 cells, underscoring the complexity of luminal B breast cancer genomic alterations and the potential interaction between multiple oncogenes affecting the biology and drug sensitivities of these tumors.

Although therapies targeting signaling pathways that complement ER α activity have demonstrated some improvement in the treatment of ER+ breast cancer, resistance and lack of biomarkers are still common clinical challenges. The work presented here identified NSD3 as a potential biomarker for SERD response and ASH2L as a potential biomarker for palbociclib response in endocrine-resistant tumors. The 8p11-p12 amplicon represents not only a source of therapy response markers, but understanding the mechanism of action of the oncogenes present in this genomic region provides the potential for development of novel therapies that will affect the genomic and epigenomic events responsible for tumorigenesis. Indeed, epigenetic therapies are under clinical investigation and have demonstrated some success in the treatment of breast and other cancer types (Kerdivel *et al.* 2013, Ades *et al.* 2014). This work on NSD3 and ASH2L provides additional evidence that can be utilized for the development and novel therapies and improvement of those already under clinical investigation.

c. Epigenetic therapies for ER+ breast cancer

Unlike genetic alterations, epigenetic changes leading to cancer are reversible (Lo and Sukumar 2008, Simon and Lange 2008, Kristensen *et al.* 2009). Coupled with

increased understanding of the histone modifying enzymes dysregulated in cancer and their downstream effects, the potential therapeutic benefits of targeting these factors is becoming apparent (Morishita and di Luccio 2011). Of the epigenetic drugs, DNMT and HDAC inhibitors are the best-studied. Use of these drugs has identified the need to better understand optimal timing of epigenetic therapy, appropriate biomarkers, and specificity of chromatin-modifying enzymes for tailored therapeutic benefit (Lustberg and Ramaswamy 2009, Pathiraja *et al.* 2010, Cai *et al.* 2011).

HDAC inhibitors (HDACi) have been explored in several disease states, including ER+ breast cancer (Thomas and Munster 2009). HDACi are implicated in cell cycle arrest by nuclear export of cyclin D1, which interacts with histone modifying enzymes to execute its transcriptional program, and by favoring hyperacetylation of genes, including pro-apoptotic genes, leading to their expression (Alao *et al.* 2004, Inoue and Fry 2015). HDACi themselves do not discriminate transcription of pro- versus anti-apoptotic genes, leaving certain tumors exposed to the possibility of HDACi-induced accelerated growth until biomarkers can be established to predict this differential response (Lo and Sukumar 2008, Lustberg and Ramaswamy 2009). HDAC inhibition also re-sensitizes cells to endocrine therapies by interrupting the interaction of HDACs with DNMTs, reversing the DNA methylation-induced silencing of ESR1 (Allred *et al.* 2004, Kristensen *et al.* 2009, Thomas and Munster 2009, Abdel-Hafiz and Horwitz 2015). This mechanism, however, only affects tumors where the mechanism of endocrine resistance is loss of ER α expression. Alternatively, HDACi have been implicated in hyperacetylation of the chaperone protein HSP90 (Lo and Sukumar 2008, Lustberg and Ramaswamy 2009). ER α is one of the many client proteins of HSP90, so hyperacetylation that destabilizes HSP90 results in degradation of ER α . HDACi, however, can also alter the chromatin

structure, allowing histone acetylation-mediated opening of genetic material for increased transcription by ER α (Margueron *et al.* 2004). The multiple and potentially conflicting mechanisms by which HDACi function highlight the need to better understand epigenetic factors and tailor inhibition toward remedy of specific dysregulated processes.

Clinical investigation of HDACi has provided an important step forward in the use of epigenetic therapy to treat cancer (Lustberg and Ramaswamy 2011, Connolly and Stearns 2012, Walsh *et al.* 2016). Since histone methylation is not as well-understood as DNA methylation and histone acetylation, HMT inhibition (HMTi) is not as developed as inhibition of other epigenetic enzymes (Morishita and di Luccio 2011). As the field of epigenomics progresses, however, the importance of this mechanism of gene regulation has become clear and HMTi is advancing (Morishita and di Luccio 2011, French *et al.* 2014, Liu *et al.* 2014). Several groups have used large databases such as GISTIC and TCGA to determine optimal factors for drug targeting and EZH2, MLL, and the NSD family of HMTs have been identified as some of the most ideal candidates (Liu *et al.* 2014, Michalak and Visvader 2016). EZH2 inhibitors have progressed furthest of the HMTi class, but even these drugs have only reached early stage clinical trials (Garapaty-Rao *et al.* 2013, Curry *et al.* 2015, Michalak and Visvader 2016, Sato *et al.* 2017). Other HMTi remain under preclinical investigation and require additional *in vitro* studies of HMT activity and mechanisms of action, such as those described in this work, for continued advancement of this field (Liu *et al.* 2014, Katoh 2016, Michalak and Visvader 2016).

EZH2 is a PcG protein implicated in H3K27 methylation-mediated transcriptional repression and is one of the best-studied HMT enzymes to date (Lo and Sukumar 2008, Pathiraja *et al.* 2010, Grzenda *et al.* 2011). It functions in polycomb repressive complexes (PRC) and is antagonized by the Trx group proteins such as ASH2L and the

MLL complexes (Simon and Lange 2008, Grzenda *et al.* 2011, Huang *et al.* 2011). HMT inhibitors (HMTi) have been primarily targeted to EZH2 and have been designed based on the paradigm that histone methylation is a negative regulator of tumor suppressors, and therefore inhibition of EZH2 and other PcG factors will alleviate this repression and halt cell cycle progression (Curry *et al.* 2015, Sato *et al.* 2017). There is some evidence to indicate that this strategy may be efficacious as EZH2 inhibitors indeed demonstrate reduced growth in tumor cell lines *in vitro* (Garapaty-Rao *et al.* 2013). Unfortunately, these therapies are highly dose-dependent and require further investigation to determine the precise timing for optimal treatment (Lustberg and Ramaswamy 2009, Garapaty-Rao *et al.* 2013). Several combination therapies have been tested in an attempt to circumvent these issues and have displayed more success than individual compounds, however these studies have also revealed the need to better understand the histone modifications at particular loci to optimize HMTi therapies as global inhibition is not necessarily the best strategy in all cases (Lo and Sukumar 2008, Curry *et al.* 2015, Sato *et al.* 2017). Several companies are developing additional HMT inhibitors currently, including specific EZH2 inhibitors as well as generalized SET domain inhibitors, which would not only target repressive histone methyltransferases but also transcriptional activators such as NSD3 and the MLL family proteins (Michalak and Visvader 2016).

Another strategy by which HMT activity can be targeted is via chromatin-interacting proteins such as those of the chromatin-reader bromodomain and chromodomain families. Many HMT enzymes, NSD3 and ASH2L included, rely on these reader proteins for recruitment to directed sites on the chromatin. Bromodomain inhibitors have been under development and testing and have shown promising results in the clinic (French *et al.* 2014, Borbely *et al.* 2015). These chromatin readers, however,

are promiscuous and broad inhibition of their activity has unknown implications. One advantage to this strategy of epigenetic inhibition is that non-SET domain-containing proteins, such as ASH2L and NSD3-S, are also inhibited in the manner. NSD3-S is known to rely on the BRD family of bromodomain proteins for chromatin tethering, and inhibition of BRD4 has demonstrated abrogated NSD3-S interaction with chromatin (Shen *et al.* 2015). NSD3-S bound to BRD4 also binds other factors, such as the chromodomain protein CHD8, a potential novel drug target in cancer (Shen *et al.* 2015). Another bromodomain protein, ANCCA, is implicated in recruitment of MLL complexes to histones (Zou *et al.* 2014). These chromatin-reading protein families are candidates for drug development and understanding their mechanism of action and effects on the epigenomic state of cancer cells is essential to optimizing their therapeutic benefits.

Epigenetic therapies represent a novel arm of therapeutic investigation and, though still in the early stages of development compared to many other cancer treatment strategies, comprise a promising source of compounds with the potential to revolutionize cancer treatment. The work presented here on NSD3 and ASH2L, both associated with transcriptional activation by histone methylation activity, challenges the current paradigm that epigenetic factors function as oncogenes by transcriptional repression of tumor suppressors. The antagonistic relationship of these trithorax group proteins on the polycomb group counterparts such as EZH2 is an interesting and extremely complicated topic of future investigation. Overall, it is clear that further investigation of the specific actions of epigenetic factors dysregulated in cancer is necessary in order to advance the field of epigenomics and identify efficacious strategies for targeting the biological effects of these alterations in patients.

4.3. Concluding Remarks

Breast cancer is the most common cancer in women and second leading cause of cancer death in women in the United States, resulting in the loss of 40,000 lives each year (Morris and Carey 2007, Chang 2012, 2014, Lumachi *et al.* 2015, Selli *et al.* 2016). Great strides have been made over the last four decades in the diagnosis and treatment of breast cancer patients, however there remains much progress to be made. Resistance to endocrine therapies is still a major clinical challenge in ER+ breast cancer and the need to understand mechanisms of resistance and develop novel therapeutics is urgent. Identification of intrinsic subtypes of breast cancer, classification of tumors based on expression profiles, and technological advancements coupled with the development of large databases tracking genomic alterations in primary breast tumors has allowed novel biological mechanisms of tumorigenesis to be elucidated and investigated. Similarly, the field of epigenomics has opened a novel avenue of investigation into tumor biology and identified a suite of potential therapeutic candidates and biomarkers in histone methyltransferase enzymes.

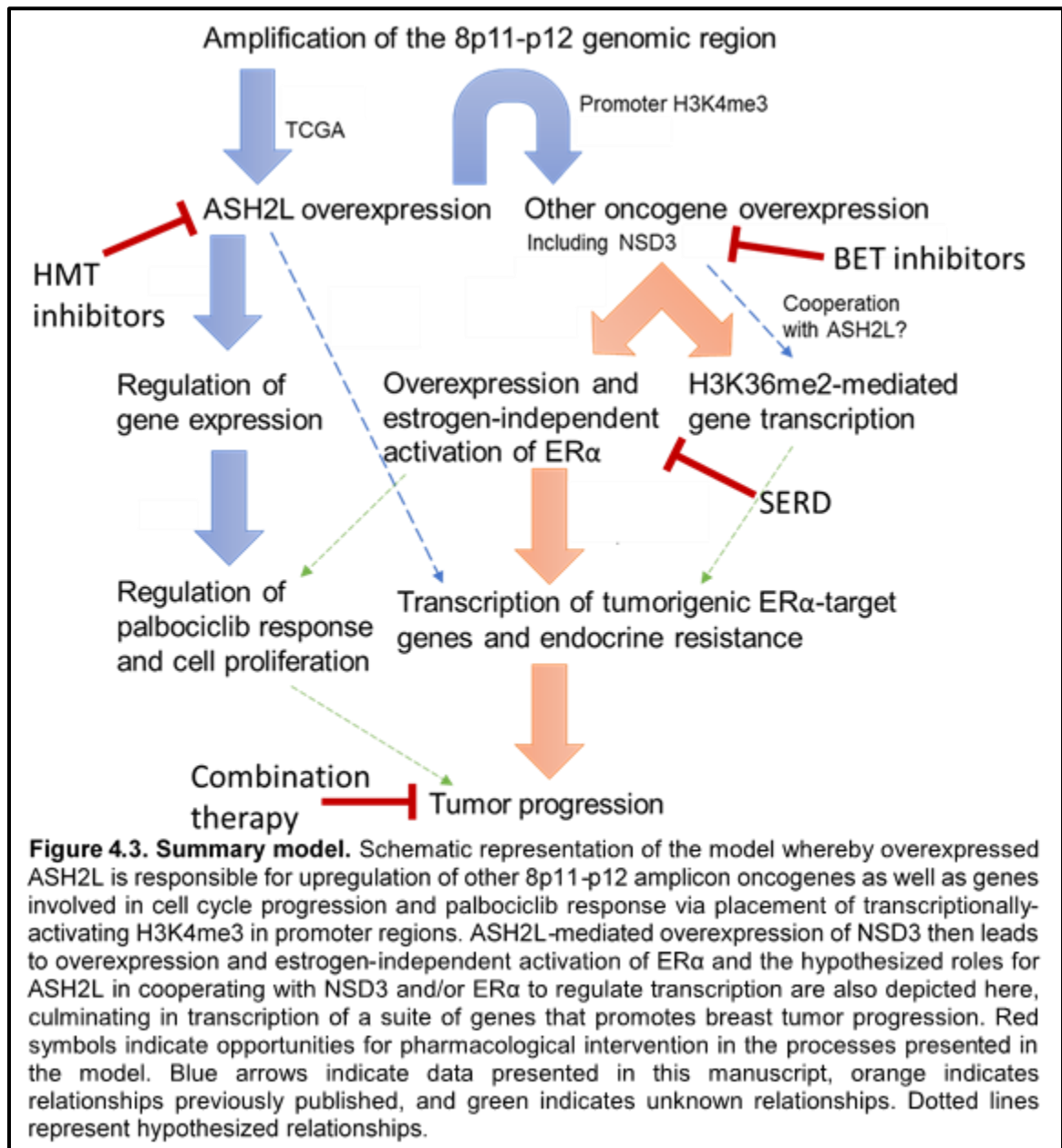
At the cross-road between genomic and epigenomic alterations in cancer lies amplification-induced overexpression of oncogenes that modify the histone code. The 8p11-p12 amplicon is found in 15% of primary breast tumors and harbors three epigenetic modifiers of chromatin, two of which, NSD3 and ASH2L, are implicated in regulation of histone methylation and transcriptional activation. NSD3 has been previously validated as an oncogene (Yang *et al.* 2010, Mahmood *et al.* 2013), however little was known about the biological role of the two isoforms of NSD3. This work established a link between amplification and overexpression NSD3 and overexpression and estrogen-independent activation of ER α (Figure 4.3). We have identified and

described here a novel mechanism of endocrine resistance in luminal B breast cancer and demonstrated a need for improved therapies that reduce receptor activity irrespective of estrogen status. Additional work is required to fully understand the implications of the non-catalytic short isoform of NSD3 and the mechanism behind NSD3-induced overexpression and activation of ER α .

ASH2L has been identified by several groups as a candidate oncogene from the 8p11-p12 region (Ray *et al.* 2004, Garcia *et al.* 2005, Gelsi-Boyer *et al.* 2005, Cornen *et al.* 2014), however this epigenetic factor has been understudied in cancer to date. The data presented here identify a role for ASH2L in regulation of H3K4me3 specifically in the promoter regions of genes associated with cell cycle progression, epigenetic regulation of chromatin, and palbociclib response. We also demonstrated that knockdown of ASH2L reduced expression of NSD3 and ER α , extending our understanding of the relationship between these oncogenes (Figure 4.3). It is clear from the data presented in this work and the unanswered questions that remain that the underlying biology of 8p11-p12 amplicon oncogene-mediated epigenetic dysregulation is complex. Further investigation of the transcriptional regulation of gene expression by NSD3 and ASH2L, cooperation between these oncogenes, effects on the proteome, and the mechanism of estrogen-independent ER α activation will provide insight into the essential biology of a significant subset of breast cancer patients at risk of succumbing to their disease due to endocrine therapy resistance.

Histone methyltransferases are increasingly recognized not just for their potential as drug targets but also as biomarkers for therapeutic response (Connolly and Stearns 2012, Chen *et al.* 2014, Michalak and Visvader 2016). NSD3 and ASH2L both have the

potential to be direct drug targets due to their oncogenic effects on transcription and cell behavior, and these oncogenes and the 8p11-p12 amplicon also have the potential to be utilized as biomarkers to predict treatment response to SERD and cell cycle therapies. The work presented here provides a rationale to include survey of NSD3 and ASH2L expression in clinical trials investigating these types of compounds. The downstream



processes and pathways under control of these two epigenetic oncogenes can be targeted therapeutically, extending the future implications of this study. The work presented here provides the foundation for a multitude of additional lines of investigation and has the potential to be translated into novel therapeutic strategies to improve survival for an important group of patients with ER+ breast cancer.

CHAPTER 5: Materials and Methods

5.1. Cell culture

All cells were cultured at 37°C in 10% CO₂.

5.1a. SUM-44. Cells were cultured in serum-free Ham's F-12 medium supplemented with 1 µg/ml hydrocortisone, 1 mg/ml bovine serum albumin, 10 mM HEPES, 5mM ethanolamine, 5 µg/ml transferrin, 10 nM tiiodothyronine, 50 nm sodium selenite, 25 µg/ml gentamicin, 2.5 µg/ml fungizone, and 5 µg/ml insulin. For estrogen-free culture conditions, phenol red-free Ham's F-12 media was substituted for normal Ham's F-12 with all the above supplements. 3 µg/ml puromycin was used for selection and maintenance of shRNA-transduced SUM-44 cells.

5.1b. SUM-52. Cells were cultured in Ham's F-12 medium supplemented with 5% fetal bovine serum, 1 µg/ml hydrocortisone, 25 µg/ml gentamicin, 2.5 µg/ml fungizone, and 5 µg/ml insulin. 2 µg/ml puromycin was used for selection and maintenance of sRNA-transduced SUM-52 cells.

5.1c. MCF-7 and CAMA-1. Cells were cultured in DMEM supplemented with 10% fetal bovine serum, 25 µg/ml gentamicin, and 2.5 µg/ml fungizone. 2 µg/ml puromycin was used for selection and maintenance of sRNA-transduced MCF-7 and CAMA-1 cells.

5.1d. MCF10A. Cells were cultured in serum-free Ham's F-12 medium supplemented with 1 µg/ml hydrocortisone, 1 mg/ml bovine serum albumin, 10 mM HEPES, 5mM ethanolamine, 5 µg/ml transferrin, 10 nM tiiodothyronine, 50 nm sodium selenite, 25 µg/ml gentamicin, 2.5 µg/ml fungizone, 10 ng/ml EGF and 5 µg/ml insulin. 1 µg/ml puromycin was used for selection and maintenance of sRNA-transduced MCF10A cells.

5.1e. ZR-75-1. Cells were cultured in RPMI supplemented with 10% fetal bovine serum, 25 µg/ml gentamicin, and 2.5 µg/ml fungizone.

5.2 Antibodies

Antibodies used in these studies were diluted in 5% milk and used at a dilution of 1:1000 for immunoblot unless otherwise stated. Antibodies include:

NSD3 (WHSC1L1): Proteintech 11345-1-AP; Vakoc Lab antibody (Shen *et al.* 2015)

ER α : Cell Signaling 8644S, Santa Cruz HC-20 (1:50 dilution for ER α ChIP-PCR cocktail); NeoMarkers ER Ab-10 (TE111.5D11) (1:50 dilution for ER α ChIP-PCR cocktail)

pS167 ER α : Cell Signaling 5587S

ASH2L: Bethyl A300-489A; 1:1000 for immunoblot and 1:50 for IP

H3K4me3: Abcam ab8580; 1:1000 for immunoblot and 1:50 for ChIP-seq

FOXA1: Abcam ab109760

AKT1: Cell Signaling 2938S

BRD2: Cell Signaling 5848S

BRD4: Cell Signaling 13440S

Cyclin D1: Cell Signaling 2926P (courtesy Dr. Carroll Lab)

Ki-67: Dako A0047 (courtesy Dr. Carroll Lab)

PI3 Kinase: Abcam ab137815

PLK1: Abcam ab47867

IgG: Cell Signaling 3900S

β -actin: Cell Signaling 3700S

5.3. shRNA constructs

Lentiviral shRNA expression vectors from the pLKO shRNA catalog were purchased from Sigma. The vectors used were the NSD3-short vector TRCN0000415241, NSD3-total vectors TRCN000425711, TRCN0000015615, and TRCN0000015616, ASH2L

vectors TRC0000019275 and TRC0000019276, ESR1 vector TRCN0000003301 and LacZ control vector. Plasmid DNA for all constructs was obtained using the Promega PureYield plasmid midiprep system (A2495) according to manufacturer's instructions.

5.4. Lentiviral production and transformation

Lentivirus was prepared using Sigma Mission lentiviral packaging system (Sigma, shp-001) in 293FT packaging cells following manufacturer's instructions. Briefly, each construct was co-transfected into 293FT cells with Sigma pLKO shRNA vectors and Lipofectamine 2000 in antibiotic-free media. Virus was harvested 48 hours after transfection, filtered, aliquoted, and stored at -80°C until use. Target cells were transduced with virus in growth media supplemented with 5 µg/ml polybrene using 0.5-1.0 ml virus per 1 million cells. Cells were selected for resistance marker expression and maintained in puromycin-containing growth media (1-3 µg/ml as listed above) beginning 24-48 hours after infection. Cells were cultured at least 5 days to allow expression of the construct.

5.5. Immunoblotting

Cells were plated and growth to 75-90% confluency. Cells were treated as indicated, either with drug compounds or shRNA infection, for the specified timepoints. Cells were lysed in buffer containing 20mM Tris-HCl (pH 8.0), 137 mM NaCl, 1% NP40, 10% glucerol, 1 mM Na₃VO₄, and 1x protease inhibitor cocktail (Calbiochem 539131). Protein concentrations were measured by Bradford assay (Bio-Rad). Laemmli sample buffer was added to the lysates and the samples were boiled for 5 min before being separated by electrophoresis on SDS-polyacrylamide gels (Bio-Rad). After transferring the proteins to polyvinylidene difluoride (PVDF) membranes, blots were probed overnight at 4°C with the indicated antibodies. Blots were washed 3x10 min in 1x tris-buffered saline with

tween 20 (TBST), probed 1 hour with the appropriate secondary antibody, incubated 1 min in ECL and developed on a Konica SRX-101A medical film processor. After developing, membranes were re-probed with a new primary antibody or discarded.

5.6. Proliferation assays

Proliferation assays were performed in 6-well culture plates seeded in triplicate with 200,000 cells per well. At each timepoint, cells were washed once with PBS and agitated on a rocker table with 0.5 ml HEPES/MgCl₂ buffer (0.01 M HEPES and 0.015 M MgCl₂) for 5 min. Cells were then lysed for 10 min with addition of 50 µl of an ethyl hexadecyldimethylammonium solution and nuclei were counted using a Z1 Coulter Counter (Beckman Coulter, Brea, CA, USA) according to manufacturer's instructions. Data are reported as averages where error bars represent +/- one standard deviation.

5.7. Drug treatment proliferation assays

Drug treatment assays were performed in 6-well culture plates seeded in triplicate with 250,000 - 500,000 cells per well. Cells were treated every 24 or 48 hours (2-5 treatments total) with the indicated drug compound and concentration. When control wells reached 90% confluence, cells were washed once with PBS and agitated on a rocker table with 0.5 ml HEPES/MgCl₂ buffer (0.01 M HEPES and 0.015 M MgCl₂) for 5 min. Cells were then lysed for 10 min with addition of 50 µl of an ethyl hexadecyldimethylammonium solution and nuclei were counted using a Z1 Coulter Counter (Beckman Coulter, Brea, CA, USA) according to manufacturer's instructions. Counts were normalized to the average of the untreated samples and are reported as averages where error bars represent +/- one standard deviation.

5.8. Colony forming assay

Cells were plated in triplicate in 6-well plates at varying clonal cell densities. MCF7 cells were plated at 5,000 cells per well and SUM-44 cells at 15,000 cells per well. MCF7 cells were cultured as normal. SUM-44 cells required 1:1 ratio of regular media to conditioned media from SUM-44 cells growing at high density. Puromycin-supplemented media was used in these assays to maintain selection of infected cells. Media was changed 24 hours after plating and then 7 days later. Colonies formed for two weeks and then were fixed with 1 ml/well 3.7% paraformaldehyde for 20 minutes at RT. Colonies were stained with 1 ml/well 0.2% crystal violet for 15 minutes at RT and de-stained with dH₂O. Colonies were allowed to dry prior to imaging, counting, and quantification on the GelCount System from Oxford Optronix.

5.9. qRT-PCR

Total RNA was harvested using a Qiagen RNeasy Plus Mini Kit (74136) according to manufacturer's instructions. RNA was quantified on the NanoDrop 2000c spectrophotometer and 2 ug RNA utilized for each cDNA reaction using the iScript Adv cDNA Kit for RT-qPCR (172-5038) according to manufacturer's instructions. Quantitative RT-PCR was then performed using 5 ng of cDNA per reaction in triplicate for each primer and sample pair in Roche FastStart Universal SYBR Green Master (Rox) mix (04913914001). Cycling conditions were 95°C for 10 min, then 40 cycles of 95°C 10 sec, 51°C 10 sec, 68°C 40 sec. GAPDH primers (IDT PrimeTime qPCR Primer set Hs.PT.39a.22214836) were used as control for each sample, analyzed by the $\Delta\Delta C_t$ method (Livak and Schmittgen 2001). Values are reported as averages of triplicate wells where error bars represent +/- one standard deviation. Primer sets were designed using IDT custom parameters and conditions for each primer pair are as reported below.

| Name | Sequence 5'-3' | Tm (°C) | %GC |
|-----------|------------------------|---------|------|
| ASH2L – F | CTCCGTGGATGAAGAGAA | 51.1 | 50.0 |
| ASH2L – R | GGTAGACAGGATGAGGTATC | 51.2 | 50.0 |
| ESR1 – F | GCTTCGATGATGGGCTTACT | 54.9 | 50.0 |
| ESR1 – R | CCTGATCATGGAGGGTCAAATC | 55.3 | 50.0 |
| FBXO5 – F | GCCTCAAAGCCTGTATTC | 50.8 | 50.0 |
| FBXO5 – R | CAAATCCACAGCCTTCTC | 50.7 | 50.0 |
| EZH2 – F | TGACTGCTTCCTACATCC | 51.1 | 50.0 |
| EZH2 – R | CTTTGCTCCCTCCAAATG | 51.0 | 50.0 |
| TTK – F | GTTGTGCCTGGATCTAAAC | 51.0 | 47.4 |
| TTK – R | CCAGAGGTTCTTGAAATG | 50.7 | 47.4 |
| BUB1 – F | GGTTAATCCAGCACGTATG | 50.8 | 47.4 |
| BUB1 – R | ACTGGTGTCTGCTGATAG | 51.1 | 50.0 |

5.10. Immunoprecipitation

Whole cell lysate was harvested using the buffer and protocol described under section 5.6 or in FAK buffer supplemented with 1 mM Na₃VO₄, and 1x protease inhibitor cocktail. Samples were measured by Bradford assay (Bio-Rad) and diluted with lysis buffer to 1000 µg protein per reaction. Antibodies were added at 1:50 dilution and samples incubated overnight at 4°C with rotation. Protein A/G beads were incubated with lysate/antibody samples for 1 hour at RT with rotation prior to washing 3x in TBST with 1x protease inhibitor cocktail. Protein was eluted in 50 µl 1x laemmli sample buffer (diluted to 1x with lysis buffer), boiled 5 min, and 25 µl loaded per lane on SDS-polyacrylamide gels (Bio-Rad). Whole cell lysate samples were created in parallel from the same samples prior to incubation with antibody and flow through was collected prior to wash steps. IgG as well as targeted antibodies were used. Gels were transferred, probed, and developed as described in section 5.5.

5.11. Microarray

RNA integrity was verified on an Agilent 2200 TapeStation (Agilent Technologies, Palo Alto, CA). 100-200 ng of total RNA will be used to prepare cRNA utilizing Ambion

Illumina TotalPrep RNA Amplification Kit (Thermo Fisher Scientific, MA). 0.75 µg of cRNA per sample was hybridized to Illumina's (HumanHT-12 v4.0 Expression BeadChip following the manufacturer's WGEX Direct Hybridization protocol (Illumina, CA). Processed array were scanned on an Illumina HiScan. Raw data was produced using Illumina Genome Studio followed by differential gene expression analysis utilizing Partek Genomics Suite (St. Louis, MO).

5.12. RNA-seq

Total RNA was prepared using a Qiagen RNeasy Plus Mini Kit and processed by the MUSC Genomics core for 2 x 125 cycles, paired-end RNA sequencing on an Illumina HiSeq 2500. RNA integrity was verified on an Agilent 2200 TapeStation (Agilent Technologies, Palo Alto, CA). A total of 100-200 ng of total RNA was used to prepare RNA-seq libraries using the TruSeq RNA Sample Prep kit following the manufacturer's instructions (Illumina, San Diego, CA). Sequencing was performed on an Illumina HiSeq 2500. Samples were demultiplexed using CASAVA (Illumina, San Diego, CA). Fastq files were used to map reads to the human genome (hg19, UCSC) utilizing Tophat2 with default settings. Samples were prepared in triplicate as biological replicates and sequenced simultaneously.

5.13. Chromatin immunoprecipitation (ChIP)

5.13a. Chromatin isolation and shearing. For each ChIP, 8-15 million cells (1-2 15 cm dishes) per treatment condition were used as starting material and processed with the Covaris truChIP chromatin shearing reagent kit (Covaris, 520154) according to manufacturer's instructions. Briefly, cells were first washed with RT PBS then crosslinked using 2 mM disuccinyl-glutamate in PBS at RT for 30 min followed by fixation in 1x Covaris fixing buffer with 1% formaldehyde for 5 min (MCF-7) or 2.5 min

(SUM-44). After quenching 5 min in Covaris quenching buffer, cells were washed and scraped in 5 ml/plate cold 1x PBS, spun at 7,500xg for 5 min at 4°C, washed in PBS, then resuspended in 1x lysis buffer and transferred to a microfuge tube. The samples were incubated 10 min with rotation at 4°C, spun at 1,700xg for 5 min at 4°C, resuspended in 1x wash buffer, incubated 10 min with rotation at 4°C, and spun at 1,700xg 5 min at 4°C. The pellets were then washed twice in 1x shearing buffer without resuspension using the same pelleting conditions as above. Upon final wash, pellets were resuspended in 1 ml shearing buffer and transferred to a Covaris glass sonication tube. Pellets of duplicate samples were combined at this step to 1 ml total volume for shearing. Each sample was sheared on the Covaris S220 series sonicator under high cell ChIP standard conditions for 10 min (MCF-7) or 8 min (SUM-44). Sheared chromatin was then transferred to a DNA LoBind tube, centrifuged at 10,000xg for 10 min at 4°C, and transferred to a clean DNA LoBind tube for storage at 4°C (up to 72 hours).

5.13b. ChIP reaction setup. ChIP reactions were set up in duplicate (IgG control, H3K4me3), triplicate (ER α), or quadruplicate (NSD3) according to antibody efficiency. Reactions included 900 μ l ChIP dilution buffer (0.01% SDS, 1.10% Triton X-100, 1x TE buffer pH 8.0, 167 mM NaCl), 100 μ l sheared chromatin, 10 μ l (1x) protease inhibitor cocktail (Thermo, 78442), and 4 μ g antibody as indicated. Reactions were incubated at 4°C with end-to-end rotation overnight.

5.13c. Epitope verification. Upon first use of a new ChIP antibody, a 10 μ l aliquot of each sheared chromatin sample was mixed with 10 μ l of laemmli sample buffer, and run as a normal western blot (see section 5.5) to verify that the shearing process did not disrupt the epitope to be used in the ChIP process.

5.13d. Size fragment verification. Upon first use of a new cell line, including knockdown cells of a previously used cell line, a 25 μ l aliquot of each sheared chromatin sample was analyzed by Agilent 2200 TapeStation (Agilent Technologies, Palo Alto, CA) according to manufacturer's instructions.

5.13e. Chromatin washing and DNA elution. Protein A/G beads were pre-blocked with 0.5% BSA in PBS and 20 μ l beads with 10 μ l protease inhibitor cocktail added to each ChIP reaction at 4°C for 1 hour with end-to-end rotation. Supernatant was removed and beads were washed 4x in wash buffer (1x TE buffer pH 8.0, 0.5 M LiCl, 100 mM NaCl, 0.10% sodium deoxycholate, 1% Triton X-100; recipe courtesy of the Brown Lab) and 2x in 1x TE pH 8.0. Beads were resuspended in 50 μ l 1x TE buffer pH 8.0 with 2 μ l RNase and incubated with input samples (10 μ l non-ChIP'd sheared chromatin, 40 μ l 1x TE, 2 μ l RNase) for 30 min at 37°C. 50 μ l elution buffer (0.2 M sodium bicarbonate, 2% SDS) and 2.5 μ l proteinase K were added to each sample and incubated at 65°C overnight with shaking (1400 rpm). DNA was then purified using AMPure XP beads (Beckman Coulter, A6381) according to manufacturer's instructions and quantified by PicoGreen DNA kit (Thermo, 7605).

5.13f. Preparation for sequencing. Sequencing libraries were prepared from ChIP DNA by the MUSC Genomics Core Facility with Rubicon ThruPLEX library preparation kits and sequenced as 35 bp single-end reads on an Illumina HiSeq 2500. Libraries for three biological replicates were prepared and sequenced for each sample type.

5.14 Bioinformatics and Statistical Analysis

5.14a. Microarray. Data were normalized using the linear and LOWESS (LOcally WEighted Scatterplot Smoothing) method (Yang *et al.* 2002). Normalized data were imported into GeneSpring for analysis. Statistical significance of differentially expressed

genes was determined using four replicate measurements for each probe (gene). A t-test was performed with the null hypothesis that the normalized log fold changes reflecting the change in gene expression (44/NS) equal zero. The Benjamini and Hochberg multiple test correction was used to determine the false discovery rate (FDR) (Benjamini and Hochberg 1995).

5.14b. RNA-seq. Paired end sequencing was performed on RNA samples using an Illumina HiSeq 2500 with each sample sequenced to a depth of ~50 million reads. Data was subjected to Illumina quality control (QC) procedures (>80% of the data yielded a Phred score of 30), and preprocessing using Trimmomatic, which removed adapter sequences and filtered low quality reads (Bolger *et al.* 2014). Further data QC was performed using FastQC prior to aligning the reads to the human genome hg19 using Tophat2 (Kim *et al.* 2013). The resulting SAM files were sorted and inputted into the Python package HTSeq to generate count data for gene-level differential expression analyses. In order to infer differential signal within the data sets with robust statistical power, we utilized DESeq2 (Love *et al.* 2014). Transcript count data from DESeq2 analysis of the samples were sorted according to their adjusted p-value or q-value, which is the smallest false discovery rate (FDR) at which a transcript is called significant. FDR adjustment is needed with large data sets such as RNAseq. FDR is the expected fraction of false positive tests among significant tests and was calculated using the Benjamini-Hochberg multiple testing adjustment procedure (Benjamini and Hochberg 1995). Using the transcript count data from DESeq2 analysis, we selected transcripts with negative log fold change values, indicating decreased expression in test versus control samples, and $p < 0.1$. This consensus gene set was then used for downstream

analysis, including comparison between different shRNA constructs to generate a more statistically stringent list of genes.

5.14c. ChIP-seq. Single end sequencing was performed on ChIP DNA using an Illumina HiSeq 2500 with each sample sequenced to a depth of ~50 million reads. Data was subjected to Illumina quality control (QC) procedures (data yielded Phred scores >30). Further data QC was performed using FastQC prior to aligning the reads to the human genome hg19 using Bowtie2. Aligned reads were converted from SAM to BAM format, sorted, and indexed. BED format files were obtained from BAM files. Peaks were called with the MACS version 2 peak caller (Zhang *et al.* 2008). ChIP samples were compared to matched input samples to generate peak sets for each replicate, which were then compared to matched condition biological replicates as described in Chapter 3, section 2 using an FDR cutoff of 0.4. Consensus peak sets generated by replicate overlap were used for downstream analysis, including comparison between treatment conditions.

5.14d. Gene Ontology and Pathway Analysis. Various data comparisons were performed between ChIP-seq, RNA-seq, and microarray gene lists as described in Chapters 2 and 3. Statistical analysis of Gene Ontology and other processes, pathways, and interactions was performed on these gene lists by gene list enrichment analysis using the ToppGene suite (Chen *et al.* 2009). P-values and percentage of genes in input compared to annotated gene lists in ToppFun are reported in results sections with Bonferroni corrected p-values and absolute number of genes aligning to each process reported in Appendices according to gene set (See List of Appendices on page v.).

5.14e. General Statistics. Statistical analysis was performed in Microsoft excel. Student's t-test was used and two-tail p-values reported. Graphs with error bars represent +/- one standard deviation unless otherwise reported.

5.15. Patient tumor cell culture

Samples were obtained according to IRB protocol (Pro00048028). Using sterile technique, samples were aliquoted to 50 ml falcon tubes, spun at 1,000 rpm for 5 min at RT, and the supernatant removed and properly discarded. Cells were resuspended in 1x Hank's Buffered Saline Solution (HBSS), consolidated, and spun again at 1,000 rpm for 5 min at RT. Supernatant was removed and resuspension and spin step was repeated. To lyse red blood cells, 9 ml sterile water was added to the tubes followed immediately by 1 ml 10x HBSS. Tubes were spun again at 1,000 rpm for 5 min at RT. Supernatant was removed and cells were resuspended in Ham's F-12 media supplemented with insulin, hydrocortisone, and 5% FBS (see section 5.1b). Cells were counted and plated in 6-well plates at a density of 1 million cells/well. Cells were cultured in various media types and supplements of estradiol but could not be cultured more than a few weeks. One well was lysed for western blotting after 2.5 weeks in culture and blotted for NSD3 and ER α expression according to section 5.5.

REFERENCES CITED

"<a systematic evaluation of miRNA mRNA interactions involved in the migration and invasion of breast cancer cells.pdf>."

(2012). "Comprehensive molecular portraits of human breast tumours." Nature **490**(7418): 61-70.

(2014). "SEER Cancer Statistics Factsheets: Lung Cancer." Retrieved February 13, 2014, from <http://seer.cancer.gov/statfacts/html/lungb.html>.

Abdel-Hafiz, H. A. and K. B. Horwitz (2015). "Role of epigenetic modifications in luminal breast cancer." Epigenomics **7**(5): 847-862.

Ades, F., D. Zardavas, I. Bozovic-Spasojevic, L. Pugliano, D. Fumagalli, E. de Azambuja, G. Viale, C. Sotiriou and M. Piccart (2014). "Luminal B breast cancer: molecular characterization, clinical management, and future perspectives." J Clin Oncol **32**(25): 2794-2803.

Alao, J. P., E. W. Lam, S. Ali, L. Buluwela, W. Bordogna, P. Lockey, R. Varshochi, A. V. Stavropoulou, R. C. Coombes and D. M. Vigushin (2004). "Histone deacetylase inhibitor trichostatin A represses estrogen receptor alpha-dependent transcription and promotes proteasomal degradation of cyclin D1 in human breast carcinoma cell lines." Clin Cancer Res **10**(23): 8094-8104.

Ali, A. and S. Tyagi (2017). "Diverse roles of WDR5-RbBP5-ASH2L-DPY30 (WRAD) complex in the functions of the SET1 histone methyltransferase family." J Biosci **42**(1): 155-159.

Ali, A., S. N. Veeranki and S. Tyagi (2014). "A SET-domain-independent role of WRAD complex in cell-cycle regulatory function of mixed lineage leukemia." Nucleic Acids Res **42**(12): 7611-7624.

Allali-Hassani, A., E. Kuznetsova, T. Hajian, H. Wu, L. Dombrovski, Y. Li, S. Graslund, C. H. Arrowsmith, M. Schapira and M. Vedadi (2014). "A Basic Post-SET Extension of NSDs Is Essential for Nucleosome Binding In Vitro." J Biomol Screen **19**(6): 928-935.

Allred, D. C., P. Brown and D. Medina (2004). "The origins of estrogen receptor alpha-positive and estrogen receptor alpha-negative human breast cancer." Breast Cancer Res **6**(6): 240-245.

Angrand, P. O., F. Apiou, A. F. Stewart, B. Dutrillaux, R. Losson and P. Chambon (2001). "NSD3, a new SET domain-containing gene, maps to 8p12 and is amplified in human breast cancer cell lines." Genomics **74**(1): 79-88.

Angus, L., N. Beije, A. Jager, J. W. Martens and S. Sleijfer (2016). "ESR1 mutations: Moving towards guiding treatment decision-making in metastatic breast cancer patients." Cancer Treat Rev **52**: 33-40.

Ariazi, E. A., J. L. Ariazi, F. Cordera and V. C. Jordan (2006). "Estrogen receptors as therapeutic targets in breast cancer." Curr Top Med Chem **6**(3): 181-202.

Atlas, T. C. G. (2015). "cBioPortal." Retrieved Feb 2, 2015, 2015, from <http://www.cbioportal.org/index.do>.

Avdic, V., P. Zhang, S. Lanouette, A. Voronova, I. Skerjanc and J. F. Couture (2011). "Fine-tuning the stimulation of MLL1 methyltransferase activity by a histone H3-based peptide mimetic." FASEB J **25**(3): 960-967.

Azim, H. A., L. Kassem, I. Treilleux, Q. Wang, M. A. El Enein, S. E. Anis and T. Bachelot (2016). "Analysis of PI3K/mTOR Pathway Biomarkers and Their Prognostic Value in Women with Hormone Receptor-Positive, HER2-Negative Early Breast Cancer." Transl Oncol **9**(2): 114-123.

Benjamini, Y. and Y. Hochberg (1995). "Controlling the False Discovery Rate: A Practical and Powerful Approach to Multiple Testing." Journal of the Royal Statistical Society. Series B (Methodological) **57**(1): 289-300.

Bennett, R. L., A. Swaroop, C. Troche and J. D. Licht (2017). "The Role of Nuclear Receptor-Binding SET Domain Family Histone Lysine Methyltransferases in Cancer." Cold Spring Harb Perspect Med.

Bergamaschi, A., Y. H. Kim, P. Wang, T. Sorlie, T. Hernandez-Boussard, P. E. Lonning, R. Tibshirani, A. L. Borresen-Dale and J. R. Pollack (2006). "Distinct patterns of DNA copy number alteration are associated with different clinicopathological features and gene-expression subtypes of breast cancer." Genes Chromosomes Cancer **45**(11): 1033-1040.

Bernard-Pierrot, I., N. Gruel, N. Stransky, A. Vincent-Salomon, F. Reyal, V. Raynal, C. Vallot, G. Pierron, F. Radvanyi and O. Delattre (2008). "Characterization of the recurrent

8p11-12 amplicon identifies PPAPDC1B, a phosphatase protein, as a new therapeutic target in breast cancer." Cancer Res **68**(17): 7165-7175.

Bhan, A., I. Hussain, K. I. Ansari, S. A. Bobzean, L. I. Perrotti and S. S. Mandal (2014). "Histone methyltransferase EZH2 is transcriptionally induced by estradiol as well as estrogenic endocrine disruptors bisphenol-A and diethylstilbestrol." J Mol Biol **426**(20): 3426-3441.

Bilal, E., K. Vassallo, D. Toppmeyer, N. Barnard, I. H. Rye, V. Almendro, H. Russnes, A. L. Borresen-Dale, A. J. Levine, G. Bhanot and S. Ganesan (2012). "Amplified loci on chromosomes 8 and 17 predict early relapse in ER-positive breast cancers." PLoS One **7**(6): e38575.

Blobel, G. A., S. Kadauke, E. Wang, A. W. Lau, J. Zuber, M. M. Chou and C. R. Vakoc (2009). "A reconfigured pattern of MLL occupancy within mitotic chromatin promotes rapid transcriptional reactivation following mitotic exit." Mol Cell **36**(6): 970-983.

Bolger, A. M., M. Lohse and B. Usadel (2014). "Trimmomatic: a flexible trimmer for Illumina sequence data." Bioinformatics **30**(15): 2114-2120.

Borbely, G., L. A. Haldosen, K. Dahlman-Wright and C. Zhao (2015). "Induction of USP17 by combining BET and HDAC inhibitors in breast cancer cells." Oncotarget **6**(32): 33623-33635.

Butler, J. S., Y. H. Qiu, N. Zhang, S. Y. Yoo, K. R. Coombes, S. Y. Dent and S. M. Kornblau (2017). "Low expression of ASH2L protein correlates with a favorable outcome in acute myeloid leukemia." Leuk Lymphoma **58**(5): 1207-1218.

Butler, J. S., C. I. Zurita-Lopez, S. G. Clarke, M. T. Bedford and S. Y. Dent (2011). "Protein-arginine methyltransferase 1 (PRMT1) methylates Ash2L, a shared component of mammalian histone H3K4 methyltransferase complexes." J Biol Chem **286**(14): 12234-12244.

Cadoo, K. A., M. N. Fornier and P. G. Morris (2013). "Biological subtypes of breast cancer: current concepts and implications for recurrence patterns." Q J Nucl Med Mol Imaging **57**(4): 312-321.

Cai, F. F., C. Kohler, B. Zhang, M. H. Wang, W. J. Chen and X. Y. Zhong (2011). "Epigenetic therapy for breast cancer." Int J Mol Sci **12**(7): 4465-4487.

Caldon, C. E., C. M. Sergio, J. Kang, A. Muthukaruppan, M. N. Boersma, A. Stone, J. Barraclough, C. S. Lee, M. A. Black, L. D. Miller, J. M. Gee, R. I. Nicholson, R. L. Sutherland, C. G. Print and E. A. Musgrove (2012). "Cyclin E2 overexpression is associated with endocrine resistance but not insensitivity to CDK2 inhibition in human breast cancer cells." Mol Cancer Ther **11**(7): 1488-1499.

Cao, F., Y. Chen, T. Cierpicki, Y. Liu, V. Basrur, M. Lei and Y. Dou (2010). "An Ash2L/RbBP5 heterodimer stimulates the MLL1 methyltransferase activity through coordinated substrate interactions with the MLL1 SET domain." PLoS One **5**(11): e14102.

Carey, L. A., C. M. Perou, C. A. Livasy, L. G. Dressler, D. Cowan, K. Conway, G. Karaca, M. A. Troester, C. K. Tse, S. Edmiston, S. L. Deming, J. Geradts, M. C. Cheang, T. O. Nielsen, P. G. Moorman, H. S. Earp and R. C. Millikan (2006). "Race, breast cancer subtypes, and survival in the Carolina Breast Cancer Study." JAMA **295**(21): 2492-2502.

Chang, M. (2012). "Tamoxifen resistance in breast cancer." Biomol Ther (Seoul) **20**(3): 256-267.

Chanrion, M., V. Negre, H. Fontaine, N. Salvetat, F. Bibeau, G. Mac Grogan, L. Mauriac, D. Katsaros, F. Molina, C. Theillet and J. M. Darbon (2008). "A gene expression signature that can predict the recurrence of tamoxifen-treated primary breast cancer." Clin Cancer Res **14**(6): 1744-1752.

Cheang, M. C., S. K. Chia, D. Voduc, D. Gao, S. Leung, J. Snider, M. Watson, S. Davies, P. S. Bernard, J. S. Parker, C. M. Perou, M. J. Ellis and T. O. Nielsen (2009). "Ki67 index, HER2 status, and prognosis of patients with luminal B breast cancer." J Natl Cancer Inst **101**(10): 736-750.

Chen, J., E. E. Bardes, B. J. Aronow and A. G. Jegga (2009). "ToppGene Suite for gene list enrichment analysis and candidate gene prioritization." Nucleic Acids Res **37**(Web Server issue): W305-311.

Chen, Y., F. Cao, B. Wan, Y. Dou and M. Lei (2012). "Structure of the SPRY domain of human Ash2L and its interactions with RbBP5 and DPY30." Cell Res **22**(3): 598-602.

Chen, Y., J. McGee, X. Chen, T. N. Doman, X. Gong, Y. Zhang, N. Hamm, X. Ma, R. E. Higgs, S. V. Bhagwat, S. Buchanan, S. B. Peng, K. A. Staschke, V. Yadav, Y. Yue and H. Kouros-Mehr (2014). "Identification of druggable cancer driver genes amplified across TCGA datasets." PLoS One **9**(5): e98293.

Cobain, E. F. and D. F. Hayes (2015). "Indications for prognostic gene expression profiling in early breast cancer." Curr Treat Options Oncol **16**(5): 23.

Comsa, S., A. M. Cimpean and M. Raica (2015). "The Story of MCF-7 Breast Cancer Cell Line: 40 years of Experience in Research." Anticancer Res **35**(6): 3147-3154.

Connolly, R., H. Li, R. C. Jankowitz, Z. Zhang, M. A. Rudek, S. C. Jeter, S. Slater, P. Powers, A. C. Wolff, J. H. Fetting, A. M. Brufsky, R. Piekarz, N. Ahuja, P. W. Laird, H. Shen, D. J. Weisenberger, L. Cope, J. G. Herman, G. Somlo, A. Garcia, P. A. Jones, S. B. Baylin, N. E. Davidson, C. Zahnow and V. Stearns (2016). "Combination Epigenetic Therapy in Advanced Breast Cancer with 5-Azacitidine and Entinostat: A Phase II National Cancer Institute/Stand Up to Cancer Study." Clin Cancer Res.

Connolly, R. and V. Stearns (2012). "Epigenetics as a therapeutic target in breast cancer." J Mammary Gland Biol Neoplasia **17**(3-4): 191-204.

Cooke, S. L., J. C. Pole, S. F. Chin, I. O. Ellis, C. Caldas and P. A. Edwards (2008). "High-resolution array CGH clarifies events occurring on 8p in carcinogenesis." BMC Cancer **8**: 288.

Cornen, S., A. Guille, J. Adelaide, L. Addou-Klouche, P. Finetti, M. R. Saade, M. Manai, N. Carbuccia, I. Bekhouche, A. Letessier, S. Raynaud, E. Charafe-Jauffret, J. Jacquemier, S. Spicuglia, H. de The, P. Viens, F. Bertucci, D. Birnbaum and M. Chaffanet (2014). "Candidate luminal B breast cancer genes identified by genome, gene expression and DNA methylation profiling." PLoS One **9**(1): e81843.

Crowe, B. L., R. C. Larue, C. Yuan, S. Hess, M. Kvaratskhelia and M. P. Foster (2016). "Structure of the Brd4 ET domain bound to a C-terminal motif from gamma-retroviral integrases reveals a conserved mechanism of interaction." Proc Natl Acad Sci U S A **113**(8): 2086-2091.

Cui, X., R. Schiff, G. Arpino, C. K. Osborne and A. V. Lee (2005). "Biology of progesterone receptor loss in breast cancer and its implications for endocrine therapy." J Clin Oncol **23**(30): 7721-7735.

Curry, E., I. Green, N. Chapman-Rothe, E. Shamsaei, S. Kandil, F. L. Cherblanc, L. Payne, E. Bell, T. Ganesh, N. Srimongkolpithak, J. Caron, F. Li, A. G. Uren, J. P. Snyder, M. Vedadi, M. J. Fuchter and R. Brown (2015). "Dual EZH2 and EHMT2 histone methyltransferase inhibition increases biological efficacy in breast cancer cells." Clin Epigenetics **7**: 84.

Dabydeen, S. A. and P. A. Furth (2014). "Genetically engineered ERalpha-positive breast cancer mouse models." Endocr Relat Cancer **21**(3): R195-208.

Damaskos, C., S. Valsami, M. Kontos, E. Spartalis, T. Kalampokas, E. Kalampokas, A. Athanasiou, D. Moris, A. Daskalopoulou, S. Davakis, G. Tsourouflis, K. Kontzoglou, D. Perrea, N. Nikiteas and D. Dimitroulis (2017). "Histone Deacetylase Inhibitors: An Attractive Therapeutic Strategy Against Breast Cancer." Anticancer Res **37**(1): 35-46.

De Marchi, T., J. A. Foekens, A. Umar and J. W. Martens (2016). "Endocrine therapy resistance in estrogen receptor (ER)-positive breast cancer." Drug Discov Today **21**(7): 1181-1188.

Demers, C., C. P. Chaturvedi, J. A. Ranish, G. Juban, P. Lai, F. Morle, R. Aebersold, F. J. Dilworth, M. Groudine and M. Brand (2007). "Activator-mediated recruitment of the MLL2 methyltransferase complex to the beta-globin locus." Mol Cell **27**(4): 573-584.

Demircan, B., L. M. Dyer, M. Gerace, E. K. Lobenhofer, K. D. Robertson and K. D. Brown (2009). "Comparative epigenomics of human and mouse mammary tumors." Genes Chromosomes Cancer **48**(1): 83-97.

Dou, Y., T. A. Milne, A. J. Ruthenburg, S. Lee, J. W. Lee, G. L. Verdine, C. D. Allis and R. G. Roeder (2006). "Regulation of MLL1 H3K4 methyltransferase activity by its core components." Nat Struct Mol Biol **13**(8): 713-719.

Douglas, J., K. Coleman, K. Tatton-Brown, H. E. Hughes, I. K. Temple, T. R. Cole and N. Rahman (2005). "Evaluation of NSD2 and NSD3 in overgrowth syndromes." Eur J Hum Genet **13**(2): 150-153.

Dowsett, M., R. I. Nicholson and R. J. Pietras (2005). "Biological characteristics of the pure antiestrogen fulvestrant: overcoming endocrine resistance." Breast Cancer Res Treat **93 Suppl 1**: S11-18.

Dutt, A., A. H. Ramos, P. S. Hammerman, C. Mermel, J. Cho, T. Sharifnia, A. Chande, K. E. Tanaka, N. Stransky, H. Greulich, N. S. Gray and M. Meyerson (2011). "Inhibitor-sensitive FGFR1 amplification in human non-small cell lung cancer." PLoS One **6**(6): e20351.

Ellis, M. J., L. Ding, D. Shen, J. Luo, V. J. Suman, J. W. Wallis, B. A. Van Tine, J. Hoog, R. J. Goiffon, T. C. Goldstein, S. Ng, L. Lin, R. Crowder, J. Snider, K. Ballman, J. Weber, K. Chen, D. C. Koboldt, C. Kandoth, W. S. Schierding, J. F. McMichael, C. A. Miller, C.

Lu, C. C. Harris, M. D. McLellan, M. C. Wendl, K. DeSchryver, D. C. Allred, L. Esserman, G. Unzeitig, J. Margenthaler, G. V. Babiera, P. K. Marcom, J. M. Guenther, M. Leitch, K. Hunt, J. Olson, Y. Tao, C. A. Maher, L. L. Fulton, R. S. Fulton, M. Harrison, B. Oberkfell, F. Du, R. Demeter, T. L. Vickery, A. Elhammali, H. Piwnica-Worms, S. McDonald, M. Watson, D. J. Dooling, D. Ota, L. W. Chang, R. Bose, T. J. Ley, D. Piwnica-Worms, J. M. Stuart, R. K. Wilson and E. R. Mardis (2012). "Whole-genome analysis informs breast cancer response to aromatase inhibition." Nature **486**(7403): 353-360.

Ellis, M. J., M. Dixon, M. Dowsett, R. Nagarajan and E. Mardis (2007). "A luminal breast cancer genome atlas: progress and barriers." J Steroid Biochem Mol Biol **106**(1-5): 125-129.

Elsheikh, S. E., A. R. Green, E. A. Rakha, D. G. Powe, R. A. Ahmed, H. M. Collins, D. Soria, J. M. Garibaldi, C. E. Paish, A. A. Ammar, M. J. Grainge, G. R. Ball, M. K. Abdelghany, L. Martinez-Pomares, D. M. Heery and I. O. Ellis (2009). "Global histone modifications in breast cancer correlate with tumor phenotypes, prognostic factors, and patient outcome." Cancer Res **69**(9): 3802-3809.

Erfani, P., J. Tome-Garcia, P. Canoll, F. Doetsch and N. M. Tsankova (2015). "EGFR promoter exhibits dynamic histone modifications and binding of ASH2L and P300 in human germinal matrix and gliomas." Epigenetics **10**(6): 496-507.

Ernst, P. and C. R. Vakoc (2012). "WRAD: enabler of the SET1-family of H3K4 methyltransferases." Brief Funct Genomics **11**(3): 217-226.

Eroles, P., A. Bosch, J. A. Perez-Fidalgo and A. Lluch (2012). "Molecular biology in breast cancer: intrinsic subtypes and signaling pathways." Cancer Treat Rev **38**(6): 698-707.

Ethier, S. P. (1996). "Human breast cancer cell lines as models of growth regulation and disease progression." J Mammary Gland Biol Neoplasia **1**(1): 111-121.

Ethier, S. P., M. L. Mahacek, W. J. Gullick, T. S. Frank and B. L. Weber (1993). "Differential isolation of normal luminal mammary epithelial cells and breast cancer cells from primary and metastatic sites using selective media." Cancer Res **53**(3): 627-635.

Falahi, F., M. van Kruchten, N. Martinet, G. A. Hospers and M. G. Rots (2014). "Current and upcoming approaches to exploit the reversibility of epigenetic mutations in breast cancer." Breast Cancer Res **16**(4): 412.

Fang, R., A. J. Barbera, Y. Xu, M. Rutenberg, T. Leonor, Q. Bi, F. Lan, P. Mei, G. C. Yuan, C. Lian, J. Peng, D. Cheng, G. Sui, U. B. Kaiser, Y. Shi and Y. G. Shi (2010). "Human LSD2/KDM1b/AOF1 regulates gene transcription by modulating intragenic H3K4me2 methylation." Mol Cell **39**(2): 222-233.

Fedele, P., N. Calvani, A. Marino, L. Orlando, P. Schiavone, A. Quaranta and S. Cinieri (2012). "Targeted agents to reverse resistance to endocrine therapy in metastatic breast cancer: where are we now and where are we going?" Crit Rev Oncol Hematol **84**(2): 243-251.

Feng, Q., Z. Zhang, M. J. Shea, C. J. Creighton, C. Coarfa, S. G. Hilsenbeck, R. Lanz, B. He, L. Wang, X. Fu, A. Nardone, Y. Song, J. Bradner, N. Mitsiades, C. S. Mitsiades, C. K. Osborne, R. Schiff and B. W. O'Malley (2014). "An epigenomic approach to therapy for tamoxifen-resistant breast cancer." Cell Res **24**(7): 809-819.

Fossati, A., D. Dolfini, G. Donati and R. Mantovani (2011). "NF-Y recruits Ash2L to impart H3K4 trimethylation on CCAAT promoters." PLoS One **6**(3): e17220.

French, C. A., S. Rahman, E. M. Walsh, S. Kuhnle, A. R. Grayson, M. E. Lemieux, N. Grunfeld, B. P. Rubin, C. R. Antonescu, S. Zhang, R. Venkatramani, P. Dal Cin and P. M. Howley (2014). "NSD3-NUT fusion oncoprotein in NUT midline carcinoma: implications for a novel oncogenic mechanism." Cancer Discov **4**(8): 928-941.

Gao, J., B. A. Aksoy, U. Dogrusoz, G. Dresdner, B. Gross, S. O. Sumer, Y. Sun, A. Jacobsen, R. Sinha, E. Larsson, E. Cerami, C. Sander and N. Schultz (2013). "Integrative analysis of complex cancer genomics and clinical profiles using the cBioPortal." Sci Signal **6**(269): p11.

Garapaty-Rao, S., C. Nasveschuk, A. Gagnon, E. Y. Chan, P. Sandy, J. Busby, S. Balasubramanian, R. Campbell, F. Zhao, L. Bergeron, J. E. Audia, B. K. Albrecht, J. C. Harmange, R. Cummings and P. Trojer (2013). "Identification of EZH2 and EZH1 small molecule inhibitors with selective impact on diffuse large B cell lymphoma cell growth." Chem Biol **20**(11): 1329-1339.

Garapaty, S., C. F. Xu, P. Trojer, M. A. Mahajan, T. A. Neubert and H. H. Samuels (2009). "Identification and characterization of a novel nuclear protein complex involved in nuclear hormone receptor-mediated gene regulation." J Biol Chem **284**(12): 7542-7552.

Garcia, M. J., J. C. Pole, S. F. Chin, A. Teschendorff, A. Naderi, H. Ozdag, M. Vias, T. Kranjac, T. Subkhankulova, C. Paish, I. Ellis, J. D. Brenton, P. A. Edwards and C.

Caldas (2005). "A 1 Mb minimal amplicon at 8p11-12 in breast cancer identifies new candidate oncogenes." Oncogene **24**(33): 5235-5245.

Gelsi-Boyer, V., B. Orsetti, N. Cervera, P. Finetti, F. Sircoulomb, C. Rouge, L. Lasorsa, A. Letessier, C. Ginestier, F. Monville, S. Esteyries, J. Adelaide, B. Esterni, C. Henry, S. P. Ethier, F. Bibeau, M. J. Mozziconacci, E. Charafe-Jauffret, J. Jacquemier, F. Bertucci, D. Birnbaum, C. Theillet and M. Chaffanet (2005). "Comprehensive profiling of 8p11-12 amplification in breast cancer." Mol Cancer Res **3**(12): 655-667.

Geyer, F. C., D. N. Rodrigues, B. Weigelt and J. S. Reis-Filho (2012). "Molecular classification of estrogen receptor-positive/luminal breast cancers." Adv Anat Pathol **19**(1): 39-53.

Grzenda, A., T. Ordog and R. Urrutia (2011). "Polycomb and the emerging epigenetics of pancreatic cancer." J Gastrointest Cancer **42**(2): 100-111.

Guccione, E., C. Bassi, F. Casadio, F. Martinato, M. Cesaroni, H. Schuchlantz, B. Luscher and B. Amati (2007). "Methylation of histone H3R2 by PRMT6 and H3K4 by an MLL complex are mutually exclusive." Nature **449**(7164): 933-937.

Guertin, D. A., K. V. Guntur, G. W. Bell, C. C. Thoreen and D. M. Sabatini (2006). "Functional genomics identifies TOR-regulated genes that control growth and division." Curr Biol **16**(10): 958-970.

Habashy, H. O., D. G. Powe, T. M. Abdel-Fatah, J. M. Gee, R. I. Nicholson, A. R. Green, E. A. Rakha and I. O. Ellis (2012). "A review of the biological and clinical characteristics of luminal-like oestrogen receptor-positive breast cancer." Histopathology **60**(6): 854-863.

Hartman, J., A. Strom and J. A. Gustafsson (2009). "Estrogen receptor beta in breast cancer--diagnostic and therapeutic implications." Steroids **74**(8): 635-641.

Haverty, P. M., J. Fridlyand, L. Li, G. Getz, R. Beroukhim, S. Lohr, T. D. Wu, G. Cavet, Z. Zhang and J. Chant (2008). "High-resolution genomic and expression analyses of copy number alterations in breast tumors." Genes Chromosomes Cancer **47**(6): 530-542.

He, C., F. Li, J. Zhang, J. Wu and Y. Shi (2013). "The methyltransferase NSD3 has chromatin-binding motifs, PHD5-C5HCH, that are distinct from other NSD (nuclear

receptor SET domain) family members in their histone H3 recognition." J Biol Chem **288**(7): 4692-4703.

Hervouet, E., P. F. Cartron, M. Jouvenot and R. Delage-Mourroux (2013). "Epigenetic regulation of estrogen signaling in breast cancer." Epigenetics **8**(3): 237-245.

Holland, D. G., A. Burleigh, A. Git, M. A. Goldgraben, P. A. Perez-Mancera, S. F. Chin, A. Hurtado, A. Bruna, H. R. Ali, W. Greenwood, M. J. Dunning, S. Samarajiwa, S. Menon, O. M. Rueda, A. G. Lynch, S. McKinney, I. O. Ellis, C. J. Eaves, J. S. Carroll, C. Curtis, S. Aparicio and C. Caldas (2011). "ZNF703 is a common Luminal B breast cancer oncogene that differentially regulates luminal and basal progenitors in human mammary epithelium." EMBO Mol Med **3**(3): 167-180.

Howell, A. (2006). "Pure oestrogen antagonists for the treatment of advanced breast cancer." Endocr Relat Cancer **13**(3): 689-706.

Huang, L., S. Zhao, J. M. Frasor and Y. Dai (2011). "An integrated bioinformatics approach identifies elevated cyclin E2 expression and E2F activity as distinct features of tamoxifen resistant breast tumors." PLoS One **6**(7): e22274.

Huang, N., E. vom Baur, J. M. Garnier, T. Lerouge, J. L. Vonesch, Y. Lutz, P. Chambon and R. Losson (1998). "Two distinct nuclear receptor interaction domains in NSD1, a novel SET protein that exhibits characteristics of both corepressors and coactivators." EMBO J **17**(12): 3398-3412.

Huang, Y., S. Nayak, R. Jankowitz, N. E. Davidson and S. Oesterreich (2011). "Epigenetics in breast cancer: what's new?" Breast Cancer Res **13**(6): 225.

Ignatiadis, M. and C. Sotiriou (2013). "Luminal breast cancer: from biology to treatment." Nat Rev Clin Oncol **10**(9): 494-506.

Ikegawa, S., M. Isomura, Y. Koshizuka and Y. Nakamura (1999). "Cloning and characterization of ASH2L and Ash2l, human and mouse homologs of the Drosophila ash2 gene." Cytogenet Cell Genet **84**(3-4): 167-172.

Inoue, K. and E. A. Fry (2015). "Aberrant expression of cyclin D1 in cancer." Sign Transduct Insights **4**: 1-13.

Irish, J. C., J. N. Mills, B. Turner-Ivey, R. C. Wilson, S. T. Guest, A. Rutkovsky, A. Dombkowski, C. S. Kappler, G. Hardiman and S. P. Ethier (2016). "Amplification of WHSC1L1 regulates expression and estrogen-independent activation of ERalpha in SUM-44 breast cancer cells and is associated with ERalpha over-expression in breast cancer." Mol Oncol.

Jacques-Fricke, B. T. and L. S. Gammill (2014). "Neural crest specification and migration independently require NSD3-related lysine methyltransferase activity." Mol Biol Cell **25**(25): 4174-4186.

Johnston, S. J. and K. L. Cheung (2010). "Fulvestrant - a novel endocrine therapy for breast cancer." Curr Med Chem **17**(10): 902-914.

Johnston, S. R., L. A. Martin, J. Head, I. Smith and M. Dowsett (2005). "Aromatase inhibitors: combinations with fulvestrant or signal transduction inhibitors as a strategy to overcome endocrine resistance." J Steroid Biochem Mol Biol **95**(1-5): 173-181.

Jovanovic, J., J. A. Ronneberg, J. Tost and V. Kristensen (2010). "The epigenetics of breast cancer." Mol Oncol **4**(3): 242-254.

Judes, G., A. Dagdemir, S. Karsli-Ceppioglu, A. Lebert, M. Echegut, M. Ngollo, Y. J. Bignon, F. Penault-Llorca and D. Bernard-Gallon (2016). "H3K4 acetylation, H3K9 acetylation and H3K27 methylation in breast tumor molecular subtypes." Epigenomics **8**(7): 909-924.

Kang, D., H. S. Cho, G. Toyokawa, M. Kogure, Y. Yamane, Y. Iwai, S. Hayami, T. Tsunoda, H. I. Field, K. Matsuda, D. E. Neal, B. A. Ponder, Y. Maehara, Y. Nakamura and R. Hamamoto (2013). "The histone methyltransferase Wolf-Hirschhorn syndrome candidate 1-like 1 (WHSC1L1) is involved in human carcinogenesis." Genes Chromosomes Cancer **52**(2): 126-139.

Kao, J., K. Salari, M. Bocanegra, Y. L. Choi, L. Girard, J. Gandhi, K. A. Kwei, T. Hernandez-Boussard, P. Wang, A. F. Gazdar, J. D. Minna and J. R. Pollack (2009). "Molecular profiling of breast cancer cell lines defines relevant tumor models and provides a resource for cancer gene discovery." PLoS One **4**(7): e6146.

Karlsson, E., M. A. Waltersson, J. Bostner, G. Perez-Tenorio, B. Olsson, A. L. Hallbeck and O. Stal (2011). "High-resolution genomic analysis of the 11q13 amplicon in breast cancers identifies synergy with 8p12 amplification, involving the mTOR targets S6K2 and 4EBP1." Genes Chromosomes Cancer **50**(10): 775-787.

Katoh, M. (2016). "Mutation spectra of histone methyltransferases with canonical SET domains and EZH2-targeted therapy." Epigenomics **8**(2): 285-305.

Kawabe, Y., Y. X. Wang, I. W. McKinnell, M. T. Bedford and M. A. Rudnicki (2012). "Carm1 regulates Pax7 transcriptional activity through MLL1/2 recruitment during asymmetric satellite stem cell divisions." Cell Stem Cell **11**(3): 333-345.

Kerdivel, G., G. Flouriot and F. Pakdel (2013). "Modulation of estrogen receptor alpha activity and expression during breast cancer progression." Vitam Horm **93**: 135-160.

Kim, D., G. Pertea, C. Trapnell, H. Pimentel, R. Kelley and S. L. Salzberg (2013). "TopHat2: accurate alignment of transcriptomes in the presence of insertions, deletions and gene fusions." Genome Biol **14**(4): R36.

Kim, J. H., A. Sharma, S. S. Dhar, S. H. Lee, B. Gu, C. H. Chan, H. K. Lin and M. G. Lee (2014). "UTX and MLL4 coordinately regulate transcriptional programs for cell proliferation and invasiveness in breast cancer cells." Cancer Res **74**(6): 1705-1717.

Kim, S., S. Natesan, G. Cornilescu, S. Carlson, M. Tonelli, U. L. McClurg, O. Binda, C. N. Robson, J. L. Markley, S. Balaz and K. C. Glass (2016). "Mechanism of Histone H3K4me3 Recognition by the Plant Homeodomain of Inhibitor of Growth 3." J Biol Chem **291**(35): 18326-18341.

Kim, S. M., H. J. Kee, N. Choe, J. Y. Kim, H. Kook, H. Kook and S. B. Seo (2007). "The histone methyltransferase activity of WHISTLE is important for the induction of apoptosis and HDAC1-mediated transcriptional repression." Exp Cell Res **313**(5): 975-983.

Knudsen, E. S. and A. K. Witkiewicz (2016). "Defining the transcriptional and biological response to CDK4/6 inhibition in relation to ER+/HER2- breast cancer." Oncotarget **7**(43): 69111-69123.

Kristensen, L. S., H. M. Nielsen and L. L. Hansen (2009). "Epigenetics and cancer treatment." Eur J Pharmacol **625**(1-3): 131-142.

Kristensen, V. N., T. Sorlie, J. Geisler, A. Langerod, N. Yoshimura, R. Karesen, N. Harada, P. E. Lonning and A. L. Borresen-Dale (2005). "Gene expression profiling of breast cancer in relation to estrogen receptor status and estrogen-metabolizing enzymes: clinical implications." Clin Cancer Res **11**(2 Pt 2): 878s-883s.

- Kumar, R., D. Q. Li, S. Muller and S. Knapp (2016). "Epigenomic regulation of oncogenesis by chromatin remodeling." Oncogene **35**(34): 4423-4436.
- Kumler, I., A. S. Knoop, C. A. Jessing, B. Ejlersen and D. L. Nielsen (2016). "Review of hormone-based treatments in postmenopausal patients with advanced breast cancer focusing on aromatase inhibitors and fulvestrant." ESMO Open **1**(4): e000062.
- Kuo, A. J., P. Cheung, K. Chen, B. M. Zee, M. Kioi, J. Lauring, Y. Xi, B. H. Park, X. Shi, B. A. Garcia, W. Li and O. Gozani (2011). "NSD2 links dimethylation of histone H3 at lysine 36 to oncogenic programming." Mol Cell **44**(4): 609-620.
- Kwek, S. S., R. Roy, H. Zhou, J. Climent, J. A. Martinez-Climent, J. Fridlyand and D. G. Albertson (2009). "Co-amplified genes at 8p12 and 11q13 in breast tumors cooperate with two major pathways in oncogenesis." Oncogene **28**(17): 1892-1903.
- Li, Y., J. Han, Y. Zhang, F. Cao, Z. Liu, S. Li, J. Wu, C. Hu, Y. Wang, J. Shuai, J. Chen, L. Cao, D. Li, P. Shi, C. Tian, J. Zhang, Y. Dou, G. Li, Y. Chen and M. Lei (2016). "Structural basis for activity regulation of MLL family methyltransferases." Nature **530**(7591): 447-452.
- Li, Y., P. Trojer, C. F. Xu, P. Cheung, A. Kuo, W. J. Drury, 3rd, Q. Qiao, T. A. Neubert, R. M. Xu, O. Gozani and D. Reinberg (2009). "The target of the NSD family of histone lysine methyltransferases depends on the nature of the substrate." J Biol Chem **284**(49): 34283-34295.
- Lim, E., G. Tarulli, N. Portman, T. E. Hickey, W. D. Tilley and C. Palmieri (2016). "Pushing estrogen receptor around in breast cancer." Endocr Relat Cancer **23**(12): T227-T241.
- Lin, I. H., D. T. Chen, Y. F. Chang, Y. L. Lee, C. H. Su, C. Cheng, Y. C. Tsai, S. C. Ng, H. T. Chen, M. C. Lee, H. W. Chen, S. H. Suen, Y. C. Chen, T. T. Liu, C. H. Chang and M. T. Hsu (2015). "Hierarchical clustering of breast cancer methylomes revealed differentially methylated and expressed breast cancer genes." PLoS One **10**(2): e0118453.
- Liu, G., A. Bollig-Fischer, B. Kreike, M. J. van de Vijver, J. Abrams, S. P. Ethier and Z. Q. Yang (2009). "Genomic amplification and oncogenic properties of the GASC1 histone demethylase gene in breast cancer." Oncogene **28**(50): 4491-4500.

Liu, L., S. Kimball, H. Liu, A. Holowatyj and Z. Q. Yang (2014). "Genetic alterations of histone lysine methyltransferases and their significance in breast cancer." Oncotarget.

Livak, K. J. and T. D. Schmittgen (2001). "Analysis of relative gene expression data using real-time quantitative PCR and the 2(-Delta Delta C(T)) Method." Methods **25**(4): 402-408.

Lo, P. K. and S. Sukumar (2008). "Epigenomics and breast cancer." Pharmacogenomics **9**(12): 1879-1902.

Locke, W. J., E. Zotenko, C. Stirzaker, M. D. Robinson, R. A. Hinshelwood, A. Stone, R. R. Reddel, L. I. Huschtscha and S. J. Clark (2015). "Coordinated epigenetic remodelling of transcriptional networks occurs during early breast carcinogenesis." Clin Epigenetics **7**: 52.

Loi, S., C. Sotiriou, B. Haibe-Kains, F. Lallemand, N. M. Conus, M. J. Piccart, T. P. Speed and G. A. McArthur (2009). "Gene expression profiling identifies activated growth factor signaling in poor prognosis (Luminal-B) estrogen receptor positive breast cancer." BMC Med Genomics **2**: 37.

Lonning, P. E., T. Sorlie and A. L. Borresen-Dale (2005). "Genomics in breast cancer-therapeutic implications." Nat Clin Pract Oncol **2**(1): 26-33.

Love, M. I., W. Huber and S. Anders (2014). "Moderated estimation of fold change and dispersion for RNA-seq data with DESeq2." Genome Biol **15**(12): 550.

Lumachi, F., D. A. Santeufemia and S. M. Basso (2015). "Current medical treatment of estrogen receptor-positive breast cancer." World J Biol Chem **6**(3): 231-239.

Luo, J., S. Liu, S. Leung, A. A. Gru, Y. Tao, J. Hoog, J. Ho, S. R. Davies, D. C. Allred, A. L. Salavaggione, J. Snider, E. R. Mardis, T. O. Nielsen and M. J. Ellis (2017). "An mRNA Gene Expression-Based Signature to Identify FGFR1-Amplified Estrogen Receptor-Positive Breast Tumors." J Mol Diagn **19**(1): 147-161.

Luscher-Firzlaff, J., I. Gawlista, J. Vervoorts, K. Kapelle, T. Braunschweig, G. Walsemann, C. Rodgarkia-Schamberger, H. Schuchlantz, S. Dreschers, E. Kremmer, R. Lilischkis, C. Cerni, A. Wellmann and B. Luscher (2008). "The human trithorax protein hASH2 functions as an oncoprotein." Cancer Res **68**(3): 749-758.

Lustberg, M. B. and B. Ramaswamy (2009). "Epigenetic targeting in breast cancer: therapeutic impact and future direction." Drug News Perspect **22**(7): 369-381.

Lustberg, M. B. and B. Ramaswamy (2011). "Epigenetic Therapy in Breast Cancer." Curr Breast Cancer Rep **3**(1): 34-43.

Mahmood, S. F., N. Gruel, R. Nicolle, E. Chapeaublanc, O. Delattre, F. Radvanyi and I. Bernard-Pierrot (2013). "PPAPDC1B and WHSC1L1 are common drivers of the 8p11-12 amplicon, not only in breast tumors but also in pancreatic adenocarcinomas and lung tumors." Am J Pathol **183**(5): 1634-1644.

Mancuso, M. R. and S. A. Massarweh (2016). "Endocrine therapy and strategies to overcome therapeutic resistance in breast cancer." Curr Probl Cancer **40**(2-4): 95-105.

Mann, K. M., J. M. Ward, C. C. Yew, A. Kovochich, D. W. Dawson, M. A. Black, B. T. Brett, T. E. Sheetz, A. J. Dupuy, D. K. Chang, A. V. Biankin, N. Waddell, K. S. Kassahn, S. M. Grimmond, A. G. Rust, D. J. Adams, N. A. Jenkins and N. G. Copeland (2012). "Sleeping Beauty mutagenesis reveals cooperating mutations and pathways in pancreatic adenocarcinoma." Proc Natl Acad Sci U S A **109**(16): 5934-5941.

Margueron, R., V. Duong, A. Castet and V. Cavailles (2004). "Histone deacetylase inhibition and estrogen signalling in human breast cancer cells." Biochem Pharmacol **68**(6): 1239-1246.

McKeage, K., M. P. Curran and G. L. Plosker (2004). "Fulvestrant: a review of its use in hormone receptor-positive metastatic breast cancer in postmenopausal women with disease progression following antiestrogen therapy." Drugs **64**(6): 633-648.

Melchor, L., M. J. Garcia, E. Honrado, J. C. Pole, S. Alvarez, P. A. Edwards, C. Caldas, J. D. Brenton and J. Benitez (2007). "Genomic analysis of the 8p11-12 amplicon in familial breast cancer." Int J Cancer **120**(3): 714-717.

Messier, T. L., J. A. Gordon, J. R. Boyd, C. E. Tye, G. Browne, J. L. Stein, J. B. Lian and G. S. Stein (2016). "Histone H3 lysine 4 acetylation and methylation dynamics define breast cancer subtypes." Oncotarget **7**(5): 5094-5109.

Michalak, E. M. and J. E. Visvader (2016). "Dysregulation of histone methyltransferases in breast cancer - Opportunities for new targeted therapies?" Mol Oncol **10**(10): 1497-1515.

Miller, W. R., A. Larionov, L. Renshaw, T. J. Anderson, J. R. Walker, A. Krause, T. Sing, D. B. Evans and J. M. Dixon (2009). "Gene expression profiles differentiating between breast cancers clinically responsive or resistant to letrozole." J Clin Oncol **27**(9): 1382-1387.

Miyamoto, K. and T. Ushijima (2005). "Diagnostic and therapeutic applications of epigenetics." Jpn J Clin Oncol **35**(6): 293-301.

Mohammed, H., I. A. Russell, R. Stark, O. M. Rueda, T. E. Hickey, G. A. Tarulli, A. A. Serandour, S. N. Birrell, A. Bruna, A. Saadi, S. Menon, J. Hadfield, M. Pugh, G. V. Raj, G. D. Brown, C. D'Santos, J. L. Robinson, G. Silva, R. Launchbury, C. M. Perou, J. Stingl, C. Caldas, W. D. Tilley and J. S. Carroll (2015). "Progesterone receptor modulates ERalpha action in breast cancer." Nature **523**(7560): 313-317.

Morishita, M. and E. di Luccio (2011). "Cancers and the NSD family of histone lysine methyltransferases." Biochim Biophys Acta **1816**(2): 158-163.

Morishita, M. and E. di Luccio (2011). "Structural insights into the regulation and the recognition of histone marks by the SET domain of NSD1." Biochem Biophys Res Commun **412**(2): 214-219.

Morishita, M., D. Mevius and E. di Luccio (2014). "In vitro histone lysine methylation by NSD1, NSD2/MMSET/WHSC1, and NSD3/WHSC1L." BMC Struct Biol **14**(1): 25.

Morris, C. and A. Wakeling (2002). "Fulvestrant ('Faslodex')--a new treatment option for patients progressing on prior endocrine therapy." Endocr Relat Cancer **9**(4): 267-276.

Morris, S. R. and L. A. Carey (2007). "Molecular profiling in breast cancer." Rev Endocr Metab Disord **8**(3): 185-198.

Mungamuri, S. K., S. Wang, J. J. Manfredi, W. Gu and S. A. Aaronson (2015). "Ash2L enables P53-dependent apoptosis by favoring stable transcription pre-initiation complex formation on its pro-apoptotic target promoters." Oncogene **34**(19): 2461-2470.

Nagamatsu, G., S. Saito, T. Kosaka, K. Takubo, T. Kinoshita, M. Oya, K. Horimoto and T. Suda (2012). "Optimal ratio of transcription factors for somatic cell reprogramming." J Biol Chem **287**(43): 36273-36282.

Nagaraj, G. and C. Ma (2015). "Revisiting the estrogen receptor pathway and its role in endocrine therapy for postmenopausal women with estrogen receptor-positive metastatic breast cancer." Breast Cancer Res Treat **150**(2): 231-242.

Nagarajan, S., E. Benito, A. Fischer and S. A. Johnsen (2015). "H4K12ac is regulated by estrogen receptor-alpha and is associated with BRD4 function and inducible transcription." Oncotarget **6**(9): 7305-7317.

Netanel, D., A. Avraham, A. Ben-Baruch, E. Evron and R. Shamir (2016). "Expression and methylation patterns partition luminal-A breast tumors into distinct prognostic subgroups." Breast Cancer Res **18**(1): 74.

Nguyen, P., G. Bar-Sela, L. Sun, K. S. Bisht, H. Cui, E. Kohn, A. P. Feinberg and D. Gius (2008). "BAT3 and SET1A form a complex with CTCFL/BORIS to modulate H3K4 histone dimethylation and gene expression." Mol Cell Biol **28**(21): 6720-6729.

Nicholson, R. I. and S. R. Johnston (2005). "Endocrine therapy--current benefits and limitations." Breast Cancer Res Treat **93 Suppl 1**: S3-10.

Noberini, R. and T. Bonaldi (2017). "A Super-SILAC Strategy for the Accurate and Multiplexed Profiling of Histone Posttranslational Modifications." Methods Enzymol **586**: 311-332.

Osmanbeyoglu, H. U., R. Pelossof, J. F. Bromberg and C. S. Leslie (2014). "Linking signaling pathways to transcriptional programs in breast cancer." Genome Res **24**(11): 1869-1880.

Paska, A. V. and P. Hudler (2015). "Aberrant methylation patterns in cancer: a clinical view." Biochem Med (Zagreb) **25**(2): 161-176.

Patel, A., V. Dharmarajan, V. E. Vought and M. S. Cosgrove (2009). "On the mechanism of multiple lysine methylation by the human mixed lineage leukemia protein-1 (MLL1) core complex." J Biol Chem **284**(36): 24242-24256.

Patel, A., V. E. Vought, V. Dharmarajan and M. S. Cosgrove (2011). "A novel non-SET domain multi-subunit methyltransferase required for sequential nucleosomal histone H3 methylation by the mixed lineage leukemia protein-1 (MLL1) core complex." J Biol Chem **286**(5): 3359-3369.

Patel, A., V. E. Vought, S. Swatkoski, S. Viggiano, B. Howard, V. Dharmarajan, K. E. Monteith, G. Kupakuwana, K. E. Namitz, S. A. Shinsky, R. J. Cotter and M. S. Cosgrove (2014). "Automethylation activities within the mixed lineage leukemia-1 (MLL1) core complex reveal evidence supporting a "two-active site" model for multiple histone H3 lysine 4 methylation." J Biol Chem **289**(2): 868-884.

Pathiraja, T. N., V. Stearns and S. Oesterreich (2010). "Epigenetic regulation in estrogen receptor positive breast cancer--role in treatment response." J Mammary Gland Biol Neoplasia **15**(1): 35-47.

Perou, C. M., T. Sorlie, M. B. Eisen, M. van de Rijn, S. S. Jeffrey, C. A. Rees, J. R. Pollack, D. T. Ross, H. Johnsen, L. A. Akslen, O. Fluge, A. Pergamenschikov, C. Williams, S. X. Zhu, P. E. Lonning, A. L. Borresen-Dale, P. O. Brown and D. Botstein (2000). "Molecular portraits of human breast tumours." Nature **406**(6797): 747-752.

Pritchard, K. I. (2013). "Endocrine therapy: is the first generation of targeted drugs the last?" J Intern Med **274**(2): 144-152.

Pullirsch, D., R. Hartel, H. Kishimoto, M. Leeb, G. Steiner and A. Wutz (2010). "The Trithorax group protein Ash2l and Saf-A are recruited to the inactive X chromosome at the onset of stable X inactivation." Development **137**(6): 935-943.

Qi, J., L. Huo, Y. T. Zhu and Y. J. Zhu (2014). "Absent, small or homeotic 2-like protein (ASH2L) enhances the transcription of the estrogen receptor alpha gene through GATA-binding protein 3 (GATA3)." J Biol Chem **289**(45): 31373-31381.

Rahman, S., M. E. Sowa, M. Ottinger, J. A. Smith, Y. Shi, J. W. Harper and P. M. Howley (2011). "The Brd4 extraterminal domain confers transcription activation independent of pTEFb by recruiting multiple proteins, including NSD3." Mol Cell Biol **31**(13): 2641-2652.

Raica, M., I. Jung, A. M. Cimpean, C. Suciuc and A. M. Muresan (2009). "From conventional pathologic diagnosis to the molecular classification of breast carcinoma: are we ready for the change?" Rom J Morphol Embryol **50**(1): 5-13.

Rakha, E. A. and A. R. Green (2017). "Molecular classification of breast cancer: what the pathologist needs to know." Pathology **49**(2): 111-119.

Rampalli, S., L. Li, E. Mak, K. Ge, M. Brand, S. J. Tapscott and F. J. Dilworth (2007). "p38 MAPK signaling regulates recruitment of Ash2L-containing methyltransferase

complexes to specific genes during differentiation." Nat Struct Mol Biol **14**(12): 1150-1156.

Ray, M. E., Z. Q. Yang, D. Albertson, C. G. Kleer, J. G. Washburn, J. A. Macoska and S. P. Ethier (2004). "Genomic and expression analysis of the 8p11-12 amplicon in human breast cancer cell lines." Cancer Res **64**(1): 40-47.

Reis-Filho, J. S. and L. Pusztai (2011). "Gene expression profiling in breast cancer: classification, prognostication, and prediction." Lancet **378**(9805): 1812-1823.

Reis-Filho, J. S., P. T. Simpson, N. C. Turner, M. B. Lambros, C. Jones, A. Mackay, A. Grigoriadis, D. Sarrio, K. Savage, T. Dexter, M. Iravani, K. Fenwick, B. Weber, D. Hardisson, F. C. Schmitt, J. Palacios, S. R. Lakhani and A. Ashworth (2006). "FGFR1 emerges as a potential therapeutic target for lobular breast carcinomas." Clin Cancer Res **12**(22): 6652-6662.

Reynisdottir, I., A. Arason, B. O. Einarsdottir, H. Gunnarsson, J. Staaf, J. Vallon-Christersson, G. Jonsson, M. Ringner, B. A. Agnarsson, K. Olafsdottir, R. Fagerholm, T. Einarsdottir, G. Johannesdottir, O. T. Johannsson, H. Nevanlinna, A. Borg and R. B. Barkardottir (2013). "High expression of ZNF703 independent of amplification indicates worse prognosis in patients with luminal B breast cancer." Cancer Med **2**(4): 437-446.

Rijnkels, M., E. Kabotyanski, M. B. Montazer-Torbati, C. Hue Beauvais, Y. Vassetzky, J. M. Rosen and E. Devinoy (2010). "The epigenetic landscape of mammary gland development and functional differentiation." J Mammary Gland Biol Neoplasia **15**(1): 85-100.

Robertson, J. F. (2007). "Fulvestrant (Faslodex) -- how to make a good drug better." Oncologist **12**(7): 774-784.

Robertson, J. F., J. Lindemann, S. Garnett, E. Anderson, R. I. Nicholson, I. Kuter and J. M. Gee (2014). "A good drug made better: the fulvestrant dose-response story." Clin Breast Cancer **14**(6): 381-389.

Rosati, R., R. La Starza, A. Veronese, A. Aventin, C. Schwienbacher, T. Vallespi, M. Negrini, M. F. Martelli and C. Mecucci (2002). "NUP98 is fused to the NSD3 gene in acute myeloid leukemia associated with t(8;11)(p11.2;p15)." Blood **99**(10): 3857-3860.

Ross-Innes, C. S., R. Stark, A. E. Teschendorff, K. A. Holmes, H. R. Ali, M. J. Dunning, G. D. Brown, O. Gojis, I. O. Ellis, A. R. Green, S. Ali, S. F. Chin, C. Palmieri, C. Caldas

and J. S. Carroll (2012). "Differential oestrogen receptor binding is associated with clinical outcome in breast cancer." Nature **481**(7381): 389-393.

Saloura, V., T. Vougiouklakis, M. Zewde, X. Deng, K. Kiyotani, J. H. Park, Y. Matsuo, M. Lingen, T. Suzuki, N. Dohmae, R. Hamamoto and Y. Nakamura (2017). "WHSC1L1-mediated EGFR mono-methylation enhances the cytoplasmic and nuclear oncogenic activity of EGFR in head and neck cancer." Sci Rep **7**: 40664.

Saloura, V., T. Vougiouklakis, M. Zewde, K. Kiyotani, J. H. Park, G. Gao, T. Karrison, M. Lingen, Y. Nakamura and R. Hamamoto (2016). "WHSC1L1 drives cell cycle progression through transcriptional regulation of CDC6 and CDK2 in squamous cell carcinoma of the head and neck." Oncotarget **7**(27): 42527-42538.

Sato, T., M. Cesaroni, W. Chung, S. Panjarian, A. Tran, J. Madzo, Y. Okamoto, H. Zhang, X. Chen, J. Jelinek and J. J. Issa (2017). "Transcriptional Selectivity of Epigenetic Therapy in Cancer." Cancer Res **77**(2): 470-481.

Schiff, R., S. Massarweh, J. Shou and C. K. Osborne (2003). "Breast cancer endocrine resistance: how growth factor signaling and estrogen receptor coregulators modulate response." Clin Cancer Res **9**(1 Pt 2): 447S-454S.

Schram, A. W., R. Baas, P. W. Jansen, A. Riss, L. Tora, M. Vermeulen and H. T. Timmers (2013). "A dual role for SAGA-associated factor 29 (SGF29) in ER stress survival by coordination of both histone H3 acetylation and histone H3 lysine-4 trimethylation." PLoS One **8**(7): e70035.

Scott, S. M., M. Brown and S. E. Come (2011). "Emerging data on the efficacy and safety of fulvestrant, a unique antiestrogen therapy for advanced breast cancer." Expert Opin Drug Saf **10**(5): 819-826.

Selli, C., J. M. Dixon and A. H. Sims (2016). "Accurate prediction of response to endocrine therapy in breast cancer patients: current and future biomarkers." Breast Cancer Res **18**(1): 118.

Shan, L., X. Li, L. Liu, X. Ding, Q. Wang, Y. Zheng, Y. Duan, C. Xuan, Y. Wang, F. Yang, Y. Shang and L. Shi (2014). "GATA3 cooperates with PARP1 to regulate CCND1 transcription through modulating histone H1 incorporation." Oncogene **33**(24): 3205-3216.

Shen, C., J. J. Ipsaro, J. Shi, J. P. Milazzo, E. Wang, J. S. Roe, Y. Suzuki, D. J. Pappin, L. Joshua-Tor and C. R. Vakoc (2015). "NSD3-Short Is an Adaptor Protein that Couples BRD4 to the CHD8 Chromatin Remodeler." Mol Cell **60**(6): 847-859.

Shiu, K. K., R. Natrajan, F. C. Geyer, A. Ashworth and J. S. Reis-Filho (2010). "DNA amplifications in breast cancer: genotypic-phenotypic correlations." Future Oncol **6**(6): 967-984.

Simon, J. A. and C. A. Lange (2008). "Roles of the EZH2 histone methyltransferase in cancer epigenetics." Mutat Res **647**(1-2): 21-29.

Sircoulomb, F., N. Nicolas, A. Ferrari, P. Finetti, I. Bekhouche, E. Rousselet, A. Lonigro, J. Adelaide, E. Baudelet, S. Esteyries, J. Wicinski, S. Audebert, E. Charafe-Jauffret, J. Jacquemier, M. Lopez, J. P. Borg, C. Sotiriou, C. Popovici, F. Bertucci, D. Birnbaum, M. Chaffanet and C. Ginestier (2011). "ZNF703 gene amplification at 8p12 specifies luminal B breast cancer." EMBO Mol Med **3**(3): 153-166.

Sorlie, T., C. M. Perou, C. Fan, S. Geisler, T. Aas, A. Nobel, G. Anker, L. A. Akslen, D. Botstein, A. L. Borresen-Dale and P. E. Lonning (2006). "Gene expression profiles do not consistently predict the clinical treatment response in locally advanced breast cancer." Mol Cancer Ther **5**(11): 2914-2918.

Sorlie, T., C. M. Perou, R. Tibshirani, T. Aas, S. Geisler, H. Johnsen, T. Hastie, M. B. Eisen, M. van de Rijn, S. S. Jeffrey, T. Thorsen, H. Quist, J. C. Matese, P. O. Brown, D. Botstein, P. E. Lonning and A. L. Borresen-Dale (2001). "Gene expression patterns of breast carcinomas distinguish tumor subclasses with clinical implications." Proc Natl Acad Sci U S A **98**(19): 10869-10874.

Sorlie, T., R. Tibshirani, J. Parker, T. Hastie, J. S. Marron, A. Nobel, S. Deng, H. Johnsen, R. Pesich, S. Geisler, J. Demeter, C. M. Perou, P. E. Lonning, P. O. Brown, A. L. Borresen-Dale and D. Botstein (2003). "Repeated observation of breast tumor subtypes in independent gene expression data sets." Proc Natl Acad Sci U S A **100**(14): 8418-8423.

Sotiriou, C., S. Y. Neo, L. M. McShane, E. L. Korn, P. M. Long, A. Jazaeri, P. Martiat, S. B. Fox, A. L. Harris and E. T. Liu (2003). "Breast cancer classification and prognosis based on gene expression profiles from a population-based study." Proc Natl Acad Sci U S A **100**(18): 10393-10398.

Southall, S. M., P. S. Wong, Z. Odho, S. M. Roe and J. R. Wilson (2009). "Structural basis for the requirement of additional factors for MLL1 SET domain activity and recognition of epigenetic marks." Mol Cell **33**(2): 181-191.

Souza, P. P., P. Volkel, D. Trinel, J. Vandamme, C. Rosnoblet, L. Heliot and P. O. Angrand (2009). "The histone methyltransferase SUV420H2 and Heterochromatin Proteins HP1 interact but show different dynamic behaviours." BMC Cell Biol **10**: 41.

Stec, I., G. J. van Ommen and J. T. den Dunnen (2001). "WHSC1L1, on human chromosome 8p11.2, closely resembles WHSC1 and maps to a duplicated region shared with 4p16.3." Genomics **76**(1-3): 5-8.

Steelman, L. S., A. M. Martelli, L. Cocco, M. Libra, F. Nicoletti, S. L. Abrams and J. A. McCubrey (2016). "The therapeutic potential of mTOR inhibitors in breast cancer." Br J Clin Pharmacol **82**(5): 1189-1212.

Steward, M. M., J. S. Lee, A. O'Donovan, M. Wyatt, B. E. Bernstein and A. Shilatifard (2006). "Molecular regulation of H3K4 trimethylation by ASH2L, a shared subunit of MLL complexes." Nat Struct Mol Biol **13**(9): 852-854.

Still, I. H., M. Hamilton, P. Vince, A. Wolfman and J. K. Cowell (1999). "Cloning of TACC1, an embryonically expressed, potentially transforming coiled coil containing gene, from the 8p11 breast cancer amplicon." Oncogene **18**(27): 4032-4038.

Streicher, K. L., Z. Q. Yang, S. Draghici and S. P. Ethier (2007). "Transforming function of the LSM1 oncogene in human breast cancers with the 8p11-12 amplicon." Oncogene **26**(14): 2104-2114.

Suzuki, S., N. Kurabe, I. Ohnishi, K. Yasuda, Y. Aoshima, M. Naito, F. Tanioka and H. Sugimura (2015). "NSD3-NUT-expressing midline carcinoma of the lung: first characterization of primary cancer tissue." Pathol Res Pract **211**(5): 404-408.

Tabarestani, S., M. Motallebi and M. E. Akbari (2016). "Are Estrogen Receptor Genomic Aberrations Predictive of Hormone Therapy Response in Breast Cancer?" Iran J Cancer Prev **9**(4): e6565.

Taketani, T., T. Taki, H. Nakamura, M. Taniwaki, J. Masuda and Y. Hayashi (2009). "NUP98-NSD3 fusion gene in radiation-associated myelodysplastic syndrome with t(8;11)(p11;p15) and expression pattern of NSD family genes." Cancer Genet Cytogenet **190**(2): 108-112.

Tan, C. C., K. V. Sindhu, S. Li, H. Nishio, J. Z. Stoller, K. Oishi, S. Puttreddy, T. J. Lee, J. A. Epstein, M. J. Walsh and B. D. Gelb (2008). "Transcription factor Ap2delta associates with Ash2l and ALR, a trithorax family histone methyltransferase, to activate Hoxc8 transcription." Proc Natl Acad Sci U S A **105**(21): 7472-7477.

Tan, C. C., M. J. Walsh and B. D. Gelb (2009). "Fgfr3 is a transcriptional target of Ap2delta and Ash2l-containing histone methyltransferase complexes." PLoS One **4**(12): e8535.

Tang, P. and G. M. Tse (2016). "Immunohistochemical Surrogates for Molecular Classification of Breast Carcinoma: A 2015 Update." Arch Pathol Lab Med **140**(8): 806-814.

Thomas, S. and P. N. Munster (2009). "Histone deacetylase inhibitor induced modulation of anti-estrogen therapy." Cancer Lett **280**(2): 184-191.

Turner-Ivey, B., S. T. Guest, J. C. Irish, C. S. Kappler, E. Garrett-Mayer, R. C. Wilson and S. P. Ethier (2014). "KAT6A, a chromatin modifier from the 8p11-p12 amplicon is a candidate oncogene in luminal breast cancer." Neoplasia **16**(8): 644-655.

Turner-Ivey, B., E. L. Smith, A. C. Rutkovsky, L. S. Spruill, J. N. Mills and S. P. Ethier (2017). "Development of mammary hyperplasia, dysplasia, and invasive ductal carcinoma in transgenic mice expressing the 8p11 amplicon oncogene NSD3." Breast Cancer Res Treat.

Turner, N., A. Pearson, R. Sharpe, M. Lambros, F. Geyer, M. A. Lopez-Garcia, R. Natrajan, C. Marchio, E. Iorns, A. Mackay, C. Gillett, A. Grigoriadis, A. Tutt, J. S. Reis-Filho and A. Ashworth (2010). "FGFR1 amplification drives endocrine therapy resistance and is a therapeutic target in breast cancer." Cancer Res **70**(5): 2085-2094.

Turner, N. C., J. Ro, F. Andre, S. Loi, S. Verma, H. Iwata, N. Harbeck, S. Loibl, C. Huang Bartlett, K. Zhang, C. Giorgetti, S. Randolph, M. Koehler and M. Cristofanilli (2015). "Palbociclib in Hormone-Receptor-Positive Advanced Breast Cancer." N Engl J Med **373**(3): 209-219.

Ullius, A., J. Luscher-Firzlauff, I. G. Costa, G. Walsemann, A. H. Forst, E. G. Gusmao, K. Kapelle, H. Kleine, E. Kremmer, J. Vervoorts and B. Luscher (2014). "The interaction of MYC with the trithorax protein ASH2L promotes gene transcription by regulating H3K27 modification." Nucleic Acids Res **42**(11): 6901-6920.

van 't Veer, L. J., H. Dai, M. J. van de Vijver, Y. D. He, A. A. Hart, M. Mao, H. L. Peterse, K. van der Kooy, M. J. Marton, A. T. Witteveen, G. J. Schreiber, R. M. Kerkhoven, C. Roberts, P. S. Linsley, R. Bernards and S. H. Friend (2002). "Gene expression profiling predicts clinical outcome of breast cancer." Nature **415**(6871): 530-536.

Vedadi, M., L. Blazer, M. S. Eram, D. Barsyte-Lovejoy, C. H. Arrowsmith and T. Hajian (2017). "Targeting human SET1/MLL family of proteins." Protein Sci.

Veeck, J. and M. Esteller (2010). "Breast cancer epigenetics: from DNA methylation to microRNAs." J Mammary Gland Biol Neoplasia **15**(1): 5-17.

Wagner, E. J. and P. B. Carpenter (2012). "Understanding the language of Lys36 methylation at histone H3." Nat Rev Mol Cell Biol **13**(2): 115-126.

Walsh, L., W. M. Gallagher, D. P. O'Connor and T. Ni Chonghaile (2016). "Diagnostic and Therapeutic Implications of Histone Epigenetic Modulators in Breast Cancer." Expert Rev Mol Diagn **16**(5): 541-551.

Wan, M., J. Liang, Y. Xiong, F. Shi, Y. Zhang, W. Lu, Q. He, D. Yang, R. Chen, D. Liu, M. Barton and Z. Songyang (2013). "The trithorax group protein Ash2l is essential for pluripotency and maintaining open chromatin in embryonic stem cells." J Biol Chem **288**(7): 5039-5048.

Wang, G., G. Liu, X. Wang, S. Sethi, R. Ali-Fehmi, J. Abrams, Z. Zheng, K. Zhang, S. Ethier and Z. Q. Yang (2012). "ERLIN2 promotes breast cancer cell survival by modulating endoplasmic reticulum stress pathways." BMC Cancer **12**: 225.

Wang, G. G., L. Cai, M. P. Pasillas and M. P. Kamps (2007). "NUP98-NSD1 links H3K36 methylation to Hox-A gene activation and leukaemogenesis." Nat Cell Biol **9**(7): 804-812.

Wang, J., Y. Zhou, B. Yin, G. Du, X. Huang, G. Li, Y. Shen, J. Yuan and B. Qiang (2001). "ASH2L: alternative splicing and downregulation during induced megakaryocytic differentiation of multipotential leukemia cell lines." J Mol Med (Berl) **79**(7): 399-405.

Wang, Z. Y. and L. Yin (2015). "Estrogen receptor alpha-36 (ER-alpha36): A new player in human breast cancer." Mol Cell Endocrinol **418 Pt 3**: 193-206.

Wen, H., Y. Li, Y. Xi, S. Jiang, S. Stratton, D. Peng, K. Tanaka, Y. Ren, Z. Xia, J. Wu, B. Li, M. C. Barton, W. Li, H. Li and X. Shi (2014). "ZMYND11 links histone H3.3K36me3 to transcription elongation and tumour suppression." Nature **508**(7495): 263-268.

Wesierska-Gadek, J., T. Schreiner, M. Gueorguieva and C. Ranftler (2006). "Phenol red reduces ROSC mediated cell cycle arrest and apoptosis in human MCF-7 cells." J Cell Biochem **98**(6): 1367-1379.

Wu, H., J. Min, V. V. Lunin, T. Antoshenko, L. Dombrovski, H. Zeng, A. Allali-Hassani, V. Campagna-Slater, M. Vedadi, C. H. Arrowsmith, A. N. Plotnikov and M. Schapira (2010). "Structural biology of human H3K9 methyltransferases." PLoS One **5**(1): e8570.

Wu, J., S. Liu, G. Liu, A. Dombkowski, J. Abrams, R. Martin-Trevino, M. S. Wicha, S. P. Ethier and Z. Q. Yang (2012). "Identification and functional analysis of 9p24 amplified genes in human breast cancer." Oncogene **31**(3): 333-341.

Xiao, Y., C. Bedet, V. J. Robert, T. Simonet, S. Dunkelbarger, C. Rakotomalala, G. Soete, H. C. Korswagen, S. Strome and F. Palladino (2011). "Caenorhabditis elegans chromatin-associated proteins SET-2 and ASH-2 are differentially required for histone H3 Lys 4 methylation in embryos and adult germ cells." Proc Natl Acad Sci U S A **108**(20): 8305-8310.

Yang, Y. H., S. Dudoit, P. Luu, D. M. Lin, V. Peng, J. Ngai and T. P. Speed (2002). "Normalization for cDNA microarray data: a robust composite method addressing single and multiple slide systematic variation." Nucleic Acids Res **30**(4): e15.

Yang, Z. Q., D. Albertson and S. P. Ethier (2004). "Genomic organization of the 8p11-p12 amplicon in three breast cancer cell lines." Cancer Genet Cytogenet **155**(1): 57-62.

Yang, Z. Q., G. Liu, A. Bollig-Fischer, C. N. Giroux and S. P. Ethier (2010). "Transforming properties of 8p11-12 amplified genes in human breast cancer." Cancer Res **70**(21): 8487-8497.

Yang, Z. Q., G. Liu, A. Bollig-Fischer, R. Haddad, A. L. Tarca and S. P. Ethier (2009). "Methylation-associated silencing of SFRP1 with an 8p11-12 amplification inhibits canonical and non-canonical WNT pathways in breast cancers." Int J Cancer **125**(7): 1613-1621.

Yang, Z. Q., K. L. Streicher, M. E. Ray, J. Abrams and S. P. Ethier (2006). "Multiple interacting oncogenes on the 8p11-p12 amplicon in human breast cancer." Cancer Res **66**(24): 11632-11643.

Yates, J. A., T. Menon, B. A. Thompson and D. A. Bochar (2010). "Regulation of HOXA2 gene expression by the ATP-dependent chromatin remodeling enzyme CHD8." FEBS Lett **584**(4): 689-693.

Yuan, W., M. Xu, C. Huang, N. Liu, S. Chen and B. Zhu (2011). "H3K36 methylation antagonizes PRC2-mediated H3K27 methylation." J Biol Chem **286**(10): 7983-7989.

Zhang, Q., L. Zeng, C. Shen, Y. Ju, T. Konuma, C. Zhao, C. R. Vakoc and M. M. Zhou (2016). "Structural Mechanism of Transcriptional Regulator NSD3 Recognition by the ET Domain of BRD4." Structure **24**(7): 1201-1208.

Zhang, X., X. Mu, O. Huang, Z. Xie, M. Jiang, M. Geng and K. Shen (2013). "Luminal breast cancer cell lines overexpressing ZNF703 are resistant to tamoxifen through activation of Akt/mTOR signaling." PLoS One **8**(8): e72053.

Zhang, X., K. Tanaka, J. Yan, J. Li, D. Peng, Y. Jiang, Z. Yang, M. C. Barton, H. Wen and X. Shi (2013). "Regulation of estrogen receptor alpha by histone methyltransferase SMYD2-mediated protein methylation." Proc Natl Acad Sci U S A **110**(43): 17284-17289.

Zhang, Y., T. Liu, C. A. Meyer, J. Eeckhoute, D. S. Johnson, B. E. Bernstein, C. Nusbaum, R. M. Myers, M. Brown, W. Li and X. S. Liu (2008). "Model-based analysis of ChIP-Seq (MACS)." Genome Biol **9**(9): R137.

Zhou, Z., R. Thomsen, S. Kahns and A. L. Nielsen (2010). "The NSD3L histone methyltransferase regulates cell cycle and cell invasion in breast cancer cells." Biochem Biophys Res Commun **398**(3): 565-570.

Zhu, L., Q. Li, S. H. Wong, M. Huang, B. J. Klein, J. Shen, L. Ikenouye, M. Onishi, D. Schneidawind, C. Buechele, L. Hansen, J. Duque-Afonso, F. Zhu, G. M. Martin, O. Gozani, R. Majeti, T. G. Kutateladze and M. L. Cleary (2016). "ASH1L Links Histone H3 Lysine 36 Dimethylation to MLL Leukemia." Cancer Discov **6**(7): 770-783.

Zou, J. X., Z. Duan, J. Wang, A. Sokolov, J. Xu, C. Z. Chen, J. J. Li and H. W. Chen (2014). "Kinesin family deregulation coordinated by bromodomain protein ANCCA and histone methyltransferase MLL for breast cancer cell growth, survival, and tamoxifen resistance." Mol Cancer Res **12**(4): 539-549.

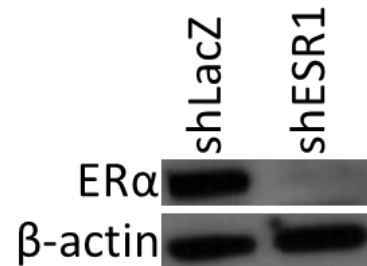
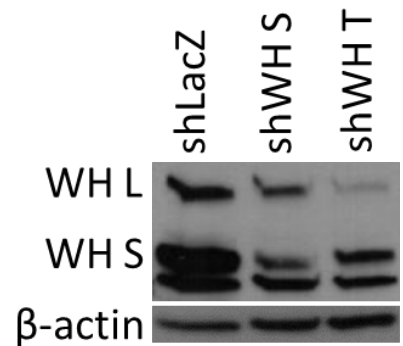
APPENDIX A. NSD3-S and ESR1 knockdown microarray results.

Immunoblots (lower right) for ER α and NSD3 (WH) following knockdown of ESR1 or NSD3, respectively, corresponding to microarray samples appear below. Venn Diagram represents genes in the ESR1 knockdown compared to LacZ control (left) or NSD3 knockdown compared to LacZ control (right). Overlapping (left) or NSD3-unique (right) gene sets were analyzed in ToppFun to produce the tables found below the diagram. Full gene lists and associated statistical measures can be located at https://www.researchgate.net/profile/Jamie_Mills2/publications. File NSD3-short knockdown microarray DOI: 10.13140/RG.2.2.13586.25286 and file ESR1 knockdown microarray DOI: 10.13140/RG.2.2.11908.53126.



| Biological Process | P-value |
|--|----------|
| Vesicle-mediated transport | 3.30E-04 |
| ER to Golgi vesicle-mediated transport | 3.70E-04 |
| Pigment metabolic process | 7.00E-04 |
| Pigment biosynthetic process | 8.20E-04 |
| Intracellular transport | 8.20E-04 |

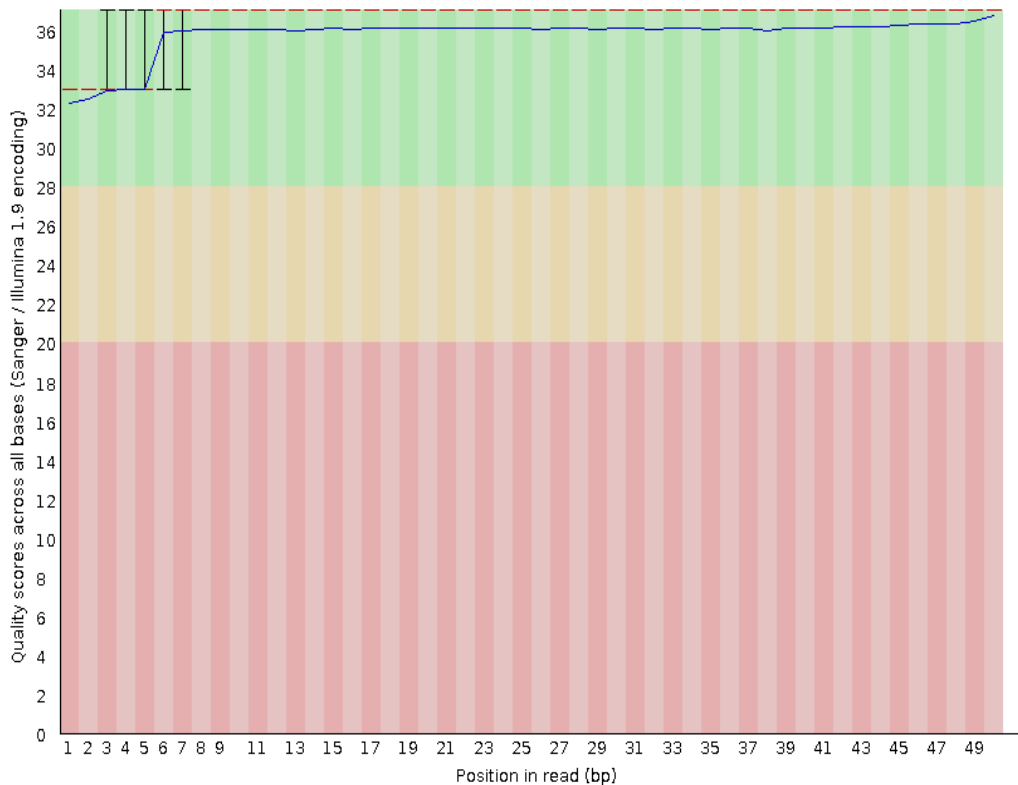
| Biological Process | P-value |
|---|----------|
| Mitotic cell cycle | 1.00E-24 |
| Cell Cycle | 1.00E-24 |
| Mitotic cell cycle process | 1.00E-24 |
| DNA metabolic process | 1.00E-24 |
| Cell cycle process | 1.00E-24 |
| Mitotic nuclear division | 1.60E-22 |
| Organelle fission | 9.30E-22 |
| Nuclear Division | 1.00E-21 |
| Organelle organization | 1.20E-21 |
| DNA replication | 4.40E-21 |
| Cell division | 4.70E-21 |
| Mitotic cell cycle phase transition | 1.50E-20 |
| Cell cycle phase transition | 2.80E-20 |
| DNA strand elongation | 8.80E-19 |
| DNA strand elongation involved in DNA replication | 8.90E-19 |

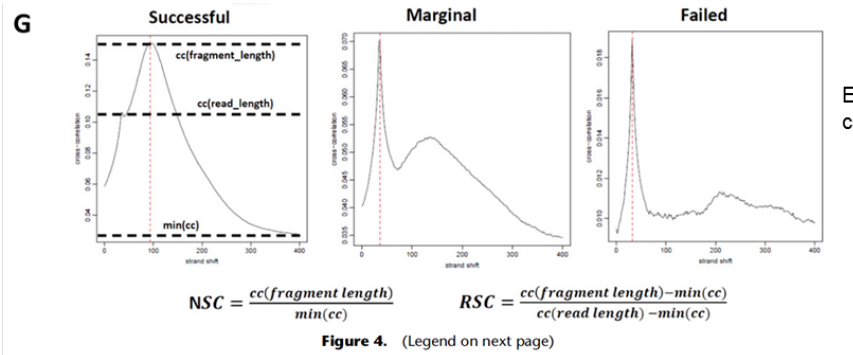


APPENDIX B. H3K4me3 ChIP-seq quality control and enrichment reports.

Output from sequencing quality control measures appears in the table below. The figure represents Phred scores for the ChIP-seq sequencing run. All samples are nearly identical, therefore only one is presented (shASH2L-A-H3K4me3). Cross-correlation plots appear on page 208 and enrichment plots on page 209.

| Sample-Name | Total Sequences | Type | # reads | %GC |
|-------------------------|-----------------|-------|----------|-----|
| 2247_shASH2L-A-H3K4me3 | 28430917 | ChIP | 28387407 | 45 |
| 2248_shASH2L-A-input | 28847916 | Input | 28819172 | 41 |
| 2249_shASH2L-B-H3K4me3 | 28142484 | ChIP | 28057625 | 43 |
| 2250_shASH2L-B-input | 35706228 | Input | 35668119 | 43 |
| 2251_shASH2L-C-H3K4me3 | 35126397 | ChIP | 34986667 | 51 |
| 2252_shASH2L-C-input | 32529399 | Input | 32449969 | 43 |
| 2253_shLacZ18-A-H3K4me3 | 32483014 | ChIP | 32393402 | 48 |
| 2254_shLacZ18-A-input | 33296775 | Input | 33219481 | 44 |
| 2255_shLacZ19-B-H3K4me3 | 35198935 | ChIP | 35069303 | 49 |
| 2256_shLacZ19-B-input | 35411340 | Input | 35328228 | 43 |
| 2257_shLacZ20-C-H3K4me3 | 34957285 | ChIP | 34835920 | 49 |
| 2258_shLacZ20-C-input | 46720830 | Input | 46614287 | 41 |

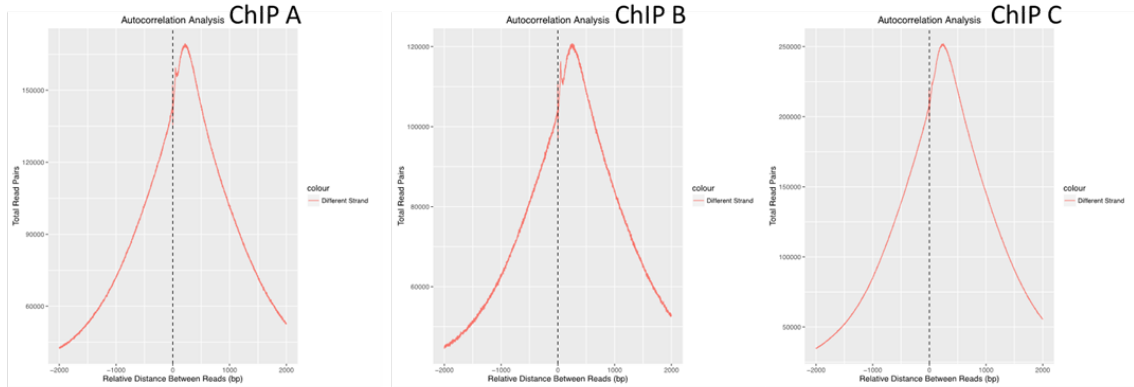




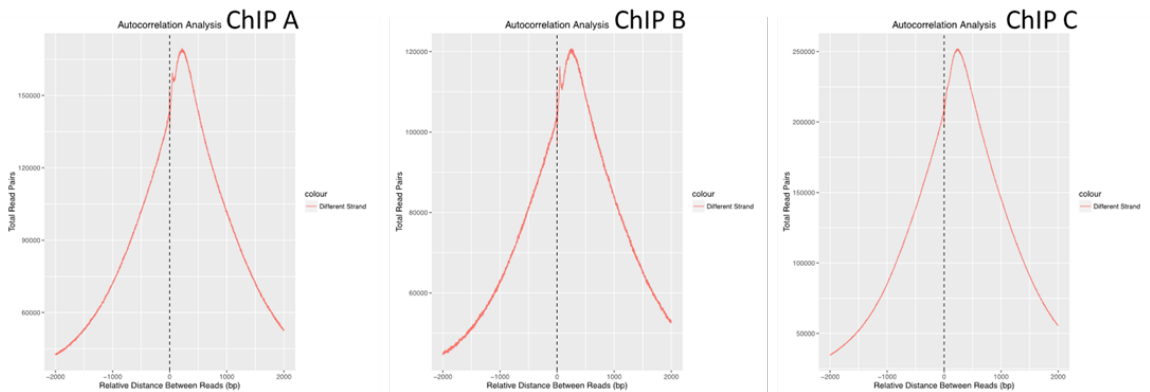
Example of successful cross-correlation plots

Figure 4. (Legend on next page)

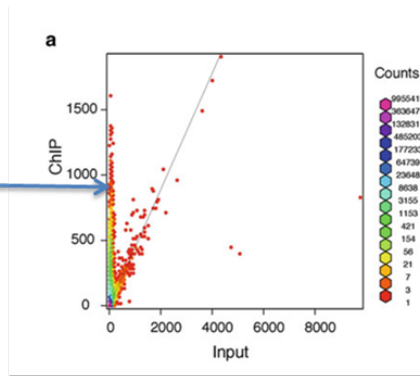
LacZ H3K4me3 ChIP samples



ASH2L H3K4me3 ChIP samples

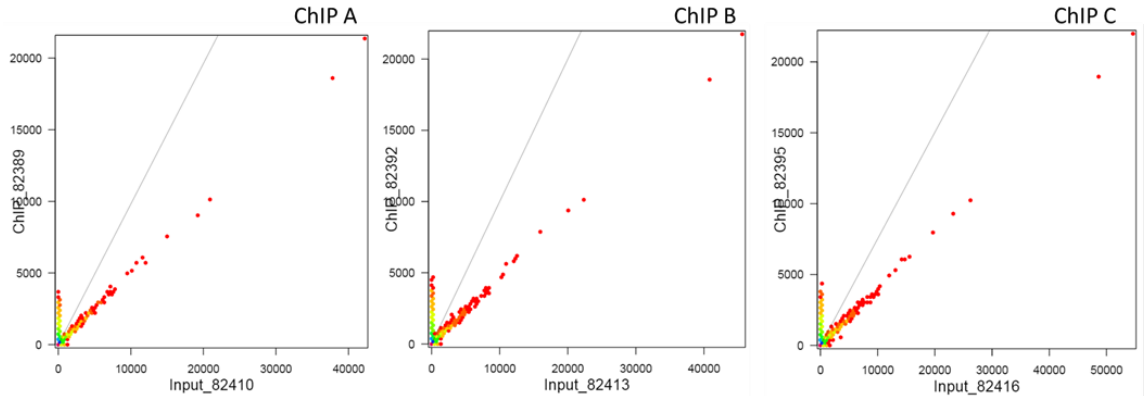


Example:
Hoping for a peak
here

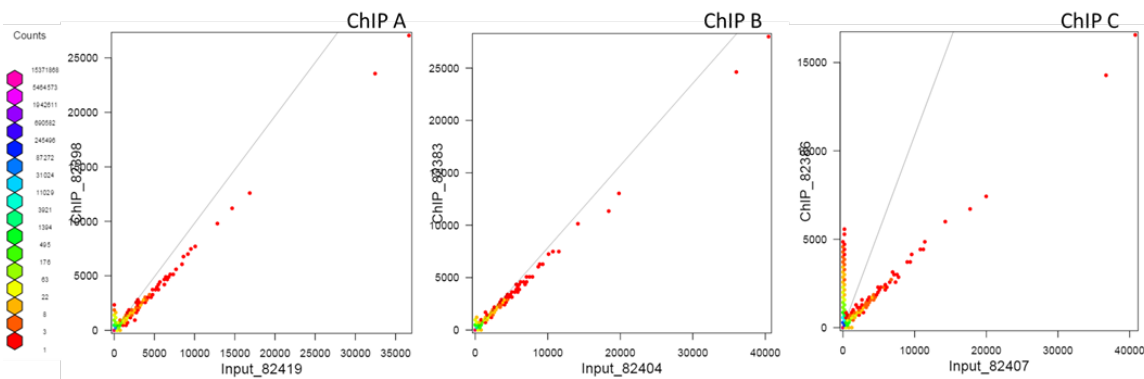


Example of successful
enrichment plots

LacZ H3K4me3 ChIP samples



ASH2L H3K4me3 ChIP samples



APPENDIX C. H3K4me3 ChIP-seq peak datasets: LacZ control and ASH2L knockdown.

Output lists from MACS2 ChIP-seq analysis can be found at https://www.researchgate.net/profile/Jamie_Mills2/publications. File H3K4me3 ChIP-seq MACS2 shLacZ DOI: 10.13140/RG.2.2.21345.71526 and file H3K4me3 ChIP-seq MACS2 shASH2L DOI: 10.13140/RG.2.2.28056.60162.

APPENDIX D. Gene Lists: overall H3K4me3 ChIP-seq peaks.

Output lists from MACS2 ChIP-seq analysis Venn Diagrams comparing LacZ and ASH2L overall gene lists appear in this appendix. These lists correspond to **Figure 3.2-D** but do not report the 13,090 genes in common.

| | | | | | |
|------------------------------|--------------|--------------|--------------|--------------|--------------|
| LacZ only (2,251) | L1TD1 | KCNH6 | MIR6124 | C1orf131 | CLEC14A |
| LOC100133669 | PKIG | KCNH7 | LOC101927854 | COL14A1 | LOC101060091 |
| HTR6 | GSTM5 | FBXO15 | SNORA59A | CPZ | DCN |
| HTR7 | KCNC1 | PKP1 | SNORA59B | APOA4 | MIR941-1 |
| LURAP1L | KCNC2 | LOC100505716 | ADAM18 | CEBPE | MIR1289-1 |
| FAM19A2 | KCNC3 | LOC100289495 | BRMS1 | TULP4 | RPS6KB1 |
| BBX | LOC283683 | KCNF1 | LOC105376331 | IL21R | SNORA31 |
| FAM19A1 | LOC79999 | HTR1F | LOC101927865 | LOC401312 | TYW5 |
| FAM19A5 | LOC100288181 | TNFSF13B | PLD5 | LOC100505625 | LOC101927694 |
| FAM19A3 | BBC3 | MBL2 | KCNV1 | EVI2A | SNORA24 |
| EXOC3-AS1 | NEFH | C1R | RPS6KA2-AS1 | LOC100288254 | CYP2E1 |
| GSTK1 | MYBPC3 | LOC284950 | SPINK14 | MAB21L2 | NGEF |
| WDR83OS | MYBPC1 | KCNJ1 | LOC101927881 | C1orf116 | ACTL7B |
| DHDH | MYBPC2 | COL26A1 | MIR6165 | LOC100506869 | FPR3 |
| BCR | KCND1 | KCNJ8 | TBX22 | SPRR2F | FPR2 |
| ORAI3 | KCND2 | ANKRD62P1- | TBX18 | SLC35D3 | C2 |
| ORAI2 | KCND3 | PARP4P3 | CD6 | UBA6-AS1 | GLYATL1 |
| AGTR1 | GSTO1 | CDRT15 | CD5 | LOC101927907 | GRIN2C |
| VOPP1 | GTF2H2B | MIR4776-1 | MXN1-AS1 | XCR1 | GRIN3B |
| ORAI1 | PKN3 | LGALS9 | MIR6132 | LOC101927914 | SNORA84 |
| AGTR2 | SYNPO2 | INHBA-AS1 | CFH | LOC440895 | DIO3OS |
| COL13A1 | GSTP1 | NKAIN3 | ELL2 | SLC35F4 | CCDC162P |
| TARSL2 | PTAFR | SLC10A6 | MOCS2 | SIPA1L1 | F8 |
| SHMT1 | KCNA2 | LOC101805491 | MOCS3 | TCEAL2 | F9 |
| B3GLCT | KCNA3 | FAM193A | PLIN1 | EMC8 | SNORA68 |
| PLBD1-AS1 | LOC642423 | SSNA1 | PLIN5 | NFYA | DPY19L1P1 |
| T | KIAA2022 | LOC101927822 | DIO2-AS1 | C6orf58 | FGF14-AS1 |
| RDH11 | KCNA5 | FAM35A | CKM | C3orf79 | SNORA98 |
| RDH16 | KCNA6 | FAM196B | HAO2-IT1 | CLEC19A | GC |
| RDH14 | ADAM28 | LOC101927839 | DNM3OS | NPC1L1 | SNORA90 |
| RDH13 | ADAM32 | LOC101927847 | DIO2 | LDLRAD4-AS1 | GGT3P |
| GSTM3 | ADAM30 | ENPP2 | MIRLET7I | DAO | SNORA87 |
| PKIB | POFUT2 | MIR6125 | LOC439933 | DNAJC3-AS1 | UBE2D4 |
| | MYBPHL | LOC101927849 | C1orf158 | C3orf22 | LOC102724784 |

| | | | | | |
|--------------|-----------|--------------|--------------|---------------|--------------|
| TNFRSF11B | CHGA | TDRD12 | RGS20 | ACY3 | RAB32 |
| SOCS2 | LSP1P3 | LOC339059 | NRIP3 | ZNF587B | RAB36 |
| COL28A1 | NCRUPAR | KCNAB3 | RGS22 | FSHB | LOC102723344 |
| BDNF | PNMT | RBBP4 | CLASP1 | PRSS3P2 | CSPG4 |
| TNFRSF10C | MIR6086 | MROH8 | LOC101927798 | FSHR | HPN-AS1 |
| SNORA80B | RPL32 | RPL13AP3 | DLK1 | SNORA17A | SLC13A1 |
| SH2D4B | MIR6083 | SLC46A2 | NOBOX | GCK | SLC13A2 |
| CECR1 | ABCA13 | MIR320B1 | RABL6 | EPGN | HERC2P9 |
| LOC102723427 | MIR6089 | IQCF2 | CDCA5 | CFHR2 | FBXL22 |
| CECR3 | GPR179 | TSHZ1 | CDCA8 | CFHR1 | CALML3 |
| PTPRZ1 | MIR6071 | TSHZ2 | TPBGL | CFHR5 | MIR7978 |
| SLITRK1 | DKK3 | FAM180A | LOC400553 | SLX4IP | TKTL2 |
| SLITRK6 | CPED1 | SRGAP2-AS1 | F13B | SNORA11B | XXYLT1-AS1 |
| ENTPD1 | SNORA74B | RAB40AL | LOC150935 | SNORA111 | GPR37L1 |
| AARD | MIR6078 | CX3CL1 | LOC101243545 | FTO-IT1 | CYCSP52 |
| MST1L | MEG9 | ANKRD7 | SLC7A3 | SYT2 | EFCAB6-AS1 |
| LOC102724710 | OCSTAMP | B3GNT5 | PTF1A | HIGD2B | TWIST2 |
| SWI5 | VTRNA2-1 | FAM181B | FRY | SYT8 | USP32P1 |
| TG | CPEB1 | FAM181A | LOC100132735 | SYT6 | HBM |
| TH | GPR182 | AKAP6 | CIR1 | CTD-3080P12.3 | LOC100288748 |
| SNAR-C3 | FRMPD2B | AKAP4 | MFNG | MS4A7 | RAB6C |
| SLC7A13 | ELN | LOC100506682 | NDC80 | ANKS3 | HDC |
| SNAR-C5 | GPR132 | LOC100506688 | IGSF11 | AGPAT4 | GABRP |
| SNAR-C4 | SNORA70B | OLAH | RLBP1 | SPOCK3 | FAIM2 |
| HYAL1 | RNF165 | LOC102724804 | LOC389602 | SPOCK1 | NANOS2 |
| FAM170A | RNF139 | PPY2P | LOC102724511 | ACKR2 | NANOS3 |
| SNAR-B1 | LIMD1-AS1 | CIB4 | TTC39C | CISTR | LOC55338 |
| CRIP3 | CHML | CIB3 | MCM3AP | ACMSD | HRASLS2 |
| SNAR-A7 | GPR156 | FAM186A | PCBP2-OT1 | ZFPM2-AS1 | SCUBE1 |
| CRIP2 | MYBPH | ELMO1 | PRKCQ-AS1 | C10orf55 | LOC100144595 |
| LOC101927623 | GPR142 | DLG1 | NFIA-AS2 | H19 | CETN4P |
| ECD | KRT8P41 | TGFBI | MIR6516 | LOC102723362 | LOC642943 |
| PHOX2A | COL16A1 | ANKRD44-IT1 | MIR7846 | TIMP3 | OACYLP |
| LOC101928977 | CHRM3-AS2 | HSPB9 | MIR6513 | TIMP1 | USP46-AS1 |
| CHD5 | CHPF | LRRC74A | EIF1B | LOC388242 | EPB41L4A-AS2 |
| LOC101927640 | ERG | BBOX1-AS1 | MIR6504 | TP53TG5 | CCBE1 |
| RGPD4-AS1 | IQCA1 | C5orf66-AS1 | MIR6502 | C10orf91 | CNBD1 |
| FAM178B | PAUPAR | KCNA10 | LOC101926940 | LOC102724652 | SPARCL1 |
| LOC101928988 | PPIAL4A | ECT2L | SMIM10L2A | LOC102724651 | MIR5095 |

| | | | | | |
|--------------|--------------|---------------|--------------|--------------|--------------|
| NYAP2 | TM4SF4 | SERPINE1 | NTSR1 | CCDC18-AS1 | ACOXL |
| SNORD2 | TM4SF1 | EARS2 | TVP23C-CDRT4 | AGR2 | LOC100996624 |
| MGC34796 | CCAT2 | ACOT8 | NTSR2 | JAM3 | LOC100996634 |
| LOC339568 | STX1B | LOC400661 | NMBR | LINC00989 | CNR2 |
| MIR6715A | LOC103312105 | SERPINA3 | VCX2 | CYSRT1 | LOC100996635 |
| PTH2R | PPP1R3A | C17orf50 | MIR7705 | EFEMP1 | LINC00911 |
| PGAM4 | TSPAN8 | SERPINB5 | ESM1 | UGT2B10 | LINC00901 |
| ERVFRD-1 | TSPAN1 | HSPA1L | CEACAM3 | ATP11C | NALCN-AS1 |
| LOC100652999 | BPIFB2 | LOC102724484 | NRN1L | LGSN | MRGBRE |
| BEND3P3 | PPP1R1C | C17orf67 | ADRB3 | SRSF5 | WDR72 |
| GPR65 | MIR550A1 | TUSC8 | CEACAM6 | LVCAT5 | WDR77 |
| LRRC70 | ANKRD18B | ATP8A2 | ESRG | LOXHD1 | LINC00882 |
| LRRC71 | MIR550A3 | TUSC3 | MIR217HG | TMEM26-AS1 | SYNJ2-IT1 |
| SLC9C1 | AKR1B1 | C17orf99 | C10orf107 | OVOL1-AS1 | LOC649133 |
| LOC100129316 | KIF23 | TECTA | C10orf113 | BFSP2 | MIR8067 |
| SH2D6 | PDZRN3 | RNF216-IT1 | C10orf126 | ZBTB20-AS4 | MIR8065 |
| SLC9A3 | TMPRSS9 | SLX1B-SULT1A4 | BDKRB1 | UGT2B28 | LINC00842 |
| SLC9A4 | STX19 | C17orf80 | MIR5197 | ARL13A | LINC00845 |
| LOC100505920 | RXR8 | ITPR1 | MIR5189 | GZMB | MIR8059 |
| GPR87 | PRLH | ATP8B4 | C14orf119 | SRD5A3-AS1 | LINC00877 |
| GPR88 | RXRG | TECRL | RWDD3 | ANPEP | IGLL5 |
| GPR85 | RFTN1 | PSCA | LOC100192426 | WWC2-AS1 | IGLL1 |
| GPR84 | MIAT | SYCP1 | KIAA1024L | FAM9B | LINC00865 |
| LOC100287072 | PRND | PSD3 | C14orf105 | MTRNR2L6 | LINC00867 |
| LRRC52 | DOK5 | SLC24A2 | LOC400997 | MTRNR2L3 | LINC00861 |
| LOC100130331 | FUT9 | SEMA3D | ZC3H12D | ANKFN1 | RERGL |
| SLC38A4 | MIR5008 | SEMA3B | LOC158434 | CACNA2D3-AS1 | SSUH2 |
| LOC100287010 | EGFR-AS1 | ANKRD30B | NPBWR2 | LOC100287792 | MIR8082 |
| IQCH-AS1 | LOC102724297 | CMA1 | RPS14P3 | C6orf141 | MAP3K19 |
| LOC100129345 | AFF2 | MIR1972-2 | FAM111A | LOC102724096 | DRC3 |
| L3MBTL4 | B3GALT5-AS1 | SYCP3 | MRVI1 | ETS1 | MIR8079 |
| PRCD | ELMO1-AS1 | LOC101926908 | HLA-DRB1 | FAM3B | PARD3-AS1 |
| IFI16 | SSTR1 | LMAN1L | PGCP1 | PHGR1 | CSTL1 |
| SLC12A2 | CRMP1 | SLC6A12 | LINC00977 | ACOT12 | PLA2G12B |
| FCGR2B | CLMP | PLPP1 | LINC00970 | LINC00922 | DNAJC7 |
| FCGR2C | PDLIM4 | SLC6A20 | LINC00971 | UBA7 | HCG17 |
| ZNF790-AS1 | PLA2G2F | PTDSS1 | CHST9 | CNN1 | MIR135A2 |
| ANTXRPL1 | S100G | DPH5 | CHST7 | LINC00954 | GJA10 |
| HNF1B | LL22NC01-81G | LOC100505795 | LINC00967 | LOC102724053 | OR7E156P |

| | | | | | |
|--------------|--------------|--------------|--------------|---------------|--------------|
| PWRN4 | LYN | THEMIS | PATL2 | SLC9A3R1 | PEBP4 |
| FEZF2 | NOX3 | RPGRIP1L | SCGB2A2 | FRG2DP | NRTN |
| PWRN2 | DLEU1-AS1 | TAC4 | VSTM2A | TBXAS1 | FAM150B |
| CTD-2151A2.1 | UCN3 | TAC1 | KCNJ13 | SP140L | WBP11P1 |
| AMIGO2 | FLVCR2 | SLC52A1 | KCNIP4 | LINC00581 | RARRES3 |
| ZDHHC22 | VWC2L-IT1 | BMP5 | KCNJ15 | LINC00578 | VIL1 |
| GDPD4 | OR14A16 | BMP2 | PARTICL | LINC00570 | OR51A2 |
| PPP2CA | LOC338694 | CPS1 | HABP2 | LINC00571 | MUC21 |
| EGFLAM | LOC103344931 | PNLIPRP2 | VCX3B | LINC00572 | C1orf94 |
| ANKRD34C-AS1 | LYRM2 | USP12-AS1 | ARHGAP26-IT1 | MIR486-2 | ADGRE5 |
| LINC00838 | LOC653786 | CDHR3 | OTOG | SMIM18 | ADGRF1 |
| CDH26 | CCDC144CP | RAB40A | RAB39A | MUC5AC | ADGRF4 |
| LINC00824 | MYLK2 | SRD5A1P1 | CXCR6 | LINC00563 | PKD1L1 |
| MIR3622B | NRROS | LOC653712 | DISC2 | SPACA7 | ASB15 |
| MRS2P2 | CXCL17 | NPVF | AAMDC | LINC00592 | EYA1 |
| GAGE10 | CXCL14 | LAMB3 | CTAGE10P | LINC00593 | LOC105375650 |
| MFSD4 | CPB2 | SCIMP | SNAR-A12 | TBX5 | GABRG2 |
| COL6A3 | DSEL | BCL6B | CPLX3 | PINK1 | FAM169B |
| AKNAD1 | CPA4 | FAM231D | KLRC3 | LINC00589 | HYALP1 |
| CDH17 | C7orf65 | FAM231B | CXCL8 | CPNE8 | LINC00400 |
| CDH19 | FOXN1 | SKP1P2 | SPO11 | CPNE7 | MIR7151 |
| LTF | SMARCA5-AS1 | NBAT1 | DOCK9 | CYP3A7-CYP3A5 | MIR7150 |
| CST9L | C7orf69 | NKX2-3 | LOC100288911 | ZNF890P | LINC00434 |
| LTK | SCHIP1 | PCSK6-AS1 | LINC00538 | NUDCD1 | LINC00424 |
| ATP1A4 | CELF3 | CDK15 | LINC00523 | OR51Q1 | CEP83 |
| ATP1A2 | DSG1 | FAM101A | LINC00524 | FMR1-AS1 | PAM |
| OPCML | SLC25A11 | COL21A1 | LINC00525 | SFTPB | MESP2 |
| NOS2 | MFF | GCNT4 | LINC00520 | SFTPC | AIFM2 |
| SAMD14 | SLC25A31 | LOC145474 | CRABP1 | SLC25A25-AS1 | HADHB |
| LIPC | NSMCE2 | GUCA2A | SHANK2-AS3 | DEPDC4 | CEP63 |
| LIPM | SFRP1 | TRMT5 | LINC00558 | HSD17B3 | MIR4472-2 |
| GABARAPL3 | CTXN3 | BEST2 | LINC00559 | OSM | ALOX5 |
| CSNK2A3 | COL9A1 | BEST3 | CRB2 | MYO9B | GPC5-AS1 |
| FLJ31356 | RERG-AS1 | BEST1 | LINC00511 | ACTL8 | GABRA5 |
| HS3ST3A1 | MLN | NEUROD1 | IL12RB2 | SMAD1-AS1 | DHRS1 |
| HACD2 | DIRC3 | LOC100130691 | LINC00507 | FAM133CP | DHRS9 |
| LY9 | PLVAP | WEE2-AS1 | CENPO | LOXL3 | AGBL1-AS1 |
| MIR1973 | ACRBP | NEB | ADGRL3 | NR3C1 | LINC00499 |
| GPIHBP1 | MIR1910 | BNC1 | CDKL4 | LOXL2 | LINC00494 |

| | | | | | |
|--------------|-----------|--------------|--------------|---------------|-----------|
| FRMD4A | FAM163A | ANP32A-IT1 | C11orf86 | IGSF1 | PRPF38A |
| VASH1 | TRPV5 | DIAPH3-AS1 | LINC00609 | PYHIN1 | MIR548D2 |
| GOLGA8G | NR2E1 | SPATA12 | LINC00606 | KLLN | LARP7 |
| PIP | AMTN | MIR3156-2 | LINC00603 | SERP2 | L1CAM |
| LINC00460 | MIR7110 | MGC16025 | PRSS45 | TFEC | LGALS17A |
| LINC00462 | MIR7111 | LOC100996455 | LINC00639 | LOC102546299 | MIR130A |
| CHMP1B2P | MIR7109 | EDA2R | MIR548AE1 | TFF1 | MIR3973 |
| HMGCS2 | CLDN2 | ANO4 | CCL17 | MRRF | EMX2OS |
| MIR1273E | CLDN1 | ANO5 | BRD4 | ETNPPL | NBPF25P |
| MIR1273H | PSMD5 | ANO1 | PRSS35 | MGC32805 | SCTR |
| LOC100130880 | FAM133A | RAMP3 | LINC00626 | GALNT12 | BBOX1 |
| LINC00485 | IDO1 | SLC30A8 | C11orf53 | EFTUD1 | BMP8B |
| LMF2 | CLCNKB | NPSR1-AS1 | NKX6-3 | SCGN | MIR3938 |
| THSD4 | AGAP2 | LINC00709 | LHCGR | COL4A3 | LINC01467 |
| CCDC70 | MRPL14 | CTB-12O2.1 | NKX6-2 | SCG2 | LINC01468 |
| LINC00476 | AGAP4 | COL5A2 | ITGA11 | MGAT4EP | MIR1343 |
| LINC00477 | COL24A1 | LINC00701 | VAC14-AS1 | RALYL | LINC00160 |
| LINC00469 | TDP2 | LINC00702 | NACAD | DKFZp434J0226 | BRE-AS1 |
| CCDC60 | WFIKKN1 | SCARF2 | LOC145845 | AGAP6 | LINC01483 |
| KLHDC7B | SNAR-H | GALNT8 | LOC102546228 | HKDC1 | LINC01485 |
| OR52N2 | EFCAB9 | TEX13A | LINC00692 | CAMK1G | LINC01482 |
| OR52M1 | MYT1L-AS1 | HSP90AB4P | DUSP26 | GMPR2 | RFXANK |
| CTAGE15 | MIR3689C | FAM132A | POM121L2 | TFPI | G6PC2 |
| C2CD4A | LEFTY1 | FAM132B | SLC16A12-AS1 | B3GAT1 | SP5 |
| TRPM1 | MRPL47 | GALNT4 | RP1 | PGLYRP2 | SP9 |
| TRPM5 | SMTNL2 | BPESC1 | C4orf45 | MIR3929 | LINC01479 |
| LOC105747689 | COL11A1 | FAM131C | LINC00687 | MIR3935 | MIR548A1 |
| HEPACAM2 | TMEM75 | RPLP0P2 | MRLN | EPSTI1 | MIR548A3 |
| PRL | PSMB3 | TMEM92-AS1 | SALRNA3 | MIR548F5 | MSLN |
| CLDN14 | CEPT1 | LINC00648 | KLF3 | MIR548F4 | UNC80 |
| HNRNPH2 | TMCO3 | LINC00644 | C4orf26 | UNC5C | LINC01426 |
| CLDN17 | WARS2-IT1 | LINC00683 | PCED1B-AS1 | MIR3923 | LINC01422 |
| CST6 | PTOV1-AS2 | GALR3 | MYOZ2 | MIR3925 | LINC01423 |
| CST5 | RBPMS | LINC00675 | MUCL1 | MIR3924 | MSMB |
| IFNB1 | DCDC5 | LINC00667 | FANK1-AS1 | SCO1 | CERS3 |
| KBTBD8 | PTPRC | PRSS23 | SMIM2 | MIR3920 | MIR548AQ |
| CHRN2 | MIR8071-1 | MYOM2 | IGSF5 | FAXDC2 | MIR548AV |
| LMO3 | FASLG | LINC00615 | SMIM5 | ADAMTS12 | MIR548AD |
| PYY | RDH10-AS1 | LINC00613 | IGSF6 | ADAMTS14 | MIR548AC |

| | | | | | |
|--------------|---------------|--------------|------------|-------------|-------------|
| LINC01416 | FREM3 | MTTP | LINC00313 | BRINP2 | LSM3 |
| MIR548AL | ZSCAN10 | C12orf80 | LINC00304 | BRINP1 | MIR1206 |
| MIR548AM | FAM120AOS | C12orf71 | TEDDM1 | C9orf129 | MIR1207 |
| MTUS2-AS1 | ADAMTSL1 | C12orf74 | DSCAML1 | FAM181A-AS1 | MIR1208 |
| NOP56 | GAST | LINC01270 | MIR3714 | GABRG3-AS1 | MIR1202 |
| PDCD1 | ASAP1-IT2 | LINC01272 | LINC01609 | TAF11 | MIR1200 |
| LINC01432 | ANGPTL2 | ZNF341-AS1 | TUBA3E | ASB5 | LINC00269 |
| STH | ANGPTL4 | LINC01268 | LINC01608 | LINC01507 | LSP1 |
| MIR1293 | LNX1-AS1 | LINC01266 | VENTXP7 | OR11I | SGCD |
| TNFSF18 | OLFML3 | LINC01256 | NRG3-AS1 | LINC01525 | LINC01549 |
| MSR1 | LINC01354 | LINC01258 | ASPRV1 | PRCAT47 | LINC01543 |
| DDIAS | LINC01350 | LINC01298 | LINC00383 | LINC01526 | LINC01544 |
| TNFSF12 | TNF | TM4SF20 | ADCYAP1 | LINC01523 | PROSER2-AS1 |
| APOBEC3A | TNR | LINC01287 | OVCH1-AS1 | GSDMC | ASPG |
| MIR1284 | LINC01344 | MIR26A1 | MIR374B | RNASE10 | NLGN3 |
| LDHAL6B | TOX | LINC01280 | CPAMD8 | TMEM196 | LINC01571 |
| LINC00052 | LINC01333 | LOC100128993 | LINC00399 | ZFAT-AS1 | LINC00240 |
| SYP | LINC01335 | ZMAT4 | BCL2L14 | LINC01510 | LINC00243 |
| C14orf1 | LINC01375 | CPSF2 | CNTNAP2 | LINC01512 | LINC01574 |
| MRPS34 | LINC01370 | SELV | LINC00330 | TMEM182 | LINC01570 |
| PRICKLE2 | TPR | UCN | MIR378G | MIR5689HG | MIR1256 |
| GAD2 | ESPNP | HEPH | MIR378I | SLC2A14 | MIR1252 |
| APTR | LINC01361 | C15orf43 | LINC00359 | CACNA1C-IT2 | LINC00238 |
| LINC01399 | LINC00028 | C15orf53 | LINC00348 | OR1M1 | LINC00239 |
| CLYBL-AS1 | LINC00029 | C15orf54 | LINC00343 | TMEM159 | LINC01564 |
| TGM1 | SYNE3 | GBP2 | MMADHC | LINC01594 | CDRT7 |
| TGM6 | LINC01304 | NXF5 | ART4 | LINC01591 | LINC01559 |
| RAG2 | PROX1-AS1 | MUC6 | ARSI | DOCK4-AS1 | LINC00222 |
| TGM4 | LINC01307 | CAPN14 | TAS2R38 | LINC01581 | LINC01553 |
| CARTPT | DKFZP586I1420 | FSIP2 | CCNJL | DEFB112 | LINC01554 |
| FGF11 | LINC01331 | LINC01621 | TAS2R60 | SSBP3-AS1 | CBLN1 |
| STEAP3-AS1 | TTN | LINC01622 | BANK1 | CALCRL | SCARNA3 |
| PRICKLE2-AS3 | RNU11 | ZFYVE19 | DEFB132 | LINC00282 | CD101 |
| IL1RL2 | LINC01322 | LINC01612 | DEFB130 | ASMT | KPRP |
| OXCT1 | MIR147A | LINC01614 | BANF1 | ANKRD29 | PDE1C |
| TGS1 | HDAC11 | LINC00320 | BANF2 | LINC00276 | ATP13A5-AS1 |
| ZPLD1 | AQP7 | KCND3-AS1 | PDGFRA | ANKRD24 | UBAC2 |
| MSANTD1 | AQP5 | LINC00310 | VCX | ANKRD22 | GDF7 |
| MBNL1 | TXK | LINC00311 | HS1BP3-IT1 | LINC00271 | SCARNA5 |

| | | | | | |
|--------------|--------------|--------------|--------------|-----------|--------------|
| SCARNA6 | SYT16 | MMS19 | MYLK | TMEM198B | PMCHL1 |
| CLIC6 | SUGCT | LOC101928008 | FLJ16171 | LINC01140 | PMCHL2 |
| CLIC5 | TSPAN18 | LOC101929331 | JPH2 | LINC01141 | OR5T2 |
| STAB2 | LOC154449 | CDC14C | JPH3 | NBPF7 | AACSP1 |
| PRMT5 | HHIP | ARMC2-AS1 | MYOG | LINC01137 | BZW1 |
| LINC01499 | LOC63930 | SNRPN | MYOC | LINC01176 | LINC01106 |
| RAPSN | RIIAD1 | BAIAP2-AS1 | MIR1537 | LINC01170 | LINC01107 |
| TLDC2 | LOC101929199 | LOC101929384 | SH3BP5-AS1 | C5orf64 | LINC01102 |
| THRB-AS1 | STAT5A | LOC101928052 | LINC01227 | C5orf67 | LINC01103 |
| PPP1R26-AS1 | REG4 | EIF2B1 | TCP11 | C5orf66 | LINC01105 |
| MANEA | CTB-178M22.2 | LOC101929395 | S100A2 | LINC01164 | ADAM8 |
| PDE8B | CD200 | CATSPER3 | FRMD1 | LINC01162 | LINC01133 |
| AMY1B | IL20 | ANGPT2 | FRMD3 | LINC01163 | LINC01126 |
| ASIC4 | TBX2-AS1 | SNX29P1 | FRMD7 | CRYBB2 | MSC-AS1 |
| ASIC3 | WFDC3 | KIAA0586 | LINC01213 | RGS5 | SERINC4 |
| DNAJC16 | IL18 | P2RX2 | S100A9 | ARID2 | TUBA8 |
| FRMD6-AS2 | EHD4-AS1 | LOC101928093 | S100A8 | RGS8 | GOLGA8CP |
| TMEM100 | IL19 | TRY2P | GIMD1 | GGT1 | DMRTA2 |
| OR2F1 | PABPC3 | KRT3 | LINC01247 | RGS7 | TEX36-AS1 |
| ARID3C | MGAT2 | TLN2 | LINC01248 | MAT1A | TNNI1 |
| MGC15885 | IL34 | TLN1 | MIR4444-1 | CALCB | LINC01070 |
| NDST4 | NUDT7 | PGAM1P5 | B3GALT6 | NXPH2 | LOC101929064 |
| GATA4 | | ZOR1E2 | CLLU1 | LOC286437 | C6orf222 |
| PYDC2 | OR5K1 | ZNRF2P2 | LINC01235 | KTN1-AS1 | LINC01095 |
| HOXC12 | EPHA5-AS1 | SOSTDC1 | NALT1 | CHURC1 | LINC01096 |
| LOC100507065 | FBN3 | TLR9 | EFCAB11 | CNTFR | LINC01091 |
| LOC100268168 | C8orf49 | TLR7 | ATP7B | ARIH2OS | LINC01093 |
| LOC101929207 | SNTG1 | TLR4 | UPP2 | UNC13D | GOLGA8IP |
| FAM201A | TFAP2D | FLJ42627 | LOC101929034 | HNRNPKP3 | OR6B3 |
| LIMS3 | TMEM233 | ANXA10 | SHCBP1L | HOXB1 | LINC01085 |
| GMDS-AS1 | FBN1 | PCDHA10 | LINC01206 | LOC442497 | LOC101929099 |
| ADIPOQ | GRM7-AS2 | PRPF4 | LINC01204 | HIF1A | CIDEB |
| LINC01010 | RER1 | EFNA2 | CTCFL | KIAA0319L | LINC01082 |
| LOC101929241 | MAN1B1 | PI4KA | ATP5S | H3F3C | CCT6A |
| MFSD6L | LOC100507006 | MIR8069-1 | XRCC4 | FOXG1-AS1 | LINC01029 |
| CTAG2 | NYNRIN | MIR1825 | XRCC3 | H2AFY2 | TNNT2 |
| LOC101929282 | ZC2HC1B | COLEC11 | INTS12 | HIF3A | LINC01016 |
| TSPAN32 | NAIF1 | MKNK1-AS1 | LINC01151 | PDCD4-AS1 | LINC01017 |
| KCTD21 | TPRG1 | OPA1-AS1 | C5orf46 | NBPF13P | TOR4A |

| | | | | | |
|--------------|--------------|--------------|---------------|--------------|--------------|
| RANBP1 | MIR4424 | FBXW12 | LOC101927123 | MIR4499 | PADI4 |
| STEAP4 | MIR4427 | SPINK8 | LOC101927131 | MIR4494 | PADI6 |
| ARHGAP44 | MIR4422 | GRIP2 | ADCY4 | MIR3165 | MIR569 |
| BASP1 | TRIM63 | PCP4 | LOC101927142 | ACTRT1 | MIR577 |
| PDIA2 | MIR4418 | OR9Q1 | ARFRP1 | MIR4481 | MIR570 |
| ARHGAP19 | TRIM54 | LOC284080 | FGD6 | LOC102467226 | LOC101929413 |
| A2ML1 | TRIM52 | LOC100506127 | TPMT | PDPN | MIR587 |
| NMRAL1 | MIR1302-1 | CNTN5 | NDUFC2-KCTD10 | DRT15L2 | TRAM2-AS1 |
| ARHGAP23 | MIR1302-4 | CNTN6 | LOC101927166 | MIR3153 | LOC285629 |
| NPY6R | MIR1302-5 | CNTN1 | FGF7 | MIR4470 | LOC101929420 |
| MIR2909 | C16orf86 | CNTN2 | CSGALNACT1 | LOC102467212 | RAB11B-AS1 |
| OPRM1 | MIR1302-6 | TNFAIP3 | TMEM178B | LOC102467213 | LOC101928105 |
| CYP1B1-AS1 | TP63 | CYTIP | EDAR | LOC102467214 | ELOVL3 |
| LOC101929625 | GIN1 | LOC100507477 | ZNF793 | LOC102467217 | LOC101929439 |
| MIR30B | SLPI | SHROOM3 | DDX11L5 | TNKS2-AS1 | POU5F2 |
| MIR30A | TRIM15 | TCAF2P1 | LOC101927189 | MIR4478 | LOC101929448 |
| TEX40 | RIN3 | SHROOM4 | LOC101927190 | MIR3146 | LOC101929452 |
| TIPARP-AS1 | NACAP1 | LOC100507468 | SVILP1 | MIR3140 | LOC101929450 |
| MOV10L1 | MIR4325 | SUMO1P3 | CTDSPL | MIR4474 | LOC101928135 |
| LMCD1-AS1 | MIR4328 | EMC3-AS1 | MIR4532 | TCTEX1D4 | KPNA7 |
| BTBD19 | MIR4320 | SLC3A1 | MIR3201 | LOC100507334 | LOC101928140 |
| LOC101928322 | FER1L4 | LOC101929608 | DDC-AS1 | MIR3181 | UNQ6494 |
| MIR340 | SPHKAP | TTC13 | MFAP3 | MIR184 | BEAN1 |
| NANOG | MIR4311 | PRSS1 | MIR3139 | LOC100507351 | LOC101929488 |
| LOC101928333 | MIR4310 | WIPF1 | MIR4465 | LRRTM3 | SCGB2B3P |
| LOC101927023 | MIR4312 | NPIPB11 | MIR4460 | HLX-AS1 | SRD5A2 |
| MIR30C2 | OR9G1 | SLC4A5 | MIR3123 | LOC101929709 | LOC101928162 |
| RIC3 | ECM1 | EVA1A | MIR3122 | LOC101929717 | LOC102467655 |
| SNX17 | GRIK5 | GJA4 | MIR4450 | IQCG | ZNF658 |
| DPP10-AS1 | NMRK1 | RSPH6A | ZNF829 | IQCK | ZNF652 |
| LY6K | MIR4300HG | LOC101928435 | MIR4442 | ALDH1A2 | POMT2 |
| LOC101927053 | MIR4290HG | MIR205 | MIR4439 | DAW1 | WISP1 |
| LOC101928386 | MIR5691 | FAM171A1 | MIR4431 | MIR139 | WISP2 |
| LOC101927055 | SCARNA26A | GJC2 | MIR4430 | MIR145 | C2orf81 |
| LY6H | CYP8B1 | MIR211 | ZCCHC13 | ERVH48-1 | EVADR |
| PARD6G-AS1 | LOC100507406 | PLAC1 | C2CD3 | MIR554 | MIR6829 |
| IP6K3 | MIR5682 | LOC101928449 | MIR3173 | MIR556 | MIR6811 |
| RHPN1-AS1 | GRIP1 | LOC101929771 | VWA2 | SLC5A7 | ZNF721 |
| LOC101927087 | SPINK4 | LOC101928443 | MIR3169 | PADI3 | MIR6761 |

| | | | | | |
|---------------------|----------------------|------------------|-----------------------------------|-------------------------|--------------|
| MIR6757 | LOC100507175EDNRA | | ANAPC1P1 | LOC100506526MIR3653 | |
| LOC441601 | MIR455 | MIR6888 | LOC101927450MIR4798 | CXorf65 | |
| MIR6741 | CRACR2A | MIR6889 | LOC101928782NBPF20 | MAGEL2 | |
| DCTN1-AS1 | LOC101928201CA3-AS1 | | RPL13AP20 | MAP1LC3C | LOC284632 |
| LOC101241902SLC6A5 | | MIR6884 | LOC101927460DDR2 | | MIR605 |
| CHRD2 | LOC101928211JMJD6 | | AFMID | SNORD17 | TMEM132B |
| FER1L6-AS2 | SLC6A4 | WFDC11 | LOC101927472TBC1D30 | | MIR618 |
| ACADL | LOC101929541MIR6854 | | LOC101927481LOC101928708LOC644762 | | |
| TMEM150C | GLI2 | MIR5590 | MIR4802 | FAM71D | REEP2 |
| ACTN1-AS1 | LOC100507195MIR4269 | | SPP2 | ZNF33BP1 | REEP6 |
| MIR544B | RIPPLY2 | MIR4268 | ZNF469 | FAM71C | SNORD137 |
| | 4A-MIR7A2P1 | MIR4263 | POM121L4P | CAV3 | MIR3692 |
| FRMD8P1 | OCA2 | CLU1OS | MIR708 | CAV1 | CEBPA-AS1 |
| MIR6772 | LOC101929563MPPED1 | | CASC6 | IRAIN | GRTP1-AS1 |
| MIR6773 | LOC101928233MIR4254 | | OLFML2A | LOC101927406LURAP1L-AS1 | |
| VIPR1-AS1 | LOC101928241MIR5692B | | CASC1 | LOC101928738PECAM1 | |
| DUOXA2 | SULF1 | CACNA1C-AS2 | RBM5-AS1 | NAT8B | MIR3686 |
| CAPN3 | LOC101929577GLYCAM1 | | SPATA8 | LOC101927412MIR2355 | |
| SATL1 | POU4F1 | S100A7L2 | BRIX1 | LOC101927416MIR3681 | |
| MIR548Q | FIG4 | KRT78 | ODF4 | LOC283177 | RPEL1 |
| CCDC148 | MIR421 | MIR4297 | POM121L12 | TTI1 | NLRC3 |
| MIR548X | SARM1 | MIR4282 | ISY1 | NAV3 | NLRC4 |
| CCDC140 | FILIP1 | GPR158-AS1 | ELFN1 | SNORD46 | MIR3678 |
| LOC100507205SLC28A2 | | COBLL1 | ZNF408 | LOC101927421MIR3672 | |
| TREH | CSF3R | MIR4289 | PGM3 | LOC101928896MIR365B | |
| ZNF385D | ZNF559 | MIR4288 | UGT2A3 | LOC101927560MIR4999 | |
| LOC285593 | LOC101928273MIR4284 | | UGT2A1 | DDX11 | MIR3664 |
| NHEG1 | SKINTL | MIR4287 | SPTB | LOC101927571MIR3660 | |
| LOC440311 | SLC15A3 | MIR4270 | ITGAD | LOC101927592CBLC | |
| DBX1 | SLC15A5 | MIR4272 | SPATC1 | DEAR | MAGEA9 |
| MIR492 | STX18-IT1 | MIR4276 | ITGA8 | LYPLAL1-AS1 | METT11 |
| CCDC185 | HOPX | MIR4275 | UGT2B7 | MIR629 | MIR2278 |
| CCDC182 | ZNF536 | MIR34A | CFAP58-AS1 | ABCC12 | LOC100506403 |
| CCDC179 | EFHB | KRT82 | LOC728730 | MIR3616 | HNCAT21 |
| CREB3L3 | KIAA1671 | KRT85 | MIR4771-2 | KIAA1024 | SLC22A16 |
| MS4A15 | LOC101928298CMTM3 | | CYP4B1 | MIR635 | SLC22A11 |
| LOC100507144MIR4302 | | LOC153910 | CAHM | MIR634 | DCST1 |
| PIH1D3 | BACH1-IT2 | MIR383 | UNC93A | MIR645 | GPBP1L1 |
| LOC101929529SKOR1 | | LOC101928778NAIP | | ABI3BP | UBL4B |

| | | | | |
|-----------------------|-------------------------------|----------------------|--------------|--------------|
| NBR2 | LOC101927285GPC6 | MIR4743 | PTCHD3 | |
| HILS1 | F13A1 | LOC102723831ARMCX4 | PTCHD4 | |
| IGSF11-AS1 | MIR944 | CD69 | MIR4735 | LOC100506207 |
| LOC101928812TPRG1-AS2 | GSN-AS1 | JMJD1C-AS1 | GDF10 | |
| H1FOO | C9orf92 | EP300 | MIR4725 | POU6F2-AS1 |
| CHMP4A | C9orf62 | LOC100132057UGT3A2 | AXL | |
| LOC101928834NCK1 | OSCAR | MIR4720 | MIR2053 | |
| NLRP8 | ATP11A-AS1 | SH3PXD2A-AS1DSCR8 | LOC102467080 | |
| NLRP1 | SLCO1B7 | GUCY2EP | LOC729987 | NUP50-AS1 |
| GAS2L2 | MIR4655 | RASGRP2 | SSX8 | OR5AC2 |
| LOC100133050LOC645752 | SIRPB2 | MIR4708 | APLNR | |
| LOC101927523MIR4651 | A4GALT | MIR4715 | HDGFL1 | |
| LOC101927526MIR4654 | DDX53 | MIR4713 | ABCG2 | |
| YBX2 | NDUFB9 | TMIGD1 | ALK | PPP4R1L |
| MIR592 | MIR4644 | NDUFS1 | C16orf47 | PLCXD3 |
| CASP4 | MIR4643 | DDX25 | MIR4789 | MIR95 |
| VWC2L | MIR938 | LOC101928516MIR4786 | FAM60A | |
| LOC440446 | MIR933 | ATP6V1B1-AS1 TRAF2 | RMND5A | |
| LOC283299 | C9orf57 | GNAT1 | TRAF1 | ZNF189 |
| LOC100506497SNORD45A | DAPK1 | LOC729970 | THSD4-AS2 | |
| SND1-IT1 | C9orf24 | LOC101927359MIR4777 | THSD4-AS1 | |
| LOC101928539IL12A | LOC101927354MIR2117 | LOC101927311 | | |
| CCDC148-AS1 | ZNF436-AS1 | GPN3 | MIR4774 | |
| RBFOX3 | LOC102723854LOC101928694LUZP6 | | | |
| EID3 | LRRN4 | MIR874 | CLEC3A | |
| ZNF277 | CD28 | MIR4703 | CLEC3B | |
| ABCB4 | CD22 | LOC101927379MIR4766 | | |
| ABCB5 | DIRAS3 | 5NMIR4767 | | |
| LOC100132111CCR8 | SCARNA18 | | 4-Sep | |
| LOC101927244CCR7 | LOC101927391MIR4762 | | | |
| LOC283440 | CD36 | RPS3 | MGAT4C | |
| LOC101927243CCR2 | GPR1 | CLEC2B | | |
| CLUL1 | CD53 | FMO1 | MIR4755 | |
| LOC101927257RTCA-AS1 | FMO4 | ABCC5-AS1 | | |
| LRRD1 | GLCCI1 | SCARNA27 | FAM65B | |
| FOXCUT | MKRN9P | LHX4-AS1 | STAM | |
| FABP3 | KIF25-AS1 | FMOD | MIR4676 | |
| KCCAT333 | GPC3 | CDH6 | FAM69C | |
| NCF4 | LOC102723828CDH5 | VLDLR | | |

| | | | | | |
|-------------------|---------------|----------------|----------|--------------|--------------|
| ASH2L only | PARP3 | KPTN | SNORD104 | KRT16P33 | SNAR-A6 |
| (416) | NOL8 | DNAJC27 | KRTCAP2 | KRT16P34 | FAM171B |
| BLM | TMEM9B-AS1 | FRMD6-AS1 | ABCA2 | KRT16P35 | LRWD1 |
| DRAP1 | AKT1S1 | SGSH | PIGG | KRT16P36 | MIR6087 |
| TAX1BP3 | WBP11 | SH3YL1 | C9orf85 | KRT16P37 | PKI55 |
| VPS35 | RBM18 | SMPD4 | ZNF174 | KRT16P38 | GPR150 |
| C1orf109 | PREPL | NUDT2 | ZNF143 | KRT16P39 | ABHD8 |
| C6orf52 | UGDH | KCTD10 | TIGD7 | KRT16P40 | CHRD |
| GBAT2 | FAM161B | UBE2M | GPATCH11 | KRT16P41 | PPIAL4F |
| TYW3 | HAGLR | YTHDF3 | PHOSPHO2 | KRT16P42 | FAM27L |
| SNORA57 | HIF1A-AS1 | OTUD6B-AS1 | KRT16P4 | KRT16P43 | RNF32 |
| SNORA7A | PSMA7 | FTSJ2 | KRT16P5 | KRT16P44 | OVOL1 |
| PSMD5-AS1 | AASDHPPT | RASAL2-AS1 | KRT16P6 | KRT16P45 | FRG2 |
| PCSK7 | ATG9A | RQCD1 | KRT16P7 | KRT16P46 | RELL2 |
| MRPS7 | TEN1 | DPY19L3 | KRT16P8 | KRT16P47 | NFKBIB |
| CHFR | RIC8B | PRR19 | KRT16P9 | KRT16P48 | HSPB3 |
| STRN3 | MORN2 | SKA2 | KRT16P10 | KRT16P49 | POLN |
| LOC101927795 | KLC4 | HOXC5 | KRT16P11 | KRT16P50 | SYS1 |
| ACP2 | NACC1 | METTL18 | KRT16P12 | FBXO18 | SNORA11E |
| CDC37 | USP46 | TGIF2-C20orf24 | KRT16P13 | IGF1R | LDB2 |
| ERMARD | SCO2 | ALKBH6 | KRT16P14 | DIAPH2-AS1 | TIMP4 |
| TIMM9 | DZIP3 | GID8 | KRT16P15 | GRM3 | SOCS2-AS1 |
| NIFK-AS1 | KRIT1 | NCAPD2 | KRT16P16 | REREP3 | GPNMB |
| RPRD1B | SDF4 | ZNF891 | KRT16P17 | SSTR5-AS1 | RPL10A |
| ILK | SDF2 | SMC5 | KRT16P18 | HECW1 | MIR663B |
| GTF2H1 | DKFZP434I0714 | LOC101928438 | KRT16P19 | ST3GAL3 | ESCO2 |
| GTF2F1 | RNASEH1 | PAAF1 | KRT16P20 | DGUOK-AS1 | LEF1 |
| C17orf89 | CAPN15 | PPHLN1 | KRT16P21 | LOC401324 | CKS2 |
| RAD51 | PRDM10 | RIPK2 | KRT16P22 | LOC102723769 | SH2D7 |
| CMC2 | GATC | ELOVL2 | KRT16P23 | FAM47E | HIST2H4B |
| PSMB8-AS1 | HIST1H2BG | MIR6733 | KRT16P24 | FPGT | LOC388436 |
| IFT122 | HELQ | CCDC122 | KRT16P25 | SPECC1L | C14orf180 |
| SRSF9 | ST7-OT4 | CCDC189 | KRT16P26 | DBI | TTY23B |
| MIR1184-2 | CAPN10 | ZNF271P | KRT16P27 | PRKAR1B | MIR3914-1 |
| MKKS | RAB11FIP2 | NUDT16 | KRT16P28 | DPY19L1P2 | ESX1 |
| YY1AP1 | ZBED5 | HPS4 | KRT16P29 | PCSK2 | MAMDC2 |
| CIRBP-AS1 | THYN1 | MIPEP | KRT16P30 | SNAR-C2 | LINC00960 |
| WDR54 | ERP44 | ITGA3 | KRT16P31 | MRPS9 | LINC00999 |
| COG8 | STAG2 | QRSL1 | KRT16P32 | SNAR-A3 | LOC100129520 |

| | | | | |
|---------------|----------------|----------------|--------------|----------------|
| TMEM63B | EEF1E1 | ARL2 | TRIM48 | RNMT |
| MTRNR2L9 | RPL36A-HNRNPW1 | WTR1 | LOC101927100 | SERF1A |
| HAVCR1P1 | ALPI | DHX29 | STT3A-AS1 | MIR607 |
| PRDM5 | CEP76 | LINC00293 | LOC101928495 | MIR3621 |
| ZNF670-ZNF695 | GNPTG | DEFB115 | DAB1 | MIR3680-2 |
| FAM122B | GABRA2 | LINC00207 | MIR4528 | LHFPL3 |
| BLOC1S5 | CCDC47 | TRMT44 | MFAP1 | BMPR1B |
| FAM126B | NPIPA7 | CORO7 | STXBP4 | LOC101928851 |
| PHACTR3 | CCDC58 | TMEM138 | PDCD11 | THBS2 |
| DNAJC4 | NPIP3 | ATP6V1D | ZNF816 | PID1 |
| PARVB | ISPD-AS1 | GDNF | ZCCHC17 | TAPBPL |
| ATP5J2-PTCD1 | PTN | POLDIP2 | MIR198 | LOC101927237 |
| GDPD3 | KLHDC3 | SGTA | LGALS8-AS1 | DFFB |
| CD40LG | ALDH16A1 | TMEM234 | MKRN2OS | PIGB |
| STARD4 | LOC650226 | XPC | MIR3191 | ZNF214 |
| NELFE | MRPL32 | PCDHA2 | LOC285696 | ZBTB25 |
| MYLK3 | RBPJL | LL22NC03-75H11 | MIR588 | DDX54 |
| SLC25A40 | KIF20A | TXNL4B | IFNG-AS1 | NDUFS8 |
| RBM14-RBM4 | DCLRE1B | SCRN3 | SLC16A1 | NDUFS6 |
| NPC2 | OSTF1 | FOXD4L1 | FNDC5 | LOC100133331 |
| NEGR1-IT1 | BUD31 | ANGPT1 | ZNF716 | LCE3A |
| FKBP1A | TCF24 | SHISA8 | LOC440300 | CDK4 |
| LOXL1-AS1 | ANKRD26P1 | H2AFJ | CCDC121 | AMN |
| NPR1 | RHO | LINC01232 | CCDC137 | SPAG5 |
| RAB4B-EGLN2 | CACNG1 | LINC01203 | KIAA0391 | TP53TG3B |
| MUT | HRAT92 | LYSMD1 | FIBP | MIR4283-2 |
| WNT10A | HTR7P1 | TTY3B | MIR423 | MIR4674 |
| PRDX6 | MCPH1 | PAX1 | MIR4300 | C7orf55-LUC7L2 |
| GCOM1 | USP20 | FZD10-AS1 | JMJD4 | |
| PMF1-BGLAP | DDIT3 | PPAN-P2RY11 | JMJD8 | |
| TIPARP | MSH3 | SLX1A-SULT1A3 | MIR4265 | |
| ARHGAP1 | TGM2 | GOLT1B | PACRG | |
| KHDRBS2 | LINC01346 | MOSPD2 | PSMA3-AS1 | |
| C14orf39 | LINC01340 | DUXAP10 | NUDT21 | |
| LRTOMT | LINC01356 | TEX41 | MAP1LC3B | |
| LINC00564 | TENM4 | FGFR1OP2 | TBC1D3H | |
| LOC102606465 | HIST1H2BB | LOC101929646 | LOC100506585 | |
| ALG5 | RBMXL1 | PABPC5-AS1 | RSPH9 | |
| ALG2 | PFKFB2 | LOC101929681 | MIR663AHG | |

APPENDIX E. Gene Lists and ToppFun Analysis: promoter only H3K4me3 ChIP-seq peaks.

Output lists from MACS2 ChIP-seq analysis Venn Diagrams comparing LacZ and ASH2L promoter peaks only gene lists appear in this appendix. These lists correspond to **Figure 3.3-A**. ToppFun analysis for the 2,035 LacZ only genes can be found at this link: https://toppgene.cchmc.org/output.jsp?userdata_id=dade9860-36b3-4a1b-b16f-e3507b08ff76.

| | | | | | |
|-------------------------|--------------|---------------|---------------|--------------|--------------|
| <u>LacZ only</u> | ITGB8 | TYMP | ATG14 | SNORA71D | DXO |
| <u>(2,035)</u> | SAP30L | LOC654841 | CDK19 | SDHA | BZW2 |
| MIR760 | RBL2 | BBS9 | FTSJ2 | DNAH7 | AZIN1 |
| DDHD2 | EXOC3 | MIR378A | TADA3 | POLD2 | METTL21A |
| LSM1 | CCNE2 | SMG7 | TMEM127 | STK16 | PLCG1-AS1 |
| ASH2L | RELL2 | CCT7 | RABL2A | ZHX2 | GNAI1 |
| ITGB1BP1 | HADHA | NEURL2 | GLI3 | NUDT1 | MORN2 |
| FGFR1 | MIR4757 | UPP1 | NFS1 | TRAF3IP2-AS1 | RABL2B |
| WHSC1L1 | KHK | EFNA5 | DES1 | MIR4651 | ANKS1A |
| TMEM56- | EPB41L4A | SNX3 | SBDSP1 | SRD5A1 | ZNF655 |
| RWDD3 | LINC00472 | ARPC1A | ADGRF3 | TRIAP1 | TBC1D22A |
| BRE | ERO1B | CBY1 | LOC100506127 | DOCK4 | NSL1 |
| SUPT7L | LOC653602 | ZDHHC14 | STRADB | ST5 | TIGD6 |
| ZNF79 | DYNLRB1 | RPS21 | HIVEP2 | PARD3B | RB1CC1 |
| GEN1 | PGM3 | ABHD1 | MBOAT2 | LRRC73 | UNC50 |
| ALG8 | LRWD1 | ZFAND2A | Sep7 | TAP1 | LRRC16A |
| DNAJC27 | ATP6V0E2-AS1 | ZNF496 | TTC31 | FAF2 | FAHD2A |
| AGBL5 | SSH3 | SLX1A-SULT1A3 | DKFZP434I0714 | AK9 | EIF1B-AS1 |
| LOC728024 | CENPO | SHARPIN | LOC100996437 | ARFRP1 | PLPP1 |
| AGBL5-AS1 | TNRC18 | MAF1 | BTBD9 | SATB2 | TBCC |
| CCDC121 | SF3B6 | PRKAG2-AS1 | ZNF786 | SERAC1 | ZFP36L2 |
| LOC102723729 | NIFK-AS1 | DNTTIP1 | COA4 | DHX57 | TSGA10 |
| FAM228B | MTRR | LOC154761 | PCIF1 | CRNDE | ZNF142 |
| MYCNOS | IRX5 | MPLKIP | AP5Z1 | MDH2 | EPB41L1 |
| CPSF3 | TTC21A | AMMECR1L | RING1 | ERCC3 | PPP1R21 |
| ADAM9 | SCAMP1-AS1 | ZDHHC3 | ZNF346 | PCOLCE-AS1 | ZNF277 |
| GPN1 | LOC101928222 | ZNF860 | POLR3F | TCAF2 | PHF3 |
| SNX17 | SFT2D1 | FOXO3 | PAX8-AS1 | C6ORF120 | TMEM237 |
| DNAJC27-AS1 | GRM8 | NLN | ASB3 | ACVR2B-AS1 | ZFP2 |
| WDR35 | TPST1 | LZTS3 | ZNF398 | SMPD4 | UXS1 |
| PRR3 | CDPF1 | RNASET2 | CPSF2 | MAVS | C22ORF23 |
| KLHL7 | NANP | PLEKHA2 | CYP51A1 | HCG17 | POP1 |
| PITPNM1 | RBM33 | DEPDC1B | SGMS1 | SMPD2 | LOC100505771 |

| | | | | | |
|--------------------|------------|--------------|--------------|-----------|-------------|
| PLOD3 | AUP1 | E2F3 | AP4M1 | NSMAF | EFHC1 |
| PSMA2 | MCM7 | LOC100289230 | SNORA71E | DZANK1 | MNX1 |
| FAHD2B | EAF1 | FAM134A | IFT43 | PHF14 | MRPL36 |
| HEY2 | SNORA3A | RAB23 | PLAG1 | COL4A3BP | TUBA4A |
| ZNF250 | COL4A4 | NSMCE2 | RPL15 | AHI1 | COP55 |
| KIAA0196 | SUCLG1 | MFSD14A | ATG9A | MTBP | TOMM6 |
| OSTM1 | DNAJC30 | MOGS | MLLT4 | RAB22A | KIAA0141 |
| PSEN2 | CHKB-CPT1B | TIGD1 | PGAP1 | C5ORF15 | SNORA9 |
| STRIP2 | TMEM60 | NCOA7 | BRD9 | ZBTB49 | LINC01024 |
| RSBN1L | LMBRD2 | MRPL32 | MOSPD3 | C2ORF68 | TUBB2A |
| SPATA2 | PNKD | PIGF | RIPK2 | TTI1 | POLR1C |
| STK36 | CHRA1 | BUD31 | SGK1 | ARPC2 | CIR1 |
| WDPCP | AZI2 | TYW5 | FZD5 | LYPD6 | FOXP4-AS1 |
| TMEM43 | CEBPB-AS1 | RPRD1B | URGCP | TP53I3 | ST3GAL5-AS1 |
| ZNF664- FAM101A | RTKN | TMEM170B | ALKBH4 | PDE10A | SLC35B4 |
| ZNF292 | TTC30B | ST3GAL1 | RBSN | BRD2 | PPIC |
| CPSF4 | FBXO32 | ATXN1 | FIGN | C14ORF178 | C2ORF76 |
| FBXL6 | PRR15 | LHX4 | LOC100288181 | SUCLG2 | TMEM198 |
| TMEM243 | CEP68 | ZNF141 | VPS50 | EIF6 | ROPN1L-AS1 |
| SLF1 | MTHFD1L | C20ORF27 | ALG12 | PDAP1 | SLC25A46 |
| PRKCE | C8ORF33 | GMDS-AS1 | XRCC6 | COPS6 | LOC150776 |
| ING2 | GLI4 | MFSD9 | DDX11 | FAM120B | EIF3B |
| SLC12A9 | NOL7 | NCAPG2 | CNOT8 | AP3B1 | FOXN2 |
| KCTD13 | FLJ38576 | PLEKHA8 | CHCHD7 | GFOD1 | IRAK1BP1 |
| NOD1 | EFCAB6 | MBLAC1 | IFT22 | BYSL | FRMD6 |
| UGP2 | FAHD2CP | TMEM129 | PCED1A | EIF5B | STK4 |
| DARS-AS1 | TBPL1 | PPP3CA | SNHG15 | HIP1 | LIPT1 |
| SNX13 | SAP130 | PFDN6 | ABLIM2 | KIZ | MIA3 |
| LINC01124 | HSF1 | SCO2 | APLF | UGDH-AS1 | IKBKB |
| ICA1L | MKLN1 | NDUFAF2 | ZNF622 | METTL1 | ERBB2IP |
| RNF4 | EGR1 | ZNF7 | PSMG3 | ZBTB9 | FGFR10P |
| ANAPC1 | FBXW7 | RMND5B | STAG3L1 | CDK11B | CACNA2D1 |
| CRNKL1 | PSMB8 | OSBPL8 | QRSL1 | AP4S1 | NUP50-AS1 |
| CDK6 | CLCN7 | WDYHV1 | FKBP14 | ZRANB3 | RPIA |
| GDF9 | ZNF623 | LOC100288152 | NIPBL | GABBR1 | MRPS27 |
| FER | SP4 | RAE1 | RASA1 | CCNG2 | THOC7 |
| TRIM36 | SPAG1 | CCDC146 | GAK | ATRAID | RAET1K |
| ZNF252P C2 | ETF1 | RGS2 | RMDN2 | PRIM2 | ANKRA2 |
| MBLAC2 | FAM114A2 | THEM6 | PSMB8-AS1 | STAG3L2 | SBDS |
| | TMPPE | ARHGEF5 | NDUFS6 | ABRA1 | HSPA4 |
| | COPG2 | SOX12 | PEX1 | TRIM52 | DBNDD2 |

| | | | | | |
|----------|--------------|---------|-----------|------------|--------------|
| FASTK | CIDCEP | ARL6IP6 | ARL15 | CUX1 | MAT2A |
| EPHA4 | LIFR-AS1 | CCDC115 | KIAA1841 | MAFF | SMIM15 |
| SMAD1 | EDEM2 | TMEM192 | PCYOX1L | MTX3 | KLF10 |
| BLCAP | HDAC3 | OTULIN | BRIX1 | BARD1 | COX5B |
| SMAP1 | MAPK3 | NOP14 | MIR7111 | SUPT3H | MRPL33 |
| OGFRP1 | HEATR5B | LTV1 | ZNF775 | GPANK1 | LRRC14 |
| ANKIB1 | TAX1BP1 | IFRD1 | PPP1R12A | CARF | HARS |
| CUL9 | IRS1 | UFSP1 | DPM1 | PANK2 | ARHGEF35 |
| WDFY3 | PRKAG1 | PDCD2 | CTDSP1 | CASP8AP2 | SLC12A2 |
| ARMC10 | HIST2H2AA3 | NEMP2 | TLK1 | ST3GAL5 | CHPF |
| CLASP1 | ASCC3 | RPS6KA2 | GID8 | CEP55 | ZBED5-AS1 |
| NXT1 | SPRY1 | ZNRD1 | NFYA | BTBD3 | CLHC1 |
| GNPDA1 | LOC100129518 | RFC2 | AFAP1 | ACAA1 | LINC01117 |
| DLL1 | PNO1 | COBLL1 | FBXO48 | GNMT | PPIL3 |
| ACTA2 | LTBP1 | MOB4 | CDK5RAP1 | INHBB | YWHAZ |
| RETSAT | IL15 | ABHD18 | SEMA4F | FAM161A | TTL |
| ALDH6A1 | LNPEP | PLEC | R3HDM1 | PUS1 | ANKHD1 |
| CSE1L | ZSWIM6 | LRRC61 | HTT-AS | ESRP1 | STK32B |
| C5ORF22 | ZNF343 | RPS27A | C2ORF81 | ETV1 | ZNF721 |
| EIF2AK3 | CCT6P1 | SEC61G | KIAA0825 | RALY | FAM184A |
| AKAP9 | RPP40 | NOP16 | HIST1H4A | MITF | WDR75 |
| HOMER1 | RPL26L1 | JADE2 | ZNF75A | ASAP1 | TMEM230 |
| ATG10 | PDSS2 | FBXO4 | LRRC6 | POMZP3 | MRPS30 |
| NIF3L1 | RDH10 | FOXP4 | USP46-AS1 | HOXC13-AS | CFAP36 |
| CDC40 | MIR6850 | PDGFA | TAF2 | SNRPE | SREK1IP1 |
| GVQW2 | LOC100129917 | FAM126B | WDR54 | LMBR1 | NCAPH2 |
| KRIT1 | ITPA | EIF3L | OR2A1-AS1 | ERCC8 | ZC3H3 |
| ZNF76 | MRPL14 | BAG6 | ATF6B | LINC01184 | NSA2 |
| C4ORF46 | GTSE1 | DDR1 | CCDC109B | PAIP2 | C8ORF37 |
| TSEN2 | LYAR | SELO | WDR46 | TSTA3 | PPID |
| PUF60 | NRF1 | NUDT6 | MZT2B | ZRSR2 | RAB24 |
| EPC2 | LOC101927795 | ICA1 | NDUFA6 | SYNCRIP | CCT6A |
| TMEM177 | STXBP5 | ZNF706 | TPD52L2 | NTPCR | LOC101928530 |
| CENPM | CEBPZ | DHX35 | GGCX | EMC3-AS1 | TECPR1 |
| ZSCAN32 | RQCD1 | UGDH | KIAA1715 | CITED2 | NUP50 |
| TMEM217 | RNF181 | MIR933 | KCND3 | NR3C2 | PSMB1 |
| CNPPD1 | VPS13B | DHX29 | SLC38A9 | TRERF1 | SKIV2L |
| FGD5-AS1 | TMEM9B | CWC27 | BRD1 | PAXIP1-AS1 | PDE5A |
| PGM2 | SIRT5 | MED7 | PCNA-AS1 | PTDSS1 | PLCB4 |
| HSPA4L | ZNF696 | PAK1IP1 | ANXA4 | DIMT1 | THUMPD3 |
| VPS13C | TCP1 | NDUFA2 | GDE1 | AFTPH | GALK2 |

| | | | | | |
|--------------|--------------|--------------|--------------|--------------|--------------|
| C5ORF45 | SNW1 | LOC728743 | GPATCH11 | PHOSPHO2 | HIST1H2BN |
| SHPRH | KLHL8 | TTK | LOC101927157 | ZSCAN31 | SEMA4C |
| RBPJ | FAM229B | C1ORF112 | DCAF17 | PPT2-EGFL8 | LINC01012 |
| GINM1 | MRPL51 | CLPTM1L | DDX41 | TDG | HMGCR |
| XRCC4 | PRPF6 | DIDO1 | WASF1 | MCFD2 | SERPINB6 |
| STMND1 | NR4A2 | CCT5 | UMAD1 | PLCL1 | RAP1GDS1 |
| CKMT2-AS1 | SPAG16 | SLC25A27 | IRF5 | LOXL3 | HNRNPDL |
| PIGG | BCAP29 | MRPS7 | LOC100294362 | ORC4 | TRIQK |
| LOC100132356 | KLHDC3 | NDUFB3 | LOC344967 | BLOC1S1 | DYNC1L11 |
| LINC01003 | RAD52 | RAD17 | APBB3 | SLX4IP | GGT7 |
| AUTS2 | EIF4E | TDP2 | INTS1 | LZTFL1 | ST13 |
| CHAC2 | TRIP6 | SLC35B3 | LRRC1 | CHSY3 | DUS4L |
| TNPO1 | CENPH | ZNF619 | SLC16A1 | EP300-AS1 | NDUFB9 |
| DENND3 | HELZ | HRSP12 | MROH1 | C9ORF78 | WTAP |
| WDR60 | CCDC88A | PPP4R3B | EMC3 | HIF1A | CROT |
| BRI3 | MCM8 | GTF2IRD1P1 | TTC23L | MTMR12 | ITPR1 |
| MUT | ATL2 | ATP5I | FOXQ1 | VWA3B | USP39 |
| RNF103-CHMP3 | TRAPPC13 | KIF20A | LOC100133669 | MEA1 | CDKN2AIP |
| CDS2 | PYGB | LOC101929710 | CNOT6L | PDP1 | CAMKMT |
| RARS2 | AIG1 | AVL9 | FAM151B | PRELID2 | WBSCR27 |
| PREPL | CLOCK | THADA | CXCR4 | EPHB6 | OTX1 |
| ORC2 | RRM2B | ZSCAN16-AS1 | RTN1 | B3GALT6 | NUDCD1 |
| CTC-338M12.4 | SLC18B1 | LSM3 | ZNF815P | INSIG1 | UBE2B |
| OXNAD1 | CTSO | CASP3 | RWDD4 | PREX1 | TFAP2A |
| JRK | LOC100287944 | ARFIP1 | ZNF789 | HELQ | BMP2K |
| RTN4 | RBM48 | PYGO2 | LYRM4 | WDSUB1 | TMED2 |
| GSS | TAB2 | PLCD1 | CARD10 | RTN4IP1 | BOLA3 |
| NAPRT | RPL23AP7 | MEIS1 | ADSL | ZNF584 | LINC00899 |
| C6ORF52 | TNPO3 | FBXO5 | RNF139-AS1 | TGFA | NOA1 |
| FAM160A1 | NDUFS1 | FAM86EP | PRMT3 | HLA-H | PTPRA |
| AKR7A2 | SOWAHC | TP53TG1 | CPSF3L | SESN1 | FAM47E-STBD1 |
| NRN1 | STK19 | LRP12 | C6ORF226 | SLC4A11 | KRBA1 |
| TOP1MT | NCAPH | LOC100505921 | TPMT | RNF123 | DOPEY1 |
| ZNF131 | ZNF2 | LETM1 | SKP2 | ATP13A2 | MRPL2 |
| CNPY4 | GZF1 | CYP4V2 | FANCD2 | PTPN18 | SAMD10 |
| MIR4469 | ABALON | RGMB-AS1 | TRIM41 | FARS2 | DCK |
| DPY19L4 | YIPF3 | TRAM2 | ADA | KMT2E-AS1 | PLK4 |
| HNRNPA2B1 | GPR155 | RNGTT | WAPL | HCFC1 | PRKRA |
| KLC4 | KIF15 | MDH1B | AK6 | GATA2-AS1 | PLEKHN1 |
| NDRG1 | ERMARD | DENND6B | C9ORF9 | TMEM161B-AS1 | JADE1 |
| FAM86DP | POLH | RPS23 | LOC221946 | | PRICKLE4 |

| | | | | | |
|--------------|--------------|------------|--------------|-----------|--------------|
| SMARCAL1 | NAA15 | SLC25A40 | ICE1 | CFAP221 | SLC1A5 |
| HIST1H2BD | TTC37 | SCOC | USP37 | CLIC1 | FGFR4 |
| ST7-OT4 | ZC3H14 | ACVR1C | SLBP | RANBP3 | SYS1-DBNDD2 |
| TMEM161B | BTD | JARID2-AS1 | MDGA1 | TBC1D14 | LIPA |
| LOC101929709 | TRAPPC9 | MED25 | DLX2-AS1 | COPG1 | METAP2 |
| SLC10A7 | LCA5 | SNORA13 | HDAC11-AS1 | USP49 | DAP3 |
| MCEE | SLC17A5 | TMEM30A | FAXC | FAM86HP | TGFBRAP1 |
| TST | ENPP4 | MKL1 | NPHP1 | PSRC1 | LSM5 |
| TCTE3 | STX11 | YTHDF3-AS1 | PTGES2 | ZNF10 | CTDSPL |
| PMS2P1 | RPF2 | MRPL9 | EHBP1 | MMAA | LOC153684 |
| LOC101926913 | RBM24 | C1ORF159 | EMC6 | FLOT1 | STX18 |
| STAG3L4 | FAM135A | PPWD1 | NR1D2 | ZNF382 | MRPS2 |
| KCNK12 | IQGAP2 | COQ6 | ZKSCAN8 | AIMP2 | MOCS2 |
| LYRM2 | SIX2 | TMEM67 | MIR3661 | EXD3 | C20ORF194 |
| UBE2D3 | LRRFIP2 | HGS | HMGB2 | KCTD7 | CDC25C |
| FIS1 | GSTCD | IRAIN | ACVR1B | MIR6791 | ADD1 |
| FBXO30 | ACOT8 | TFAP2A-AS1 | COMMD1 | PHF10 | KIAA1429 |
| PSMA7 | CEP250 | HM13-AS1 | BAG2 | NDUFA12 | FUBP3 |
| PCBP1-AS1 | RASA4 | NPY5R | DBN1 | PSMG2 | YIPF5 |
| LSM14B | OTUD6B-AS1 | ZNF709 | BIN1 | HSPD1 | LYRM4-AS1 |
| MFAP3L | TMEM128 | MROH8 | GPSM3 | TRAPPC11 | SLC25A32 |
| TMCO6 | ACTR3 | SCRIB | RHPN1-AS1 | PLOD1 | CCDC74A |
| PSMG3-AS1 | NEMP1 | WWC2 | FAM86B1 | C19ORF52 | RBM42 |
| NDUFAF5 | ANKZF1 | GTF2I | AKAP7 | RPS12 | BRD8 |
| CCDC136 | CRLS1 | SAFB | TFB1M | CFLAR | TMEM203 |
| TAF6 | PXT1 | CEP44 | CDC37 | NAGA | YTHDF3 |
| PSIP1 | TSNARE1 | GGA3 | RGS19 | DAXX | KIAA0319 |
| MACROD2 | UFL1 | SNORA17A | PPIP5K2 | PAICS | FBXL20 |
| ZNF596 | DMC1 | LOC553103 | PMS1 | METAP1D | C12ORF60 |
| GALNT10 | MOB1B | CD3EAP | ITGA9-AS1 | MIR4792 | UBE2C |
| STAM | LOC101929231 | DBF4 | MIR6821 | LOC731157 | KLHL18 |
| ARHGEF18 | ITPR1-AS1 | GHR | MIR6875 | PARK2 | C5ORF56 |
| TRMT11 | CTNND2 | RAVER1 | HIST1H2BK | NEU1 | FGD6 |
| TBC1D32 | LOC100652758 | PASK | POLR1A | SLC30A6 | LOC100287015 |
| SNORD54 | IRX2 | DTX3 | ADAT2 | ATXN7L1 | TAF9 |
| RRP8 | SLCO4A1 | BFSP1 | PDCD6 | PMEP1A | CCNT2 |
| RPL7L1 | HEXA | PRRT3-AS1 | SDCCAG3 | LRPAP1 | NELFB |
| CHMP4C | MTA3 | ARF4 | STRN | USP20 | REPIN1 |
| POLR2H | MPST | MAU2 | STK25 | NUP188 | KCNIP3 |
| PLEKHA3 | MIR6892 | GGA1 | LOC101926935 | FAM53A | NR2C2 |
| NCK2 | GTF2F1 | C17ORF80 | THAP5 | ACBD4 | TXLNG |

| | | | | | |
|-------------|--------------|--------------|-----------|------------|------------|
| TEX10 | JAKMIP1 | ZNF561-AS1 | SMARCE1 | DNAJC28 | KCNK15-AS1 |
| PRPF31 | TSG101 | PAQR8 | CELSR1 | RFX3 | RECQL4 |
| EZH2 | NABP1 | NUS1 | CEP76 | ZNF230 | MRPL12 |
| SLC30A4 | NBEAL1 | NUDT4P1 | ORMDL1 | C17ORF89 | PTMA |
| ZNF8 | HIST2H4B | LOC102723824 | THCAT158 | ERF | C18ORF54 |
| RASA4B | H1FX-AS1 | STARD7-AS1 | GLT8D1 | SMARCD3 | NEK1 |
| CDK16 | GNPDA2 | TUBB | PRPF4 | ZNF567 | GLYCTK |
| FAAP100 | CLDN4 | SMC1A | LRCH4 | COPS7B | UBE2G2 |
| ST7-AS1 | TATDN1 | FAM86B3P | FST | SNORD52 | ANO10 |
| SIGMAR1 | WNT7B | RPL7A | ZNF470 | ELOVL2-AS1 | ZNF239 |
| SERINC1 | SCARNA13 | NAT14 | MBTD1 | ABT1 | SEC14L1 |
| SEC22C | HIST1H2AG | ARHGEF16 | FAM134C | CISD2 | LOC284930 |
| PCDH7 | SGCE | AGPAT1 | ZNF790 | COQ4 | HIST1H2BG |
| SGOL1 | FAM86B2 | SDCBP2 | FAM86JP | POLRMT | ZSCAN26 |
| MAP3K14-AS1 | AP5S1 | NUFIP1 | ASPH | MKKS | ZBTB12 |
| SNORD84 | SUGP2 | MRGBP | KIAA1958 | RAI14 | ZNF717 |
| CAPN7 | LOC100507053 | GPAT3 | RBBP8 | SUCO | PNPLA6 |
| STIM2 | TGS1 | GMPPA | BOD1L1 | NDUFA8 | TPRKB |
| INSIG2 | TTLL12 | PEX26 | BZW1 | CSTF1 | XRCC2 |
| PCBP1 | NOXA1 | FAM110A | MYADM | SNX5 | FAM210A |
| MAP4K4 | MFSD10 | MAD2L1 | SNTA1 | HBP1 | TM7SF2 |
| FBXO38 | LINC00602 | ACAD8 | MMP16 | PPM1L | CERK |
| SIPA1L3 | EXTL3 | SPPL2B | ANKRD31 | HMGNA4 | ZNF594 |
| ZYX | RRM1 | PNISR | SYS1 | TAF4B | PLIN2 |
| GABPB1 | APBB2 | COQ5 | SRRD | PEX13 | TEF |
| TMEM167A | MANEA-AS1 | MTIF2 | TFEB | KHDC1 | LRRC37A3 |
| RASGRP3 | PRR34 | NME2 | SUZ12P1 | CHCHD5 | SMIM7 |
| OXLD1 | AMZ2 | CBX7 | SKIDA1 | RIBC2 | CAPNS1 |
| CHERP | SNORD12B | CEP72 | USP5 | ATP2C1 | TYK2 |
| ANAPC10 | C1GALT1C1L | GMNN | HAUS8 | HSD11B1L | AKAP1 |
| TBC1D16 | DCTD | CETN3 | ERP44 | USP34 | NDUFV3 |
| C3ORF58 | RAB3A | EWSR1 | TNFRSF10A | ASF1B | OSMR-AS1 |
| HOMER3 | MAFG | ZDHHC9 | PEX3 | BUB1 | LINC00652 |
| ZBTB21 | UBE2V1 | CDADC1 | C2ORF27B | MICB | SLC25A1 |
| MIR615 | TAF8 | BEND3 | SDHAP3 | RRP1B | PTCH1 |
| DNPEP | POMK | CCDC157 | HIST1H2AJ | CENPP | USP40 |
| TMEM198B | STK11IP | PPP1R18 | HIST1H3B | GPR108 | UBE2E1-AS1 |
| MCPH1 | PITRM1 | KRT18 | ARID3A | PTCD3 | NIPAL2 |
| SQSTM1 | SNAI1 | USP6NL | OSMR | NNT-AS1 | ELFN2 |
| CALM2 | NUDCD2 | GATA6 | C17ORF67 | DNAJB2 | XAB2 |
| SKIV2L2 | RPS18 | MET | NCBP2 | RFXANK | P3H4 |

| | | | | | |
|------------|------------|------------|-------------|--------------|-----------|
| SCLY | LENG8 | RNMT | UTP18 | RNASEH1 | SMARCAD1 |
| MIF4GD | PHF1 | ZIC3 | S1PR5 | LOC100506990 | NOL4L |
| MIB1 | ZFYVE28 | BCAS3 | PTRH1 | MIR375 | TSEN34 |
| LRRC8A | LIMCH1 | IFT20 | HIST1H2AE | PLEKHH3 | MIR425 |
| SLC38A7 | GM2A | PARP2 | TIAM1 | FRG1HP | WDR91 |
| PTPN23 | ODF2 | MORN4 | AFF1 | NDUFA11 | R3HDM4 |
| LMTK3 | ISOC2 | CDKN2B-AS1 | LOC644656 | ARSG | L3MBTL1 |
| PGLS | RAET1E-AS1 | RRAGD | RIOK1 | ZC2HC1C | TRIM35 |
| RIOK2 | STXBP4 | FNDC3B | GNAS | ENTHD2 | PQLC1 |
| SACM1L | LGALSL | IKBKAP | WDR5 | PRR18 | SYNE4 |
| HN1 | MIR4754 | LOC389765 | ID1 | RPS6KB1 | KIAA1468 |
| SMKR1 | KIAA1328 | GSTA4 | PAPD7 | TEN1-CDK3 | AP1M1 |
| THOC1 | THAP7-AS1 | WBP2 | DTD2 | CEP126 | PEG10 |
| KDSR | UBA5 | ZNF529 | CBR3-AS1 | HPCAL1 | NADK2 |
| GMFB | FBXL12 | PPAN | OTUD6B | HSPBP1 | MYRIP |
| SGSH | MTRF1L | ANKRD17 | TBCB | SLC25A14 | BLOC1S5 |
| HIST1H2AM | KANSL1L | ACAA2 | ANKRD37 | CCDC171 | CPLX1 |
| RNU86 | POLR3D | BBS12 | HGH1 | POLR2D | PPP1R11 |
| PCBP4 | RPL12 | C3ORF14 | GAD1 | RPP25L | PDK2 |
| TPGS2 | MRPL30 | SLC44A4 | IKZF2 | CLTCL1 | C18ORF8 |
| NUTF2 | ZSCAN16 | LINC01336 | RSPH1 | TNPO2 | TRAF2 |
| STMN3 | DLG1-AS1 | PHF5A | BPGM | LOC101928438 | COPE |
| PLRG1 | TOPORS-AS1 | FAM73B | OSGIN2 | PSMC5 | ABCG1 |
| TLR5 | SGPP2 | ORAI2 | ZNF829 | ZNF580 | LPP |
| ACVR1 | CERCAM | SSNA1 | ABTB1 | LOC100272217 | BCL11A |
| VPS13A-AS1 | DGCR6L | SOX9 | LPIN3 | NCALD | C6ORF62 |
| C8ORF59 | C5ORF66 | RPL9 | SNORA26 | PECR | AMZ2P1 |
| RUFY1 | MRPS23 | INAFM1 | NDUFB2-AS1 | DLX4 | UBE2O |
| MAN1B1-AS1 | TIPARP-AS1 | LOC389641 | TCF19 | NPAS2 | RRAGA |
| ZNF197 | NDUFA13 | MIR6790 | REEP6 | POP4 | RPS28 |
| PTPDC1 | TTC3 | DUSP18 | GTPBP2 | LINC01607 | TUSC2 |
| TCTEX1D2 | ELOVL2 | KLHL2 | MED12L | PITPNB | FANCC |
| CEP78 | OXSM | CCDC137 | ATG12 | SH3BGR | ENPP5 |
| DTWD2 | DPY19L3 | RASL11B | SLC25A23 | HIST1H2BH | TTC28-AS1 |
| PRCC | PDE6D | LRRC45 | PDE11A | ZNF570 | CGGBP1 |
| SNRNP200 | ANKRD33B | SYNJ1 | CMYA5 | SNX30 | PLCD3 |
| C2ORF73 | ZBTB2 | HERC2P2 | SEPSECS-AS1 | MIR330 | PIGX |
| ACSL6 | NFKBIL1 | ZNF830 | PAQR3 | UBL5 | PAF1 |
| MIR34AHG | BECN1 | CENPQ | HIST1H2AK | JMJD6 | ARHGEF3 |
| SIRT2 | TBCK | C19ORF33 | ZDHH4 | MIR4665 | VAV2 |
| LOC145694 | MIR1204 | NREP | TEFM | PSMG1 | TMEM135 |

| | | | | | |
|----------|--------------|----------|--------------|--------------|--------------|
| NDUFA5 | ZNF793 | HMBOX1 | | 2-Sep ZNF573 | CCM2 |
| SUN2 | FBXO10 | GOLGA2 | FBXO7 | PNPLA7 | HNRNPUL1 |
| CDC14B | AURKA | NKILA | ZNF566 | SLC26A11 | JUNB |
| SWI5 | DST | HMMR | CABYR | ANO2 | MSH3 |
| MSL1 | ACP1 | WSB1 | ASAH1 | C19ORF66 | THAP4 |
| ARMC9 | LOC100507564 | SRP72 | RPL10 | GRB2 | PINX1 |
| TRIP12 | PIK3CA | GPR107 | TRIM46 | ZNF571 | ITGA3 |
| COX11 | FZD3 | THAP9 | CWC25 | ADAMTS19-AS1 | SSH2 |
| SEPSECS | DCLRE1A | DGCR6 | SH3YL1 | SPIRE1 | PPP1R10 |
| HPS4 | NCK1 | SNAP25 | ZNF569 | MIR4530 | NEK11 |
| VEGFC | KIAA1524 | AKT1S1 | UVSSA | LINC00667 | RAB3C |
| SYBU | EBNA1BP2 | ZNF565 | RAP2B | B3GALNT1 | TBC1D5 |
| CLPTM1 | NF1 | ZNF700 | TXNRD2 | GADD45G | TMX3 |
| PNPO | SETD2 | DIRC2 | BLOC1S3 | NARF | ADAM17 |
| MCTP1 | ACOX3 | USP43 | SVOPL | AP2A1 | TXNIP |
| DIP2A | RANGAP1 | SPRYD3 | TXNDC5 | C11ORF68 | NME6 |
| EDN1 | CAPN10-AS1 | SLC16A2 | TNRC6B | MIR4664 | LOC100128398 |
| NOTCH1 | KLHL26 | GYS1 | MRPL41 | ADGRL1 | POLR2I |
| GOLGA1 | TESK1 | MYO19 | SYCE3 | VAMP2 | MIR8069-2 |
| HIST1H3H | TOPBP1 | CENPE | CAB39 | RIC1 | TBC1D2 |
| ZNF322 | SNRPD2 | CCDC39 | SORBS3 | LAMB1 | NUP62 |
| EPN1 | INSR | SEC24B | SSR4 | KIF9-AS1 | ASTN2 |
| AIMP1 | DCTN4 | NUDT18 | CCDC43 | SUPT5H | KHDRBS3 |
| SMIM19 | CDKN2A | C9ORF40 | RND1 | ZNF473 | RALBP1 |
| GSDMD | DNAJC7 | MAFA | NRM | GPRIN1 | UBXN7 |
| FLAD1 | TSPAN33 | NCL | IL1R1 | MCCC1 | MAPRE2 |
| STRA13 | LOC101929762 | MAPT-IT1 | AXIN1 | C19ORF44 | HNRNPUL2- |
| CANX | HIST1H3G | MAPK11 | MRPL27 | SCP2 | BSCL2 |
| CYTH1 | CDC20B | RCHY1 | TTC39C-AS1 | CEP112 | ZNF311 |
| PAQR5 | TMEM147 | CNBP | ANKRD6 | CEBPA | MED16 |
| ARHGDI1 | KCTD2 | ZNF446 | MED22 | DENND4A | ARVCF |
| TMCO3 | ATP13A1 | EXOC7 | MSX2 | NXF1 | PI4KA |
| ZNF791 | FKRP | DALRD3 | LARP7 | MRPL1 | ADRB2 |
| ZNF845 | SNHG16 | SLCO5A1 | RAD18 | MYPOP | DDX5 |
| TP53I13 | SS18L1 | ADNP-AS1 | RFX1 | LDOC1L | CCDC74B |
| CPQ | ZNF436-AS1 | RHOQ | LOC100419583 | HCG25 | DTYMK |
| MTERF4 | KIF4A | DNASE1L1 | RNF152 | TAOK1 | ARIH2OS |
| INTU | SEC61B | SLC25A33 | RBM12B-AS1 | CTDP1 | EPM2AIP1 |
| POLE4 | MPND | ABCB8 | FAM162A | THAP8 | ZNF561 |
| RBM18 | HIRA | PEX12 | CDKN1C | SLC2A11 | NDUFA3 |
| JAK2 | COMMD10 | SLC16A3 | FAM207A | GRHL2 | SNORA16A |

| | | | | |
|-----------|------------|-------------|--------------------------|--------------|
| TRIM37 | UBA6 | MGC57346 | <u>ASH2L only</u> | SNRNP40 |
| SNORD58B | CELSR3-AS1 | EEF1D | <u>(1,240)</u> | POLA2 |
| RUNDC1 | ZMYM3 | NUDT16 | | MIR5700 |
| ZNF354C | HNRNPL | SCARB2 | STK32C | HIST2H2BF |
| AGPAT5 | ARMC1 | XRCC1 | PHTF1 | AGO3 |
| ATP5G1 | WDR89 | SS18L2 | PTPRE | RCOR2 |
| BAG1 | ESCO2 | BCL2L12 | PIFO | MAP4K2 |
| PPP1R26 | SLC1A1 | LOC728323 | WNT2B | LMO7DN |
| SDSL | SEC24B-AS1 | ALYREF | SYT6 | GDF11 |
| PLEKHH2 | POLQ | C21ORF58 | PWWP2B | LMO7 |
| SH3GL1 | PARP3 | AASDH | EBF3 | MEGF6 |
| SH3BP2 | CECR5 | HPS5 | LRRC27 | ELP4 |
| NKX3-2 | DLX1 | NOL8 | ATP5F1 | MYCL |
| EBAG9 | GUCD1 | LINC01534 | DTX4 | TMEM138 |
| HMG20B | ALG3 | WDR62 | FAM196A | ATP8B2 |
| PSMD5-AS1 | LIN54 | SUPT6H | LOC643355 | PATL1 |
| CASKIN2 | SNORD61 | NNT | ORC1 | FZD10 |
| IRGQ | ME2 | CAPN10 | WDR74 | CLYBL |
| ZNF607 | MIR4674 | RRP9 | RNU11 | PITHD1 |
| IDUA | SAMD4B | RNF214 | ST7L | PDE3A |
| ZNF846 | ADCY3 | MIR4523 | LOC101928034 | RILPL1 |
| KMT2B | MRPS18C | TEN1 | FAM76A | GON4L |
| ARHGFEF6 | SIRT6 | CCDC58 | BSDC1 | ATP11A |
| FAIM | LINC01431 | LACC1 | HMG2 | LINC01167 |
| UBXN8 | ABHD17C | TRIM32 | HIST2H3C | CHST11 |
| MSL2 | SEC16A | HIST1H2BM | KCNC4 | KMO |
| DCAF16 | FLT3 | DIS3 | B4GALNT4 | CHID1 |
| EIF4ENIF1 | C9ORF69 | SPATA13 | RHOF | MIR9-1 |
| MRPL34 | POT1-AS1 | PSMD5 | KDF1 | GMEB1 |
| PRR7 | SLC35G1 | VRK3 | AZIN2 | ABHD13 |
| LSS | TECR | RNASEH1-AS1 | LOC646626 | DPYSL4 |
| PIGP | ASXL3 | LOC339874 | LINC00365 | NELL2 |
| JAK1 | RUBCN | CCDC25 | HSPB11 | ZFP91 |
| DEDD2 | INVS | MIR4449 | ZNF740 | LOC101928414 |
| MAP1LC3A | DUSP4 | NFKBIB | GALNT2 | TMCC2 |
| PAXBP1 | MIS18A | C9ORF163 | LETMD1 | FAAP20 |
| SNORD50B | SNHG5 | NIP7 | DLEU1 | ZNF385A |
| ZNF879 | CC2D1A | ZGRF1 | ITGA7 | POU6F1 |
| PSMD7 | ADARB1 | FAM47E | NRXN2 | ZNF326 |
| NBR2 | ALG2 | | CMPK1 | DEF8 |
| MYO1B | MRPS12 | | HECTD3 | PSMB2 |

| | | | | | |
|--------------|--------------|--------------|--------------|--------------|-----------|
| USPL1 | DAGLA | ANAPC15 | SSBP3 | PKN2 | FNDC5 |
| CACNB3 | STARD10 | GALNT4 | ARHGEF2 | KCNH3 | ADAMTSL3 |
| FANK1 | TMEM39B | ANKRD63 | DNAJC3 | RAB3IL1 | RNVU1-20 |
| PPFIA2 | RGL1 | ZMYM2 | HOXC-AS3 | ZCCHC11 | PCDH17 |
| METTL21B | LATS2 | PFKFB2 | PGBD5 | POLR3GL | SDHAF2 |
| SNORD15A | DNALI1 | PLEKHB1 | BLACAT1 | PPP1R1A | ATP2C2 |
| ZNF664 | HS6ST3 | EIF4G2 | RASSF7 | BORA | HIST2H4A |
| LOC101927204 | PADI2 | ZBTB41 | KCNC1 | HMGA2 | SWT1 |
| PDE3B | MSRB3 | YBX1 | TMCC3 | SLC22A18 | C1ORF145 |
| LOC101927583 | LRTOMT | SAMD11 | C1ORF53 | P4HA3 | SYT17 |
| USP12 | TMEM53 | PDE1B | GUCY1A2 | GOLGA8A | DIXDC1 |
| SETDB2 | AHCTF1 | COL16A1 | PPP2R5B | LOC101927318 | SCFD1 |
| TUB | LOC101929234 | NES | TESC | TSC22D1 | TTC39A |
| SPATA1 | NDFIP2-AS1 | LRRC63 | GTF2H3 | INPP5B | PAH |
| TMEM200B | TNS2 | CDH15 | PHLDA2 | PLBD1-AS1 | BCL2L14 |
| GSE1 | PRICKLE1 | C11ORF91 | RFX5 | CACNA1C | B3GALNT2 |
| RAD54L | SNAI3 | KRT8 | ERMAP | KIF2C | CAND1.11 |
| ZBTB7B | DDX55 | ARL14EP | SF1 | SPATA6 | S100A16 |
| PXMP2 | EVA1B | ARV1 | RCAN3 | DYNLRB2 | SHF |
| SPRYD4 | GTF2B | LOC101928443 | MANEAL | FAM78B | SMPD3 |
| RAB30 | CLP1 | KCNT2 | DAPK2 | ESRRA | GOLGA8F |
| DNAJA3 | PNRC2 | BEND5 | PLCG2 | MAF | GOLPH3L |
| PHC2 | SCUBE2 | VANGL2 | SERPING1 | KCNK2 | HMCN1 |
| ALKBH3 | TAF6L | GAN | CYB5R2 | TPBGL | HELB |
| PUSL1 | TRMT112 | FAM86C1 | TCTN1 | IGFALS | SLC4A8 |
| LOC101928737 | TUFT1 | KCNJ11 | WDR11-AS1 | MZT1 | SIVA1 |
| LOC101928043 | SLC3A2 | TMEM266 | CFAP45 | LOC100287036 | TRIM34 |
| LOC101929657 | KCTD14 | ZNF687 | LOC100132057 | USP35 | CUEDC2 |
| EIF3J-AS1 | CELF3 | THBS1 | CNIH3 | NADK | ETV6 |
| MCOLN2 | BPNT1 | SMIM22 | CHRM3 | KCNQ4 | CELF1 |
| FMNL3 | HMGB1 | NUDT4 | MSI1 | RAP2A | AMDHD1 |
| COLCA1 | SMYD2 | BCAR1 | WDR26 | LRRK2 | UBE2L6 |
| EIF4G3 | JDP2 | SPG20-AS1 | GJB2 | ATF7IP | MIR5087 |
| SHISA2 | ZBTB8OS | LHX9 | SPDYC | DISP2 | VPS36 |
| LIX1L | RWDD3 | FNDC3A | INPP5A | ROM1 | CSNK2A2 |
| QSOX1 | DR1 | FAM103A1 | LOC284648 | DOC2A | ZCCHC14 |
| ZC3H12C | CACNA1C-AS1 | SP1 | MIR7155 | TMC7 | SCN8A |
| FAM124A | RBM26 | MIR190B | TRIM67 | FAM183A | ST3GAL4 |
| LOC100288798 | ZMYM5 | PRRG4 | MCF2L-AS1 | MIR5691 | PLA2G4B |
| GPBP1L1 | KCTD10 | SNHG1 | INTS6 | ZNF778 | LINC01144 |
| HNRNPA1L2 | CCDC24 | ALG14 | MIPEP | IFNLR1 | PPFIA4 |

| | | | | | |
|--------------|------------|----------|-----------|-----------|--------------|
| KMT5A | ZNF644 | ZNF597 | NQO1 | ALG5 | COX15 |
| IRX6 | CCDC83 | C11ORF1 | GLUD1P3 | SOX5 | C14ORF37 |
| HYPK | C1ORF27 | ADAMTS7 | GLB1L2 | HS2ST1 | IRAK4 |
| PLPP4 | EFEMP2 | PTPN6 | PLK3 | MKNK1 | GAS6 |
| SYT7 | STYK1 | ARPC5 | DYDC2 | EXOSC8 | LOC101928979 |
| ARHGEF25 | MKI67 | MPPED2 | MTMR10 | YOD1 | SHOC2 |
| TMEM87A | LINC00939 | TMX2 | SYNC | CALCOCO1 | ANP32AP1 |
| NUP93 | PIGBOS1 | TAT-AS1 | CPEB3 | EXD2 | LOC283922 |
| PRC1 | TMEM126B | RIMKLA | BCL9L | LINC00346 | ANKRD2 |
| C10ORF54 | AP5B1 | SYT13 | USP3 | KCNK13 | CENPJ |
| PHF11 | NPAS3 | HSPA7 | DHRS12 | ITPRIP | PRDM10 |
| KIAA1804 | MAB21L3 | FALEC | FGF9 | RAB30-AS1 | C16ORF71 |
| FUCA1 | PLEKHG4 | ARID5B | ONECUT1 | EHF | MRPS31P5 |
| PLEKHD1 | TPT1 | MAP1LC3B | SMIM2-AS1 | AIM1L | NSUN4 |
| RGMA | POMT2 | CYB5B | ATMIN | ALG6 | TIMM10 |
| TK2 | KLHDC4 | LBHD1 | FGGY | TMEM126A | CACHD1 |
| TTBK2 | CALB2 | TDRD5 | MMP25 | KIAA1217 | C11ORF74 |
| ZNF140 | MRPS35 | RBPMS2 | PTPN20 | RPS27L | TBX6 |
| LINGO1 | SLC2A1 | MIR4692 | AGAP11 | ARNT2 | SPNS2 |
| MSANTD2 | FLJ37453 | POU3F1 | FMN1 | FOX3D-AS1 | XRCC6BP1 |
| EEF1DP3 | DYNC1LI2 | CIB2 | LOXL4 | FOXA1 | IQSEC3 |
| RNF6 | ITFG1-AS1 | PRSS27 | CORO1A | MEIOB | C16ORF74 |
| MMACHC | RRP15 | SNX33 | RTN4RL2 | FREM2 | USP54 |
| PLLP | UGGT2 | SHCBP1 | XYLT1 | C11ORF45 | FAM25A |
| MIR4500HG | SLC16A7 | MSANTD4 | TRIM13 | CHRM1 | COQ9 |
| CATSPER2 | DNAJC3-AS1 | FTH1 | HSPA12A | ITGB1 | CYP2J2 |
| CHD4 | NPAT | GPR161 | MRE11A | TMEM256 | LOC101929574 |
| GUCY2EP | TPTE2 | ST3GAL2 | LINC00434 | TMEM167B | MAD2L2 |
| LOC101929340 | TENM4 | SETD6 | RHOBTB1 | IFIT3 | KIF22 |
| SNHG21 | STOX1 | SFR1 | ZNF248 | SUPV3L1 | GPS2 |
| MIR3124 | DMAP1 | SLC43A2 | UTP20 | ARHGEF12 | MIR4513 |
| EEA1 | KCNJ5 | LIPT2 | GRID1 | KBTBD6 | NRG3 |
| RAB39A | LINC01572 | CTSC | C11ORF70 | ESRRG | DHX38 |
| HNRNPA1P10 | NTHL1 | ABCG4 | TDRD3 | ATM | TMOD2 |
| UCHL3 | PLXNC1 | LIG4 | LYRM1 | PKD1L2 | GLIS2-AS1 |
| WDR81 | ACBD7 | NEGR1 | BEAN1 | ARNT | LOC105376671 |
| ESYT1 | SEMA6D | RAP1A | LOC644919 | ZNF263 | MAEL |
| INO80 | FAM81A | NCDN | BEST3 | PKMYT1 | PRIMA1 |
| BARX2 | PLEKHO1 | GJC2 | CBFA2T3 | TEKT1 | ACTR1A |
| ZFPL1 | SVIL | CDT1 | ADD3-AS1 | IGSF9B | RUSC1-AS1 |
| BMF | NPR1 | FAM216A | NME3 | KCNQ10T1 | CCDC64B |

| | | | | | |
|--------------|--------------|-----------|--------------|--------------|--------------|
| B4GALNT1 | LINC00871 | SLC25A21 | SPA17 | LOC81691 | ACSM3 |
| LOC283140 | USP2 | USP3-AS1 | MIR5093 | FLT1 | HOXC9 |
| LOC105447648 | RPS17 | RIMS3 | FAM63A | AK4 | FAM90A1 |
| RXFP4 | PRUNE | A2M-AS1 | NMNAT1 | FBXO33 | MAFTRR |
| SPRED1 | ANO9 | PAN3-AS1 | LNX2 | ZZEF1 | ANAPC16 |
| FZD10-AS1 | SPTB | BEGAIN | KCNIP2 | SORT1 | ADPRM |
| BAIAP3 | PKNOX2 | LGR5 | DNAJC16 | CIDEB | MYO1C |
| LARP6 | CELF6 | VWA2 | WNT4 | SNORD49B | RAVER2 |
| ZNF436 | PC | CHD8 | C11ORF97 | ADAMTSL4 | CSTF2T |
| SAXO2 | APOLD1 | HTR7 | ADPRHL1 | C10ORF10 | PLXDC2 |
| TMEM255B | ZDHHC24 | NLK | FHOD1 | TP73 | MRPL55 |
| FAM181A-AS1 | AARS | BBS10 | LRRC38 | MIR497HG | RFX7 |
| CXCL16 | LINC01461 | NDUFB1 | SNORD45C | MED31 | ACIN1 |
| ATP1A1 | PFKFB3 | SEMA7A | DHDDS | SLX1B | CPEB1 |
| ARMC4 | RNASEK- | NOP9 | KIAA1462 | CHMP4A | CTNS |
| FSIP1 | C17ORF49 | MIR193BHG | TLCD2 | ENOX1 | ZNF25 |
| NPIPA7 | SAT2 | AGBL4 | ARPIN | SMIM1 | ADPGK |
| GRK5 | PVRL1 | ANKFY1 | SPAG5 | SAMD4A | DBNDD1 |
| TSHR | AURKB | RPS6KA4 | BIRC3 | WSCD1 | GRIK4 |
| PKM | C11ORF80 | NFYC-AS1 | LOC101929089 | MIR7846 | SNORD42B |
| FPGT | ARHGAP22 | CFAP70 | MXI1 | MIR9-3HG | KCTD11 |
| SLC11A2 | SRSF11 | GRHL3 | SNRNP25 | FAM57A | ALOX15P1 |
| SHISA6 | CTC1 | HHEX | ABCC4 | PALB2 | CISTR |
| NFIA | SPAG7 | PPP1R36 | LOC283575 | SIAE | HIC1 |
| NRDC | CCDC6 | ACOT7 | FAM25C | ZDHHC1 | LOC102723809 |
| HMOX2 | TMEM57 | PROSER1 | C11ORF71 | APITD1 | PRPSAP2 |
| LRRC8D | ZFP69B | BDKRB2 | CDKL1 | PIK3AP1 | ARL6IP1 |
| MTHFR | MIR365A | PTPRB | PLD2 | LINC00437 | ERCC4 |
| TRABD2B | BIRC2 | TMC5 | NIPAL3 | PARS2 | DBT |
| DNAJC14 | DEXI | STAM-AS1 | RPAIN | MIR132 | NAA60 |
| SMCO4 | ZNF684 | ANKDD1A | APLP2 | C1ORF168 | HS3ST3A1 |
| FAM13C | TLL2 | TSPAN2 | MED11 | UBTD1 | RHBDL1 |
| ZRANB2 | RPL13 | PDCD6IPP2 | SALL2 | EDC3 | FBXO2 |
| TAF1D | LINC00466 | SC5D | PITPNM3 | SV2B | POLR2A |
| SLC45A1 | DCUN1D2 | TRIM33 | SELL | LOC101928453 | LINC01515 |
| TMEM254-AS1 | GPRC5B | LRRC40 | SULT1A2 | NXN | GCOM1 |
| PCAT29 | EFCAB7 | SCN4B | PGM1 | DGKA | TTC36 |
| NUDT7 | SLC25A30-AS1 | ADRB1 | ADRA2A | CCSER2 | RBM4B |
| MAN1C1 | GFOD2 | HOXC5 | DLG4 | MEIS3P1 | FLJ36000 |
| TUBGCP2 | PGR | ANKRD52 | STIP1 | NPRL3 | NCOR1 |
| NRGN | DDX19A | FMO9P | NECAP1 | RGS6 | HBA2 |

| | | | | | |
|--------------|--------------|-------------|------------|-----------|---------------|
| TSC22D1-AS1 | NEUROG3 | RBM7 | MIR6859-2 | ASPG | FAM111A |
| SULT1A1 | HBA1 | BMP8B | ZNF219 | WBP1L | DDX11L9 |
| MTOR | WDR63 | C1ORF233 | MIR6859-3 | SREBF1 | NBEAP1 |
| RNF167 | C14ORF93 | USP2-AS1 | BAMBI | EFCAB14 | MIR4708 |
| CELSR2 | LOC100190986 | MORN1 | PPP4R4 | RPS13 | PTEN |
| FAM64A | NIPA1 | ABR | GLRX5 | LTB4R | KBTBD3 |
| COX10 | FAM155A | C16ORF52 | MIR4307HG | WHAMMP3 | EML5 |
| DPAGT1 | MIR3175 | PRTFDC1 | PRCP | RPP30 | SUGT1 |
| STXBP6 | MTIF3 | SESN3 | USP28 | RERE | SERINC4 |
| CD164L2 | DEPDC1-AS1 | MFSD6L | MBTPS1 | RNF187 | USP31 |
| ALDH3B2 | TMEM120B | DENND2D | PHF23 | ASAH2B | DDX23 |
| ANKRD35 | SLC2A4 | ROR1 | MIR6732 | TCTEX1D4 | LEPROT |
| TINF2 | C15ORF59 | EPHA10 | IGF2 | LINC01481 | GNRHR2 |
| DACT1 | DIO3 | CYP26A1 | CYB5D1 | HSD11B2 | ACADVL |
| TYW3 | ZSWIM7 | ARHGAP32 | TANGO6 | ALDOC | BBOX1 |
| TAF13 | MIR4492 | SERPINA1 | TNFSF12 | FLCN | CLCF1 |
| HAX1 | POLR1D | LOC440300 | AUNIP | CRISPLD2 | LOC101929613 |
| LOC101928162 | LOC101926933 | TMEM107 | SLC2A1-AS1 | CFAP58 | MIR3176 |
| PDSS1 | IREB2 | TVP23B | SCMH1 | TRNP1 | RASAL2 |
| LRIG3 | HPCAL4 | SIRT1 | GLI1 | PPP2R1B | LOC101054525 |
| CASKIN1 | RPL26 | MPDU1 | FBXO44 | CHAC1 | TLL5 |
| LDB1 | HYDIN | PTCHD2 | TACC2 | SEPN1 | ZNF592 |
| AK5 | ALDH1A3 | ARRB2 | USP21 | BMP8A | MYBBP1A |
| ZDHHC16 | MT1A | RAB1B | KIF11 | SHBG | LINC00359 |
| MAP3K9 | EML1 | ARMC3 | ETFA | CREB3L1 | MTERF2 |
| NATD1 | LINC00842 | RAB11FIP2 | CYB5D2 | C1R | CEP83-AS1 |
| PRKCCQ | C15ORF61 | C10ORF11 | BRSK2 | PMP22 | C11ORF88 |
| UBXN10-AS1 | DYNC2H1 | MSS51 | CRB1 | LAMB3 | JMJD7-PLA2G4B |
| MIR4691 | MFSD13A | TOM1L2 | DERL2 | PDE2A | DISC1 |
| WBP4 | GRTP1 | PTGER2 | MCOLN3 | KIAA0754 | PPP1R14D |
| EIF1AD | SPNS1 | CYB5RL | HSPA2 | KIF1BP | ESR2 |
| MKX-AS1 | OAF | SNORA48 | RAB40C | MIR4487 | ADIPOR2 |
| NEDD8-MDP1 | LOC100288846 | SOS2 | ADAMTS17 | SMC3 | SRPR |
| TNRC6A | IL10RA | GPR3 | IFI27L2 | LOC284023 | C1QL4 |
| BCL6B | SLC5A11 | SLX1A | GYLTL1B | ALDH4A1 | SPIRE2 |
| SPAG5-AS1 | FAM107B | EGR2 | PMVK | DDX11L10 | CTH |
| LOC100506022 | LOC102724933 | MIR6775 | SMG5 | RBBP4 | GNPAT |
| WRAP53 | TRIM3 | LOC728392 | FAF1 | IPO13 | HP1BP3 |
| C17ORF107 | CT62 | TMX2-CTNND1 | HOXC12 | KMT2A | DPY19L2 |
| POMGNT1 | MRPS31 | SARM1 | ZZZ3 | C15ORF48 | SNORD55 |
| GNAO1 | RNF207 | TPM3 | ETNK2 | FAM111B | PALMD |

| | | | | |
|--------------|--------------|--------------|--------------|-----------|
| LOC102724467 | SLC25A45 | SDHD | LAMC1 | KIN |
| DIAPH3 | LTBP2 | SERINC2 | P2RY6 | ZCCHC24 |
| RTCA | SFXN4 | MGRPRX3 | TMTC2 | ACY3 |
| CDC42BPA | NHLRC4 | EXOC3L4 | PTGER3 | BACE1 |
| FOSL1 | ORMDL2 | GCHFR | GBP4 | ADAM8 |
| POLR2L | ZG16B | NR0B2 | LOC101929718 | KIAA0895L |
| POTEB3 | RAB3B | SSX2IP | GPATCH4 | NDUFS8 |
| PRKCQ-AS1 | AGO4 | MKL2 | DLG2 | RAB2B |
| NLRP14 | NEURL1 | PIGK | FAR2 | PAQR7 |
| SCNN1B | B4GALNT3 | SH2D5 | TMEM69 | CKS1B |
| TRIM6 | LRRC8C | ARID1A | LINC00866 | LMO3 |
| ZNF214 | COMMD6 | STIL | E2F8 | UBAC2-AS1 |
| FAM160A2 | NME4 | KAZN | GORAB | NUBP2 |
| HYI | SPRY2 | LRRC52 | HERC1 | ATP5S |
| PSKH1 | UPF2 | TM9SF2 | OTOG | |
| SSTR5-AS1 | CIT | ST3GAL4-AS1 | CAMK2G | |
| GOLGA6L7P | SPPL2A | VAMP1 | LGALS8 | |
| DDX11L1 | DDN | ABCC11 | ATG101 | |
| POU2F3 | LINC00638 | LOC101928322 | TUBB3 | |
| HIST2H2BA | EP400NL | DNAJA4 | CPB2-AS1 | |
| ARHGAP1 | LOC101927045 | FAM83G | TTF2 | |
| FANCA | ACTR10 | C1ORF220 | ALG1 | |
| FOXO6 | PACSIN3 | ABCD2 | COA7 | |
| SHC1 | HINFP | C10ORF2 | USP15 | |
| ELOVL1 | LINC00938 | HIPK3 | RORA | |
| GOT1 | TRNAU1AP | CFAP54 | LOC101928069 | |
| CCDC144CP | SDC3 | TLN2 | FOXM1 | |
| TLX1NB | YRDC | SSU72 | CCKBR | |
| UFM1 | NUMA1 | C15ORF57 | ZMYM6NB | |
| ZC3H13 | SAMD13 | SYNM | LOC103171574 | |
| TGM1 | CDYL2 | RPS14P3 | CAPN1 | |
| CDC7 | SLC25A35 | ALDH1A2 | EFNB2 | |
| LRRC32 | ANAPC5 | MIR4537 | PCBD1 | |
| JMJD4 | MED18 | PGLYRP4 | ZNF281 | |
| KIF18A | TIGD3 | MTMR11 | LOC100996455 | |
| CAP1 | HTR6 | GLYCAM1 | RMI2 | |
| RSRC2 | SYT8 | SNX22 | INTS7 | |
| MIR4710 | MUC1 | LINC01488 | ASB7 | |
| SBF2-AS1 | HNRNPUL2 | MIR484 | FGF11 | |
| NBEA | REEP3 | CCDC85B | MDK | |
| HAS3 | F2 | CD59 | KCNQ1 | |

| | | | | | |
|---------------------------|-----------|--------------|--------------|--------------|--------------|
| Common (1,282) | ADAM15 | DYNLL1 | ATHL1 | SLC12A6 | PGAP2 |
| RSBN1 | TFB2M | UBQLN4 | PIGV | PRKAB2 | CD81-AS1 |
| MAGI3 | OSCP1 | TSACC | LMNA | CD63 | ARL1 |
| SLC16A1-AS1 | MIR7641-2 | TPRG1L | TRAPPC3 | CCT2 | AXDND1 |
| WDR77 | NT5DC3 | LINC01389 | APIP | LOC148413 | TMEM5 |
| HIPK1-AS1 | TDRKH | TMEM59 | LINC01128 | KLHL17 | LOC101928580 |
| GSTM4 | MRPL20 | LOC101927415 | SMIM12 | SMAP2 | TMEM52 |
| BAG5 | FBXO3 | AASDHPPT | FRMD5 | ELF3 | DPH6-AS1 |
| LRIG2 | RNF121 | TAGLN2 | SLCO3A1 | TMEM179B | LYPLAL1 |
| RPLP0 | E2F7 | ANKLE2 | CPTP | RARG | HIST2H2AA4 |
| METTL10 | EEF1G | PIBF1 | FOXJ3 | RBM15 | PMM2 |
| CNN3 | C11ORF57 | C11ORF73 | RASSF3 | TROVE2 | IPO9-AS1 |
| PEX10 | METTL20 | GGPS1 | UBAC2 | KBTBD4 | PPCS |
| EIF5 | EIF2S1 | ARHGEF7 | COX4I1 | MIR203A | RBM34 |
| XRCC3 | LINC01351 | ATF1 | ASIC1 | LOC101927495 | RPAP3 |
| PPP1R13B | TOLLIP | UBR4 | SH3BP5L | QSER1 | GALE |
| CCDC64 | PEF1 | NAV2 | COX20 | TMEM9B-AS1 | SNX1 |
| RAB35 | TMPO-AS1 | PDIK1L | C1ORF131 | SLC50A1 | BCAR3 |
| RNF141 | CAPZB | MIR2276 | STAT6 | DEDD | ZNF143 |
| ZFYVE21 | CSAD | EIF3J | DIABLO | TUBGCP4 | FAM213B |
| B3GNT4 | ATP6V1D | EXOC8 | ANGEL2 | TSPAN31 | TATDN3 |
| LINC00959 | NCSTN | CAPS2 | MTF1 | RAD51AP1 | PACS2 |
| PLEK2 | ITGA5 | SPPL3 | LYRM5 | RIT1 | LPCAT4 |
| LOC101928068 | EIF2B1 | CCND1 | S100A13 | ZCCHC17 | FURIN |
| TKFC | SYDE2 | PLEKHA8P1 | MVK | RBBP5 | WSB2 |
| CAPRIN2 | CCDC59 | EFNA1 | LOC101927587 | AKT1 | RNU6-2 |
| PYM1 | UBE3B | MAGOH | SYF2 | ZMYND11 | MIB2 |
| PSMD9 | USF1 | LOC101929224 | PPHLN1 | TMEM80 | VEZT |
| AMPD2 | VPS33A | PSMD13 | PARPBP | DDX51 | HRAS |
| RSF1 | SOCS4 | RHOG | ANP32E | SRRM1 | TP53BP1 |
| NUSAP1 | TAF1A-AS1 | MIR6733 | SPRYD7 | BROX | SLC38A1 |
| CAMKK2 | DCLRE1B | KCTD21-AS1 | TSSC4 | ZNF605 | DTWD1 |
| LOC100505666 | C1ORF109 | ENO1-AS1 | LRRC41 | CORO1C | CD82 |
| TPCN1 | KIAA1033 | HIST2H2BE | MFSD5 | TSPAN4 | RRAS2 |
| ACTR6 | PHRF1 | GDPD5 | GATC | EMSY | AP3B2 |
| BLM | TMEM56 | P3H1 | IBA57 | DDIAS | NOC2L |
| NEDD1 | SNORA57 | ART5 | SRSF9 | AQP11 | TAF5L |
| PBXIP1 | POLR3B | PKP2 | BRAP | NDUFAF1 | SRP14 |
| BTBD10 | MIR3652 | HEATR1 | FKBP11 | AP4E1 | POLE |
| CAPN5 | ZC3H10 | FADS2 | ILK | PCCA | ZNF891 |
| | TMEM79 | RAB3IP | NAA40 | TPR | TARBP2 |

| | | | | | |
|-----------|-----------|--------------|--------------|--------------|------------|
| MIR5187 | PKP3 | KIF26A | RNF34 | CHP1 | TMEM54 |
| SCAF11 | PGM2L1 | SHMT2 | SPCS2 | HMGCL | SMAGP |
| CEP170B | UBN1 | TTC13 | CES2 | LOC148709 | TCF12 |
| NADSYN1 | SLC43A1 | ZNF821 | BTBD6 | ITPKA | FLYWCH2 |
| PAK6 | GPT2 | VPS33B | NHLRC2 | MCRS1 | TRMT1L |
| C12ORF49 | CRTC3-AS1 | MIR616 | P2RY2 | ADCK3 | MVD |
| RNPS1 | ARNTL | LOC100996255 | VPS45 | RIC8B | GBAT2 |
| RAB13 | SLC25A22 | TERF2IP | TTLL7 | ZNF768 | MLLT10 |
| TINAGL1 | MRTO4 | SH3D21 | LOC100288069 | MTA1 | CFDP1 |
| C16ORF59 | PRDM11 | PLBD2 | ADAL | HSDL1 | SLC30A7 |
| STARD9 | TSC2 | SPATA33 | EPS8L2 | GNS | ZNF500 |
| ACD | TMEM234 | NOP10 | KSR2 | DNAJC17 | NUDT21 |
| IST1 | PQLC2 | HEBP1 | SYT1 | LOC643339 | RBM8A |
| SNRNP35 | PRPF38A | BICD1 | MMS19 | CCDC189 | HHAT |
| FZD4 | EFTUD1 | LRRC4C | ABCA3 | NDUFA4L2 | THAP2 |
| YY1AP1 | GPR89A | USB1 | ADAR | NAGPA-AS1 | MIR1915 |
| ISG20L2 | ABCB10 | TOLLIP-AS1 | ILF2 | VAMP4 | MYCBP |
| SNAP47 | FOXN3 | CCNF | ARHGAP5 | C16ORF95 | ADCY9 |
| ING1 | TNFRSF19 | INAFM2 | LINC00936 | ATG16L2 | UBALD1 |
| PAAF1 | COX14 | ZNF785 | GAPDH | MLEC | TMEM72-AS1 |
| SOCS2 | CRYL1 | ISCU | F3 | KIAA0430 | INPPL1 |
| TMED5 | GPR137 | AEBP2 | KMT5B | ZNF84 | PPFIBP2 |
| SHISA9 | PTBP2 | SDR39U1 | BMS1P5 | ZNF503-AS2 | SMAD6 |
| CDCA5 | SMARCC2 | MAGOHB | TPP2 | ALG11 | MAP2K5 |
| GNAI3 | KCTD21 | DENND5B | PDIA3 | DDX11-AS1 | PARD3 |
| PIP5K1A | SMARCD1 | WARS2 | IDH3A | PGAM5 | C14ORF119 |
| IKBIP | ZFP69 | HCFC2 | RCBTB1 | RSL1D1 | LOC643770 |
| SERF2 | MRPL48 | TP53BP2 | ZBTB18 | MIR762 | MDM2 |
| FGF14-IT1 | C1ORF101 | PFKP | MRPL49 | MIR4512 | SNORA14B |
| KRTCAP2 | TXNDC12 | DVL1 | USP24 | DMXL2 | FAM86FP |
| SUOX | RNF41 | DGAT2 | | 5-Mar KATNB1 | GOLT1B |
| NUDT22 | TBC1D24 | MTFR1L | RANBP10 | NUP133 | RAB6A |
| NUF2 | UBAP2L | RPL4 | EEF2KMT | ANKRD13C | CHTF8 |
| POLR3C | DNAJC24 | AAGAB | NIT1 | NFAT5 | ENSA |
| DUS2 | XPO4 | ZNF668 | RASSF8 | LLPH-AS1 | NR1H3 |
| TRAPP2L | GALNT6 | GNPTG | FLJ10038 | PEX11B | RNF111 |
| UVRAG | COG8 | TSPAN9 | C14ORF79 | C15ORF41 | C14ORF80 |
| PTDSS2 | CD2BP2 | SDF4 | ZBED5 | FOS | GPR19 |
| TMEM50A | PCED1B | TJP1 | APH1B | LOC100147773 | FEN1 |
| TMTC3 | PAOX | SCYL2 | TCP11L1 | ARMC5 | SLC2A13 |
| MAPKAPK5 | EXO1 | CMC2 | UBE2Q2 | RCC2 | NUTM2A-AS1 |

| | | | | | |
|--------------|-------------|------------|--------------|------------|----------|
| KIF14 | RCE1 | FAHD1 | SLX4 | MAN2C1 | IL15RA |
| TMEM183B | IGSF9 | INTS4 | POLL | TRIP4 | RSU1 |
| NUTM2B-AS1 | VPS29 | SLC7A6OS | DDIT3 | CASC2 | KCNAB2 |
| LRRC57 | MIR200C | PARGP1 | PHKB | PIF1 | VPS35 |
| TXNL4B | LAMTOR5-AS1 | CHEK1 | BORCS5 | AHSA1 | TXNDC17 |
| COQ7 | CDK2 | SLIRP | SDF2 | KLHL35 | HENMT1 |
| CDIPT | TMEM51 | CIART | PHYH | NCAPD3 | KIAA0586 |
| TSR3 | FLVCR1 | DOCK9-AS2 | PYGL | DCAF11 | PCDH9 |
| DHCR7 | PLEKHG6 | DICER1 | OAZ3 | VIM-AS1 | KCNMB4 |
| NAB2 | TARS2 | HNRNPF | TAF12 | EMC8 | TCP11L2 |
| DLL4 | HTATIP2 | PIK3CD-AS2 | SNORD74 | CUL4A | LIN7C |
| CHTF18 | FAM213A | CIAPIN1 | STARD5 | CAMTA1 | NCKAP5L |
| RAB27A | LRP1 | CIPC | GFRA1 | ENKD1 | L3HYPDH |
| AFG3L1P | ICE2 | TSR1 | ADK | GTF2IP20 | HECTD2 |
| LOC100506844 | TMEM208 | HMG20A | GPR158 | PTPN14 | NOP2 |
| NCAPD2 | SLC37A4 | TGFB2-AS1 | RELA | GPALPP1 | MEIS2 |
| TIGAR | PLEKHG5 | LRRC20 | ARHGAP11B | FBXL19-AS1 | CKAP5 |
| FRA10AC1 | MIR6741 | NFATC4 | HIRIP3 | M6PR | MIR210HG |
| MTMR2 | GPN3 | LYSMD1 | ZNF488 | ATP1A1-AS1 | GSTO2 |
| ARHGEF17 | CCNY | CEP170 | MANSC1 | SUV39H2 | DLG5 |
| ATP5C1 | TMEM254 | GMPR2 | 15-Sep | SNORD68 | YAP1 |
| GDAP2 | SKA3 | CCPG1 | TCEB2 | C10ORF111 | MADD |
| ANKRD42 | AP3M1 | CREBL2 | LOC102724571 | RCOR3 | CREBBP |
| DUT | CCDC122 | SMG6 | LRRC28 | GALNS | CLSTN3 |
| FANCM | HIF1A-AS1 | MIR22HG | CASP9 | BTG2 | NMRAL1 |
| MRPS11 | GABARAPL2 | CFL2 | DCAF6 | MIR3656 | HSPA6 |
| CDKN2C | HOXC-AS2 | TEAD4 | RNPC3 | LDHA | OPTN |
| PDDC1 | DPF3 | PRKRIR | HIST2H2AC | PIAS3 | IGHMBP2 |
| FAM168A | C10ORF25 | RPAP2 | CASC4 | ACP2 | HSPA14 |
| RPLP2 | SLC39A13 | MTX1 | THYN1 | SEC14L5 | NARFL |
| RPUSD4 | TCHP | AKAP11 | ZNF213-AS1 | CCNL2 | PLEKHO2 |
| SVIL-AS1 | NEBL-AS1 | ICMT | LINC00115 | EMC4 | DHRS4L2 |
| FBXL8 | DUSP10 | ZC3H7A | NEK9 | TM9SF1 | MRPL43 |
| ACBD5 | CTAGE5 | MTHFSD | SBF2 | ADM | CNST |
| AIP | LRP6 | SOCS1 | RPPH1 | PPFIA1 | SNORD60 |
| CARHSP1 | SFMBT2 | C14ORF142 | TRAPPC4 | NDUFA9 | ZWINT |
| ATAD3A | TAF3 | RABGAP1L | LRRC16B | BMS1P6 | GSTZ1 |
| HYKK | GPR176 | FAM212B | MIR4515 | ERLIN1 | ORC6 |
| IFT140 | CCDC82 | DRAP1 | MLST8 | CCDC88C | ZNF174 |
| ASH1L | ATE1 | SUSD4 | CENPL | RAPGEF3 | ZNF689 |
| UBC | RNLS | FAM24B | ATF6 | TMEM219 | RIC8A |

| | | | | | |
|--------------|------------|--------------|--------------|----------|--------------|
| BLOC1S6 | LRFN4 | SH2B1 | TROAP | AP1G2 | ACADSB |
| ZBTB1 | ENO4 | FRMD6-AS1 | PRDM2 | POU2F1 | NME7 |
| ASUN | ST8SIA1 | SLC39A9 | IDH2 | MYO9A | ARID4A |
| RNASE4 | B9D1 | MSTO2P | POLDIP2 | CYP1A1 | ZNF641 |
| DYRK3 | SEZ6L2 | CHST15 | CDC123 | GLUD1P7 | FTO |
| NRP1 | VAV3 | SNHG10 | CFAP43 | MIEF2 | CNTROB |
| AP5M1 | TIMM8B | EXOC5 | ZFP3 | RNF166 | SCO1 |
| CCDC84 | METTL15 | NUP107 | RSPRY1 | LCOR | DDX12P |
| PANK1 | CORO1B | NDUFV1 | APEX1 | OGFOD1 | CDC42BPB |
| TNKS2 | LINC01134 | PEX5 | CTDNEP1 | IQCH-AS1 | SP7 |
| PAPSS2 | HEXA-AS1 | SLC16A13 | ST20 | CYLD | MFGE8 |
| SPATA7 | NFKB2 | METTL18 | TLE3 | KATNAL1 | CFL1 |
| ZNF697 | MAP4K5 | ZNF487 | MASTL | L2HGDH | ANKRD13D |
| GNB5 | RGS10 | ARHGAP42 | SLC38A6 | CCDC77 | SRM |
| SF3B3 | BAHD1 | MUTYH | SEMA4B | SEMA6C | POLG |
| RRN3 | KIAA0391 | MAPK8IP3 | C1ORF174 | COA6 | CCDC184 |
| TIMM23 | SLC25A11 | FAM21C | HAUS2 | SNHG12 | GLOD4 |
| FAM173A | ATP2A1-AS1 | FAM149B1 | SPG7 | EIF5A | ALDH9A1 |
| CWC15 | PDE8A | WDR3 | DPP3 | SLC44A3 | WDR73 |
| HPS1 | TMCO4 | STRN3 | VWA9 | IL4R | PFKM |
| MPG | VTI1A | TIMM9 | PPP3CB-AS1 | ATF3 | LRRC8B |
| RECQL | ATG13 | STX8 | FBRS | ALDH3B1 | ZCRB1 |
| ZEB1-AS1 | BMS1P4 | CENPBD1 | TMEM116 | LCMT1 | LOC102606465 |
| CIB1 | FUT8 | LOC100506023 | SPSB3 | INPP5K | TLCD1 |
| ZNF438 | ZNF32 | PEX11A | RAB26 | INSM2 | GEMIN4 |
| EMC7 | CRIP2 | RPL36AL | DDB2 | WARS | FAM86C2P |
| UBL7-AS1 | THNSL1 | RNF31 | PRKG1 | TP73-AS1 | SOCS2-AS1 |
| LOC100289511 | MIER1 | KIF1C | ENTPD7 | ARL3 | FUK |
| ASCC1 | ATG2B | SCNM1 | HES4 | MRPS34 | SEPHS1 |
| GPATCH2 | RASAL2-AS1 | CNOT2 | PRPF40B | TXNDC16 | TIGD7 |
| FAM118B | BRMS1L | DHRS4 | MRPS16 | TNFAIP1 | NSMCE1 |
| LOC101559451 | ANXA11 | GTF3C1 | CDC42SE1 | AK7 | ZKSCAN2 |
| DGKH | SLC22A17 | IKZF5 | CINP | DNAH2 | DPH5 |
| JRKL | SNX29 | FZD8 | PEMT | ERAL1 | NARS2 |
| NUDT16L1 | VPS26B | DCAF4 | LOC100130950 | INPP5F | UBFD1 |
| EHD4 | USMG5 | CAMTA2 | CEP57 | HTR7P1 | CDIP1 |
| RPA1 | DHRS4L1 | SLC19A2 | MESP1 | POMP | PSMA3-AS1 |
| DPP8 | BMPR1A | CCDC7 | KTN1 | SPG21 | ATXN7L2 |
| CHFR | FAM65A | METTL9 | LOC100130987 | PRMT5 | ARHGAP11A |
| RAD9A | BBS4 | PLA2G15 | EPC1 | PDCD11 | SETD3 |
| PLEKHH1 | RBM23 | STAT2 | LOC101929099 | PCSK7 | WDR20 |

| | | | | | |
|------------|-----------|--------------|--------------|-----------|------------|
| SRCAP | LOC399815 | RITA1 | C16ORF58 | GPAM | DCAF5 |
| WEE1 | DDHD1 | STT3A-AS1 | ECD | CDCA3 | KRTAP5-AS1 |
| TMED8 | NEURL4 | PHB2 | IQCC | WBP11 | ACTN1 |
| CDC14A | ARF1 | RANGRF | VPS11 | ATN1 | ENTPD5 |
| ZSCAN2 | SHPK | FAM21A | KIAA0319L | C10ORF131 | AP4B1 |
| PBLD | MAP3K11 | FERMT2 | LINC00612 | ZNF511 | KDM4A-AS1 |
| HEATR5A | CTNNBIP1 | FLII | C15ORF39 | SSH1 | NPC2 |
| PRSS22 | BHLHE41 | C16ORF62 | BANF1 | PPP2R3C | FAM69A |
| TBL3 | FBXO34 | PER3 | RAB5B | RHBG | ERC1 |
| HELLS | MYH10 | GTPBP4 | C14ORF132 | TIMM10B | DCTN5 |
| FHAD1 | COPS3 | FBXO18 | PAPOLA | COPS7A | PWP1 |
| NBL1 | SLC36A4 | DDX24 | CEP104 | APAF1 | SFXN3 |
| CREM | CKAP2 | NR4A1 | SFXN2 | GLMN | FGFR10P2 |
| TUFM | C16ORF13 | POLR3K | LINC01465 | EDRF1 | ELMSAN1 |
| C17ORF100 | GSG2 | ZNF839 | ERI2 | UEVLD | LINC00933 |
| SRP54 | MIR762HG | CHCHD1 | AGL | C15ORF40 | RELT |
| MYL6B | COG7 | LZIC | AMN1 | DFFB | DTL |
| CAPN15 | PML | FKBP2 | SPEN | APBB1 | PAN2 |
| GID4 | RRN3P3 | WDR37 | FAM161B | SZT2 | FCF1 |
| BTBD7 | VPS53 | COQ10A | TRIM45 | SCARB1 | MTHFD1 |
| ARID3B | SLC35A3 | DRAM2 | RPS2 | SPATA41 | CHD9 |
| DECR2 | ZNF286B | YIF1A | TMEM199 | GAS5 | LRRN2 |
| THAP10 | C11ORF24 | LINC00235 | HERC2P3 | ZNF276 | ELMOD1 |
| BCAS2 | POP5 | PHF13 | PTGR2 | DAD1 | S100BPB |
| VANGL1 | ANKS3 | KAT6B | LIN52 | RHOD | SMPD1 |
| RABGGTA | PHC1 | CLCN6 | MEX3A | OGFOD2 | FRRS1 |
| HOMEZ | ARG2 | PELI2 | PARP6 | FAN1 | STT3A |
| CYP46A1 | VWA8 | MOAP1 | MIR4687 | DDX54 | ALG9 |
| LYSMD4 | CNNM2 | ANKRD16 | LOC101928118 | SARNP | PIGB |
| TRAP1 | ATAD1 | TRIM8 | TMEM251 | SERGEF | EIF3I |
| DHRS1 | MAX | RB1 | CAPZA1 | TRMT61A | PRH1-PRR4 |
| TM9SF3 | RER1 | LOC100134368 | MGAT2 | TAF10 | MIR3178 |
| LRR1 | LINS1 | ECE1 | COPS2 | ZNF485 | INF2 |
| COX10-AS1 | NEO1 | TIMM23B | MLF2 | AMIGO1 | RASSF10 |
| WAC | TM2D3 | RTCA-AS1 | SLC25A28 | DNAL1 | ST3GAL3 |
| TDP1 | ZBTB25 | TOX4 | SLC41A1 | LIMA1 | ZMPSTE24 |
| HERC2 | PARK7 | APITD1-CORT | SASS6 | RPS6KL1 | SMG7-AS1 |
| CSGALNACT2 | AKIP1 | ACYP1 | ERCC6-PGBD3 | NFYC | MIR135B |
| MIS12 | ZNF18 | CISD1 | PPME1 | AREL1 | CEP83 |
| MCU | CCS | NUDT8 | PPP2R5C | RNF40 | MED8 |
| KDM8 | TAX1BP3 | SEC61A2 | CEPT1 | ARHGAP12 | BLOC1S2 |

| | |
|----------|--------------|
| PRDX6 | LOC101927765 |
| ARID2 | OSBPL9 |
| PLBD1 | ACOT2 |
| C12ORF65 | MPHOSPH9 |
| MRPL37 | SNORD46 |
| TPI1 | PPOX |
| CD27-AS1 | AKAP5 |
| C1ORF43 | ACAP3 |
| EXT2 | STX4 |
| ADCY6 | RAD51-AS1 |
| BCCIP | TMEM8A |
| RHNO1 | TMC3-AS1 |
| IMMP1L | C14ORF1 |
| TAPBPL | |
| ZFYVE27 | |
| GTF2H1 | |
| ISCA2 | |
| YIPF1 | |
| RAB15 | |
| HYOU1 | |
| KLHDC9 | |
| SH2B3 | |
| ZNF408 | |
| POC1B | |
| CDK2AP1 | |
| DENND2C | |
| B4GALT2 | |
| RPUSD1 | |
| SEC23A | |
| EDARADD | |
| RAD51 | |
| KIF20B | |
| LAMTOR2 | |
| WDR90 | |
| RUSC1 | |
| MIR1282 | |
| ZPR1 | |
| SNORD59A | |
| IPMK | |
| ARAP1 | |
| ANG | |

APPENDIX F. ASH2L knockdown RNA-seq results.

RNA-seq results following knockdown of ASH2L with two shRNA constructs (275 and 276). Sequencing read count data for each knockdown sample was compared to read count data for LacZ control. Genes were ranked by negative \log_2 Fold Change from control and can be found at

https://www.researchgate.net/profile/Jamie_Mills2/publications. File ASH2L 275 knockdown RNA-seq DOI: 10.13140/RG.2.2.36445.20967 and file ASH2L 276 knockdown RNA-seq DOI: 10.13140/RG2.2.23652.58249.

APPENDIX G. Gene lists and ToppFun analysis: ASH2L knockdown RNA-seq downregulated genes.

The 3,278 genes in common between the two shRNA constructs, corresponding to **Figure 3.4-A**, are reported below and ToppFun analysis on these genes can be found at this link: https://toppgene.cchmc.org/output.jsp?userdata_id=4af8986f-347e-45e2-81e8-d235a39427ed.

| | | | | |
|--------------|------------|-------------|--------------|---------|
| PGLYRP2 | PAXBP1-AS1 | RASL10B | PEG10 | C14orf1 |
| HTR6 | STX2 | FBXO38 | LOC102724933 | FAM193A |
| CAPNS1 | MBD3 | FAM90A1 | FBXO3 | FAM35A |
| PRKACA | GATSL3 | DRAP1 | FBXO5 | MRPS30 |
| ZNF19 | MCRS1 | SP2 | BSN | SH3BGRL |
| DHDH | BMP8A | SP4 | ATXN7L3 | MRE11A |
| ZNF14 | ZNF76 | SP3 | MT1A | PEX10 |
| ZNF16 | SKI | KCNK5 | CRISPLD2 | PDCL3 |
| SIGIRR | KCNG1 | APIP | SUB1 | FAM195B |
| VOPP1 | PDCD5 | SPDL1 | FLYWCH2 | KCNS3 |
| SF1 | MSI1 | NEO1 | CERKL | TACC3 |
| SHMT1 | MSI2 | CERS6 | DHX9 | HDGF |
| NPRL3 | FBXO24 | DHPS | ZBTB2 | RAD1 |
| ADAMTS15 | FADS2 | VPS13B | NEU4 | INPPL1 |
| ADAMTS13 | NEK2 | CCDC183-AS1 | RACGAP1 | IGF1R |
| PRPF38A | MAP3K6 | UHRF2 | FAM192A | TGM1 |
| TMEM254-AS1 | KCNH1 | UHRF1 | NTNG1 | PPIP5K2 |
| ZNF34 | FBXW4 | SRF | BBS1 | FAM198B |
| FRG1B | PIAS3 | LRTM2 | XBP1 | IGFLR1 |
| DHFR | MSH6 | MLLT1 | SPDYC | ENPP1 |
| LAS1L | MSH2 | U2AF1 | LOC100506990 | TGM3 |
| STRN | PKP4 | SRR | MC1R | CARD10 |
| SFXN2 | MIR210HG | KCNJ3 | FBXL3 | ZGRF1 |
| SFXN5 | BLM | NOP58 | LOC100505666 | ADAM11 |
| KCNC1 | IREB2 | GSTZ1 | APOBEC3B | SDHC |
| LOC100288181 | FBXO45 | NECAP1 | MRPS11 | DENND6B |
| KCND2 | FBXO46 | BRE | DMBX1 | GRK1 |
| KCND3 | C6orf25 | ST7 | RAC3 | GYLTL1B |
| BGN | FBXO43 | KCNK1 | LINC00052 | GRK6 |
| MMP16 | NPAS1 | SLC23A2 | PRPF40B | PIBF1 |
| RAPGEF5 | FBXO41 | SLC23A1 | CACYBP | SDK1 |
| GTF2H2B | NEK8 | CCP110 | PITPNM3 | IFT22 |
| PKN3 | NEK4 | LGALS4 | FAM193B | TAT |
| CCM2L | API5 | LGALS1 | MICU2 | IFT52 |

| | | | | |
|---------|-----------|---------------|--------------|--------------|
| GRM2 | MEX3A | C1orf189 | GLOD5 | COPG2 |
| GRM8 | CDKN1C | FKBPL | BCOR | NUPL1 |
| MYBL2 | SETD4 | SKIDA1 | TCERG1 | LOC100294145 |
| CA8 | SETD5 | LEMD3 | ZMYND8 | SPPL2B |
| MYBL1 | SETD2 | FKBP7 | MKI67 | ROGDI |
| EEF1G | CDKN1B | FKBP3 | KIAA0930 | C3orf67 |
| ELF2 | SETD6 | FKBP5 | NFU1 | EME1 |
| ELF4 | ASH2L | CNP | TANGO6 | EME2 |
| ZMYND10 | FGD5-AS1 | C1orf167 | CPT1C | GBAP1 |
| ZMYND11 | MTG2 | COPS6 | NIF3L1 | IL11RA |
| SHANK3 | TK1 | MTL5 | UHRF1BP1 | ACYP1 |
| IFT74 | RRP15 | C1orf159 | STRIP2 | MBNL1-AS1 |
| MTA1 | DENND2D | MCM7 | GSE1 | TIMELESS |
| OXCT1 | ZSCAN5A | ZC3H4 | ARGLU1 | PMEL |
| MVB12B | ASH1L | C1orf131 | C6orf99 | ISYNA1 |
| MVB12A | COPZ1 | MCM8 | GBAS | GSTCD |
| TDH | CIT | COL14A1 | C12orf75 | ALOX15 |
| RRM1 | MTF1 | MCM9 | CAB39L | PMF1 |
| RRM2 | RARA | ZC3H6 | SLC35F4 | CAMSAP1 |
| WARS2 | ANGPTL2 | SYNE4 | SIPA1L2 | EMG1 |
| CCS | RCCD1 | TRO | C6orf48 | UBB |
| CD9 | GAS6 | CEP170B | SIPA1L3 | ZMAT5 |
| SLIRP | EXOC2 | PRKG1 | GSG2 | LONRF1 |
| FRMPD4 | PLIN5 | ESPL1 | ZYG11A | LONRF2 |
| ELK1 | NFIX | MCM3 | LOC101927934 | CPSF7 |
| RRP9 | C1orf192 | MCM4 | HEG1 | CPSF6 |
| MTBP | METTTL21A | MCM5 | SCAND2P | DAK |
| ALCAM | PAPSS1 | MCM6 | CALML3-AS1 | DIAPH3 |
| PRKCI | MINOS1 | MCM2 | SDCCAG8 | PXMP2 |
| DNAAF3 | CDKN2C | DKFZP586I1420 | DTYMK | PXMP4 |
| SDSL | MOCOS | HDAC4 | TYMS | ZCCHC4 |
| NUP85 | ELP5 | HDAC2 | EMC1 | FGFR3 |
| VPS16 | ELP6 | HDAC3 | EMC6 | ZCCHC3 |
| ST3GAL3 | NFIA | DGCR11 | NOP14-AS1 | ZCCHC2 |
| PLK4 | NFIB | HDAC1 | NFYA | THRA |
| BTF3 | C1orf174 | TULP3 | FAM46B | DBI |
| C3orf18 | TNC | TTK | MTX2 | RBM3 |
| PLK3 | OIP5 | TENC1 | NFYB | HEPH |
| PLK1 | GTF2I | HDAC6 | C6orf57 | DCK |
| MEX3D | KCMF1 | VPS52 | RSG1 | ZAP70 |
| C3orf14 | MAP2K4 | C1orf106 | PRKRA | RBL1 |

| | | | | |
|--------------|--------------|--------------|--------------|-----------|
| DCX | SIRT5 | CNTNAP2 | BAIAP2L2 | BCCIP |
| RBKS | EMP2 | NXT1 | EPHA7 | CCND1 |
| NRXN1 | EMP3 | NXT2 | LOC100188947 | C11orf1 |
| DDO | SIRT3 | ATRAID | MXRA8 | C9orf106 |
| NXF1 | F7 | NGRN | ULK2 | CCNE2 |
| POC1A | F8 | MB | DXO | CCNE1 |
| BUB1 | GPRC5A | LINC00337 | MXRA7 | C9orf116 |
| HES2 | CDC42EP4 | MRPL9 | FKBP1AP1 | VCL |
| HES4 | ADSSL1 | LINC00339 | PAXIP1 | RTN3 |
| LOC91450 | CDC42EP2 | DGCR5 | RTF1 | RTN1 |
| DEK | ARF5 | DGCR2 | AARD | KLHL11 |
| PDE10A | TOB2P1 | EMX1 | ART4 | ENHO |
| ATP13A2 | STAU2 | VPS37C | DHX34 | PTPRG-AS1 |
| RBMX | UNG | RAD23A | PCBP2 | CCNB2 |
| MDC1 | GLRA2 | PIK3CA | SWI5 | CCNB1 |
| C22orf23 | UNK | DTL | ARSG | KLHL26 |
| SCAMP5 | FGF14-AS2 | LRP1 | N4BP3 | KLHL22 |
| LOC101927691 | PMS1 | LRP5 | ZBED4 | STT3A |
| EML1 | LRG1 | PRIMPOL | ARSB | STT3B |
| LOC493754 | SERBP1 | CECR1 | RAB11FIP4 | ACTL10 |
| EML6 | RIMBP3 | CECR2 | TH | YWHAE |
| HGC6.3 | HEPHL1 | CECR5 | DHX29 | YWHAB |
| NGEF | PITX1 | OR2W3 | AARS | CHD3 |
| SHOX2 | LAG3 | CECR6 | CETN2 | MEA1 |
| SDR39U1 | PPP1R16A | KATNA1 | CETN3 | PIDD1 |
| C5 | UBE2E1 | TIFA | PCSK4 | FAM178A |
| PRKAR2B | RBX1 | SLITRK6 | ENC1 | C9orf142 |
| PRKAR2A | PFKFB1 | LOC100506844 | DHX15 | SFR1 |
| RSU1 | PFKFB3 | C1orf229 | NCOA5 | DARS2 |
| NETO2 | ARL3 | CNNM3 | IMMP1L | CCNA2 |
| LINC00304 | NTPCR | C1orf226 | GREB1L | RCN3 |
| RPLP1 | BCL2L12 | LINGO1 | FAM172A | SGK223 |
| RPLP0 | SOCS3 | DUT | GCH1 | SFPQ |
| ECSIT | CPAMD8 | BAIAP2 | DEFB132 | PSRC1 |
| TUBA1C | SOCS7 | LRR1 | NEDD1 | TBC1D5 |
| TUBA1B | BRPF3 | EIF4A3 | GLB1L | CHDH |
| PP7080 | LOC100132529 | TONSL | YIPF6 | TBC1D7 |
| HEY2 | MDM2 | UBE2L6 | AUNIP | LOC150776 |
| RPLP2 | FGFR1OP | NUBP1 | TARDBP | PNKP |
| IKBIP | TUBGCP3 | UBE2L3 | MAD2L1 | TAF15 |
| ACTL6A | TUBGCP4 | TXNDC17 | KLHL36 | TAF10 |

| | | | | |
|--------------|-----------|-----------|--------------|-----------|
| C9orf173 | SLCO4A1 | ANKRD24 | CBLN3 | KPTN |
| ASB8 | RNF166 | ESRRG | SLC46A1 | TLDC1 |
| ACIN1 | PCYOX1 | LSM5 | GEMIN8P4 | STAC3 |
| QRICH1 | RNF165 | LSM3 | C21orf2 | DLC1 |
| ASB1 | RPL12 | LSM2 | LOC102724814 | TOMM7 |
| RPL30 | RPL11 | CNOT1 | MCCC2 | CIB3 |
| RPL32 | GPR153 | ZFP62 | MTUS2 | CIB1 |
| RPL34 | RNF138 | TADA3 | CARHSP1 | RDM1 |
| THYN1 | CHN2 | CNOT3 | ASTL | FBL |
| GCSH | RPL13 | SPERT | RRAGB | PTTG1 |
| RPL35 | ANKRD54 | RNF14 | VDAC1 | NUSAP1 |
| ADNP2 | RPL18 | ADRA1A | ZFPM1 | TMEM14A |
| RPL38 | RNF130 | PTBP1 | CBLL1 | TMEM14B |
| RTTN | ABI2 | RPL7A | TSHZ1 | PAM16 |
| RPL37 | ABI3 | DNMT3B | TRMT2B | ARID5B |
| ANKS1B | MSRB2 | PDDC1 | GMCL1 | TMEM134 |
| MED1 | KRT8P41 | WASH1 | NUAK1 | LMX1B |
| RPL23 | ANKRD39 | IQCB1 | NUAK2 | PDE9A |
| RPL22 | LINC00263 | EP400NL | TNRC6C-AS1 | H6PD |
| IFT80 | HJURP | HIAT1 | UBAC2 | DNAJC21 |
| LOC100131138 | DACH1 | DNMT3A | CCDC88B | ZC3H18 |
| IFT88 | GRB14 | ADRA2B | CCDC88A | SUDS3 |
| IFT81 | GRB10 | PTBP2 | CCDC88C | ZC3H13 |
| RPL27 | ANKRD31 | ADRA2A | CLIC3 | ASIC3 |
| RPL26 | ANKRD32 | PTBP3 | GDI1 | ZC3H14 |
| ALG10B | RNF44 | ASPM | OLA1 | DNAJC19 |
| NEDD4L | RNF40 | SNRPA1 | C21orf58 | DNAJC11 |
| PNPO | BSCL2 | EIF4E2 | PRMT6 | HSPA2 |
| RPL41 | CLIP3 | SSX2IP | LINC00174 | DNAJC16 |
| PRRC2B | MELK | GATA3-AS1 | MAP4K1 | FES |
| SLC16A14 | ZFP41 | SMARCD1 | PRMT5 | DLG4 |
| PRRC2A | NHP2 | NLGN2 | LINC00176 | CLASRP |
| TMEM198 | ERP27 | RBBP4 | PRMT1 | HSPB6 |
| SPEF1 | ABHD2 | PUF60 | LINC00173 | FRMD6-AS1 |
| TMEM180 | ABHD1 | RBBP8 | PRMT3 | ELAVL1 |
| PCOLCE-AS1 | OARD1 | RBBP7 | POC5 | DHTKD1 |
| GPR137 | ABL1 | MEST | B3GNT6 | TMEM104 |
| EMD | ANKRD10 | LINC00235 | RPUSD3 | TMEM107 |
| ZC3H10 | ABL2 | RNF20 | B3GNT4 | TMEM109 |
| TMEM173 | ESRRA | SMARCE1 | C21orf67 | PDE4A |
| RNF168 | ANKRD26 | ILF3-AS1 | SGK3 | POLI |

| | | | | |
|------------|--------------|---------|--------------|--------------|
| GUSB | PDGFC | NDC80 | CD207 | CACNA1F |
| POLE | LOC642852 | MCMDC2 | SLC2A4RG | TMEM240 |
| POLH | MAGOHB | FAM208A | SUGP2 | CACNA1H |
| PDE4C | FASN | TSPAN12 | DHRS13 | TMEM241 |
| CTPS2 | SLC25A21-AS1 | TSPAN11 | WFDC6 | C8orf48 |
| RNF208 | CATSPER2P1 | CEP290 | IL20 | SYCE3 |
| CTPS1 | CHAF1B | APAF1 | DHRS11 | SYCE2 |
| ARID1A | CHAF1A | PRPS1 | ZNF587B | TMEM249 |
| UPK3B | ATIC | CDC45 | PABPC4 | TFAP2B |
| PALLD | SMPD4 | ATXN1L | PABPC5 | UBE2C |
| RGS19 | LIN52 | EIF4H | DMC1 | GGH |
| POLDIP3 | SPHK2 | EIF4E | PABPC3 | UBE2A |
| PON2 | POT1 | EIF4B | PABPC1 | SYT7 |
| DBF4B | ACSBG1 | CDC5L | LOC100288637 | HIGD2A |
| STRN4 | XRCC6BP1 | FAM209B | GBA | TMEM231 |
| HSPD1 | ATL3 | TSPAN13 | PCDP1 | TMEM237 |
| POLN | WRB | SYT12 | MGAT3 | UBE2S |
| TSPEAR | ATP5A1 | EIF3L | RELT | UBE2T |
| HSPE1 | LOC100652758 | EIF3I | GCA | LOC730183 |
| MEIS3 | WTIP | EIF3F | EPGN | UBE2N |
| DLK2 | TTC30B | ATXN10 | NUDT7 | MXD3 |
| RGS10 | TTC30A | NUDT1 | MIS18A | FBN1 |
| POMK | SLC27A1 | CDC20 | NUDT8 | MS4A7 |
| RGS12 | GMDS-AS1 | EIF2D | HNRNPA2B1 | DMKN |
| POP1 | ATN1 | EPC2 | OTULIN | RERG |
| TESK2 | PLOD1 | CIRBP | ZFAND3 | SGOL2 |
| F11R | CEP250 | MFSD10 | RPP30 | SGOL1 |
| LOC642846 | CDC25C | CSNK2B | GEN1 | MAN1A2 |
| CAPN10-AS1 | CDC25A | KCTD13 | SLX4IP | LOC100130075 |
| HDGFRP2 | ACLY | KCTD18 | POU3F2 | SPIDR |
| FRS3 | SLC27A2 | EIF1B | TMEM253 | EPN2 |
| RABL3 | DLX1 | KCTD15 | SPOCD1 | TMEM210 |
| CDCA2 | CORO1A | FBF1 | SCNN1G | C8orf59 |
| CDCA3 | CORO1C | OMA1 | TMEM256 | RER1 |
| CDCA4 | IGSF21 | KALRN | SHQ1 | TMEM219 |
| CDCA5 | DHRS4-AS1 | MBTD1 | SCNN1D | AGPAT5 |
| CDCA7 | EIF4EBP2 | XRRA1 | TMEM258 | CASC10 |
| CDCA8 | SLC14A1 | CEP192 | EHBP1L1 | RAP1GDS1 |
| GATA4 | FUS | IFFO2 | PPIH | C8orf82 |
| GATA3 | FUZ | ALDH6A1 | FBN2 | AGPAT1 |
| GATA2 | DDX11-AS1 | CDC16 | CACNA1D | C8orf86 |

| | | | | |
|--------------|--------------|--------------|--------------|-------------|
| TMEM201 | TMSB15B | TTC21B | CISD3 | KANSL1L |
| PABPN1 | CACTIN | CEP112 | RPL18A | MYEF2 |
| TMEM209 | LOC100131347 | LPP-AS2 | PPP2R1A | VAX2 |
| FBRS | FAM213B | SEC16A | KAT8 | RAB11B |
| SSRP1 | TAF9B | CSPG4 | KAT7 | FAIM3 |
| MAP10 | DMTN | WDR1 | SEPHS1 | TATDN1 |
| ANKLE2 | C10orf91 | CEP164 | KRT2 | COTL1 |
| EPS8 | YTHDF2 | LOC101928053 | KRT8 | TRAPPC13 |
| DLEU1 | CSNK1A1 | SNRNP70 | FLT3LG | NANOS1 |
| CDK5RAP3 | C10orf95 | WDR5 | ESCO2 | HRASLS2 |
| CDK5RAP2 | SCAF4 | WDR6 | KRT5 | SHISA2 |
| REV1 | LOC100129046 | TTC23L | MAPK8IP1 | SHISA9 |
| GTPBP1 | ADM5 | RFC5 | SIK3 | ALG10 |
| GTPBP3 | TMEM39B | RFC3 | TLN2 | FANCD2 |
| ZC2HC1C | RAB3A | RFC4 | DNA2 | PRKAR2A-AS1 |
| PLEKHS1 | CEP120 | PLEKHG2 | SPTBN5 | PRPF8 |
| MAP1A | CEP128 | RFC1 | TWIST1 | SCUBE2 |
| PPIEL | SLC8A2 | RFC2 | HTATSF1 | SCUBE3 |
| ANAPC13 | BZRAP1 | TFDP1 | LOC100126784 | RPRD1B |
| SEH1L | SALL4 | TFDP2 | TP53BP2 | RPRD1A |
| CTBP2 | PHYHD1 | MTRF2 | TNRC18 | POU2F1 |
| ACMSD | SLC39A6 | PLEKHH2 | TP53BP1 | EIF2S1 |
| DICER1-AS1 | SLC39A4 | CATSPER3 | CCR10 | POU2F3 |
| BARD1 | PLEKHJ1 | PLEKHH3 | SETDB1 | TLX1 |
| TPRG1 | RARS2 | MTFP1 | LOC81691 | PYCR1 |
| SETD1A | TLE3 | RAB26 | FUBP3 | SOWAHD |
| IRF2BP1 | SUPT16H | RAB23 | FUBP1 | ATP5G2 |
| GP2 | CEP131 | RAB28 | TOP2A | SIX4 |
| IRF2BP2 | SPICE1 | RNGTT | COL18A1 | H2AFJ |
| ADI1 | VRK1 | KRR1 | ZNRF2P1 | SIX5 |
| C10orf82 | VRK3 | FBXL19 | VAV3 | RHBDF1 |
| GMEB1 | ILF3 | CEP152 | PSENFEN | H2AFY |
| GMEB2 | RAB36 | TPRKB | RAB6C | H2AFZ |
| YJEFN3 | RAB37 | FBXL14 | TOP3A | H2AFX |
| KRI1 | EIF4E1B | SNRNP40 | GFRA1 | RHBDF2 |
| TEAD2 | SNRPG | P2RX2 | LIME1 | PPP2R5D |
| TEAD3 | SNRPF | VAPB | MIR17HG | PPP2R5C |
| LOC100133985 | SNRPC | RAB13 | RFNG | TRAPPC6A |
| LOC148709 | SNRPA | PANK3 | ZNF8 | RFT1 |
| TAF6L | CSNK1G2 | TRAF3IP3 | ZNF7 | SKIV2L2 |
| NCOR1 | SNRPB | PPP2R2A | PSMC3IP | COLEC12 |

| | | | | |
|--------------|-----------|-----------|-----------|-------------|
| STOML2 | GGA1 | PPM1L | XRCC5 | AP2B1 |
| MAPK9 | TCOF1 | PPM1N | PPP1R21 | PLEKHA4 |
| MAPK7 | SRSF10 | PPM1J | XRCC2 | DPY19L4 |
| TMEM30B | EXTL3 | PPM1K | XRCC3 | ERCC6L |
| CKLF | SRSF11 | PPM1D | EAF1 | MIDN |
| PGAP1 | LRRC27 | BARX2 | ERAL1 | CLGN |
| PGAP2 | LRRC20 | SH3BP1 | RPL27A | PALM |
| RFX2 | UCKL1-AS1 | LINC01208 | CALM3 | ARID2 |
| PDZK1 | GPR64 | ATP9B | CALM2 | GGT1 |
| RFX1 | RUVBL2 | SH2B2 | PPP1R11 | GPANK1 |
| LOC102724386 | RUVBL1 | SLC12A2 | GPAA1 | DOK3 |
| UQCRC2 | ZFP69B | CYB5B | PPP1R10 | MZF1 |
| NCAPG | MYT1 | NICN1 | KIF14 | PSMD10 |
| NCAPH | SLC9B1 | SLC12A1 | HNF4G | NXPH4 |
| GIGYF2 | SAP30 | MBOAT1 | AP2A1 | DBIL5P |
| HSD11B2 | OLFM2 | RPL23A | BRCA1 | FUT8 |
| FIGNL1 | SLC9A5 | ATOX1 | KIF11 | KIF3A |
| MYO6 | FRMD8 | PRC1 | BRCA2 | NPHP1 |
| RHBDL1 | SAP25 | ZAK | KIF15 | ISOC1 |
| PRRT3 | SLC9A8 | PLEKHB1 | QSOX2 | CAMTA1 |
| PRRT2 | MRTO4 | IFI35 | GRIPAP1 | NPHP4 |
| IL22RA1 | LRRC56 | CCAR1 | LYNX1 | PHF10 |
| PRRT4 | TACSTD2 | TMPO | TMEM198B | PHF12 |
| GPR19 | GPR83 | TMEM194B | ZFR | PAN2 |
| EFCAB4A | CRNDE | TMEM194A | KIF25 | KIF4A |
| HSPB11 | MMP24-AS1 | PAQR4 | KIF24 | PHF13 |
| JPH3 | GPR97 | PAQR5 | KIF23 | PHF19 |
| UPF1 | EFCAB12 | HNF1A | KIF22 | LOC115110 |
| LRRC46 | EFCAB11 | TM4SF4 | NBPF1 | MAST4 |
| PGAM1 | ATP7B | STX1B | KIF27 | AFF3 |
| PGAM2 | ERC1 | PPP1R3C | KIF2C | TMEM191A |
| CCSAP | DNM1L | CD2BP2 | LINC01136 | AFF1 |
| TMC4 | CTNBL1 | L3MBTL2 | STX12 | TIMM17B |
| PTGR2 | PELP1 | PPP1R35 | DERL3 | NCBP1 |
| LRRC41 | SIGMAR1 | ANKRD19P | TMPRSS2 | AZGP1P1 |
| CKS2 | VEZF1 | TSPAN9 | RXRA | PLA2G4B |
| KANK2 | PPM1A | ERI1 | EXOSC9 | MASTL |
| LRRC14 | NT5C3B | ERI2 | EXOSC8 | ZP1 |
| LRRC15 | GIGYF1 | ERI3 | EXOSC3 | SEPT5-GP1BB |
| PELI3 | PPM1B | XRCC6 | EXOSC2 | SAMHD1 |
| GGA2 | GTF3C4 | XRCC4 | MICB | CLN6 |

| | | | | |
|-----------|-----------|-----------|--------------|--------------|
| AURKB | LOC730101 | GTF2F1 | EBF4 | PSPH |
| PARL | TRIP6 | LINC01132 | LOC101929080 | LOC101926888 |
| AURKA | UNC119 | METTL2B | BOLA3 | NPY1R |
| PDLIM1 | RAD17 | DNMT1 | GRWD1 | KCTD3 |
| TAS1R1 | RAD18 | LINC01134 | ALDH7A1 | PDIA5 |
| PDLIM4 | CDC42SE2 | RHOBTB2 | 1-Mar | ADRB2 |
| PDLIM7 | SERPINA3 | LINC01124 | C6orf203 | SEZ6L2 |
| U2SURP | SERPINA1 | SCCPDH | SRPK3 | AGER |
| MAPK10 | SPIN4 | SERINC2 | SRPK1 | DPP3 |
| MAPK11 | SPIN3 | SYCP2 | HBS1L | PDZD4 |
| R3HDM1 | SERPINA6 | PSD4 | FEN1 | ARHGAP20 |
| MBTPS2 | ING1 | HYDIN | DAZAP1 | MYH11 |
| CNTFR | FCRLB | SLC37A4 | RPPH1 | ALYREF |
| IPP | ING5 | NIPSNAP1 | ZMYM3 | IFT122 |
| IPW | TRIM9 | PAPD7 | LINC01023 | ESR1 |
| FDXR | ING2 | RPL37A | RHOH | TDRD3 |
| EARS2 | TRIM6 | SLC24A3 | NME4 | NMRAL1 |
| ACOT7 | CSRP2 | SEMA3C | AP3B2 | SMAD7 |
| TRIQK | C17orf53 | SFTPA2 | IL17RB | ARHGAP33 |
| SERPINF1 | AP3S1 | UNC93B1 | RHOB | ARHGAP30 |
| PASK | CNTD1 | DPCD | RAD51C | DESI1 |
| SYTL4 | NUDT16L1 | AP3M2 | DNASE1L2 | DESI2 |
| NISCH | C14orf169 | CTNNAL1 | LINC01016 | URB2 |
| HOXB9 | C14orf164 | ANKRD30B | RAD54B | DLEU2L |
| ACOT2 | IVD | SEMA4D | PBLD | NT5DC1 |
| ACOT1 | ITPKA | ANKRD30A | KIAA0754 | ERBB4 |
| PRR12 | HSPA14 | RPL35A | KIAA0753 | NT5DC2 |
| PRR11 | BLCAP | CDC42BPB | RAD54L | NCAM2 |
| PRR14 | MZT1 | TPCN1 | LCMT2 | REPS1 |
| ACOT4 | TM9SF1 | RAD52 | ANKMY1 | LGI1 |
| SKA3 | C17orf62 | RAD51 | RANBP1 | KDF1 |
| SKA1 | ATP8A2 | SOGA1 | FLJ30403 | NAP1L1 |
| SKA2 | CLSTN2 | DPF1 | PRSS30P | SHCBP1 |
| FAM160B2 | RTKN2 | DPF2 | DNM1P35 | NAP1L4 |
| RAD21 | TUSC1 | TNS4 | CYP2D7P | FMNL3 |
| HOXC4 | BZW2 | SKP1 | CAMK1 | NUP107 |
| PRR22 | TUBB3 | TNS1 | LY6G5B | ALKBH7 |
| PRR24 | GYG2 | TIPIN | RAB3GAP1 | ALKBH6 |
| SIVA1 | WHSC1L1 | SLC6A16 | CMIP | ALKBH5 |
| LOC284009 | IGFBP5 | SACM1L | ARHGAP40 | CACNA2D2 |
| GLUD1 | IGFBP4 | CMC2 | KNTC1 | CACNA2D4 |

| | | | | |
|--------------|--------------|--------------|-----------|-----------|
| LOC100630918 | TP53I11 | TRIM46 | PTMS | TTC36 |
| MTHFD1 | LINC00993 | E2F2 | PPP3CB | SHROOM4 |
| MTHFD2 | ATAD1 | ZNF865 | PCM1 | PTGES3L |
| SLBP | CASP8AP2 | E2F7 | PPP3CC | POLD3 |
| URI1 | ATAD5 | E2F8 | GIT1 | CYTH2 |
| MEPCE | ATAD2 | TRIM45 | SLTM | POLD1 |
| LYPD5 | SNX22 | CNBP | ARHGEF2 | POLD2 |
| LYPD6 | APEX1 | CABLES2 | PTMA | LINC00910 |
| LOH12CR1 | NCAPD2 | TRIM36 | PCNA | TTC12 |
| ATRIP | RIF1 | TRIM32 | AHCY | TTC18 |
| JAG2 | TMEM167A | TNFRSF6B | COL6A4P1 | TTC17 |
| TOE1 | LOC101928378 | C16orf80 | NOXO1 | POLE4 |
| HEXIM2 | LAPTM4B | ECI2 | FITM2 | POLE2 |
| BTBD19 | THAP9-AS1 | TRIM28 | SLX4 | COL7A1 |
| TEX30 | EFEMP1 | TRIM24 | GRIN1 | ERCC1 |
| NCAPH2 | UGT2B15 | GIN1 | NEK11 | CTBP1-AS2 |
| PBX3 | UGT2B17 | TMEM170B | NUP188 | PRSS1 |
| TEX38 | SRSF2 | SNHG15 | CELSR1 | SMC5 |
| PBX1 | SRSF3 | KEL | CELSR2 | SMC6 |
| FAM111B | SRSF6 | SNHG10 | CELSR3 | SMC3 |
| FAM111A | SRSF7 | TRIM13 | LINC00938 | FAM86FP |
| AGO1 | SRSF9 | C16orf62 | FAM3B | SMC4 |
| NCAPG2 | PKMYT1 | LOC153684 | FAM3D | SMC2 |
| KDM8 | LOC100129534 | ACTR3B | SPINK8 | FAM122B |
| TFCP2L1 | KIAA1524 | WWC2-AS2 | FBXW11 | GJA1 |
| FAM115A | RHPN1-AS1 | APELA | LOC400927 | WDR90 |
| IL18BP | UFD1L | HLTF | CCNB1IP1 | CIRBP-AS1 |
| CASP14 | ECE1 | PCK1 | LINC00925 | KIAA1468 |
| MAMDC4 | AP4M1 | B4GALNT4 | NUP160 | KIAA1467 |
| DUSP5 | GRID1 | PCK2 | LINC00957 | LUC7L |
| RING1 | TNFRSF18 | C16orf59 | LINC00958 | LINC00898 |
| IFT140 | TNFRSF19 | BRI3BP | CNTLN | LINC00899 |
| TEX14 | ZNF878 | POLA1 | NUP155 | PRSS3 |
| AGPS | TRIM58 | POLA2 | PCIF1 | LINC00893 |
| CHST1 | TNFRSF25 | TP73 | LINC00940 | LINC00894 |
| TP53I13 | DCTPP1 | GRIK5 | TTC25 | NUP210 |
| URM1 | TRIM55 | GRIK3 | TNFAIP8 | KNSTRN |
| LOC101927021 | SRSF1 | GRIK4 | LMNB2 | WDR76 |
| AGR2 | MTHFSD | LOC100129518 | LTB4R | HCFC1 |
| AGR3 | ARL13B | MTMR9LP | LMNB1 | ADCY9 |
| LINC00997 | E2F1 | LOC100996693 | MKL2 | ARMC3 |

| | | | | |
|--------------|--------------|--------------|-------------|--------------|
| NUP205 | MAMSTR | ZNF764 | MLEC | CCDC28B |
| WDR62 | TPM1 | PAAF1 | TMEM184B | CNDP2 |
| WDR65 | THOC1 | CKAP2L | PUM1 | LIG1 |
| LOC101927100 | THOC3 | CTDSPL | TRIM52-AS1 | TMEM9B-AS1 |
| GJC3 | CHD1L | SMC1A | SMU1 | LIG3 |
| NCSTN | THOC2 | C1QL4 | TPX2 | MATR3 |
| BLOC1S1 | THOC6 | ZNF75A | RPS25 | TCTEX1D2 |
| BLOC1S3 | ZNF799 | SMC1B | RPS28 | LOC440028 |
| PLAC1 | C2orf96 | DNAJC1 | ADCK2 | CDH24 |
| FDFT1 | BZRAP1-AS1 | NPEPL1 | RPS29 | TCTEX1D4 |
| WDR52 | GLT8D1 | CTDSP1 | ZNF813 | NONO |
| WDR54 | HMMR | DNAJC9 | RPS20 | ZSCAN2 |
| WDR60 | LOC101593348 | FGL1 | RPS23 | GPSM2 |
| MKS1 | ORC5 | PDHB | DCP1B | LOC100506022 |
| SMG6 | ORC4 | ZNF749 | C2CD3 | TOPBP1 |
| LINC00853 | ORC6 | LOC100130417 | ZCCHC17 | IQCC |
| HELLS | FGGY | ZNF747 | ZCCHC14 | RPS3A |
| WDR37 | ORC1 | HN1L | LRRCC1 | IQCD |
| WDR33 | UBR7 | KIAA0101 | ZCCHC24 | IQCG |
| KIFC2 | ORC3 | MFAP3 | PARP1 | IQCH |
| KIFC1 | UBR5 | UMODL1 | PARP2 | IQCK |
| ZNF724P | ZNF789 | PARS2 | ZDHHC12 | RABEP1 |
| FAM129A | FANCI | RPS15 | GP1BA | FCHSD2 |
| ADCY3 | CHTOP | DYNLL1-AS1 | WIBG | DDAH1 |
| ADCY1 | OSBPL6 | RPS14 | FYTTD1 | OAS3 |
| FGD1 | COA1 | RPS16 | AMIGO3 | AKT1S1 |
| SLC17A9 | FANCM | RPS19 | NOL9 | CDH13 |
| PPP1R7 | FANCL | RPS18 | EPPIN-WFDC6 | THOP1 |
| USP1 | FANCA | PDK3 | DRP2 | ATP1A4 |
| PCGF1 | FANCC | RPS11 | PURA | ATP1A3 |
| RSPH4A | FANCB | BRICD5 | PDPR | LIN9 |
| WDR18 | FANCG | RPS13 | GINS1 | ATP1A1 |
| LOC101928491 | FANCF | RPS12 | GINS2 | LOC100507373 |
| VMA21 | LHX2 | CRNKL1 | GINS3 | OGFRL1 |
| PCYOX1L | LHX1 | SRRM1 | GINS4 | CHSY1 |
| PARK7 | ZNF775 | NEIL3 | MLH1 | SUV420H2 |
| PPP1CC | DDX11L2 | CSTF3 | AIG1 | NSDHL |
| IPO9 | UFSP1 | RPAP3 | GRHL2 | SAMD14 |
| RIMS3 | UBTF | FXR2 | MPHOSPH9 | SAMD15 |
| HMCES | PHACTR1 | CHTF8 | ZWILCH | LIPJ |
| SLC26A10 | ZNF765 | WBSCR27 | LGALS8-AS1 | DAXX |

| | | | | |
|--------------|-------------|----------|--------------|----------|
| STARD7 | KPNB1 | SLC25A14 | COMMD3 | SNORD88B |
| AKIP1 | ZNF672 | C2orf81 | COMMD6 | ARHGEF39 |
| PADI2 | ZNF670 | ZNF624 | COMMD4 | HMGA1 |
| PARPBP | RNASEH2B | SLC25A22 | CSDE1 | BMP7 |
| OAZ3 | CPB2 | MMAB | C2orf16 | TAB2 |
| HMGXB4 | RNASEH2A | FOXJ3 | THRIL | TAB1 |
| INCA1 | PEF1 | SLC25A39 | USP27X-AS1 | RBM25 |
| ERLIN1 | TROAP | ZNF619 | RABGAP1 | NAA40 |
| ERLIN2 | MAZ | ZNF618 | CCDC104 | RBM26 |
| SASS6 | FOXO6 | SLC25A33 | DOT1L | HMGB2 |
| TRAM2-AS1 | THADA | PVRL1 | PGRMC1 | PSIP1 |
| FGFBP3 | GLIS2 | SLC25A35 | HEATR2 | ATP2A1 |
| ELOVL5 | STK31 | LPGAT1 | HEATR4 | HMGB1 |
| ELOVL2 | NPAT | FOXI3 | NPM1 | SEC61A2 |
| LOC101928103 | STK35 | ZDHHC6 | MOK | BCL7C |
| HIST2H2BE | ZNF668 | ZDHHC4 | LOC100129722 | BCL7B |
| SUMF1 | ZNF665 | FOXH1 | ALDH4A1 | ZNF385C |
| SLC29A4 | MCC | THAP3 | FKBP1A | ZNF385B |
| SLC29A2 | STK24 | ZNF718 | PER3 | RBM33 |
| TFAP2A-AS1 | STK25 | ZNF717 | ESYT1 | HS3ST3B1 |
| PROCA1 | SCGB3A1 | THAP7 | FOXA1 | ARHGEF10 |
| FSTL3 | ARHGAP11A | ZNF714 | CCDC167 | RBM17 |
| RECQL4 | CELF1 | TMEM87A | MPG | RBM14 |
| C7orf34 | MCM10 | DSN1 | SNIP1 | DYNLT1 |
| YLPM1 | NRARP | ZNF701 | OSR2 | ARHGEF19 |
| STXBP5L | SQRDL | ZNF700 | CCDC159 | PEX1 |
| MPLKIP | FOXM1 | RIMKLB | CCDC157 | PEX7 |
| ZNF696 | CAPZB | RBM10 | PCOLCE | LPHN1 |
| PECR | MDK | INTS2 | RPGRIP1L | SPOPL |
| NRROS | SUMO3 | INTS7 | UTP11L | NAA35 |
| CSE1L | ZNF649 | RCOR2 | NPNT | RBM23 |
| FAM228B | MYADML2 | RCOR1 | WBP11 | RBM24 |
| SLC16A8 | SUMO2 | SUV39H2 | CCDC151 | RBM22 |
| SLC25A42 | ZNF646 | DOC2A | CCDC150 | RBM4B |
| ZNF687 | ZNF644 | SUV39H1 | CCDC142 | BSN-AS2 |
| KPNA2 | SLC25A15 | CCDC125 | RBM8A | CCDC183 |
| PRPF4B | DBF4 | BMI1 | ARHGEF26 | CCDC170 |
| FAM227A | SLC25A17 | PEPD | CCDC148 | FAM98C |
| ACAP3 | LAMTOR5-AS1 | UTP14C | FAM95A | TAF6 |
| MAK | ZNF639 | FOXD2 | ZFHX2 | THRSP |
| KIAA1731 | SLC25A10 | CCDC114 | CCDC138 | NAA16 |

| | | | | |
|--------------|--------------|----------|----------|-----------|
| TAF4 | DISP2 | ZNF608 | CDK5R1 | LRRC14B |
| CPVL | NCL | RUSC1 | NRK | SPIB |
| CCDC173 | ZNF557 | ZNF606 | NRM | KIAA1107 |
| CCDC171 | NUTM2D | CHEK2 | NRL | C14orf79 |
| MYB | ZNF551 | CHEK1 | NUCKS1 | SYNGAP1 |
| MS4A14 | GLO1 | ARL6IP6 | TOMM20 | RAVER1 |
| LOC100507144 | GLB1L2 | RECQL | CHCHD7 | AKT1 |
| SARNP | PHF21B | FLJ37453 | DLG5-AS1 | LINC00536 |
| PIH1D2 | STIP1 | PFN4 | TOMM34 | PKNOX1 |
| NHLRC1 | ZNF876P | PFN1 | PREPL | GTSE1 |
| CDKN2B-AS1 | ZNF549 | C19orf40 | CTTNBP2 | MNX1 |
| PSMG3-AS1 | CYP4F12 | C19orf43 | LTBP4 | TSTD1 |
| NR2C2AP | CHERP | C19orf48 | CPLX3 | SKAP1 |
| NSUN5P1 | LOC101928292 | C19orf44 | ENKD1 | CRABP2 |
| F8A1 | ZNF534 | PATZ1 | TBCB | DOCK9-AS2 |
| FZD8 | PCNXL3 | FIS1 | TBCA | RNF219 |
| PA2G4 | NES | C19orf54 | TBCK | PLA2G6 |
| PPP5C | PCNXL4 | SS18L1 | MRGBP | RHOT2 |
| PLCH1 | ZNF530 | C19orf55 | CXCL9 | RNF214 |
| CDK12 | C19orf66 | SNHG5 | DOCK7 | C14orf93 |
| GLI1 | ASB16-AS1 | ZWINT | GAS6-AS2 | LINC00552 |
| PFAS | C19orf68 | C19orf57 | GAS6-AS1 | NR2F2 |
| GLI3 | ZNF525 | MYL6B | EGFL6 | CYP4F8 |
| PITPNA-AS1 | C19orf71 | PRPF19 | NS3BP | AIF1L |
| PLCB3 | LOC646719 | MTERFD1 | SENP1 | ZNF496 |
| PLCB1 | LCA5L | CCHCR1 | HSH2D | DDX12P |
| PLCB2 | SMDT1 | MIR4263 | TRNP1 | ARHGAP1 |
| ASAH1 | ZNF519 | KREMEN1 | LUC7L3 | MED19 |
| LOC101929567 | SCGB2A1 | KREMEN2 | MNS1 | MED16 |
| ZNF592 | GLS2 | KRT32 | DOCK2 | MED18 |
| CARD9 | LOC100128361 | PACS2 | DOCK1 | MECP2 |
| SAAL1 | PAXIP1-AS1 | KRT38 | LUC7L2 | MECOM |
| LRPPRC | NHS | KRT37 | TSEN34 | DLGAP5 |
| RFWD3 | UGGT2 | MIR5587 | NXN | ZNF486 |
| ALMS1 | UGGT1 | ZNF137P | TUFT1 | RMI2 |
| TRMT6 | PLCL2 | DCPS | LTC4S | RMI1 |
| ZNF574 | MND1 | AAMDC | KLRG2 | JOSD2 |
| PHLDB1 | METAP1 | CA12 | CMTM4 | BAZ1B |
| NBN | ARL6IP1 | KRT19 | CMTM6 | MED22 |
| ZNF566 | C19orf25 | KRT18 | TICRR | MED25 |
| PHLDA1 | SOX2 | TRIP13 | CMTM1 | MED20 |

| | | | | |
|-----------|--------------|--------------|--------------|------------|
| L2HGDH | NUDT12 | NAF1 | NUDCD1 | GPRIN1 |
| ZNF473 | ZCRB1 | LINC00565 | MIS18BP1 | EEF1A2 |
| ODC1 | KHDRBS1 | ITGA9 | CHAMP1 | TBC1D24 |
| CENPA | LOC285847 | ZNRF1 | LOC100506548 | WDFY1 |
| CENPC | SMYD5 | ZNRF2 | SREBF1 | C1orf74 |
| NEURL1B | AGAP11 | ZNRF3 | DUS2 | UBIAD1 |
| EXOSC10 | GMPS | HNRNPA1 | KIF9 | PKDCC |
| PRR14L | TNRC18P1 | HNRNPA0 | DEPDC1 | TCF7 |
| ZNF467 | SLC9A3R1 | HNRNPA3 | DEPDC5 | PKD1P1 |
| ZSWIM5 | HNRNPDL | CYP4B1 | GNAI3 | TBC1D13 |
| CENPU | ZNF428 | TBX6 | GNAI1 | TBC1D17 |
| CENPW | BRIX1 | HNRNPAB | GNAI2 | VIL1 |
| WNT7B | SMYD4 | SUCLA2 | RANBP3L | NAT8 |
| KIAA1161 | SMYD3 | NAGS | PNMA1 | NASP |
| CENPE | NAE1 | MYO1G | TCEB3 | UBXN11 |
| ABCB10 | NADK | SMARCB1 | TCEB1 | HOOK2 |
| CENPH | ODF2 | CRKL | RIBC1 | HOOK1 |
| ETNK2 | RABL2A | OPHN1 | RIBC2 | ALPL |
| CENPI | RABL2B | SNRPD1 | CAP2 | TCF4 |
| CENPJ | ARPC4 | CPNE3 | NOL4L | TCF3 |
| CENPK | NACA | SNRPD3 | TCEA3 | AMOTL1 |
| TAOK2 | ZNF415 | SPA17 | TTC3 | DNAL4 |
| TSR2 | CNTROB | SCAPER | RTN4IP1 | DNAL1 |
| CENPL | MIPEP | CCDC78 | CAPS | GALK1 |
| CENPM | ITGB1 | ALG6 | CRTC1 | HP1BP3 |
| CENPN | ISY1 | ACTN1 | C1orf56 | FBXL19-AS1 |
| CENPO | RMND1 | KCNK12 | LOXL3 | WHSC1 |
| CENPQ | ITGB2 | ACTN4 | BUB1B | NAV2 |
| CRAT | ITGAL | UNC93A | TTF2 | TTI2 |
| CDKN3 | NRGN | FAM76B | ACTG2 | TTI1 |
| TAF1A-AS1 | LOC728752 | CCDC87 | LOXL1 | ACTA1 |
| EXOC3L1 | EXO1 | LOC100129931 | ACTG1 | VIMP |
| EXOC3L4 | PPP6R3 | SEC14L2 | NR3C2 | FAM72B |
| GMNN | LOC100130992 | BRIP1 | EEF1B2 | OTUB1 |
| CASC5 | TMEM255B | EGR3 | AMMECR1L | RNF8 |
| CASC2 | ACTR5 | RANBP17 | TBC1D31 | ASAP2 |
| CASC3 | SPTB | WDYHV1 | NRTN | GNG3 |
| ZNF446 | MMS22L | TSPEAR-AS1 | TEKT5 | GNG4 |
| NUDT15 | LRTOMT | NOL11 | MORC4 | TRA2B |
| NUDT13 | ITGA7 | THTPA | CASK | GNG7 |
| ZNF443 | UGT2B4 | NANP | EEF1A1 | DNAI1 |

| | | | | |
|--------------|-----------|-----------|--------------|--------------|
| EYA3 | LOC283335 | CCDC12 | ZGLP1 | CHMP4A |
| MYO15B | ABCA17P | CCDC15 | POLR3H | MF12-AS1 |
| OTUD3 | ELMOD3 | LOC54944 | LINC00467 | PXN |
| GPATCH2 | GNL1 | TMEM132A | ISCA2 | HRH3 |
| XYLT2 | COL2A1 | PHKB | PNN | CLSPN |
| HNRNPU | TCP1 | MIR614 | DENR | FAM83D |
| LOC101927560 | C18orf54 | REEP5 | METTL1 | FAM83A |
| ADARB1 | ADRBK2 | REEP2 | HSD11B1L | CBX7 |
| ADARB2 | NSD1 | CNIH2 | CIRH1A | CBX6 |
| FGFRL1 | ABI3BP | DIDO1 | C2CD4C | CBX5 |
| DHRS4L2 | ZNF347 | AMD1 | MAATS1 | CBX4 |
| DDX11 | FARP2 | ADAMTS4 | ZRANB3 | CBX3 |
| FNDC3A | FARP1 | PSTPIP2 | LOC728819 | TRPV1 |
| RHNO1 | NR1H3 | EMILIN1 | RAET1E | EIF3IP1 |
| MCMBP | DHRS2 | CEBPA-AS1 | RAET1K | CAPRN1 |
| CEP78 | ZNF33A | CCDC34 | RNPS1 | TRPV4 |
| PRELID2 | CEP41 | HAUS4 | HEPACAM2 | CHMP2A |
| AFAP1L2 | ZNF331 | HAUS3 | XPO1 | SAE1 |
| ZNF384 | CHKB-AS1 | HAUS6 | XPO6 | KLHDC9 |
| NFATC3 | TM7SF2 | HAUS5 | CHMP1A | CBY1 |
| LOC155060 | CYSLTR1 | HAUS1 | TUBB | 8-Sep |
| NFATC2 | ZNF326 | CCDC74B | NHP2L1 | SPRED2 |
| HNRNPL | HMGN2 | CCDC74A | HNRNPH1 | TRPS1 |
| EHD1 | ZNF324 | NOS1AP | HNRNPH3 | CASP2 |
| HNRNPK | C18orf25 | PWARSN | CSTA | 1-Sep |
| HNRNPD | HMGN1 | THSD4 | DCST1 | SAFB |
| HNRNPC | MAGI2 | NSL1 | DCST2 | POMGNT2 |
| FARSB | CXorf65 | TGFBR3L | SLC22A31 | 2-Sep |
| CEP89 | KAT6A | FIP1L1 | MPP2 | IGDCC3 |
| CEP57 | PGP | HAUS8 | PTGES3 | AMTN |
| PHF2 | ZNF317 | POLR2A | XPO7 | PFDN6 |
| NRSN2 | TSSK6 | ASTE1 | LHFPL1 | LOC100506499 |
| PHF7 | STAMPB | HAUS7 | CT62 | FAM84B |
| ABCC11 | ZNF311 | POLR2B | KDM1A | KDM3B |
| PHF6 | CCDC24 | POLR2F | RBMX2 | PERM1 |
| PHF8 | CCDC30 | POLR2G | BACE1-AS | THBS3 |
| TCTN2 | DVL2 | CCDC77 | LOC100506469 | FAM168B |
| TCTN1 | ZNF304 | POLR2I | NRCAM | UGP2 |
| PBK | CCDC17 | ASCC1 | HADH | PCED1A |
| ZNF367 | CCDC18 | CYP51A1 | PHYH | GNA12 |
| ELMOD2 | CCDC19 | CCDC59 | HMHA1 | KDM4A |

| | | | | |
|--------------|-----------|-------------|--------------|--------------|
| KDM4B | ZNF250 | UBALD1 | SFMBT1 | DCLRE1C |
| KDM4D | PIGO | HAT1 | C9orf37 | CD81 |
| LOC101927550 | PIGP | LOC145783 | SPATA17 | GEMIN2 |
| FAM167B | TMEM52 | ISG20L2 | KIF20A | GXYLT1 |
| CDK2AP1 | MRPL37 | ZBTB17 | KIF20B | BAHCC1 |
| EHMT2 | CTCF | RBPMS | WNK4 | PPFIA3 |
| LOC101928530 | EFCAB6 | ZBTB14 | SLAMF9 | SLC30A8 |
| KRTCAP2 | MRPL35 | GOT2 | IFITM10 | SLC30A1 |
| PPP4R2 | PIGX | ZBTB12 | LRRN4 | ATAD3C |
| PPP4R4 | MRPL42 | MLXIPL | HSPA12A | HNRNPUL1 |
| PSMD3 | EDRF1 | C9orf91 | PAICS | HNRNPUL2 |
| PSMD1 | EFCAB2 | PTPRA | HSPA12B | SLC1A4 |
| ZNF287 | PSMA6 | PIN1 | ANLN | PDS5B |
| WDHD1 | MRPL50 | VPS9D1-AS1 | PTPRS | SLC1A5 |
| RBFOX2 | PSMA4 | SLC25A5-AS1 | FAM57B | H1FX |
| ZNF282 | PSMA2 | ZNF512B | DIRAS1 | PACSIN1 |
| CLDN5 | LRRC9 | FUNDC1 | FAM57A | SUPT5H |
| DDX39A | TMEM106C | HMG20B | TECR | SSH1 |
| PSME1 | PIGK | HMG20A | PTPRK | H1FO |
| ZNF275 | ZNF239 | MIR4664 | BABAM1 | LOC100996447 |
| TTYH3 | PIGM | HSP90AA1 | SPTLC1 | DDX46 |
| ZNF273 | SMTNL2 | HAX1 | RSRC1 | DDX47 |
| TTYH1 | PET112 | SYNPO2L | CCR8 | DDX42 |
| IL20RA | SRRT | ITIH4 | CCR7 | DDX50 |
| IQGAP3 | ZNF518A | MAK16 | CCR6 | NDUFS8 |
| MRPL11 | PSMB4 | PARD6G | CCT3 | NDUFS2 |
| AMZ2 | TMEM67 | NDUFB1 | LOC100128885 | NUP54 |
| ZBTB7B | HAS3 | ZBTB45 | KIF25-AS1 | DDX23 |
| LOC100133445 | FLNA | NTN1 | HSF2 | KDELC2 |
| ABCA2 | FLNB | NTN3 | CAMK2N2 | FAM132B |
| CADM4 | TMCO3 | PARD6B | CCT7 | GALNT2 |
| CADM1 | APITD1 | GANAB | CCT4 | SPATA33 |
| CADM2 | PSMC6 | KIAA1328 | TMUB1 | BUD13 |
| ABCA4 | PSMC3 | FCHO1 | RPA2 | CLUAP1 |
| ABCA7 | ZNF214 | NDUFA8 | KIF26A | NUP37 |
| PSMG1 | SAYSD1 | DONSON | RPA3 | RPL5 |
| ZNF256 | KIAA0895L | PTPN9 | SPC24 | RPL3 |
| EZH2 | ZBTB22 | CCNF | SPC25 | GABPB2 |
| ZNF253 | LOC728554 | FAM53A | LOC643072 | TRRAP |
| PIGU | ZNF207 | SCN1A | DCLRE1B | STMN2 |
| PIGT | ZBTB32 | ZFP1 | DCLRE1A | STMN3 |

| | | | | |
|--------------|-----------|-------------|----------|--------------|
| RPL8 | C11orf82 | CUL9 | DCAF16 | STAM |
| RPL9 | C11orf80 | NOTCH3 | HIRIP3 | HTR7P1 |
| RPL6 | SF3B4 | NOTCH1 | MAL2 | SPRTN |
| STMN1 | SF3B2 | AK3 | DCAF10 | ANP32B |
| DAPK3 | GPS2 | AK7 | PTPN18 | TMCC1 |
| CLPSL1 | AFP | AK8 | SPAG7 | CENPBD1 |
| ASF1B | BCLAF1 | AK9 | SPAG5 | BAP1 |
| TSPYL5 | C11orf73 | DSCR3 | SPAG6 | KLLN |
| NOLC1 | RPS3 | C11orf30 | NFASC | TRAM2 |
| LOC101928674 | LINC00634 | CLEC7A | IMPDH1 | PPCDC |
| ZNF143 | BRD9 | NACC1 | MGAT4A | HINT2 |
| ACD | RPS2 | MPDU1 | MGAT4B | LOC102723927 |
| ZNF141 | AGA | MAFA | C4orf27 | TSC22D3 |
| RDX | SF3A3 | ABHD15 | ALG1L9P | LOC102546294 |
| CDC7 | SF3A1 | AQPEP | CYP4Z1 | CCKBR |
| UPF3A | SF3A2 | SNAI3-AS1 | MYOZ1 | RBM12B |
| CDC6 | BRF1 | CDK4 | MUCL1 | LOC100507501 |
| GPN1 | PRSS36 | CDK2 | BROX | PRIM2 |
| GPN3 | C11orf58 | ALB | ARC | PRIM1 |
| TADA2A | C11orf57 | CDK1 | CEP57L1 | RBM15B |
| LINC00669 | AGBL5 | BRK1 | CCDC42B | PTCHD2 |
| ZNF136 | MORN1 | C16orf45 | XRN2 | DZANK1 |
| RET | MORN3 | DUSP16 | TFAM | CILP2 |
| MYOM1 | HYLS1 | PAGR1 | FAM64A | LOC100506207 |
| ZNF131 | DGKD | SIN3A | TELO2 | GDF11 |
| EP300-AS1 | CTNND2 | BAI2 | IGSF8 | DMRT2 |
| TCF20 | WASH2P | EFHD2 | SNORD35B | SEMA3B-AS1 |
| NUF2 | ZUFSP | EFHD1 | ANP32A | FLJ37035 |
| LINC00618 | CDH1 | BAI1 | TEX264 | GALNT14 |
| GARNL3 | RPS9 | C4orf36 | TMTC2 | GALNT16 |
| TCF19 | RPS7 | AMH | TMTC1 | DSCC1 |
| NDC1 | RPS8 | MSH5-SAPCD1 | SMIM7 | SCGN |
| TIGD3 | GPT2 | LOC145837 | IGSF9 | APLP1 |
| TAPT1-AS1 | RPS6 | LOC729970 | TMTC4 | COL4A2 |
| BRD2 | RPSA | TRAF3 | INPP5B | STK4 |
| BRD1 | C11orf35 | BHLHE40-AS1 | CYP4X1 | DMAP1 |
| AEN | TRAIP | EFHC1 | STC2 | STIL |
| TIMM22 | ARMCX4 | C4orf46 | SCAI | KIF18A |
| TIMM21 | TEX9 | LOC284837 | BANP | KIF18B |
| C11orf84 | MADD | MRM1 | CDT1 | ATG16L2 |
| KIAA1257 | TMPO-AS1 | DCAF15 | CDSN | LOC100507564 |

B4GALT2
USP37
ABCD3
USP31
CHTF18
USP39
PKD1
SLC2A8
CKS1B
HEBP1
GMPPA
AOX1
USP30
USP46
ABCC8
CKAP5
KLF16
MST1P2
USP40
SSR4P1
MCPH1
USP13
HCN3
USP10
USP19
ELOVL2-AS1
STOM
MUTYH
TCFL5
USP21
USP22
ZNF182
ZNF180

APPENDIX H. Gene lists and ToppFun analysis: ASH2L knockdown H3K4me3 ChIP-seq and RNA-seq.

The 438 genes in common between the ASH2L knockdown RNA-seq and H3K4me3 ChIP-seq, corresponding to **Figure 3.4-D**, are reported below and ToppFun analysis on these genes can be found at this

link: https://toppgene.cchmc.org/output.jsp?userdata_id=aab4d5af-6c57-42af-8c9e-6eb4b19d807d.

| | | | | |
|------------|-----------|-------------|-------------|-------------|
| ASH2L | BZW2 | AP4M1 | ALDH6A1 | GPANK1 |
| WHSC1L1 | METTL21A | PGAP1 | CSE1L | CASP8AP2 |
| BRE | GNAI1 | BRD9 | NIF3L1 | NTPCR |
| GEN1 | RABL2B | LOC10028818 | ZNF76 | NR3C2 |
| AGBL5 | NSL1 | 1 | PUF60 | PAXIP1-AS1 |
| FAM228B | PPP1R21 | XRCC6 | EPC2 | LRRC14 |
| GPN1 | TMEM237 | DDX11 | CENPM | SLC12A2 |
| CCNE2 | POP1 | CHCHD7 | FGD5-AS1 | MRPS30 |
| CENPO | PSMA2 | IFT22 | HDAC3 | NCAPH2 |
| TNRC18 | HEY2 | PCED1A | LOC10012951 | LOC10192853 |
| GRM8 | ZNF250 | SNHG15 | 8 | 0 |
| NANP | STRIP2 | PEX1 | GTSE1 | XRCC4 |
| RBM33 | ING2 | DZANK1 | VPS13B | WDR60 |
| CCT7 | KCTD13 | MTBP | SIRT5 | RARS2 |
| CBY1 | UGP2 | TTI1 | ZNF696 | PREPL |
| ABHD1 | LINC01124 | LYPD6 | TCP1 | ZNF131 |
| ZNF496 | CRNKL1 | PDE10A | ARL6IP6 | DPY19L4 |
| MPLKIP | TRIM36 | BRD2 | OTULIN | HNRNPA2B1 |
| AMMECR1L | MCM7 | COPS6 | UFSP1 | RAD52 |
| TADA3 | EAF1 | METTL1 | RFC2 | EIF4E |
| RABL2A | TTC30B | ZRANB3 | EIF3L | TRIP6 |
| GLI3 | EFCAB6 | ATRAID | DHX29 | CENPH |
| DESI1 | SP4 | PRIM2 | PCYOX1L | CCDC88A |
| PCIF1 | COPG2 | EFHC1 | BRIX1 | MCM8 |
| RING1 | RAB23 | MNX1 | ZNF775 | TRAPPC13 |
| CYP51A1 | RPRD1B | TMEM198 | CTDSP1 | AIG1 |
| POLD2 | TMEM170B | LOC150776 | NFYA | TAB2 |
| NUDT1 | ZNF141 | STK4 | R3HDM1 | NCAPH |
| AK9 | GMDS-AS1 | FGFR1OP | ZNF75A | KIF15 |
| CRNDE | NCAPG2 | RAET1K | WDR54 | POLH |
| PCOLCE-AS1 | PFDN6 | BLCAP | KCND3 | TTK |
| SMPD4 | ZNF7 | CUL9 | BRD1 | DIDO1 |
| DXO | WDYHV1 | NXT1 | BARD1 | RAD17 |

| | | | | |
|-----------|-------------|-----------|------------|-------------|
| ZNF619 | TAF6 | NUP188 | GMNN | TTC3 |
| KIF20A | PSIP1 | FAM53A | CETN3 | ELOVL2 |
| THADA | STAM | SLC1A5 | CCDC157 | ZBTB2 |
| LSM3 | ZC3H14 | LSM5 | KRT18 | TBCK |
| FBXO5 | RBM24 | CTDSPL | SMARCE1 | PARP2 |
| TRAM2 | GSTCD | LOC153684 | CELSR1 | CDKN2B-AS1 |
| RNGTT | CEP250 | CDC25C | GLT8D1 | RPL9 |
| DENND6B | DMC1 | FUBP3 | MBTD1 | CENPQ |
| RPS23 | CTNND2 | CCDC74A | RBBP8 | AFF1 |
| TTC23L | LOC10065275 | UBE2C | MMP16 | WDR5 |
| RTN1 | 8 | EZH2 | ANKRD31 | PAPD7 |
| ZNF789 | SLCO4A1 | ZNF8 | SKIDA1 | TBCB |
| CARD10 | GTF2F1 | SIGMAR1 | HAUS8 | TCF19 |
| PRMT3 | MED25 | SGOL1 | ELOVL2-AS1 | ZDHHC4 |
| FANCD2 | MRPL9 | FBXO38 | NDUFA8 | LOC10050699 |
| LOXL3 | TMEM67 | SIPA1L3 | PPM1L | 0 |
| ORC4 | TFAP2A-AS1 | TMEM167A | RIBC2 | PLEKHH3 |
| BLOC1S1 | GTF2I | CHERP | HSD11B1L | ARSG |
| SLX4IP | SAFB | TMEM198B | ASF1B | ZC2HC1C |
| EP300-AS1 | DBF4 | MCPH1 | BUB1 | SLC25A14 |
| MEA1 | RAVER1 | CALM2 | MICB | CCDC171 |
| PRELID2 | PASK | SKIV2L2 | RECQL4 | PECR |
| RTN4IP1 | GGA1 | TATDN1 | PTMA | PSMG1 |
| ATP13A2 | USP37 | WNT7B | ZNF239 | NOL4L |
| PTPN18 | SLBP | SUGP2 | ZBTB12 | TSEN34 |
| HCFC1 | NPHP1 | MFSD10 | ZNF717 | SYNE4 |
| RAP1GDS1 | EMC6 | EXTL3 | TPRKB | KIAA1468 |
| HNRNPDL | HMGB2 | RRM1 | XRCC2 | PEG10 |
| TRIQK | RHPN1-AS1 | AMZ2 | TM7SF2 | PPP1R11 |
| USP39 | RGS19 | RAB3A | SMIM7 | RPS28 |
| WBSR27 | PIIP5K2 | POMK | CAPNS1 | FANCC |
| NUDCD1 | PMS1 | RPS18 | USP40 | PIGX |
| BOLA3 | STRN | TUBB | SACM1L | SWI5 |
| LINC00899 | STK25 | SMC1A | THOC1 | PNPO |
| PTPRA | PSRC1 | RPL7A | STMN3 | NOTCH1 |
| DCK | PHF10 | AGPAT1 | TCTEX1D2 | PAQR5 |
| PLK4 | HSPD1 | MRGBP | CEP78 | TMCO3 |
| PRKRA | PLOD1 | GMPPA | ODF2 | TP53I13 |
| KCNK12 | RPS12 | MAD2L1 | KIAA1328 | POLE4 |
| FIS1 | DAXX | SPPL2B | KANSL1L | AURKA |
| PSMG3-AS1 | PAICS | CBX7 | RPL12 | |

| | |
|-------------|---------|
| LOC10050756 | PPP1R10 |
| 4 | NEK11 |
| PIK3CA | TBC1D5 |
| DCLRE1A | POLR2I |
| KIAA1524 | ZNF311 |
| SETD2 | MED16 |
| CAPN10-AS1 | ADRB2 |
| KLHL26 | CCDC74B |
| TOPBP1 | DTYMK |
| SS18L1 | AGPAT5 |
| KIF4A | SDSL |
| HMMR | PLEKHH2 |
| AKT1S1 | HMG20B |
| ZNF700 | DCAF16 |
| CENPE | PIGP |
| MAFA | ZMYM3 |
| NCL | HNRNPL |
| MAPK11 | ESCO2 |
| CNBP | CECR5 |
| ZNF446 | DLX1 |
| SLC25A33 | ADCY3 |
| SEP2 | SEC16A |
| ZNF566 | TECR |
| ASAH1 | MIS18A |
| TRIM46 | SNHG5 |
| BLOC1S3 | ADARB1 |
| SYCE3 | BCL2L12 |
| NRM | ALYREF |
| MED22 | WDR62 |
| RAD18 | RRP9 |
| RFX1 | RNF214 |
| CDKN1C | TRIM32 |
| AP2A1 | VRK3 |
| MIR4664 | ZGRF1 |
| SUPT5H | |
| ZNF473 | |
| GPRIN1 | |
| CEP112 | |
| NXF1 | |
| GRHL2 | |
| HNRNPUL1 | |

APPENDIX I. Gene lists and ToppFun analysis: ASH2L, NSD3-S, and ESR1 knockdown expression analysis and ASH2L knockdown H3K4me3 ChIP-seq overlap.

The 44 genes in common between the ASH2L knockdown RNA-seq and H3K4me3 ChIP-seq and NSD3-S and ESR1 knockdown microarrays, corresponding to **Figure 3.5-C**, are reported below and ToppFun analysis on these genes can be found at this link: https://toppgene.cchmc.org/output.jsp?userdata_id=be0407ac-a6be-4e45-b138-28ef7cb260d7.

The 320 genes that remain unique to the ASH2L knockdown RNA-seq and H3K4me3 ChIP-seq group following the comparison in **Figure 3.5-C** also appear below and ToppFun analysis on these genes can be found at this link: https://toppgene.cchmc.org/output.jsp?userdata_id=69413b86-3639-4bd6-8210-dad543db7860.

| | | | | |
|------------------|----------|-------------------|-------------|-----------|
| 44 Genes: | UBE2C | 320 Genes: | GNAI1 | CHCHD7 |
| | EZH2 | | RABL2B | IFT22 |
| CCNE2 | SGOL1 | ASH2L | NSL1 | PCED1A |
| RING1 | AMZ2 | BRE | PPP1R21 | SNHG15 |
| MCM7 | MAD2L1 | GEN1 | TMEM237 | PEX1 |
| NCAPG2 | GMNN | FAM228B | POP1 | DZANK1 |
| CSE1L | HAUS8 | GPN1 | ZNF250 | TTI1 |
| CENPM | ASF1B | TNRC18 | STRIP2 | ZRANB3 |
| TCP1 | BUB1 | GRM8 | UGP2 | ATRAID |
| RFC2 | RECQL4 | NANP | LINC01124 | PRIM2 |
| DHX29 | ELOVL2 | RBM33 | CRNKL1 | EFHC1 |
| CENPH | CENPQ | CBY1 | TRIM36 | MNX1 |
| KIF15 | DCLRE1A | ABHD1 | EAF1 | TMEM198 |
| TTK | KIAA1524 | ZNF496 | TTC30B | LOC150776 |
| KIF20A | HMMR | MPLKIP | EFCAB6 | STK4 |
| LSM3 | CENPE | TADA3 | SP4 | RAET1K |
| FBXO5 | ADCY3 | RABL2A | COPG2 | BLCAP |
| RTN1 | | GLI3 | RPRD1B | CUL9 |
| MEA1 | | DESI1 | TMEM170B | NXT1 |
| WBSCR27 | | PCIF1 | ZNF141 | NIF3L1 |
| PLK4 | | CYP51A1 | GMD5-AS1 | ZNF76 |
| PRKRA | | NUDT1 | AP4M1 | PUF60 |
| STAM | | AK9 | PGAP1 | EPC2 |
| USP37 | | CRNDE | BRD9 | FGD5-AS1 |
| SLBP | | PCOLCE-AS1 | LOC10028818 | GTSE1 |
| HMGB2 | | SMPD4 | 1 | VPS13B |
| SLC1A5 | | DXO | XRCC6 | SIRT5 |
| LSM5 | | BZW2 | DDX11 | ZNF696 |
| LSM5 | | METTL21A | | |

| | | | | |
|-------------|-------------|-----------|-------------|-------------|
| ARL6IP6 | DENND6B | RAVER1 | CCDC157 | CCDC171 |
| OTULIN | RPS23 | PASK | KRT18 | PECR |
| UFSP1 | TTC23L | GGA1 | SMARCE1 | NOL4L |
| EIF3L | ZNF789 | NPHP1 | CELSR1 | TSEN34 |
| PCYOX1L | PRMT3 | EMC6 | GLT8D1 | SYNE4 |
| ZNF775 | LOXL3 | RHPN1-AS1 | MBTD1 | KIAA1468 |
| CTDSP1 | ORC4 | PIIP5K2 | RBBP8 | PEG10 |
| NFYA | BLOC1S1 | PMS1 | MMP16 | PPP1R11 |
| R3HDM1 | SLX4IP | STRN | SKIDA1 | RPS28 |
| ZNF75A | EP300-AS1 | STK25 | ELOVL2-AS1 | PIGX |
| WDR54 | PRELID2 | PSRC1 | NDUFA8 | SWI5 |
| KCND3 | RTN4IP1 | PHF10 | PPM1L | PNPO |
| BRD1 | ATP13A2 | PLOD1 | RIBC2 | NOTCH1 |
| GPANK1 | PTPN18 | RPS12 | PTMA | PAQR5 |
| CASP8AP2 | HCFC1 | DAXX | ZBTB12 | TMCO3 |
| NTPCR | RAP1GDS1 | NUP188 | ZNF717 | TP53I13 |
| PAXIP1-AS1 | HNRNPDL | FAM53A | XRCC2 | POLE4 |
| LRRC14 | TRIQK | CTDSPL | TM7SF2 | LOC10050756 |
| SLC12A2 | NUDCD1 | CCDC74A | SMIM7 | PIK3CA |
| LOC10192853 | BOLA3 | ZNF8 | CAPNS1 | SETD2 |
| XRCC4 | LINC00899 | FBXO38 | SACM1L | CAPN10-AS1 |
| WDR60 | PTPRA | SIPA1L3 | THOC1 | KLHL26 |
| ZNF131 | DCK | CHERP | STMN3 | TOPBP1 |
| DPY19L4 | KCNK12 | TMEM198B | TCTEX1D2 | SS18L1 |
| HNRNPA2B1 | FIS1 | MCPH1 | KIAA1328 | ZNF700 |
| RAD52 | PSMG3-AS1 | CALM2 | KANSL1L | MAFA |
| EIF4E | TAF6 | SKIV2L2 | RPL12 | MAPK11 |
| TRIP6 | PSIP1 | TATDN1 | TTC3 | CNBP |
| CCDC88A | ZC3H14 | WNT7B | ZBTB2 | ZNF446 |
| MCM8 | RBM24 | SUGP2 | TBCK | SLC25A33 |
| TRAPPC13 | GSTCD | MFSD10 | CDKN2B-AS1 | SEP2 |
| AIG1 | CEP250 | EXTL3 | AFF1 | ZNF566 |
| TAB2 | DMC1 | RAB3A | WDR5 | ASAH1 |
| NCAPH | CTNND2 | POMK | PAPD7 | TRIM46 |
| POLH | LOC10065275 | TUBB | TBCB | BLOC1S3 |
| DIDO1 | SLCO4A1 | SMC1A | ZDHHC4 | SYCE3 |
| RAD17 | GTF2F1 | AGPAT1 | LOC10050699 | NRM |
| ZNF619 | MED25 | MRGBP | PLEKHH3 | MED22 |
| THADA | TFAP2A-AS1 | GMPPA | ARSG | RAD18 |
| TRAM2 | GTF2I | SPPL2B | ZC2HC1C | RFX1 |
| RNGTT | DBF4 | CBX7 | SLC25A14 | CDKN1C |

AP2A1
MIR4664
SUPT5H
ZNF473
GPRIN1
CEP112
NXF1
HNRNPUL1
PPP1R10
NEK11
TBC1D5
ZNF311
MED16
ADRB2
CCDC74B
DTYMK
PLEKHH2
HMG20B
DCAF16
ZMYM3
HNRNPL
ESCO2
CECR5
DLX1
SEC16A
TECR
MIS18A
ADARB1
ALYREF
RRP9
TRIM32
VRK3
ZGRF1